Table of Contents

Collaborating Institutions

Individuals from the following departments and institutions collaborated with the Center's faculty and staff in the research reports included in this year's publication (for individual attributions see specific reports):

Collaborating Columbia University Departments:

- Department of Biochemistry and Molecular Biophysics, Howard Hughes Medical Institute
- Department of Medicine, Division of Cardiology
- Department of Pediatrics
- Department of Radiation Oncology

Collaborating Institutions:

- Compliant Systems Integration, Inc., Rochester, NH
- Department of Experimental Oncology, Fondazione IRCSS Instituto Nazionale Tumori, Milan, Italy
- Departments of Medicine and Cell Biology, New York University Langone Medical Center, New York, NY
- Department of Natural Sciences, Hostos College of the City University of New York, New York, NY
- Department of Radiation Oncology, New York University Langone Medical Center, New York, NY
- Department of Radiation Oncology, The University of Texas Medical Branch, Galveston, TX
- GSI, Helmholtz Center for Heavy Ion Research, Munich, Germany
- Instituto de Alta Investigación, Universidad de Tarapacá, Arica, Chile
- University of Dundee, Dundee, Scotland ■

Left: The signing of the Columbia University - National Institute of Radiological Sciences (NIRS) Collaborative Agreement with Dr. Yoshiharu Yonekura, President of the NIRS and Prof. Tom K. Hei, representing Dean Lee Goldman of Columbia University Medical Center. In the back are: Dr. Yukio Uchihori (left) and Dr. Tadashi Kamada (right).

Below: Award winners at the 14th International Congress of Radiation Research in Warsaw, Poland. Radiation Research Society President Dr. Peter O'Neill presents Dr. David Brenner with the Failla Award (left). Dr. Igor Shuryak receiving the Editors' Award for best research article by a Scholar in Training from Radiation Research Editor Dr. Marc Mendonca (center). Dr. David Brenner after his Failla Award Lecture (right).

Acknowledgement of Support

In 2011 the Center for Radiological Research was supported by competitively awarded grants from the following agencies:

- Department of Defense
  - Defense Threat Reduction Agency
- Department of Energy
  - Office of Science, Office of Biological and Environmental Research [Low Dose Radiation Research Program]
- Department of Health and Human Services
  - Biomedical Advanced Research and Development Authority
  - National Institutes of Health:
    - National Cancer Institute [Program Project (P01) and Individual Research Grants (R01s)]
    - National Institute of Biomedical Imaging and Bio-engineering (P41)
    - National Institute of Allergy and Infectious Disease (U19)
    - National Institute of Environmental Health and Safety (R01s and R21)
    - National Institute of General Medical Sciences (R01)
- National Aeronautics and Space Administration

Websites

Center for Radiological Research……http://crr-cu.org
Radiological Research Accelerator Facility……http://www.raraf.org
Center for High-Throughput Minimally-Invasive Radiation Biodosimetry……....http://www.cmcr.columbia.edu
Mechanism of Bystander Effects……...…http//www.radiation-bystander.columbia.edu
Web-Rad-Train……...http://www.web-rad-train.org
Department of Radiation Oncology……http://cpmcnet.columbia.edu/dept/radoncology
Radiation Safety Office……..…..http://ehs.columbia.edu/rs.html
CRR Annual Reports (1998-present)……http://crr-cu.org/reports.htm

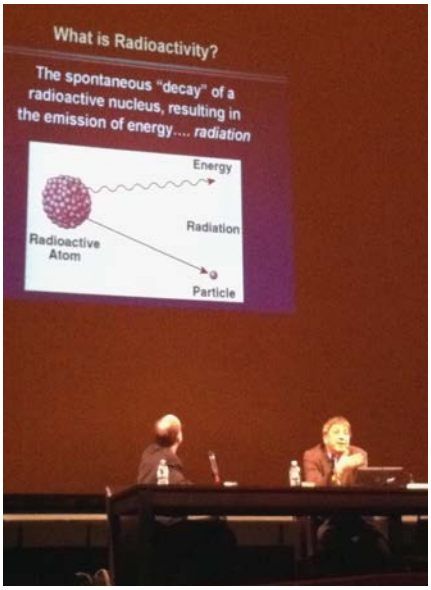

Center Director Dr. David Brenner explains the basics of radiation and the risks from the Fukushima disaster to the Metropolitan Opera Company prior to their spring tour to Japan. Information quelled irrational fears, and the Met was the first foreign performing arts organization to appear in Japan after the tsunami. Left: Met General Manager Peter Gelb watches Dr. Brenner's talk on the Met stage. Right: Dr. Brenner on the set of "Die Walküre" after his talk.

Introduction

2011 was certainly a significant year in the context of low dose radiation effects. The Fukushima disaster brought the topic firmly into the public view. Not surprisingly, predictions of the radiation-related consequences of the accident in the media varied from "millions of new cases of cancer in the northern hemisphere" (Op Ed, New York Times April 30 2011), to zero cancer cases (BBC Viewpoint, March 26 2011).

We can be pretty sure that the truth lies somewhere in between these extremes, but the reality is we don't know where. With the exception of a small number of extraordinarily brave workers inside the Fukushima Daichi plants, the radiation doses that the public have received to date (and will continue to receive for many years to come) are very low indeed - much lower than the doses for which we have epidemiological evidence of risk.

That we, in the radiation research field, have established so little about cancer risks caused by very low doses of radiation is, *prima facie*, quite surprising. After all, the health effects of ionizing radiation have been studied for a long time, and quite intensively since atomic bombs were used in World War II. But it is tough to understand cancer risks at very low radiation doses because epidemiological studies at such low levels of exposure are essentially impossible to conduct. The fundamental difficulty: about 25 percent of any population will die of cancer anyway.

But the inability to conduct an epidemiological study of low-dose radiation exposure doesn't say anything, one way or another, about whether the risks of tiny radiation doses are real. Absence of evidence is not evidence of absence.

So if low-dose radiation epidemiological studies are not feasible, what is to be done? The question becomes: How can we extrapolate radiation risks measured in epidemiological studies that can actually be done (i.e., of people who were exposed to higher doses), down to the much lower doses that are of societal interest but cannot be studied in the same way? The answer, inevitably, involves a better understanding of the basic science. What are the molecular processes whereby radiation damage to DNA results in the production of pre-malignant cells and, years later, in a frank cancer? Some of the mechanisms are likely to be similar to those for carcinogenesis in general, but because of the unique nature of radiation energy deposition, many of the mechanisms will be unique to radiation. Of course, it should not be overlooked that radiation is often used to treat cancer patients, and as such the study of these same mechanisms also has the potential to impact on improvements in radiotherapy.

The radiation risk for any given individual exposed to a very low dose of radiation will no doubt be miniscule, but what is the significance of tiny increases in individual risks, when many millions or even billions of people are exposed? In most other fields, risks to whole populations are estimated by multiplying the average individual risks by the number of people exposed, no matter how small the risk. Is this the right methodology to estimate the population risks when huge populations are exposed to very small radiation risks? There are some clues, but we really do not know, and basic science research, of the sort described in this Annual Report, is the only avenue forward here. ■

Throughout the Fukushima crisis, many news outlets called upon Dr. Brenner to help explain and interpret the evolving situation and the health risks associated with the radiological releases.

Staff News

Dr. David Brenner won the 2011 Failla Award. This award, named for Gioacchino Failla, the founder of our Center and one of the founders of the Radiation Research Society (RRS), is the highest honor bestowed by the RRS. Previous winners include our former director, Dr. Eric Hall. The presentation of the gold medal followed Dr. Brenner's award lecture entitled "Exploring the two-edged swords" and was made at the 14th International Congress of Radiation Research in Warsaw, Poland.

Dr. Tom Hei chaired the program committee for the RRS 2012 Annual Meeting, and will assume the presidency of the Society at the 2012 meeting. He was appointed Editor of *Advances in Space Research (Life Sciences)* and remains an Associate Editor of the *Journal of Radiation Research*. Dr. Hei was appointed to the scientific advisory board of the U.S. Environmental Protection Agency to evaluate a report on Libby amphibole fibers.

Dr. Howard Lieberman was appointed permanent member of the NIH RTB study section for a two-year term. He continued his position on the Scientific Advisory Board for the Israel Cancer Research Fund. In addition, he was Associate Editor for the journals *Radiation Research* and *Journal of Cellular Physiology*.

Dr. Sally Amundson was awarded tenure in the Department of Radiation Oncology. She continued as a member of the NCRP and of the Scientific Advisory Committee (SAC) of the joint U.S.-Japan Radiation Effects Research Foundation (RERF). Dr. Amundson was elected as the U.S. co-chair of the 2012 SAC. She also remained an Associate Editor of *Radiation Research.*

Dr. Charles Geard, who served for many years as the Associate Director of the Center, formally retired in 2011. He remains highly involved with the Center, especially at RARAF, and we are very grateful for his continued insight, advice and collaboration.

Several staff members left the Center in 2011, and we wish them well in their new ventures. Dr. Gengyun Wen entered a residency program in clinical psychiatry. Mr. Carl Elliston left for a medical physics position. Mr. Joshua Bernstock left for an M.D./Ph.D. program. Dr. Corinne Leloup, Dr. Aiping Zhu, Mr. Lihua Ming, and Ms. Yvette Acevedo also left the Center in 2011.

Two new Associate Research Scientists, Qingping Cui and Mikhail Repin, joined the CRR in 2011, as well as three Staff Associates, Kong Kwan Lam, Jay Perrier, and Radoslaw Pieniazek. Dr. Jie Zhang and Dr. Jihua Nie from Suzhou University were in the Center for a six-week training program in Dr. Tom Hei's laboratory.

We were delighted that several CRR members were promoted during the year. Drs. Lubomir Smilenov and Yongliang Zhao were promoted to Assistant Professor of Clinical Radiation Oncology, and Antonella Bertucci was promoted to Associate Research Scientist. ■

Laboratory Colloquia and Seminars

Three times a year, the Center organizes morning-long colloquium sessions featuring presentations of recent work by Center researchers and guest speakers. These colloquia are attended by Center staff and students, as well as by physicians and scientists from other departments at CUMC. They serve as a forum for discussions and forging future collaborations. The 2011 Colloquium Series was organized by Dr. Lubomir Smilenov.

March Colloquium:

- Dr. Gengyun Wen: "Does TGFBI affect tumor metastasis?"
- Dr. Ana Vasileva: "Adventures with a 'royal' protein in germ cells."
- Dr. Peter Golikov, Columbia Technology Ventures: "Introduction to Columbia Technology Ventures."

June Colloquium:

- Dr. Norman Kleiman, Environmental Health Sciences, CUMC: "CRR website Update: Improving all of our Internet presence."
- Dr. Mercy Davidson, Dept. of Radiation Oncology, CUMC: "Mitochondria in health and disease."
- Dr. Charles Geard: "Science and the CRR."

October Colloquium:

- Prof. Clifford Chao, Dept. of Radiation Oncology, CUMC: "Departmental update and Q&A."
- Dr. Teresa Palomero, Department of Pathology and Cell Biology, CUMC: "High-throughput sequencing at CUMC: applications and stories."
- Dr. Manuela Buonanno: "Mechanisms underlying the propagation of radiation-induced non-targeted effects."

In addition to our colloquium series, we have also welcomed a number of distinguished guest speakers from around the country and around the world. Guest speakers during 2011 included the following:

- Dr. Francesca Antonacci, University of Washington: "Structural variation of the human genome and disease predisposition."
- Dr. Takehiko Nohmi, National Institue of Sciences, Tokyo, Japan: "Genotoxicity of chemicals and radiation: tobacco, radiation and citrus fruit"
- Dr. F. Andrew Ray, Colorado State University: "Detecting chromosomal inversions using chromatid paints – use for retrospective biodosimetry."
- Dr. Peter Rez, Arizona State University: "The physics of airline security."
- Dr. Xiangchun Wang, NIH: "Functional Research of TGF Beta Pathway from Glycosylation to Ubiquitination." ■

CRR 2011 Holiday Party (l-r): Radek Pieniazek, Mikhail Repin, Alan Bigelow, Lilian Oling (upper right) Marcelo Vazquez, Antonella Bertucci, Teresa Vazquez, Jeremy Garty, Corinne Leloup, Guy Garty, (lower right) holiday prize giving: (standing): Tom Hei. (l to r in back): Guy Garty, Sasha Lyulko, Peter Grabham, David Cuniberti.

Faculty and Staff

Faculty:

DAVID J. BRENNER, Ph.D., D.Sc.
- ***Director***
- ***RARAF Director***

Higgins Professor of Radiation Biophysics
Professor of Radiation Oncology
Professor of Environmental Health Sciences
Chairman, Joint Radiation Safety Committee
Chairman, Radioactive Drug Research Committee

TOM K. HEI, Ph.D.
- ***Associate Director***
- ***Vice-Chairman, Dept. of Radiation Oncology***

Professor of Radiation Oncology
Professor of Environmental Health Sciences

ERIC J. HALL, D.Phil., D.Sc., FACR, FRCR, FASTRO
Higgins Professor Emeritus,
Special Lecturer in Radiation Oncology,
Special Research Scientist

CHARLES R. GEARD, Ph.D.
Professor Emeritus of Clinical Radiation Oncology

HOWARD B. LIEBERMAN, Ph.D.
Professor of Radiation Oncology
Professor of Environmental Health Sciences

SALLY A. AMUNDSON, Sc.D.
Associate Professor of Radiation Oncology

LUBOMIR SMILENOV, Ph.D.
Assistant Professor of Clinical Radiation Oncology

YONGLIANG ZHAO, Ph.D.
Assistant Professor of Clinical Radiation Oncology

Research Staff:

GERHARD RANDERS-PEHRSON, Ph.D.
Senior Research Scientist

ADAYABALAM BALAJEE, Ph.D.
Research Scientist

GUY GARTY, Ph.D.
Research Scientist

VLADIMIR IVANOV, Ph.D.
Research Scientist

HONGNING ZHOU, M.D.
Research Scientist

ANTONELLA BERTUCCI, PH.D.
Associate Research Scientist

ALAN BIGELOW, Ph.D.
Associate Research Scientist

CONSTANTINOS BROUSTAS, Ph.D.
Associate Research Scientist

GLORIA CALAF, Ph.D.
Adj. Associate Research Scientist

QINGPING CUI, Ph.D.
Associate Research Scientist

SHANAZ GHANDHI, Ph.D.
Associate Research Scientist

PETER GRABHAM, Ph.D.
Associate Research Scientist

JARAH MEADOR, PH.D.
Associate Research Scientist

SUNIRMAL PAUL, Ph.D.
Associate Research Scientist

BRIAN PONNAIYA, Ph.D.
Associate Research Scientist

MIKHAIL REPIN, Ph.D.
Associate Research Scientist

IGOR SHURYAK, M.D., Ph.D.
Associate Research Scientist

HELEN TURNER, Ph.D.
Associate Research Scientist

ANA VASILEVA, Ph.D.
Associate Research Scientist

CARL ELLISTON, M.S.
Senior Staff Associate

KEVIN M. HOPKINS, M.S.
Senior Staff Associate

STEPHEN A. MARINO, M.S.
Senior Staff Associate

AIPING ZHU, M.D.
Senior Staff Associate

KONG KWAN LAM
Staff Associate

JAY PERRIER
Staff Associate

RADOSLAW PIENIAZEK
Staff Associate

MARIA TAVERAS, R.N.
Research Nurse

Post-Doctoral Research Scientists:

YUNFEI CHAI, Ph.D.
HONGBO FANG, Ph.D.
ANDREW HARKEN, Ph.D.
THOMAS TEMPLIN, Ph.D.
GENYUN WEN, Ph.D.
YANPING XU, Ph.D.
ERIK YOUNG, PH.D.

Design & Instrument Shop:

GARY W. JOHNSON, A.A.S., Senior Staff Associate
- ***Design & Instrument Shop Director***

DAVID CUNIBERTI, B.A., Instrument Maker
DENNIS KEAVENEY, Instrument Maker
ROBERT C. MORTON, Instrument Maker

Technical Staff:

JOSHUA BERNSTOCK, M.S., Research Worker
LIHUA MING, M.S., Technician B
CUI-XIA KUAN, Technical Assistant

Administrative & Secretarial Staff:

MONIQUE REY, B.A., Center Administrator
LILIAN OLING, M.A., Project Manager
MARGARET LIN ZHU, M.A., Business Manager
YVETTE ACEVEDO, Administrative Assistant
ANGELA LUGO, B.A., Administrative Coordinator
ANNERYS RODRIGUEZ, Bookkeeper ■

Faculty and Staff

Front Row (l-r): Dr. Eric Hall, Dr. Sally Amundson, Dr. Tom Hei, Dr. David Brenner, Dr. Howard Lieberman, Dr. Charles Geard, Ms. Monique Rey.

2nd Row: Mr. Gary Johnson, Dr. Preety Sharma, Ms. Erica Pena, Dr. Antonella Bertucci, Ms. Maria Taveras, Dr. Congju Chen, Ms. Lilian Oling, Dr. Jarah Meador, Dr. Sasha Lyulko, Dr. Manuella Buonanno, Dr. Bo Zhang, Dr. Ana Vasileva, Ms. Angela Lugo, Dr. Peter Grabham.

3rd Row: Mr. Radek Pieniazek, Dr. Constantinos Broustas, Ms. Annerys Rodriguez, Dr. Adayabalam Balajee, Dr. Helen Turner, Dr. Shanaz Ghandhi, Dr. Vladimir Ivanov, Dr. Lubomir Smilenov.

Back Row: Mr. Roy Lam, Dr. Sunirmal Paul, Dr. Thomas Templin, Mr. David Cuniberti, Mr. Stephen Marino, Dr. Mikhail Repin, Dr. Igor Shuryak, Dr. Guy Garty, Mr. Robert Morton, Dr. Alan Bigelow, Dr. Andrew Harkin, Dr. Hongning Zhou, Dr. Erik Young, Mr. Jay Perrier, Mr. Michael Grad, Dr. Winston Liao, Mr. Kevin Hopkins, Dr. Qingping Cui.

Not Pictured: Dr. Yongliang Zhao, Dr. Gerhard Randers-Pehrson, Dr. Gloria Calaf, Dr. Brian Ponnaiya, Mr. Carl Elliston, Dr. Aiping Zhu, Dr. Kong Kwan Lam, Dr. Yunfei Chai, Dr. Hongbo Fang, Dr. Genyun Wen, Dr. Yanping Xu, Mr. Dennis Keaveney, Mr. Joshua Bernstock, Mr. Lihua Ming, Ms. Cui-Xia Kuan, Ms. Margaret Lin Zhu, Ms. Yvette Acevedo.

Imaging at the RARAF Microbeam Irradiator

Andrew D. Harken, Gerhard Randers-Pehrson, and David J. Brenner

Introduction

We are continuing to develop the imaging capabilities at the microbeam end station making use of the Electron Multiplying CCD (EMCCD) technology. We are also expanding our use of oblique illumination imaging as a long-term observational technique for monitoring cell morphology before, during and after irradiation.

Enhanced Imaging Speed

As we have previously reported, we have replaced our intensified CCD (ICCD) camera with the EMCCD, which has given us better control of our imaging capabilities. This upgrade has also enhanced the resolution of our images, while acquiring them in a significantly shorter exposure time. Figure 1 demonstrates this capability. The image in Figure 1A was acquired with the ICCD camera over ~1.5 sec and the image in Figure 1B was acquired with the EMCCD at an exposure of 0.48 msec. Both of these images were acquired using the same light intensity on the sample. Most of the acquisition time is in the image handling system for the microbeam control

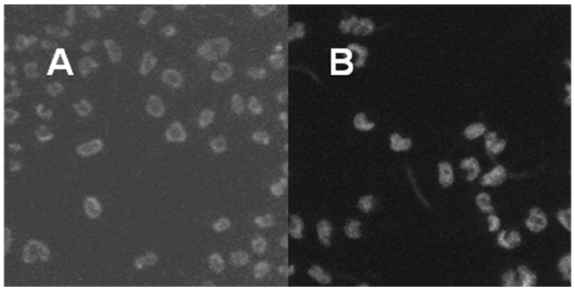

***Figure 1**. Comparison images from microbeam irradiations. Image A was acquired with the ICCD camera and image B with the EMCCD camera.*

software. This means that the actual exposure time for capturing the EMCCD image is 10 msec. The current shutter time on the lamp is ~120 msec for the fastest images. We will reduce this with the introduction of our diffraction grating light source, which can switch to the UV source line in 1 msec and away after exposure again in 1 msec, giving an overall exposure of 12 msec for a 10 msec acquisition.

Oblique Time Lapse Observational Imaging

Oblique illumination imaging uses an off-axis, above the dish light source independent of the microscope illumination pathways. The light passes through the sample dish, reflects off the beam exit window, back through the sample into the microscope objective and forms a contrast image of the sample at the camera. This technique allows us to view cells in a non-stain, no-UV illumination manner. Figure 2 is an image of A549 cells imaged with this technique.

We are expanding on our imaging capabilities to take longer observations at the microbeam end station. We have developed a time-lapse imaging routine where an image can be acquired at any time frame the experimenter requires. Figure 3 demonstrates a time-lapse series of an A549 cell finishing a division cycle. In this series, 25

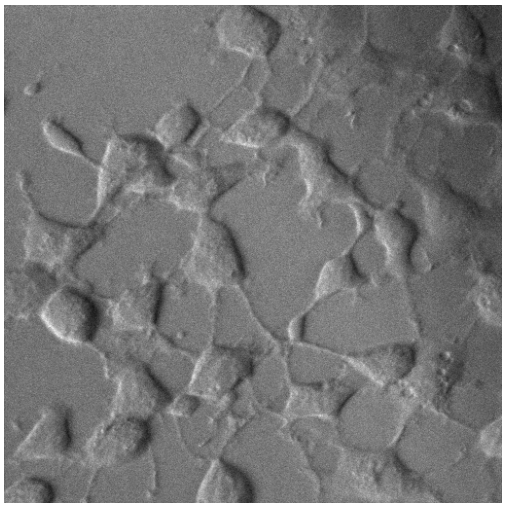

***Figure 2**. Oblique illumination image of A549 cells with no stain at 600 nm illumination.*

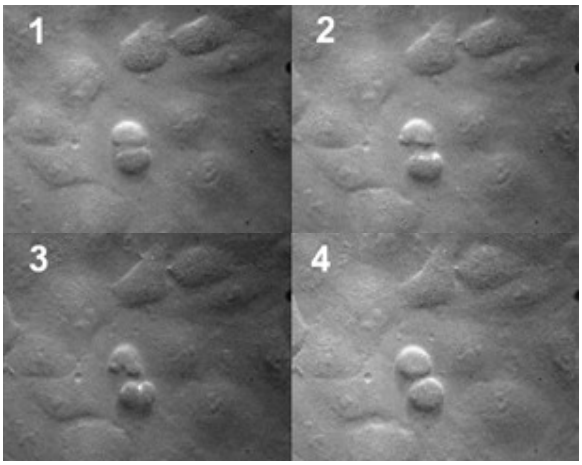

***Figure 3**. Series of images of confluent A549 cells where one of the cells is completing a division. 25 minutes elapsed between frame 1 and frame 4.*

minutes elapse between frame 1 and 4. We are continuing to develop our fluorescent and non-fluorescent imaging capabilities on our microbeam end station as our users require new and differing techniques to visualize their experimental endpoints. ■

Label-free Vibration-insensitive Interferometric Imaging of Live Cells

Oleksandra Lyulko, Gerhard Randers-Pehrson, and David Brenner

Simultaneous Immersion Mirau Interferometry (SIMI) is an epi-illumination no-stain, no-UV imaging technique, developed at the Radiological Research Accelerator Facility (RARAF). SIMI is an advanced modification of

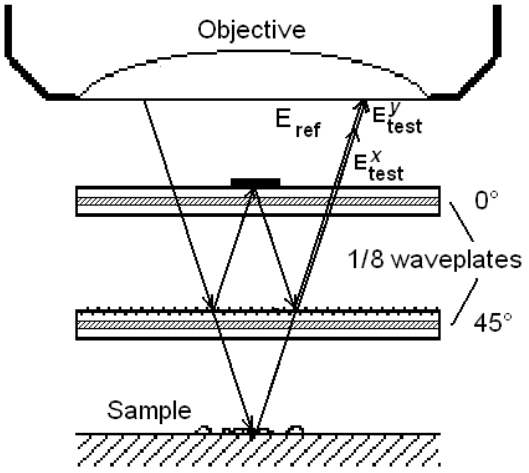

Figure 1. *Schematic of the simultaneous Mirau interferometer: a λ/8-waveplate placed in the test arm introduces a π/2 delay between the x and y components of the test beam; a second waveplate oriented at 0° equalizes the test and reference path lengths.*

Immersion Mirau Interferometry (IMI), which was developed as a label-free imaging modality for targeting live cells in medium during microbeam irradiation experiments. IMI uses phase-shifting interferometry as a data collection technique – the interference patterns are acquired consecutively as the sample is positioned at different heights with nanometer precision. This makes IMI sensitive to environmental vibrations and limits its use only to workstations with vibration isolation, which is not feasible within the geometry of the RARAF microbeam endstation. SIMI was developed to overcome this limitation. It is based on the simultaneous acquisition of all interferograms, which eliminates the effects of vibration. The schematic of SIMI design is shown in Figure 1. A λ/8 waveplate (retarder) with its fast axis at 45° to the direction of the light polarization is introduced between the beam-splitter of the interferometer and the sample. The waveplate creates a quarter-wavelength phase difference between the x and y components of the test beam upon two traversals.

Therefore, the output of the interferometer contains two interferograms with a relative phase shift of π/2. The interferograms are spatially separated by a polarization beam displacer and are recorded by the sensor of a camera. Combined with the background image, the acquired interferograms are used to reconstruct the intensity map of the specimen. To restore equal optical paths, a compensation waveplate with its axis at 0° to the polarization of light is placed into the reference path.

Polycarbonate film was selected as the retarder material because of its high accuracy of retardance (the ability to introduce phase shift) and higher acceptance angle, or an angle of incidence (AOI) for which the retardance change is relatively low, in comparison to other materials, for example, mica and quartz (Figure 2). Having uniform retardance across a wide range of AOI is important for our system because the objective compatible with the Mirau attachment has a high numerical aperture and the angles of incidence vary from 0 to 30 degrees. The windows were laminated with polycarbonate retarder film by Bolder Vision Optik (Boulder, CO).

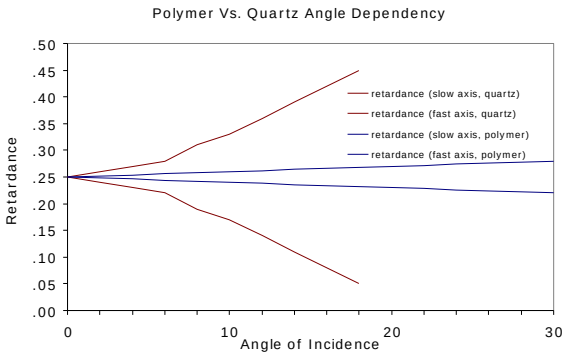

Figure 2. *Dependence of retardance on the angle of incidence (AOI) for a quartz waveplate (red line) and a polycarbonate waveplate (blue line). The polycarbonate waveplate exhibits considerably more uniform properties across different AOI than does quartz.*

Exposure of polycarbonate film to liquid causes degradation of its retardation properties. To prevent contact with medium, each waveplate was sandwiched between two thin layers of glass (Figure 1). Precision windows of thickness 0.2 and 0.3 mm were manufactured by Perkins Precision Developments (Platteville, CO). The specifications of the glass - surface quality 20/10, flatness of 1/20 of the wavelength (540 nm) and parallelism below 5 seconds - greatly exceeded the generally used standards of the optics industry. These parameters were chosen to limit the wavefront distortion

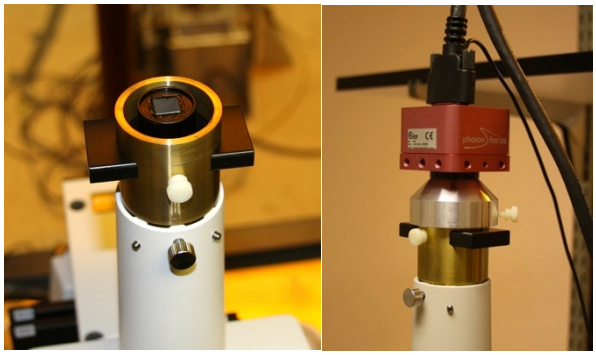

Figure 3. *SIMI microscope module. Left: the main body of the camera adaptor with the beam-displacer fitted inside; right: main adaptor body, rotatable C-mount and the camera.*

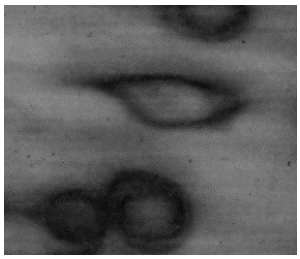

Figure 4. *SIMI image of HT 1080 fibrosarcoma cells. The cells were plated on glass slides and imaged in PBS.*

of the incident beam. The windows were coated with partially and fully reflective mirror coatings by Laseroptik GmbH, Garbsen, Germany. To preserve the components of the light polarization, the coatings were selected with low dependence of transmission, retardance and phase shift on the direction of polarization and AOI. All of the coatings are covered with protective layers to prevent

Figure 5. *Example of processing of a SIMI image of a live fibroblast: a) the grayscale image reconstructed from interferograms; b) binarized image separates pixels with intensities above or below the threshold level; c) the region within the closed contour of the cell nucleus is filled and the center of gravity is localized and marked.*

interaction with the cell medium. The new optics holders for the polarization windows and the SIMI interferometric attachment were constructed and assembled at the machine shop of the Center for Radiological Research (CRR). A custom camera adaptor, also designed and built in the CRR machine shop, allows for alignment of the system components with the light polarization (Figure 3).

The SIMI system was successfully tested for imaging of live cells in the immersion mode. Figure 4 shows a SIMI image of HT 1080 fibrosarcoma cells. The cells were cultured on glass slides in cell growth medium. Prior to imaging, the cells were transferred to phosphate buffered saline (PBS) pre-warmed to 37°C. The outlines of the cells are clearly visible and can be detected using the automated image analysis software for cell targeting developed and used at RARAF (Figure 5). ■

Center for Radiological Research 2011 Holiday Party (top row, l-r): David Brenner, Tom Hei, Lubo Smilenov, Shanaz Ghandhi, Lilian Oling, Jeremy Garty, Sasha Lyulko, (bottom row, l-r): Lilian Oling, Shanaz Ghandhi, Alan Bigelow, Erik Young.

Imaging of a Cell System to Study Chromosomal Aberration Formation at the Microbeam

Alan W. Bigelow, Brian Ponnaiya, Iris Muller[a], and Jonathan Chubb[b]

The ability of ionizing radiation to induce chromosomal aberrations has been a long-standing interest at the Center for Radiological Research, and the formation of these aberrations has been studied in a variety of systems using various methods of analyses [1-5]. Recently, the charged particle microbeam was used to examine the induction of genomic instability using a chromosomal end point [6]. It was observed that the progeny of irradiated and bystander human hamster hybrid (A_L) cells contained persistent chromosomal changes when analyzed using multicolor banding (mBAND).

Novel developments of fluorescent chromosome tags within single cells are enabling small areas on specific chromosomes as targets for the RARAF microbeam. These advances in live-cell imaging are opening new frontiers for radiobiologists to irradiate sub-cellular components located within conventional sub-cellular (nucleus or cytoplasm) targets. Pursuing our motivation 1) to investigate changes in chromosome domain dynamics as a function of targeted DNA damage, and 2) to study the mechanisms of chromosome aberration formation, we are collaborating with both Iris Muller at GSI Darmstadt and Jonathan Chubb at the University of Dundee, who have developed a triple-tagged HT1080 cell line that offers chromosome-specific targeting.

These triple-tagged HT1080 cells express red fluorescent protein (RFP), green fluorescent protein (GFP) and yellow fluorescent protein (YFP). Histone 2B is tagged with RFP and is present in all the chromosomes. Histone 3 is tagged with a photoactivable GFP variant that is also present in all the chromosomes but only fluoresces when illuminated with 405 nm light. Individual chromosomes (or even fractions of chromosomes) can be made to fluoresce in this way. In addition, bacterial LacO sequences have been integrated specifically into chromosome 11. To visualize these sequences, plasmids have been introduced into the cells that produce YFP tagged LacI protein, which binds specifically to the LacO sites. To date all these fluorescent proteins have been visualized using oil immersion optics [7]. However, microbeam studies require the targets to be visualized under either air or water objectives. Therefore, the first step towards using these cells in a microbeam experiment required the imaging of the fluorescent proteins under water immersion objectives. For these studies a Nikon 60X Water Immersion Objective Lens with a 1.27 NA was used.

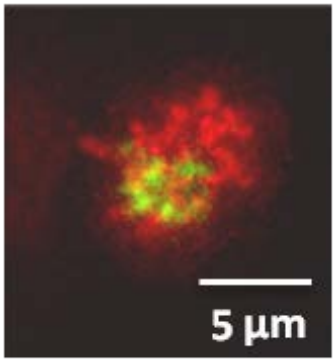

Figure 1. *Triple tagged HT1080 cell with all chromosomes expressing RFP conjugated Histone 2B (red). Only regions targeted by the UV microspot exhibit GFP fluorescence (green).*

Two approaches for chromosome specific targeting of these cells are: 1) to mark a particular chromosome region through photoactivation of GFP, and 2) to locate chromosome 11 by imaging the YFP (yellow spots). At RARAF we have performed a feasibility study for both of these approaches and found that, while we can currently photoactivate GFP on select chromosomes within a single cell nucleus, proposed technical developments will greatly enhance our ability to identify and irradiate the yellow spots on chromosome 11.

For our photoactivation trial, we used the UV microspot to initiate photoactivation of GFP by scanning the laser focal point over a small square region of the cell nucleus. Z-stack fluorescent images were subsequently

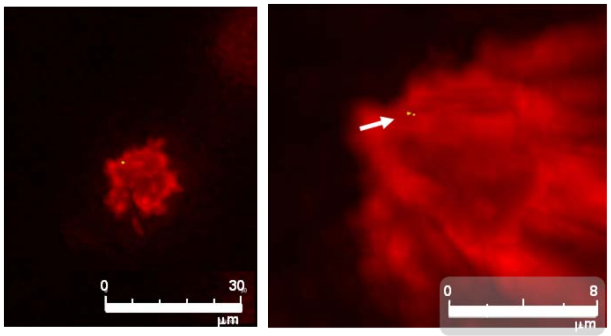

Figure 2. *Fluorescent z-stack imaging of YFP tagged LacI bound to LacO bacterial sequence introduced into HT1080 cells (yellow). Image on the right shows resolution of two copies of the sequence after image processing (arrow).*

[a]GSI, Helmholtz Center for Heavy Ion Research

[b]University of Dundee

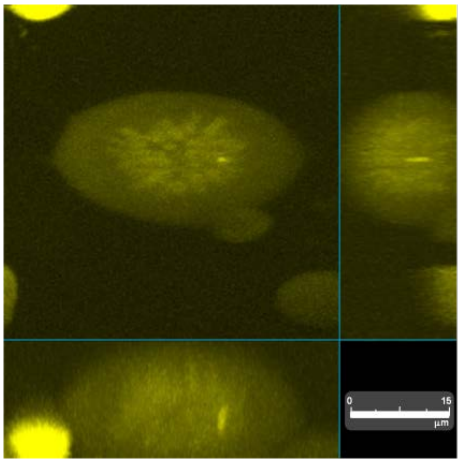

Figure 3. *Imaging of YFP tagged LacI bound to LacO bacterial sequence introduced into HT1080 cells using multiphoton microscopy.*

processed and revealed GFP signal spanning the area of the initial laser scan (Figure 1). This validated that we have the capability to define single chromosomes within a cell nucleus for targeting.

In the second approach, the YFP signal was imaged through two modes: 1) fluorescent z-stack imaging (Figure 2) and 2) multiphoton microscopy, with triple profile view (Figure 3). Autoquant debluring software was applied to both cases. A single yellow spot is discernible using both imaging techniques. Only in the case of fluorescent z-stack imaging, however, was it possible to reveal two distinct spots within the YFP region, through the application of additional processing steps. While we are optimistic that these cells enable small areas on specific chromosomes as targets for the RARAF microbeam, we also acknowledge the need for additional technologies to reliably visualize these targets in real time (without image processing steps).

Two proposed development projects that RARAF users are calling for are super resolution microscopy and a super microbeam. Stimulated Emission Depletion (STED) microscopy offers an on-line approach for super resolution microscopy of live cells with tens of nanometers resolution. Our proposed solenoid-based super microbeam aims to focus charged particles to a diameter of equivalent magnitude to reliably irradiate small areas on specific chromosomes.

In conclusion, we have successfully photoactivated GFP on histone 3 and visualized the YFP signal on chromosome 11 using water immersion optics on the microbeam end station. The ability to target a specific chromosome with the charged particle microbeam will allow us to investigate the mechanisms involved in chromosome aberration formation in a definitive manner.

References

1. Geard CR, Rossi HH. Biophysical studies with high-energy argon ions 3. Chromosomal aberrations in aerated and hypoxic Vicia faba root meristems. Radiat Res. 1977 Jun;70(3):480-93.
2. Geard CR. Initial changes in cell cycle progression of Chinese hamster V-79 cells induced by high-LET charged particles. Radiat Res. 1980 Sep;83(3):696-709.
3. Geard CR, Jenkins G. Human chromosome-specific changes in a human-hamster hybrid cell line (AL) assessed by fluorescent in situ hybridization (FISH). Int J Radiat Oncol Biol Phys. 1995. Apr 30;32(1):113-20.
4. Brenner DJ, Okladnikova N, Hande P, Burak L, Geard CR, Azizova T. Biomarkers specific to densely-ionising (high LET) radiations. Radiat Prot Dosimetry. 2001;97(1):69-73.
5. Mitchell CR, Azizova TV, Hande MP, Burak LE, Tsakok JM, Khokhryakov VF, Geard CR, Brenner DJ. Stable intrachromosomal biomarkers of past exposure to densely ionizing radiation in several chromosomes of exposed individuals. Radiat Res. 2004 Sep;162(3):257-63.
6. Hu B, Grabham P, Nie J, Balajee AS, Zhou H, Hei TK, Geard CR. Intrachromosomal changes and genomic instability in site-specific microbeam-irradiated and bystander human-hamster hybrid cells. Radiat Res. 2012 Jan;177(1):25-34.
7. Iris Muller, Shelagh Boyle, Robert H. Singer, Wendy A. Bickmore and Jonathan R. Chubb. Stable Morphology, but Dynamic Internal reorganisation of interphase human chromosomes in living cells. PLoS One. 2010 Jul 13;5(7):e11560. ■

Proton Induced Soft X-Ray Microbeam at RARAF: Biological Testing

Andrew D. Harken, Gerhard Randers-Pehrson, and David J. Brenner

Introduction

The development of the proton-induced soft x-ray microbeam for low-LET ionization of single cells and sub-cellular organelles is continuing. The x-ray microbeam has now seen the start of biological users of the microbeam, first for verification of the system and then for beginning experiments.

End Station Design

The x-ray microbeam is installed on a horizontal beam line at the Radiological Research Accelerator Facility (RARAF) [1]. Figure 1 is a schematic representation of the microbeam end station with the proton beam coming in from the right. The protons (1.8 MeV) are focused on a titanium target (Kα = 4.5 keV) using an electrostatic quadrupole quadruplet. The titanium target is cut at a 70° angle to the incident proton beam, which allows a portion of the generated x-rays to be emitted in the vertical direction. The x-rays are focused using a Fresnel zone plate diffractive optic (Zoneplates, Inc, London, UK) to a current spot size of 5 µm in diameter.

The samples are positioned using a combination micro- and nano-positioning stage (Mad City Labs, Madison, Wisconsin, USA). This design of horizontal staging allows the same biological protocols to be used on the x-ray microbeam that have been developed on thecharge-particle beam system making beam type comparative studies more easily accessible. The beam size is 5 µm in diameter, which is sufficient for nuclear and cytoplasmic irradiations as wanted by our users.

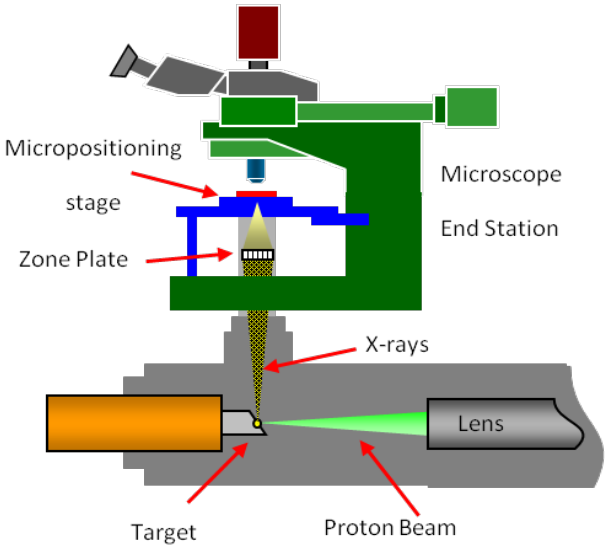

Figure 1. *Schematic diagram of the x-ray microbeam end station on the horizontal beam line at RARAF.*

Preliminary Biological Testing

The initial test for the x-ray microbeam using biological targets was to irradiate AG1522 cells with 0.1 Gy of x-rays in the nucleus. Figure 2 shows two representative cells, a sham-irradiated control cell on the left and an irradiated cell on the right. The cells were analyzed for γ-H2AX foci and the expected increase in foci in the irradiated cells was observed. This experiment is ongoing, but the results shown are typical.

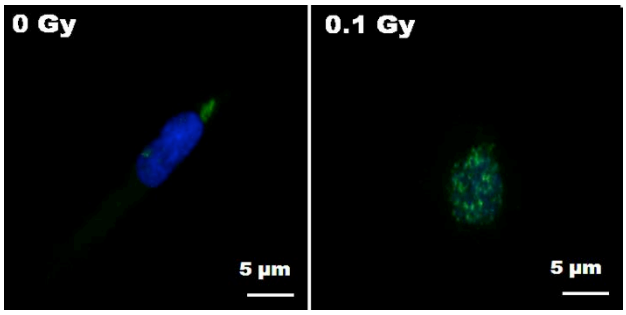

Figure 2*. AG1522 cells with the nuclear stain DAPI (blue) stained for γ-H2AX (green). These cells demonstrate the x-ray microbeam is targeting individual cells as required and that we are observing DNA damage commensurate with the delivered dose.*

Conclusion

Development of the proton induced x-ray microbeam is continuing with the biological testing and initial biological experiments. We are actively encouraging our users to consider using the x-ray microbeam at RARAF for comparison to their broad area irradiations and charged-particle microbeam irradiations.

References

1. Harken A, Randers-Pehrson G, Brenner DJ (2011) The Columbia University proton-induced soft X-ray microbeam. *Nuc. Intr. And Meth. B* **269:** 1992-6. ■

Update on the Neutron Microbeam

Yanping Xu

The neutron microbeam system has been completely installed at RARAF this year. The initial proton beam has been tested. The proton beam size optimization and the secondary neutron beam test are ongoing now.

Neutron Microbeam

The neutron microbeam beam line was assembled at RARAF (Figure 1). The whole length of the beam line from ion object aperture to Lithium Fluoride target is about 6.0 meters. Beam diagnostic/handling devices (e.g. steering magnet, shutter, beam positioning slides) and vacuum protection devices (e.g. fast valve & beam line baffle) have been installed. The detection system at the microbeam end station includes two gas chambers mounted on microscope objectives (Figure 2). One is an ionization chamber, which is for making the initial proton current and initial proton beam spot size measurements. The other is a gas proportional counter with gain, which is used for neutron detection. The imaging system includes a customized long motion horizontal microscope coupled with a CMOS camera and an X-Y-Z 3D motorized stage for holding samples (Figure 2). Both detection and imaging system control codes have been finished and tested. A remote program control network was set up in the console room. The initial proton beam current has been measured at about 2 nA. The proton beam size is about 100 µm by 150 µm diameter (Figure 3) using a large ion object aperture and an electrostatic quadruplet lens with an ABBA configuration.

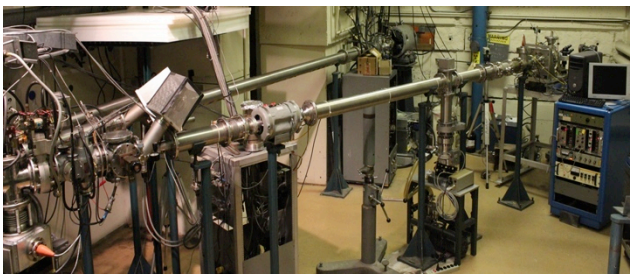

***Figure 1**. Neutron microbeam beam line*

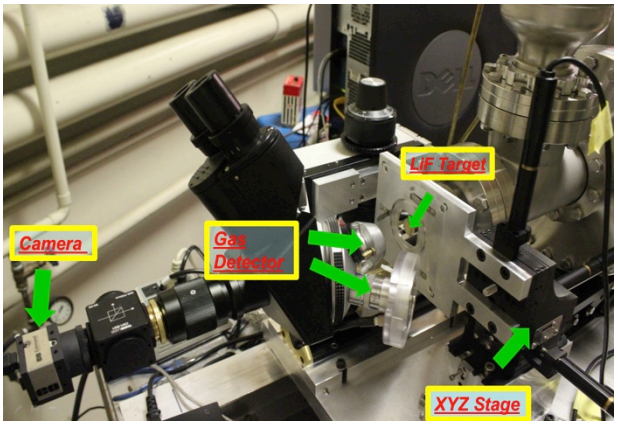

***Figure** 2. Neutron microbeam line end station*

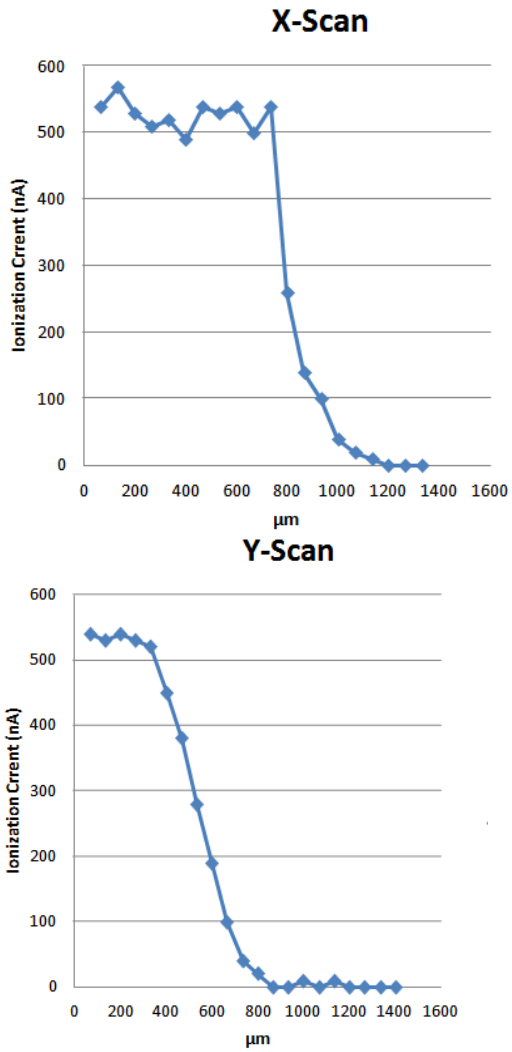

***Figure** 3. Initial proton beam size scan results*

The beam size optimization is ongoing, and we reasonably expect to be able to achieve a 20 µm diameter proton beam. Measurement and dosimetry of the secondary neutron beam spot size will be conducted once the goal for the proton beam size is met.

References

1. Xu Y, Garty G, Marino SA, Massey TN, Randers-Pehrson G, Johnson GW, Brenner DJ. (2012) Novel neutron sources at the Radiological Research Accelerator Facility. J Instrum. 7(3): C03031.
2. Xu Y, Randers-Pehrson G, Marino SA, Bigelow AW, Akselrod MS, Sykora JG, Brenner DJ. (2011) An accelerator-based neutron microbeam system for studies of radiation effects. Radiat Prot Dosimetry. 145(4): 373-6. ■

Dissemination of Information: Internet

Radoslaw Pieniazek

I am the main Administrator of the following websites, CRR: Center for Radiological Research (http://crr.columbia.edu), CMCR: Center for High-Throughput Minimally-Invasive Radiation Biodosimetry (http://cmcr.columbia.edu) and RARAF: Radiological Research Accelerator Facility (http://raraf.org).

Updates

The content of our websites is continually updated to reflect the current state of research at CRR and to answer questions interested parties may have. For example the RARAF website offers useful information such as the current month's accelerator schedule and our experiment scheduling form. We also keep users apprised of the status of new developments at RARAF through our New Developments section, which is dedicated to highlighting the current state of microbeam development and upgrades. This section includes detailed descriptions of novel new tools we are building to enhance the microbeam.

David Brenner's new website

I built a new website for CRR and RARAF director, David Brenner (http://columbia.edu/~djb3).

The new features include a modern look, user-friendly menu and "latest news" section. Visitors can also find audio podcasts and interesting links to topics such as radiation safety.

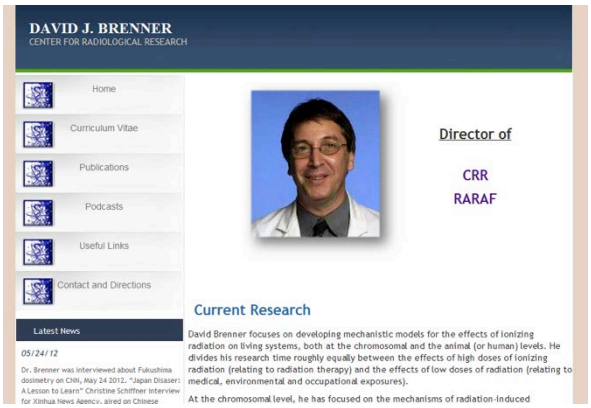

***Figure 1**. David Brenner's new website.*

The New RARAF Website

Packaging is often as important as content, so we addressed the need for a new website. An updated website is currently under construction and will be available in late summer of 2012. Until that time, the current website is available at http://raraf.org.

***Figure 2.** The new RARAF website.*

The new website has a fresher look, intended to attract future microbeam users with updated content to reflect the current state of research at RARAF. Functional menus (including a front page rotating-picture menu) were designed to easily navigate through the content. Videos will not only be visible from the microbeam online training educational materials page, but there will also be a "Featured Videos" section on the home page.

While browsing, at any point a user will be able to quickly navigate to websites like Columbia or NIBIB as well as return to the main RARAF page. In the footer, we will have information on RARAF's mailing address and links to our social media websites (LinkedIn, Facebook and YouTube Channel).

The New Developments section will be separated into specific, easy-to-spot segments, such as "Biological Systems" or "Imaging". The updated website will contain

detailed descriptions of novel new tools we are building to enhance the microbeam, such as the Neutron Microbeam, Optoelectronic Tweezers and other exciting new topics like Zebrafish.

Microbeam Online Training Course

In May of this year we held the first Microbeam Training Course at RARAF over the course of three days. An online version of the course was available to the students and all interested scientists unable to attend at http://raraf.org/educationalmaterials. The curriculum consists of PDF handouts and audio podcasts synched with the accompanying PowerPoint presentations. Next year we will expand the online materials with HD videos (720p resolution) of the RARAF staff: giving a preliminary lecture on microbeams (David Brenner), a technical tour of the accelerator facility (Stephen Marino), a demonstration of cell seeding and dish preparation (Manuela Buonanno), as well as microbeam start up with accelerator stabilization (Gerhard Randers-Pehrson). In today's world personal electronic devices are mostly portable, that is why the videos we shot can be viewed on any Internet enabled device supporting YouTube format, which includes: PCs, Macs, tablets and smartphones. To grow the material database even further, during the three-day training course we filmed every lecture (available at http://raraf.org/lectures) giving outside users and scientists the opportunity to derive knowledge from

***Figure 3**. RARAF website. Training Videos section.*

RARAF's experts in microbeam technology. We now provide access to a total of over 275 minutes of video footage related to the Microbeam Training Course.

Our goal in making these enhancements was to further develop a user-friendly research environment for the ever-growing microbeam community. ■

Celebration of Dr. Brenner's Failla Award at the 14th International Congress of Radiation Research. Top left (l to r): Debbie Brenner, Renee Brenner, David Brenner. Lower left (l to r): Bill Morgan, Tom Hei, Sally Amundson. Above (l to r): Helen Turner, Manuella Buonanno, David Brenner.

Microbeam Technology Development for Small Animal Systems

Manuela Buonanno, the RARAF team, and Collaborators

Ionizing radiation-induced biological effects *in vivo* can currently be studied at the Radiological Research Accelerator Facility (RARAF) using three animal models. This report will briefly summarize each of these three models.

C. elegans

The *C. elegans* nematode is a well-established research organism suitable for radiobiological studies. With a transparent body that can be easily observed under a microscope, *C. elegans* has a relatively small diameter (50 μm) and can be completely traversed by the charged particles generated by the RARAF microbeam, the maximum penetration of which is 450 μm. In previous microbeam protocols [1] the worms were immobilized by anesthesia and positioned by hand within 20 minutes. However, some biological endpoints, such as genetic and behavioral studies, require high-throughput irradiation/imaging capabilities without the use of drugs such as anesthetics. To meet the considerable demand for high-throughput studies from the *C. elegans* research community, we have an ongoing collaboration with **Dr. Hobert** at the Howard Hughes Medical Institute of Columbia University. In order to support high-throughput irradiation of *C. elegans*, we have implemented a microfluidic worm clamp (Figure 1), originally designed by Dr. Whitesides at Harvard University. Each clamp consists of up to 16 tapered channels with 10-μm thin bottom, to guarantee charged particle traversal. Worms are introduced into the microfluidic clamp through liquid flow between an inlet and an outlet (Figure 1A); they are immobilized in the microchannels (Figure 1B, C) and then released by reversing the flow direction in the clamp.

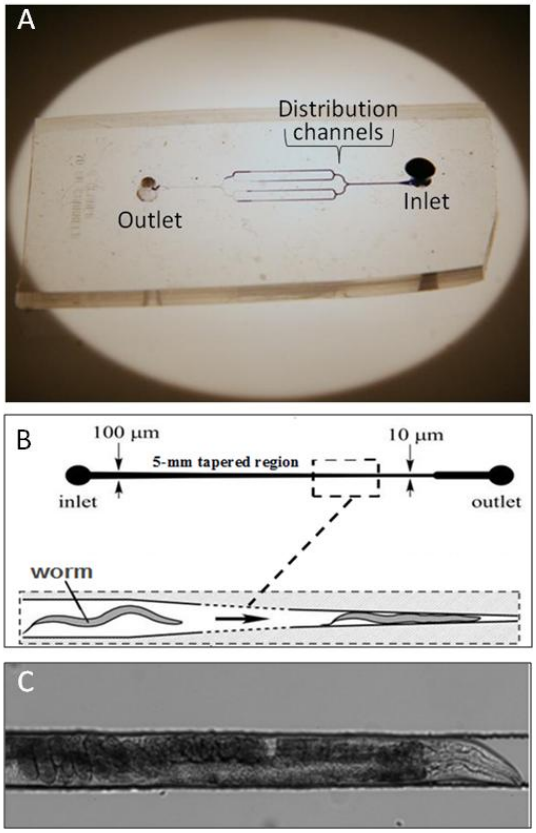

Figure 1. *A) 4-channel microfluidic device for C. elegans observation and irradiation at the microbeam. Worms move into the microfluidic channels through liquid flow between an inlet and an outlet. B) The size of each microchannel is such that young adult worms are immobilized without the use of anesthesia. C) Microscope view of an immobilized young adult C. elegans.*

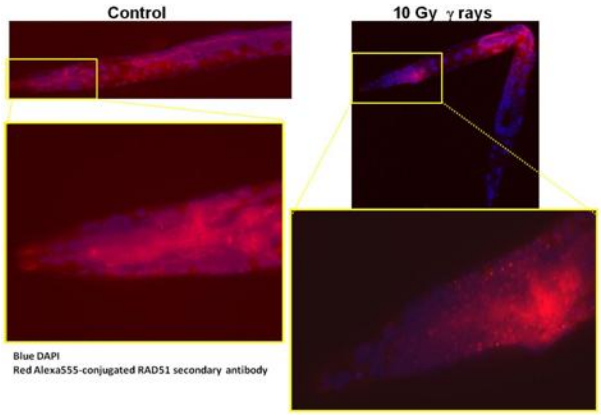

Figure 2*. Localization of RAD51 foci in wild-type C. elegans. Thirty minutes after exposure to 0 or 10 Gy from γ rays, worms were counterstained with DAPI (blue) and analyzed for RAD51 foci formation by immunohistochemistry (red). Compared to control, irradiated worms exhibited RAD51 foci mainly in the head/intestine regions.*

Ongoing experiments aim at investigating the role of DNA repair in ionizing radiation-induced bystander effects. Of particular interest is the RAD51 homolog protein, a major player in homologous recombination repair, which is required for the maintenance of genome

integrity [2]. Upon DNA damage, RAD51 protein forms subnuclear complexes that are microscopically detectible as foci, which contain many of the enzymatic activities required for efficient repair of DNA double strand breaks. By targeting a specific region of the worms with our microbeam, one can study radiation-induced bystander effects by evaluating RAD51 foci formation in sites distant from the irradiated area. For this purpose, preliminary studies were performed with γ rays to identify the location of RAD51 foci in *C. elegans*. Wild type (N2) worms were exposed to 0 or 10 Gy from ^{137}Cs γ rays. Thirty minutes after irradiation, worms were analyzed for RAD51 foci formation by immunohystochemistry. Compared to sham-irradiated *C. elegans*, γ-irradiated worms exhibited subnuclear concentrated foci particularly in the head/intestine area (Figure 2).

Future experiments will explore the induction of RAD51 foci following microbeam irradiation in both the targeted and non-targeted areas of *C. elegans*. Such an endpoint requires a relatively large number of samples that will be obtained using our microfluidic device.

Zebrafish embryos

The zebrafish (*Danio rerio*) represents a powerful model system in scientific research, since it shares a high genetic homology with humans. Zebrafish are small in size (~ 1 mm when adult) and transparent, therefore they represent a suitable model for studying biological effects of microbeam radiation exposure *in vivo*. **Dr. Targoff,** of the Pediatric Department at Columbia University, is one of our microbeam users and she studies cardiac morphogenesis in zebrafish embryos [3] (Figure 3).

Figure 3. *A 52 h post fertilization wild type zebrafish embryo. Small and transparent, it is an ideal model to investigate the biological effects of microbeam irradiation in vivo.*

Dr. Targoff's model consists of 52 h post fertilization zebrafish embryos that are genetically engineered to express a green fluorescent protein (GFP)-tagged atrium and a red fluorescent protein (RFP)-tagged ventriculum (Figure 4).

Studies on cardiac functions will soon be undertaken at RARAF using zebrafish embryos; for instance, the contribution of a specific region of the heart (e.g. atrium) to cardiac regeneration will be determined by lethally irradiating with the microbeam another region of the heart (e.g. ventriculum).

Mouse ear

Studies on ionizing radiation-induced bystander effects *in vivo* can be performed at the Columbia microbeam using a mouse ear model. The ear of a mouse, measuring approximately 13 mm in both length and width and with

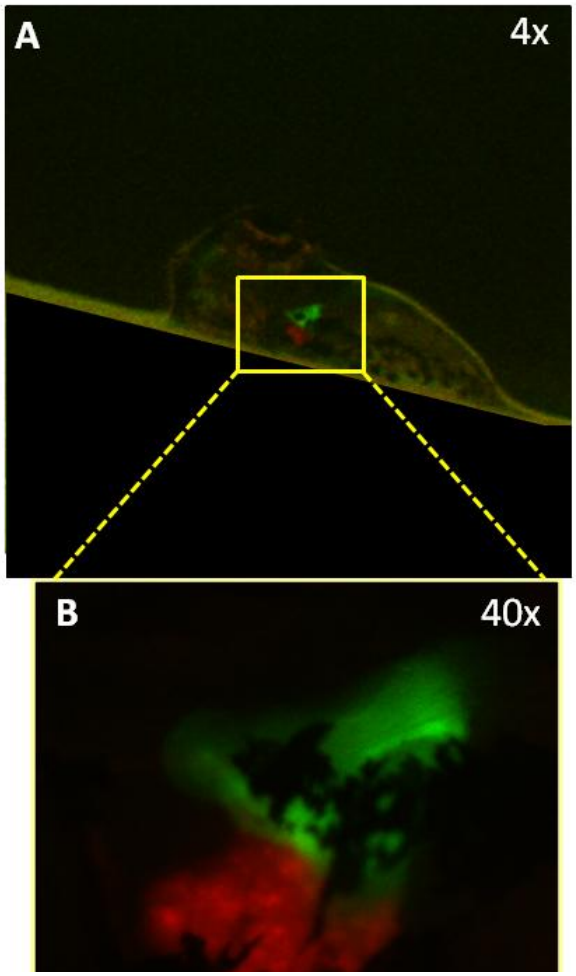

Figure 4. *A) Outline of a 52 h post fertilization zebrafish embryo under the fluorescent microscope (4x magnification) at RARAF. The zebrafish heart is delimited by the yellow rectangle. B) The cells of the atrium and the ventriculum are GFP- or RFP-tagged, respectively (40x magnification).*

an average thickness of 250 μm, can be used for bystander studies *in vivo* with our 5-MeV proton microbeam, which has a range of 350 μm. Using as support a mouse and mouse ear holder designed and built by the RARAF team and the Center for Radiological Research (CRR) Machine Shop, it is possible to irradiate a small area of a mouse ear and investigate bystander effects in the non-targeted regions (Figure 5).

Although evidence for bystander effects induced by ionizing radiation is established, the molecular mechanisms underlying these effects are not fully understood. Cell to cell intercellular communication through gap junctions has been shown to be critical for the propagation of bystander signals from irradiated to non-irradiated neighboring cells [4]. Connexin-43 (cx43) is one of the major proteins involved in gap junction intercellular communication, however studies on its role in radiation-induced bystander effects *in vivo* are limited by the fact that cx-43 deficiency is embryonic lethal. In collaboration with **Dr. Smilenov** at the CRR, we will soon be able to provide our users with a cx-43 conditional

Figure 5: *A) A mouse on the mouse ear holder at the end station of the RARAF microbeam. B) View of a small portion of the flattened mouse ear that can be a potential microbeam target. C) One region of the ear (e.g. black circle) can be targeted with our microbeam and radiation-induced bystander effects can be investigated in the non-targeted regions of the ear (e.g. regions outside the black circle).*

knockout mouse model via lentiviral transduction [5]. Briefly, SKH-1E hairless mice have been bred with the B6.129S7-*Gja1*^{tm1Dlg}/J transgenic mice in which exon 2 of the cx-43 gene is flanked by lox P sequences. This modification allows the complete knockout of the cx-43 gene by transduction of cells with lentiviral vectors containing Cre recombinase. The viral vector also contains the green fluorescent protein (GFP) gene that renders only the cx-43 knockout cells visible under the fluorescent microscope at RARAF. By targeting only cx-43-/- GFP-tagged cells, it will be possible to investigate the role of cx-43 in the propagation of bystander effects induced by microbeam irradiation *in vivo*.

Biological responses can be evaluated in irradiated versus non-irradiated regions of ear and in cx-43 knocked-out ears versus sham-irradiated ears. One biological endpoint that is of interest to many users is γH2AX foci formation. The maintenance of genomic stability requires efficient DNA double strand break repair that is mediated by the phosphorylation of multiple histone H2AX molecules near the break sites [6]. The phosphorylated H2AX (γH2AX) molecules form foci covering many megabases of chromatin. The formation of γH2AX foci is critical for efficient DNA damage response and for the maintenance of genome stability. To test whether ionizing radiation induces γH2AX foci in the mouse ear, we exposed mouse ears to 5 Gy from x-rays. Each mouse was shielded so that the sham-irradiated ear served as control. One hour after irradiation, the mouse was sacrificed and a 6 mm punch of the mouse ear was fixed and cut with a microtome. As expected, x-rays

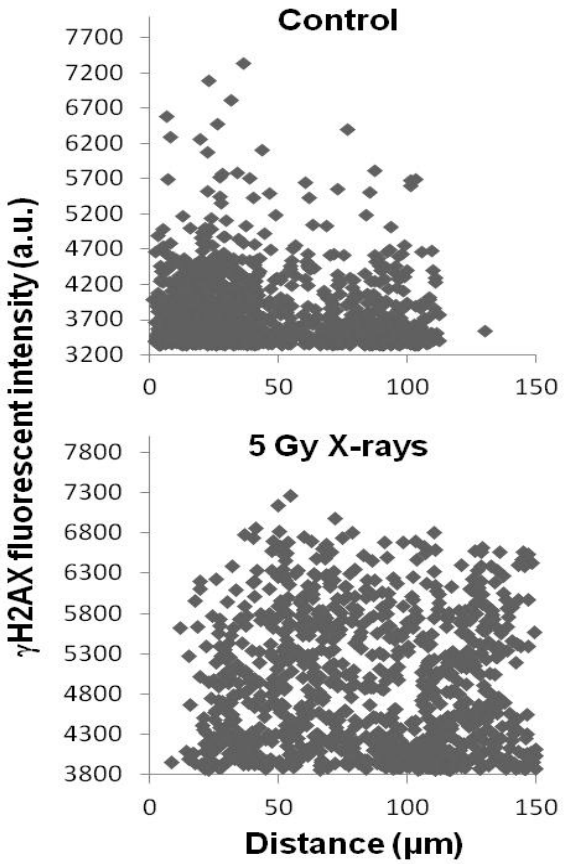

Figure 6. *γH2AX foci formation as a function of distance in a section of a mouse ear exposed to 0 or 5 Gy of x-rays. Each point represents γH2AX fluorescence signal from a single cell.*

induced γH2AX foci in the whole tissue section of the irradiated ear (Figure 6). Future experiments with the microbeam will evaluate γH2AX foci formation as a function of the distance from the targeted area in mouse ears that are deficient in gap junction intercellular communications as described above.

References

1. Bertucci A. *et al.*, J. Radiat Res (2009) 50 (Suppl.): A49-A54.
2. Tarsounas M. *et al.*, Oncogene (2003) 22: 1115–1123.
3. Targoff K.L. *et al.*, Dev Biol (2008) 322(2): 314-21.
4. Azzam E.I. *et al.*, PNAS (2001) 98(2): 473-8.
5. Shi Z. *et al.*, J Virol (2001) 75(23): 11474-82.
6. Bakkenist C.J and Kastan M.B., Nature (2003) 421: 499–506.

■

Effects of Cytoplasmic Irradiation on Respiratory Chain Functions

Bo Zhang and Tom K. Hei

Radiation-induced DNA damage such as single- and double-stranded breaks have been suggested to be the main cause of mutation and cell death. Most studies focus on nuclear DNA damage induced by radiation exposure and few have examined the biological effects on the mitochondrial genome. Previous studies from our laboratory have indicated that targeted cytoplasmic irradiation with alpha particles induces mutations at the CD59 locus in human-hamster hybrid cells, while inflicting minimal cytotoxicity [1]. These results imply that cytoplasm is an essential target for genotoxic effects induced by ionizing radiation.

Since mitochondria are ubiquitous in the cytosol of a cell, targeted cytoplasmic irradiation is likely to inflict damage to the mitochondria, particularly mitochondrial membranes. In the present study, radiation-induced mitochondrial damage, including respiratory chain function and genotoxicity, in human small airway epithelial (SAE) cells were examined using the Columbia University charged-particle microbeam that can target selected cellular sites with high precision. Briefly, exponentially growing SAE cells were plated on specially-constructed microbeam dishes with a polypropylene bottom. Cells were imaged and a defined number of alpha particles were delivered to the cytoplasm of individual cells as described [1, 2].

To investigate whether cytoplasmic irradiation affects mitochondrial respiratory chain function, cytochrome c oxidase (COX) and succinate dehydrogenase (SDH) activities were determined by histochemistry after irradiation with ten α particles (Figure 1A). Compared with untreated cells, cytoplasmic irradiated SAE cells showed an average of 50% reduction in COX staining at various time points up to 24 hours, indicating reduced respiratory chain function. The decrease in COX activity ranged from 38% of control at 2 hours to 65% at 24 hours. Interestingly, the activity of SDH, an enzyme encoded entirely by the nuclear genome, was also reduced by equivalent levels after cytoplasmic irradiation over a similar time span (0.5, 2, 4, 12, 24 hours). The enzyme histochemical data were quantified using Image J (NIH) software (Figure 1B). Statistical analyses of the image captured under a 40x objective lens were performed using Student's t-test. The differences in enzyme activities between controls and irradiated cells were highly significant (Figure 1B).

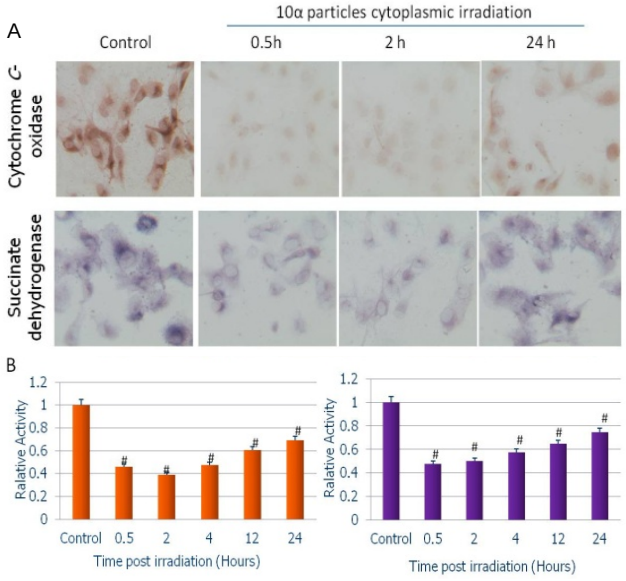

***Figure 1**. The changes of COX and SDH activity staining in SAE cells at different times after 10 α particles cytoplasmic irradiation. A) COX and SDH activities were determined by histochemical staining after 10α particles targeted to the cytoplasm. B) The time course of changes in COX and SDH activities in the SAE cells obtained from semi-quantitative analysis. #P <0.005 versus the control group. Bars indicate ± SEM. Similar results were obtained in three other experiments. In each experiment, 100 cells were scored.*

Direct DNA damage caused by ionizing radiation has been considered to be the main cause of mutation. However, the effects of mitochondria in modulating radiation-induced genotoxicity are largely unknown. In order to confirm the role of mitochondria in radiation-induced genotoxicity, the nuclear DNA was examined by assaying the frequency of micronuclei (MN) in both mitochondria dysfunctional ρ^0 and normal ρ^+ SAE cells. Compared with the ρ^+ SAE cells, ρ^0 cells had higher background MN frequency. Treatment with 10 alpha particles targeted at the nucleus induced 18% and 29% MN frequency in both ρ^0 and ρ^+ SAE cells respectively. Moreover, cytoplasmic irradiation also induced a statistically significantly increase to 12% in MN yield among SAE cells. However, cytoplasmic irradiation had no significant effect on the frequency of micronucleated ρ^0 SAE cells. These results reveal that cells without mitochondrial function are less sensitive to nuclear DNA damage induced by cytoplasmic irradiation.

Analysis of the activity of cytochrome c oxidase (COX, complex IV) and succinate dehydrogenase (SDH, complex II) was performed to evaluate mitochondrial

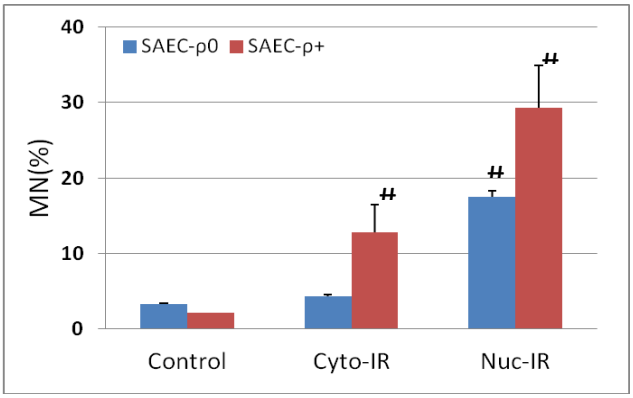

***Figure** 2. Micronuclei frequency of SAE cells induced by 10 α particles to the cytoplasm or nucleus of SAEC- ρ^0 or SAEC- ρ^+. Data represent mean ± SE of three independent experiments. In each experiment, 1000 cells were scored. # P <0.05 versus the control group.*

respiratory chain function. Usually, SDH activity is not affected by impaired mitochondrial DNA, except in the mitochondrial biogenesis process [3]. However, our histochemical analysis revealed 50% reductions of both COX and SDH activity in cells irradiated through the cytoplasm, indicating that both nuclear and mitochondrial subunits are affected among target cells. Meanwhile, to determine if the induction of mitochondrial damage by cytoplasmic irradiation has an effect on genomic instability, MN frequencies were measured in both mitochondria dysfunctional ρ^0 and normal ρ^+ SAE cells (Figure 2). Compared with untreated cells, ρ^+ SAE cells showed a 12% increase in MN frequency after cytoplasmic irradiation, however, ρ^0 SAE cells had no obvious response. It is known that direct DNA damage can induce mutation in the progeny of irradiated cells, however, our study suggested that induction of mitochondrial damage may also induce genomic instability. Therefore, extranuclear targets may have roles in mediating the genotoxic effects of radiation, and mitochondrial dysfunction induced by cytoplasmic irradiation may be considered as a potential contributor, although the exact mechanism is not known.

In conclusion, the present study showed that cytoplasmic irradiation results in mitochondrial respiratory chain dysfunction and induced genotoxicity in SAE cells. These data strengthen some of the fundamental issues regarding extranuclear targets and how cytoplasmic damage is processed in mammalian cells.

References

1. Wu L.J., Randers-Pehrson G, Waldren C.A., Geard C.R., Yu Z.Y. and Hei T.K. (1999) Targeted cytoplasmic irradiation with alpha particles induces mutations in mammalian cells. *Proc Natl Acad Sci (USA)*, **96**: 4959-4964.
2. Hong, M., Xu, A., Zhou, H., Wu, L., Randers-Pehrson, G., Santella, R.M., Yu, Z. and Hei, T.K. (2010) Mechanism of genotoxicity induced by targeted cytoplasmic irradiation. *Br J Cancer* **103**:1263-1268.
3. Ross JM, Öberg J, Brené S, Coppotelli G, Terzioglu M, Pernold K, Goiny M, Sitnikov R, Kehr J, Trifunovic A, Larsson NG, Hoffer BJ, Olson L. (2010) High brain lactate is a hallmark of aging and caused by a shift in the lactate dehydrogenase A/B ratio. *Proc. Natl Acad Sci. USA.* **10**: 20087-20092. ■

Role of Cyclooxygenase-2 in Radiation-induced Bystander Effect

Hongning Zhou, Vladimir N. Ivanov, Roy Lam, and Tom K. Hei

Radiation-induced bystander effects have clear implications for low-dose radiation risk assessment. A better understanding of the cellular and molecular mechanisms of the phenomenon will allow us to formulate a more accurate assessment of the health effects of low doses of ionizing radiation. Although radiation-induced bystander effects have been well studied in the past two decades, the precise mechanisms are still unclear.

In sub-confluent cultures or medium transfer studies, there is evidence that reactive oxygen/nitrogen species and cytokines are involved in mediating the process. On the other hand, gap junction-mediated cell-cell communications have been shown to be critical for bystander effects in confluent cultures of either human or rodent origins [1, 2]. It is likely that a combination of pathways is involved in producing a bystander response.

Using primary human fibroblasts, we showed recently that the cyclooxygenase-2 (COX2) signaling cascade,

including the activation of mitogen activated protein kinase (MAPK) pathways, plays an essential role in the bystander process [3]. Furthermore, we found that mitochondria played an important role in radiation-induced bystander effect, partially via mitochondria-dependent regulation of iNOS and COX2 signaling pathways, which are under NF-κB regulation [4]. To further confirm the role of COX2 in radiation induced bystander responses, mouse embryo fibroblasts (MEF) were generated from Cox2 knock-out mice, as well as from wild type mice. Using the Columbia University charged particle microbeam, we targeted either the nucleus or only the cytoplasm of the cell and irradiated each cell with an exact number of alpha particles. Preliminary data show that *Cox2*$^{-/-}$ MEFs have significantly lower bystander micronuclei formation after α-particle irradiation, either through nuclei or cytoplasm, compared with that of wild type MEFs (Figure 1).

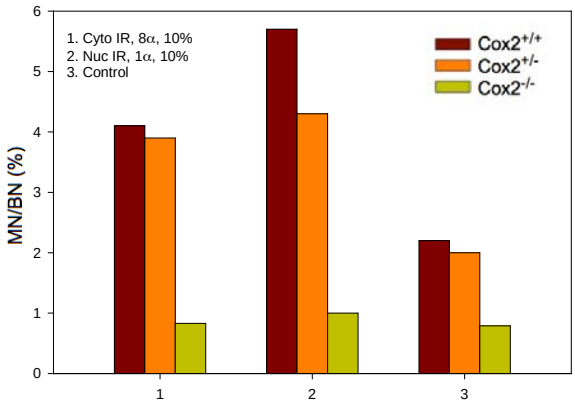

Figure 1. *Induction of micronuclei in binucleated mouse embryo fibroblasts after microbeam irradiation.*

To extend this finding to *in vivo* studies, the *Cox2* null genotype was generated in C57BL/6 *gpt* delta transgenic mice. A small area (1cm x 1cm) of the lower abdomen of the mouse was irradiated with 2 Gy x-rays, and induction of mutation and 8-OHdG formation in out-of-field lung was examined at different times. This study is currently under way.

Acknowledgements: This research was supported by funding from the National Institutes of Health Grants CA 49062, ES 12888. The Radiological Research Accelerator Facility (RARAF) is an NIH supported Resource Center through grants EB-002033 (NIBIB).

References

1. Morgan WF. (2003) Non-targeted and delayed effects of exposure to ionizing radiation: II. Radiation-induced genomic instability and bystander effects in vivo, clastogenic factors and transgenerational effects. *Radiat Res*. **159(5):** 581-96.
2. Hei TK, Zhou H, Ivanov VN, Hong M, Lieberman HB, Brenner DJ, Amundson SA, Geard CR. (2008) Mechanism of radiation-induced bystander effects: a unifying model. *J Pharm Pharmacol*. **60(8)**: 943-50.
3. Zhou H, Ivanov VN, Gillispie JA, Geard CR, Amundson S, Brenner DJ, Lieberman HB, and Hei TK. (2005) Mechanism of radiation induced bystander effect: role of COX2 signalling pathway. *Proc Natl Acad Sci USA*. **102(41)**: 14641-6.
4. Zhou H, Ivanov VN, Lien YC, Davidson M, Hei TK. (2008) Mitochondrial function and nuclear factor-kappaB-mediated signaling in radiation-induced bystander effects. *Cancer Res*. **68(7):** 2233-40. ■

Radiation oncology residents welcome Dr. Tadashi Kamada, director of charged particle therapy at NIRS in Japan. (l-r): Dr. John Ng, medical student Allen Costa, Dr. Tom Hei, Dr. Chi Zhang , Dr. Tadashi Kamada, Dr. Tony Wang, Dr. Clifford Chao, Dr. Amish Shah, Dr. David Horowitz.

Design of a Super Microbeam

Gehard Randers-Pehrson

Introduction

We began operating our microbeam at RARAF in 1994 using a 5 µm diameter aperture system. We have steadily reduced the beam size by successive systems comprising electrostatic quadrupole lenses first as single multiplets and then compound multiplets. See Bigelow, *et. al.* [1] for a review. The present system utilizes a pair of identical triplet lenses in series in a 3.8 m long vertical beam line. In normal operation we use a resolution of 0.6 to 1 µm diameter. We are limited now to a minimum beam spot of 0.4 µm by spherical and parasitic aberration inherent in quadrupole focusing systems.

Our present resolution is entirely adequate for the experiments that are routinely performed at RARAF, namely irradiating cell nuclei or other sub cellular regions of cells and for bystander studies. However, new developments in marking proteins with fluorescent tags are opening up an exciting class of experimental sub cellular targets, which are smaller than our present capabilities. Several examples are: single mitochondria, replication forks, and hybrid human-hamster cells, which have a small bit of bacterial DNA that can be tagged and visualized. We decided that we should continue to keep our facility on the cutting edge by designing the next generation of microbeams. We want a design that will produce a beam smaller than 100 nm.

Ion Focusing

There are numerous microbeam facilities worldwide as reviewed by Jamison [2]. Even though the systems with the smaller beam diameters are generally magnetic quadrupole multiplets, it has long been recognized that solenoid based systems have a potential to produce smaller spot size because they have smaller spherical aberrations and are less prone to parasitic aberrations. A compound system using an electrostatic quadrupole for the first stage and a wire wound solenoid for the final stage was proposed by Wollnik [3]. The proposal was extended by Breese [4], who proposed a system with a magnetic quadrupole first stage and superconducting solenoid for the final stage. Both systems promise a beam spot of smaller than 50 nm.

There is one operating superconducting solenoid system in Bochum, Germany. It uses a single stage design and achieves a 0.5 µm spot. We propose to construct a compound system comprising two solenoids.

Solenoid design

The solenoid design plan is to determine what coil configurations and slit arrangements will yield the smallest beam size for a given count rate. We started our lens system design with the decision that we would use the present vertical microbeam II beam line in order to retain the horizontal positioning of samples for the convenience of our users and stability of incorporated imaging systems. The total length of the system is thereby constrained to 4 meters. The second constraint is to be able to focus our most rigid beam, namely 11 MeV helium ions. The third limit is to keep the peak field strength below 8 Tesla because of limits on superconducting materials.

Calculations involve two stages. First, using an assumed coil cross section and current density, calculate the resulting field profiles using the programming suite, Superfish, available from the Los Alamos National Laboratory as a free download. Second, use the included interpolation program to obtain the fields strengths on a grid that is appropriate for a commercial ray tracing program, SIMION-8. Ray traces using various object sizes and limiting apertures are performed to determine the minimum beam spot dimensions. These calculations are performed iteratively to find the optimum design.

The present design consists of two solenoids, both with an 8T peak current. The final lens has a coil length of 12 cm and an internal diameter (ID) also equal to 12 cm. There are also shield coils with current flowing in the opposite direction to provide an active reduction of the fields outside the cryostat. The first lens has a similar field profile, but a smaller ID. The beam profile is shown in Figure 1.

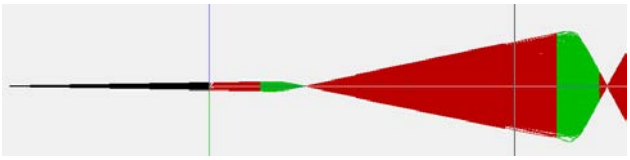

Figure 1. SIMION-8 ray tracing of proposed two solenoid lens system. Note that the vertical scale has been expanded by 500 times relative to the horizontal direction to show beam envelope.

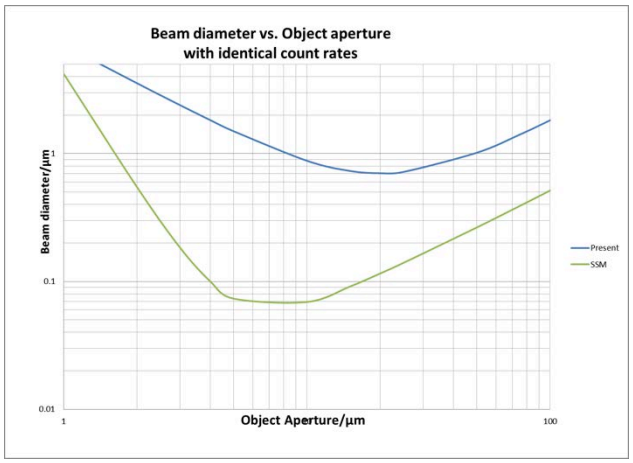

Figure 2. Predicted performance of dual solenoid nanoprobe.

Predicted performance

A series of ray tracings were calculated for various object aperture and angle-limiting aperture sizes. Figure 2 displays the expected beam diameter vs. the object aperture diameter where the angle limiter is chosen to provide the same count rate that we obtain in our present double quadrupole triplet system. We conclude that the proposed system can provide a beam with a 50 nm diameter and good count rate.

References

1. Bigelow, A.W., et al., *Single-Particle/Single Cell Ion Microbeams as Probes of Biological Mechanisms.* IEEE Transactions on Plasma Science, 2008. **36**(4): 8.
2. Jamieson, D.N., *New generation nuclear microprobe systems.* Nuclear instruments and methods B, 2001. **181**: 11.
3. Wollnik, H., M.I. Yavor, and A.G. Kalimov, *Low aberration focusing system for a proton nanoprobe.* Review of Scientific Instruments, 1998. **69**(12): 4116-4119.
4. Breese, M.B.H., D.N. Jamieson, and B.L. Doyle, *The use of solenoid lenses in a two-stage nuclear microprobe probe-forming system.* Nuclear Instruments & Methods in Physics Research Section B-Beam Interactions with Materials and Atoms, 2002. **188**: 6. ■

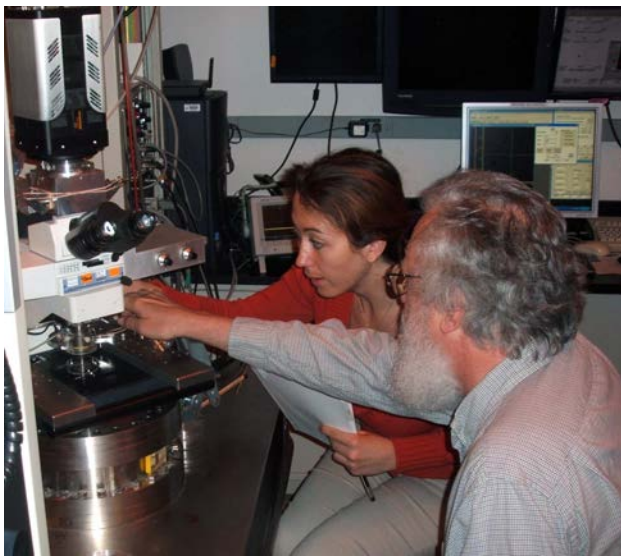

Hands-on training at the second Microbeam Training Course. Left: Dr. Charles Geard explains the manufacture of dishes for microbeam experiments to three of the students as Dr. Guy Garty looks on. Right: Dr. Gerhard Randers-Pehrson assists a student at the microbeam endstation.

A Pivotal Role of IL17-expressing γδ T Cells in Radiation-induced Pneumonitis

Winston Liao[a], K.S. Clifford Chao[a], John Munger[b], Tom K Hei, and Simon Cheng[a]

The lung is one of the most sensitive human organs to ionizing radiation, and the damage to normal lung tissue remains a major obstacle in radiotherapy targeting thoracic malignancies. Radiation causes prompt DNA, lipid and protein damage due to generation of free radicals, which results in cell death and tissue injury. Damaged-self injuries can be recognized by the immune system through damage-associated molecular patterns (DAMPs) also known as "alarmins." The immune system then recruits and activates a variety of inflammatory cells to the site of injury to eliminate dead cells and initiate wound repair [1]. Therefore, radiation-induced lung injury is essentially a continuous progression of disregulated events orchestrated from an early inflammatory process often referred to as radiation pneumonitis and a late fibrotic process known as radiation fibrosis [2].

Radiation pneumonitis, often occurring from 1 to 3 months after radiotherapy, is manifested with non-specific respiratory syndrome such as nonproductive cough, transient fever, respiratory insufficiency, dyspnea, etc. Histologically, pneumonitis lung exhibits depletion of type I pneumocytes, atypia of type II pneumocytes, alveolar wall edema, infiltration of inflammatory cells into its interstitium and alveoli [3]. Radiation induces a cascade of signaling events involving numerous cytokines, chemokines and growth factors from a variety of lung resident and infiltrated immune cells, contributing to the clinical respiratory symptoms and ultimate structural alteration of the lung. However, the major cell types and crucial mediators involved in the acute pneumonitis phase are still far from established, in contrast to the delayed fibrosis phase, where transforming growth factor-β (TGFβ) has been well-documented as a key player [4].

By using a radiation pneumonitis murine model in this study, we have identified a significant increase of pathogenic IL17-expressing γδ T cells, which are essential in radiation pneumonitis as demonstrated by mitigation of pneumonitis in γδ T cell knockout mice. Our findings reveal that disregulated innate immune response as represented by IL17-expressing γδ T cells may be a potential therapeutic target for radiation-induced lung injury.

[a] Department of Radiation Oncology, Columbia University Medical Center
[b] Departments of Medicine and Cell Biology, New York University Langone Medical Center

IL17-expressing cells are identified during radiation-induced pneumonitis, which is mainly contributed by unconventional γ δ T cells.

Murine experimental radiation-induced pneumonitis was developed by giving a single dose of 15 Gy X-ray to the whole thorax of pneumonitis-prone C3HBe/FeJ WT mice [5]. After 10 weeks, thoracic irradiation induced a 6-fold elevation of immune cell infiltration, including macrophages, lymphocytes and granulocytes, in the bronchial alveoli lavage (BAL) fluid (Figure 1A). In addition, the irradiated lungs exhibited substantially more alveolar wall edema and increased inflammatory cells in the interstitium (Figure 1B).

IL17 is a pro-inflammatory cytokine, which is extensively implicated in inflammation, infection and autoimmunity [6]. Agents including bleomycin, silica and ionizing radiation [7] that cause tissue damage through oxidative stress without infection could induce significant increases of IL17-expressing cells, which was also confirmed in our study (Figure 1C). Consistently, a substantial elevation of IL17 protein level was detected in the culture medium of single cell suspensions isolated from digested mouse lungs when the cell suspension was re-stimulated *ex vivo* with anti- CD3 and anti-CD28 antibodies for 3 days (Figure 1C). To identify the cellular sources of IL17 after irradiation, lung single cell suspension was re-stimulated *ex vivo* with PMA/ionomycin, and analyzed by flow cytometry for intracellular IL17 staining, combined with surface markers TCRαβ and TCRγδ, two well-known major sources of IL17-expressing T cells. Surprisingly, there was a marked increase of γδ T cells from the pneumonitis lungs, which also contributed to the majority of elevated IL17-expressing cells (Figure 1D). Concomitantly, the inflamed lungs upon irradiation were associated with elevated mRNA expression of acute phase proteins IL6 and TNFα, IL17 family signature cytokines IL23 and IL1β (Figure 1E), indicating a proinflammatory cytokine microenvironment that favors γδ T cell differentiation and function.

Radiation-induced pneumonitis is attenuated in γδ T cell knockout mice.

Having established that IL17-expressing γδ T cell numbers correlated well with the pathogenesis of radiation-induced pneumonitis, we sought to elucidate whether these cells mediated pneumonitis pathogenesis or if their accumulation was just a secondary effect of

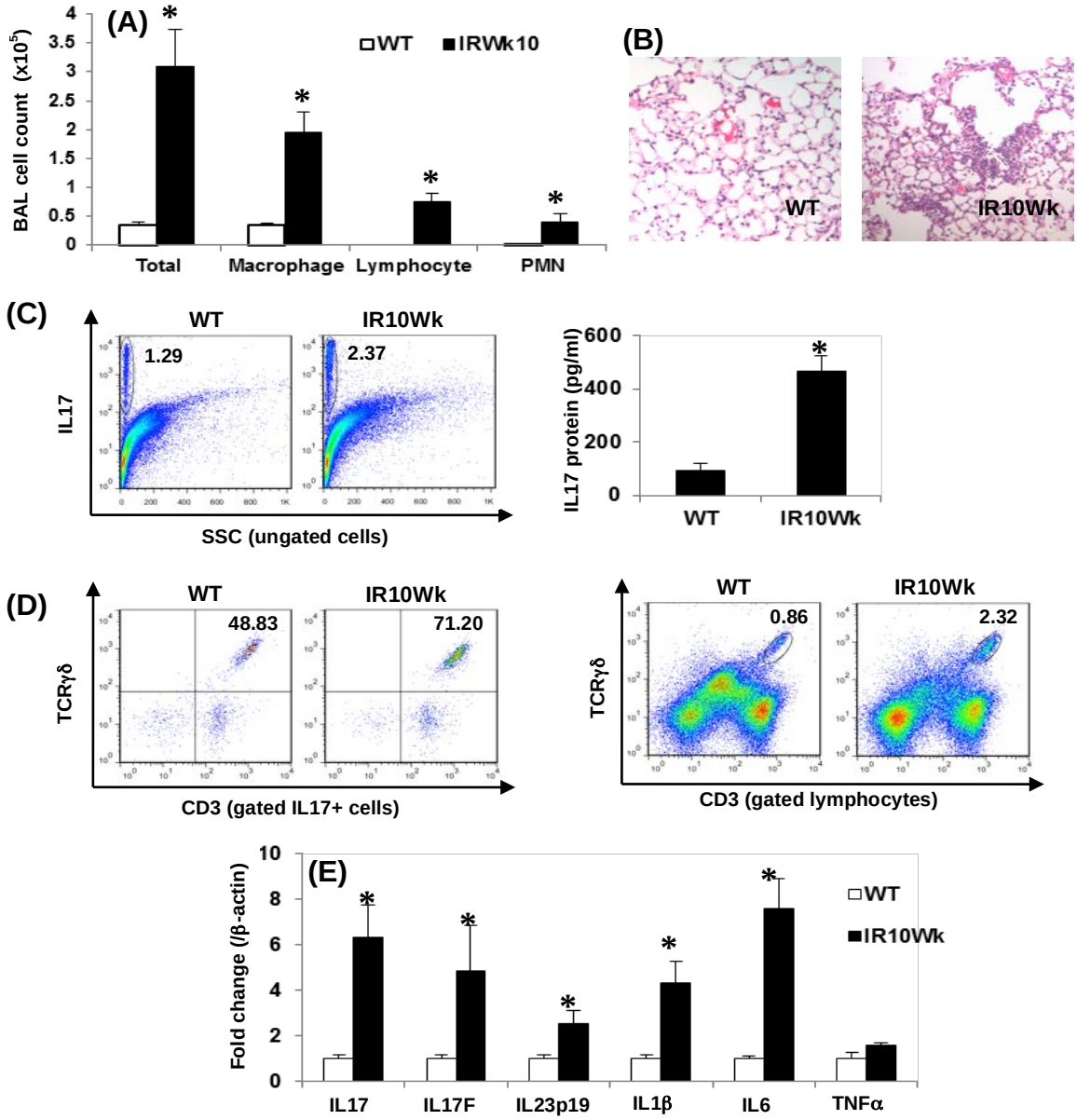

Figure 1. *Elevation of IL17-expressing γδ T cells is associated with radiation-induced pneumonitis. (A) A significant increase of immune cell infiltration into bronchial alveoli lavage (BAL) of the irradiated mice compared to non-irradiated controls. (B) Representative H&E staining of mouse lung sections showing cell infiltration into irradiated-lung interstitium. (C) A dramatic elevation of IL17 levels and IL17-expressing cells were detected from the digested lungs of irradiated mice, the majority of which were increased unconventional γδ T cells (D). (E) Proinflammatory cytokines IL17, IL17F, IL23p19, IL1β, IL6 and TNFα mRNAs were measured from digested lung tissues by qPCR. Relative mRNA level is normalized over β-actin and presented as fold-change compared to control. Data are shown as mean ± SEM. *p < 0.05.*

radiation. We obtained a γδ T cell-specific knockout mouse (dTCR), which is deficient in γδ T but has intact αβ T cells. One disadvantage of this mouse strain is its C57B6 genetic background, which normally develops marginal acute inflammation but substantial delayed fibrosis [5]. 18 Gy of X-ray was delivered to the thorax of C57B6 WT and dTCR mice, a higher dose than that applied to C3HBe/FeJ mice. WT C57B6 mice showed a lower basal percentile of pulmonary γδ T cells compared to WT C3HBe/FeJ mice, but thoracic irradiation brought this frequency to over 5 times higher (Figure 2A). Interestingly, though it was confirmed that dTCR mice were deficient in γδ T cells, they were not totally deficient in IL17 expression (Figure 2B). Surprisingly, *naïve* dTCR mice displayed a similar frequency of pulmonary IL17-expressing cells in comparison with intact WT controls, and this frequency was propagated upon radiation too, but to a significantly lower degree than that seen in irradiated WT mice. It was further found that in dTCR mice, αβ T cells compensated for IL17 expression (Figure 2B).

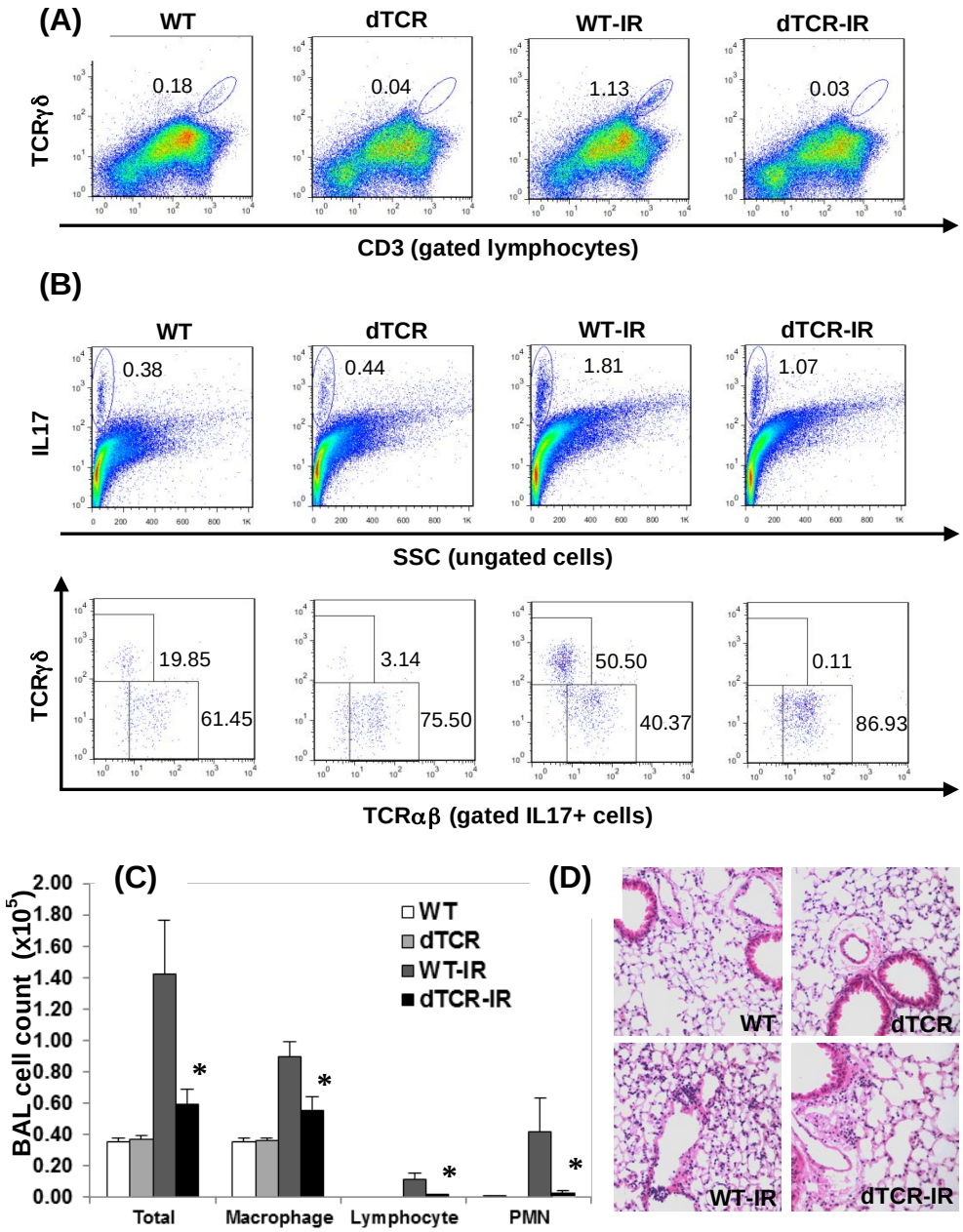

***Figure** 2. Radiation-induced pneumonitis is attenuated in γδ T cell knockout mice. (A) Thoracic irradiation provokes accumulation of γδ T cells into the lungs of WT C57B6 mice as well, whereas no γδ T cells are detected from C57B6 γδ T cell knockout mice dTCR as expected. (B) Depletion of γδ T cells significantly reduces radiation-induced total IL17-expressing cell frequency though αβ T cells appear to compensate for some expression of IL17. (C) Significant decrease of cell infiltration into the BAL of γδ T cell knockout mice. (D) Alleviated lung histopathology in γδ T cell knockout mice upon irradiation. Data are shown as mean ± SEM. *p < 0.05.*

In addition, 18 Gy thoracic X-ray exposure induced an elevation of BAL cell count including macrophages, lymphocytes and neutrophils, though the magnitude was much lower than that in irradiated C3HBe/FeJ mice. Interestingly, the absence of γδ T cells in dTCR mice markedly reduced BAL total and differential cell counts (Figure 2C). Furthermore, although radiation-induced inflammation in C57B6 mice was only sporadically displayed in histology, it was significantly mitigated in dTCR mice as shown in the representative histological images (Figure 2D).

Our results demonstrate that a significant elevation of pulmonary IL17-expressing γδ T cells correlates with radiation pneumonitis *in vivo*. In addition, mRNAs of cytokines important for IL17-expressing γδ T cell activation, IL1β and IL23, are markedly upregulated in the lungs of irradiated mice. Lastly and also importantly, radiation-induced pneumonitis is significantly attenuated in γδ T cell knockout mice, indicating a pathogenic

function of γδ T cells in radiation pneumonitis. Thus, strategies to deplete or block IL1β/IL23-stimulated IL17-expressing γδ T cells shall be of interest in mitigating pneumonitis. Taken together, our results emphasize the importance of pulmonary IL17-expressing γδ T cells to radiation-induced inflammatory response and reveal the innate immune response pathway as a potential target for therapeutic intervention in radiation lung injury.

References

1. Schaue D, McBride WH. Links between innate immunity and normal tissue radiobiology. Radiat Res 173: 406-17, 2010.
2. Graves PR, Siddiqui F, Anscher MS, Movsas B. Radiation pulmonary toxicity: from mechanisms to management. Semin Radiat Oncol 20: 201-7, 2010.
3. Tsoutsou PG, Koukourakis MI. Radiation pneumonitis and fibrosis: mechanisms underlying its pathogenesis and implications for future research. Int J Radiat Oncol Biol Phys 66: 1281-93, 2006.
4. Yarnold J, Brotons MC. Pathogenetic mechanisms in radiation fibrosis. Radiother Oncol 97: 149-61, 2010.
5. Chiang, C.S., W.C. Liu, S.M. Jung, F.H. Chen, C.R. Wu, W.H. McBride, C.C. Lee, and J.H. Hong. Compartmental responses after thoracic irradiation of mice: strain differences. Int J Radiat Oncol Biol Phys 62: 862-871, 2005.
6. Miossec, P., T. Korn, and V.K. Kuchroo. Interleukin-17 and type 17 helper T cells. N Engl J Med 361: 888-898, 2009.
7. Cappuccini, F., T. Eldh, D. Bruder, M. Gereke, H. Jastrow, K. Schulze-Osthoff, U. Fischer, D. Kohler, M. Stuschke, and V. Jendrossek. New insights into the molecular pathology of radiation-induced pneumopathy. Radiother Oncol 101: 86-92, 2011.
8. Sutton, C.E., S.J. Lalor, C.M. Sweeney, C.F. Brereton, E.C. Lavelle, and K.H. Mills. Interleukin-1 and IL-23 induce innate IL-17 production from gammadelta T cells, amplifying Th17 responses and autoimmunity. Immunity 31:331-341, 2009. ■

Celebration of Dr. Charles Geard's retirement (l-r): Margaret and Charles Geard, David Brenner, Tom Hei. Upper right (r to l): Fiona Miller, Charles Geard, Richard Miller. Lower right (l to r): Tom Hei, Sally Amundson.

ATM Kinase is Essential for an Efficient DNA Damage Response in Human Neural Stem and Differentiated Cell Types

Domenico Delia[a] and Adayabalam S. Balajee

The tissue microenvironment contains a heterogeneous mixture of stem cells (undifferentiated and multipotent), progenitor cells and specialized (differentiated) cell types. Currently, it is not clear whether or not intrinsic differences in DNA damage response mechanisms exist between different cell types and tissues. Increased incidence of leukemia and thymic lymphoma observed in A-bomb survivors of Hiroshima and Nagasaki points out that certain tissues/organs may be more susceptible to ionizing radiation (IR) induced carcinogenesis. IR induces a wide spectrum of lesions including single strand breaks (SSB), double strand breaks (DSB), base damage and DNA-protein cross-links. DNA repair efficiency for these lesions in replicative multipotent stem cells and non-replicative post-mitotic cells such as neurons is largely unknown. Since IR is a well-known carcinogen, knowledge of how different cell types in a tissue microenvironment respond to IR induced DNA damage is essential for assessing short and long-term effects of IR on human health.

In our earlier studies, we determined that the DSB repair efficiency (based on IR induced 53BP1 and gamma-H2AX foci formation and persistence) was somewhat attenuated in human adipose tissue derived mesenchymal stem cells (hAT-MSC, Lonza, USA) relative to differentiated primary skin cell types (fibroblasts, keratinocytes and melanocytes). Further, micronuclei (MN) frequency was also higher in hAT-MSC than differentiated skin cell types (fibroblasts, melanocytes and keratinocytes) after low doses of gamma rays (5cGy, 10cGy and 50cGy). To further explore the basis for DNA repair heterogeneity between stem and differentiated cell types, we recently performed a number of experiments on human neural stem/progenitor cells and in differentiated neurons. This system would allow us to systematically evaluate the DNA damage response mechanisms before and after differentiation of neural stem cells into post-mitotic neurons and mitotic glial cells (oligodendrocytes and astrocytes). The main reason for choosing the neural cell system is that many well-known radiosensitive human disorders such as ataxia telangiectasia (AT), AT-like disorder (ATLD) and Nijmegen breakage syndrome [1,2] display progressive neurodegenerative features. A better understanding of DNA damage response mechanisms mediated by ATM, ATR and DNA-PK in the neural cell system would enable us to identify the molecular cause for neurodegeneration in human radiosensitive syndromes. To directly determine the role of ATM kinase, ReNVM cells with stably suppressed *ATM* were generated by transduction of lentiviral shRNA vectors targeting the nucleotide sequences 268-286 and 1267-1285 of the *ATM* transcript. RT-PCR analysis showed an efficient suppression of *ATM* transcript by more than 90% relative to control shRNA vector transfected ReNVM cells (Figure 1A).

Initially, the effect of ATM kinase on neurogenesis was evaluated. The protocol for neuronal differentiation was essentially the same as described earlier [3]. For differentiation, cells grown as neurospheres are mechanically disaggregated for expansion and reseeded in complete medium (plus EGF and FGF) After 24 hours, a time point defined as day 0 (DO), the cells appear as doublets that are capable of generating new neurospheres with self-renewal capacity. To induce differentiation, cells were placed on poly-L-Ornithine and laminin coated slides/dishes and cultured without EGF for an additional 3 days. The medium without EGF and FGF was then replaced biweekly to promote the generation of neurons, oligodendrocytes and astrocytes. Differentiation of RenVM cells into neurons, oligodendrocytes and astrocytes were achieved at days 10, 17 and 24 respectively. Cells sampled at these three time intervals contained a homogenous population of the respective cell types. To identify different neural cell types, indirect immunofluorescence was performed using antibodies for lineage specific phenotypic markers. Antibodies specific for MAP2 (microtubule associated protein) and β-tubulin III (also known as Tuj1) were used as markers for neurons. Oligodendrocytes and astrocytes were identified by antibodies specific for GalC (Galactocerebroside) and GFAP (Glial Fibrillar Acidic Protein) respectively.

A critical step in neurogenesis (CNS) is the directed outgrowth of neurites and neurite outgrowth is reflective of neuronal maturation. Inhibition of either ATM or ATM/ATR kinases greatly affected the neuronal

[a]Department of Experimental Oncology, Fondazione IRCSS Istituto Nazionale Tumori, Milan, Italy.

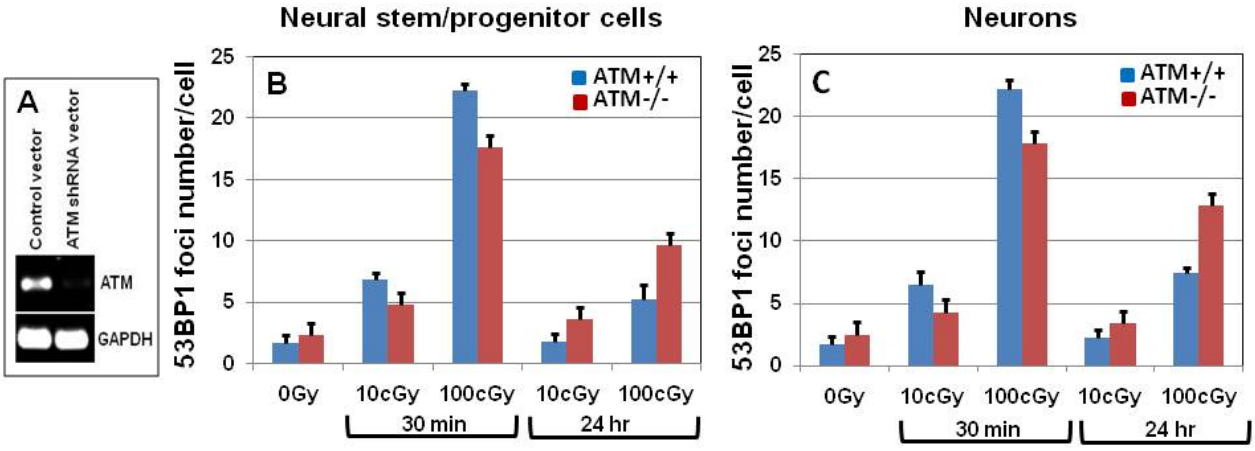

Figure 1. *(A) RT-PCR analysis of ATM mRNA in control and ATM shRNA vector transfected human neural stem/progenitor cells (ReNVM). The stably transfected clonal cells were selected by blasticidin (2μg/ml). (B) Analysis of γ-ray induced 53BP1 foci formation in ATM proficient and ATM suppressed ReNVM cells after 30 min and 24hr post-recovery times. (C) Analysis of γ-ray induced 53BP1 foci formation in ATM proficient and ATM suppressed neurons derived after differentiation of RenVM cells.*

maturation, suggestive of their importance in neurogenesis. In sharp contrast to the slow growth of *ATM* deficient primary fibroblasts, *ATM* suppressed neural progenitor cells exhibited a slightly increased proliferation potential in culture. DNA damage and repair was next assessed in neural stem/progenitor cells and neurons following exposure to varying doses (0.1Gy, 0.25Gy. 0.5Gy, 1Gy and 2.5Gy) of γ-rays. Initial induction of 53BP1 and gamma-H2AX foci reflective of DNA double strand breaks was essentially similar between *ATM* proficient neural stem/progenitor cells and differentiated neurons at all of the radiation doses examined. However, cells with persistent 53BP1 and gamma-H2AX foci analyzed 24 hours (Fig.1B and C) and 48 hours after IR exposure were consistently higher in neurons than in neural stem/progenitor cells. Consistent with this observation, MN formation was also increased in neurons as compared to neural stem/progenitor cells. Moreover, *ATM* knockdown further enhanced the proportion of neurons with persistent 53BP1 (Fig.1B and C) and gamma-H2AX foci indicating the importance of ATM mediated signaling for efficient DSB repair in neurons.

To further explore the molecular basis for the observed intrinsic differences in DSB repair efficiency between neural stem cells and differentiated neurons, a comparative expression analysis of DNA repair genes was performed in multipotent adult stem cells and differentiated neurons using a quantitative real time PCR profiler array (SA Biosciences, Frederick, MD, USA). This array contains a total of 84 genes that participate in diverse DNA damage signaling/repair pathways (Nucleotide Excision Repair, Base Excision Repair, Mismatch Repair, Non-homologous End Joining Repair and Homologous Recombination Repair). Of interest, we found that *ATM* and *DNA-PK* showed a biphasic pattern with an initial decline in expression in post-mitotic neurons followed by an elevated expression in mitotic glial cells (oligodendrocytes and astrocytes). In contrast, ATR kinase expression was drastically reduced both at mRNA and protein levels in all the differentiated neural cell types (neurons and glial cells) relative to neural stem/progenitor cells. In addition to *ATM*, *ATR* and *DNA-PK*, transcripts for many key proteins involved in DNA repair and cell cycle checkpoint regulation also showed reduced expression in newly differentiated neurons: *BRCA1, CHK1, CHK2, ERCC2, FANCG, EXO1, MLH1, MLH3, MSH2, MSH3, OGG1, PCNA, PMS1, RAD18, RAD21, RAD50, RAD51, REV1, RPA1, TP53, P73, UNG, XPA, XPC, XRCC1, XRCC2* and *XRCC3*. As efficient ATM kinase activation depends on the MRN (Mre11, Nbs1 and Rad50) complex, ReNVM cells with stable suppression of Nbs1 and Mre11 have also been generated. Currently, we are assessing the roles of Mre11 and Nbs1 gene products in adult neurogenesis and neuroprotection after exposure to low and high doses of low LET radiation. Collectively, our findings suggest that the *in vitro* neural cell model system is ideal for evaluating the role of ATM, ATR and DNA-PK in neurogenesis and neuroprotection.

References

1. Frappart PO, McKinnon PJ. Ataxia-telangiectasia and related diseases. *Neuromolecular Med* 2006;**8**:495-512.
2. Bekker-Jensen S, Lukas C, Kitagawa R, et al. Spatial organization of the mammalian genome surveillance machinery in response to DNA strand breaks. *J Cell Biol* 2006;**173**:195-206.
3. Carlessi L, De Filippis L, Lecis D, Vescovi A, Delia D. DNA-damage response, survival and differentiation in vitro of a human neural stem cell line in relation to ATM expression. *Cell Death Differ* 2009; **16**:795-806. ■

Rad9 Controls Expression of Integrin Beta1 and Invasion in Prostate Cancer Cell Lines

Constantinos G. Broustas, and Howard B. Lieberman

Introduction

Rad9 is a protein with an established role in the DNA damage response and DNA repair. As part of the Rad9-Hus1-Rad1 complex, it acts as a sensor of DNA damage that enables ATR kinase, independently recruited to the site of damage, to phosphorylate and activate its downstream effector Chk1 [1]. In recent years, however, Rad9 has been implicated in pathways not directly related to the DNA damage/repair response. Moreover, it has been shown that Rad9 can act independently of its partners Hus1 and Rad1 to transactivate a number of genes including $p21^{waf1/cip1}$ [2].

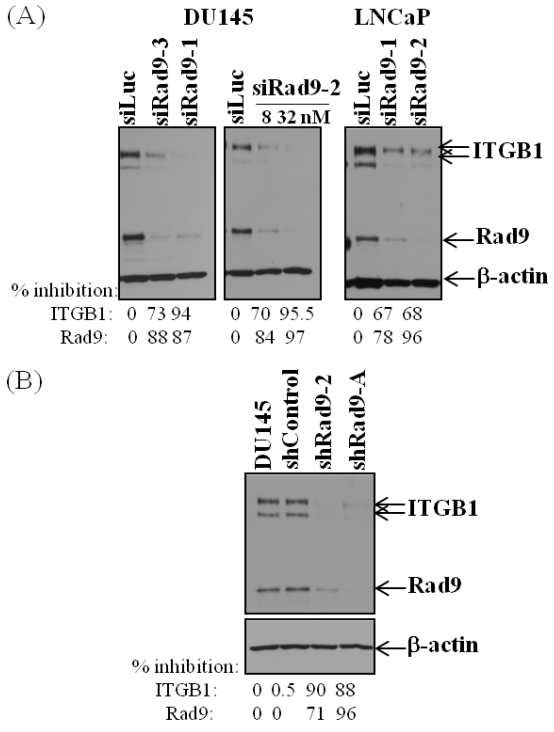

Figure 1: *(A) Rad9 expression modulates ITGB1 protein levels. Transient silencing of Rad9 in either DU145 or LNCaP cells using three different siRad9 (#1, #2, #3) suppresses ITGB1 expression. siRad9#2 was used at two different concentrations. Percent inhibition of ITGB1 and Rad9 compared with siLuc are indicated. (B) Stable downregulation of Rad9 in DU145 (clones 2 and A) results in diminished levels of ITGB1 protein compared with parental DU145 or shControl cells. Percent inhibition of ITGB1 and Rad9 compared with parental DU145 cells are indicated.*

Aberrant Rad9 expression has been associated with prostate, breast, lung, skin, thyroid and gastric cancers [1]. Previous reports showed that Rad9 is over-expressed in human prostate cancer specimens as well as prostate cancer cell lines [3]. Down-regulation of Rad9 in PC3 and DU145 human tumor cell line xenografts impairs growth in nude mice, whereas ectopic expression of Rad9 in an immortalized, nontumorigenic, prostate cell line (PWR-1E) conferred the ability to form aberrant growths in mice [3]. Furthermore, immunohistochemical analysis of normal and tumor prostate specimens showed that Rad9 expression increased along with cancer progression stages, suggesting a role for Rad9 in prostate malignant progression [3].

Prostate cancer is the most prevalent non-cutaneous type of cancer in men [4]. Despite successes in treating localized primary prostate tumors, metastatic prostate cancer poses a real challenge and remains essentially incurable. As in most types of solid cancers, metastasis is the major morbidity and mortality factor for patients with prostate cancer. An integral part of the metastatic process is the integrins. These molecules are heterodimeric αβ transmembrane receptors that connect the extracellular matrix to the cytoskeleton [5] and play important roles in migration, invasion as well as anoikis resistance [6]. In particular, β1 integrin (ITGB1) is known to confer higher survival and metastatic capacity to a number of cancer cells including those of prostate origin [7-9].

In the previous Annual Report we showed that Rad9 depletion impairs DU145 and PC3 prostate cancer cell migration and invasion. In the present report, we propose that Rad9 may influence cell migration and invasion by controlling the abundance of integrin β1.

Results

Rad9 silencing suppresses integrin β1 expression— We have previously shown that Rad9 affects migration and invasion of prostate cancer cell lines. Preliminary studies showed that DU145 cells migrated better towards fibronectin, when Rad9 levels were high. Therefore, we hypothesized that Rad9 may affect cell migration by controlling the abundance of integrin β1. Downregulation of Rad9 by transiently transfecting DU145 cells with three non-overlapping siRNAs (#1, #2, #3) reduced levels of total integrin β1 protein from 73% to 95%, depending on the siRNA (Fig. 1A, left panel). Varying the degree of Rad9 silencing using 8 nM (84% Rad9 suppression) or 32 nM (97% inhibition) of siRad9#2 reduced expression of

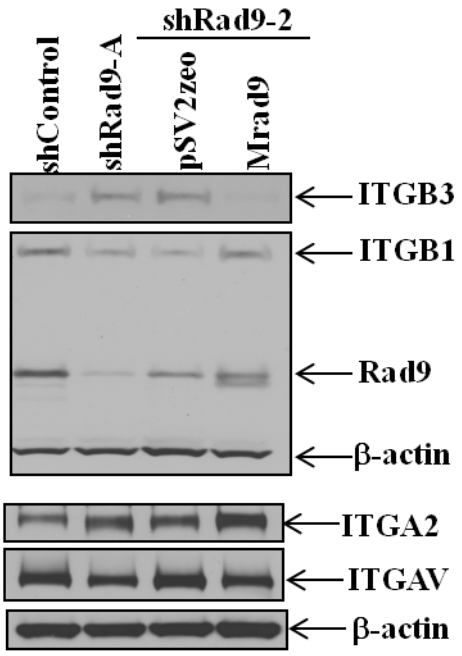

Figure 2*: Rad9 does not affect other integrins. Western blot analysis of DU145 stable clones with anti-ITGB3, anti-ITGB1, anti-Rad9 and anti-actin antibodies. Same lysates run separately and immunoblotted with anti-ITGA2 and anti-ITGAV antibodies.*

ITGB1 proportionally, that is 70% and 95.5% (Fig. 1A, middle panel). Furthermore, suppression by approximately 70% of ITGB1 protein via reducing levels of Rad9 was also observed with the LNCaP prostate cancer cell line (Fig. 1A, right panel). DU145 cells with stably reduced levels of Rad9 protein (clones shRad9-2 and shRad9-A) displayed reduced levels of ITGB1 protein (by approximately 90%) when compared with DU145 cells or shControl cells (Fig. 1B). Rad9 knockdown specifically downregulated ITGB1 as the levels of other integrins, like ITGA2 and ITGAV, were not affected (Fig. 2). In contrast, ITGB3 expression was increased in the cells where ITGB1 was reduced (Fig. 2). This was in agreement with published reports that ITGB1 exerts an inhibitory effect on ITGB3 by destabilizing ITGB3 mRNA [10].

Mrad9 expression restores integrin β1 protein levels— Transient transfection of DU145/shRad9-A cells with varying concentrations of Mrad9 plasmid showed that ITGB1 levels increased proportionally (Fig. 3A). Likewise, stable expression of Mrad9 in DU145 cells that stably suppress expression of endogenous Rad9 showed a three-fold increased expression of ITGB1 (Fig. 3B). Ectopic expression of Mrad9 affected specifically ITGB1 and it had no effect on integrins α2 and αv, whereas integrin β3 levels were diminished as a result of the increased integrin β1 levels (Fig. 2).

ITGB1 silencing abrogates Rad9-dependent invasion— Knocking down endogenous Rad9 diminished invasion of DU145 through matrigel, whereas expression of Mrad9 in DU145/shRad9 cells was able to restore invasion in these cells (Fig. 4). To assess whether ITGB1 can influence Mrad9-induced cell invasion, endogenous ITGB1 was silenced by a specific siRNA in DU145/shRad9/Mrad9 cells. As shown in Figure 4, silencing of ITGB1 reduced invasion of cells and negated

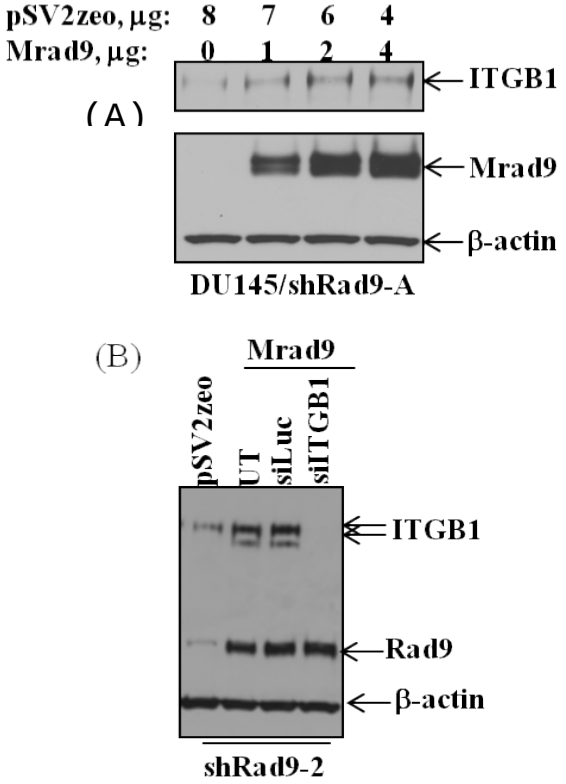

Figure 3: *(A) ectopic expression of various concentrations of Mrad9 cDNA in DU145/shRad9 clone A and immunoblotting with ITGB1, Rad9 and actin antibodies. (B) Stable expression of Mrad9 in the DU145/shRad9#2 clone restores ITGB1 levels. UT: untransfected.*

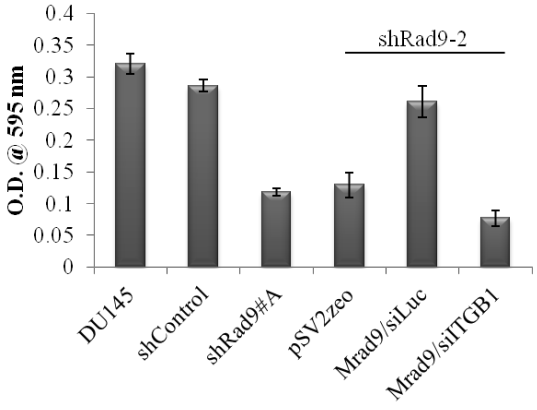

Figure 4: *DU145/shRad9 invasive capability is restored by expressing Mrad9 only when ITGB1 levels are maintained. Data are mean O.D. ± SD (n=3).*

the effect of expressed Mrad9 to levels comparable to those of cells with knockdown Rad9. These results suggest that Rad9-induced invasion may proceed through the regulation of ITGB1 expression. Re-expressing ITGB1 in DU145/shRad9 cells with reduced endogenous ITGB1 would be predicted to phenocopy the Mrad9 effect on invasion. However, ectopically expressing ITGB1 in these cells caused increased cell death, so invasion could not be assessed.

Conclusions

We have presented data that show Rad9 expression affects protein levels of ITGB1, whereas levels of other integrins remain unchanged, and this effect may control Rad9-dependent cell invasion by prostate cancer cell lines.

References

1. Broustas CG, Lieberman HB. Contributions of RAD9 to tumorigenesis. (2012) J Cell Biochem 113:742-51.
2. Yin Y, Zhu A, Jin YJ, Liu YX, Zhang X, Hopkins KM, Lieberman HB. (2004) Human RAD9 checkpoint control/proapoptotic protein can activate transcription of p21. Proc Natl Acad Sci U S A. 101:8864-9
3. Zhu A, Zhang CX, Lieberman HB. (2008) Rad9 has a functional role in human prostate carcinogenesis. Cancer Res. 68:1267-74.
4. Shen MM, Abate-Shen C. (2010) Molecular of prostate cancer: new prospects for old challenges. Genes Dev 24:1967-2000.
5. Hynes RO. (2002) Integrins: bidirectional, allosteric signaling machines. Cell 110:673-87.
6. Margadant C, Monsuur HN, Norman JC, Sonnenberg A. (2011) Mechanisms of integrin activation and trafficking. Curr Opin Cell Biol 23:607-14.
7. Hood JD, Cheresh DA. Role of integrins in cell invasion and migration. (2002) Nat Rev Cancer 2:91-100.
8. Zeng ZZ, Jia Y, Hahn NJ, Markwart SM, Rockwood KF, Livant DL. (2006) Role of focal adhesion kinase and phosphatidylinositol 3'-kinase in integrin fibronectin receptor-mediated, matrix metalloproteinase-1-dependent invasion by metastatic prostate cancer cells. Cancer Res 66:8091-9.
9. Goel HL, Breen M, Zhang J, Das I, Aznavoorian-Cheshire S, Greenberg NM, et al. (2005) beta1A integrin expression is required for type 1 insulin-like growth factor receptor mitogenic and transforming activities and localization to focal contacts. Cancer Res 65:6692-700.
10. Retta SF, Cassarà G, D'Amato M, Alessandro R, Pellegrino M, Degani S, et al. (2001) Cross talk between beta(1) and alpha(V) integrins: beta(1) affects beta(3) mRNA stability. Mol Biol Cell 12:3126-38. ■

Radiation Induced Changes in CD44 Expression and Hyaluronic Acid Synthesis in Breast Cancer Cells

Jarah A. Meador, Shanaz A. Ghandhi, and Sally A. Amundson

Recent technologies have allowed cancer stem cells (CSC) to be identified in several different tumors based on the presence or absence of specific cell surface markers. This has enabled researchers to target and study potential cancer therapeutics and cellular processes that are specific to CSCs. Al-Hajj et al [*1*] were the first to isolate and identify mammary CSCs by the surface marker expression of $CD44^{+}/CD24^{low}$ and found that 100 or fewer of these cells could form tumors in SCID mice. Breast tumors are composed of a heterogeneous cell population and the "cancer stem cell hypothesis" postulates that tumors arise from individual cells that have self-renewal ability, and stem derived progenitors are capable of tumor growth initiation and maintenance. The cancer stem cell population is small and accounts for only 0.1 to 1% of all tumor cells.

CD44 is expressed on the surface of cancer stem cells from a variety of tumor types. High CD44 expression is associated with increased risk of metastasis and poor overall patient prognosis. CD44 positive breast cancer stem cells have been shown to be highly refractory to radiation and chemotherapeutics and are enriched following radiation treatment. We examined the effect of a broad range of ionizing radiation doses on CD44 surface expression in different breast cell lines. We exposed exponentially growing 2-D cultures of non-tumorigenic (MCF10A) and breast cancer cell lines (MDA-231 and MCF-7) to gamma radiation and analyzed CD44

expression 5 days post-exposure using flow cytometry (Figure 1).

The standard CD44 form (CD44s) was measured in this assay and a change in CD44s intensity is seen in MCF10A and MDA231 5 days after exposure to gamma radiation. CD44s intensity was decreased at a dose as low as 0.01 Gy and CD44s intensity was increased in both cell lines following 10 Gy radiation exposure. Interestingly, no change in CD44s intensity was observed in MCF7 following exposure to gamma radiation. To determine the persistence of radiation induced CD44s expression changes, irradiated cells were split 5 days after culturing and CD44s expression measured one week later. All experiments were performed in triplicate. The pattern of CD44s expression was stable in progeny of irradiated cells at all doses studied (data not shown). Taken together these data show that radiation alters CD44 signaling in breast cancer cells in a dose dependent manner.

Normal breast tissue development and function is dependent upon growth factor and extracellular matrix (ECM) mediated epithelial-stromal interactions. In addition to inducing DNA damage in individual cells, ionizing radiation can cause changes in the microenvironment through activation and physical remodeling of the ECM components [*2*]. Hyaluronan or Hyaluronic acid (HA) is a major glycosaminoglycan component of the ECM and has roles in wound healing, proliferation, modulation of adhesion, and cell-cell communication. Rapid and persistent radiation induced fragmentation of HA and activation of other ECM molecules in the mouse mammary gland microenvironment have been reported [*3*, *4*]. It has long been established that radiation induced scission of HA molecules is dependent upon absorbed radiation dose [*5*, *6*]. High levels of HA have been reported in invasive breast cancer cell lines and metastatic breast tumors. CD44 is the primary cell surface receptor for HA and binding initiates a CD44 signaling cascade leading to increased cell proliferation, survival and invasion. In a study by Tsai et al. [*7*], replicative senescence and ECM remodeling was observed in human mammary fibroblasts exposed to low dose ionizing radiation.

Although it has been reported that radiation acts directly on HA by producing dose dependent fragment sizes, we wanted to know if radiation also influences the synthesis and/or turnover of HA. MDA231 cells were grown in monolayer 2-D cultures and irradiated with ^{137}Cs gamma radiation at different doses. The cells were exposed to a range of low to high dose radiation (0.1 to 10 Gy) and HA levels in the medium were assayed at 24 hr post exposure using an HA-ELISA (Figure 2). Several hours prior to irradiation the medium was replaced with serum-free medium to reduce cell growth effects on HA production. For the 5-day experiment, fresh serum-free media was added every 2 days. 24 hrs after radiation exposure we observed a dose dependent change in HA levels with the greatest decrease in HA at 0.1 Gy. HA levels were near control levels at the highest dose of 10 Gy. The pattern of HA levels in the 24hr samples remained 5 days after exposure (data not shown).The levels of hyaluronan and differences in HA chain length seen among rapidly remodeling tissues, such as tumors, are due to the concerted action of hyaluronan synthases (HAS 1-3) which produce HA polymers of different chain sizes and hyaluronidases (HYAL) that catabolize HA into fragments of defined size. A possible synergistic relationship between radiation-induced HA fragmentation and activation of HAS/HYAL signaling as an initiation or promotion event in breast tumorigenesis has not yet been studied. We measured increased HAS3 gene expression (compared to control) in MDA231 24 hr after exposure to 0.1, 2.5 or 10 Gy radiation (Figure 3). Because HA levels represent the dynamic balance of synthesis and degradation, we also measured HYAL1 expression in MDA231 at the same doses and time points and found the highest increase in HYAL1 expression following exposure to 2.5 Gy.

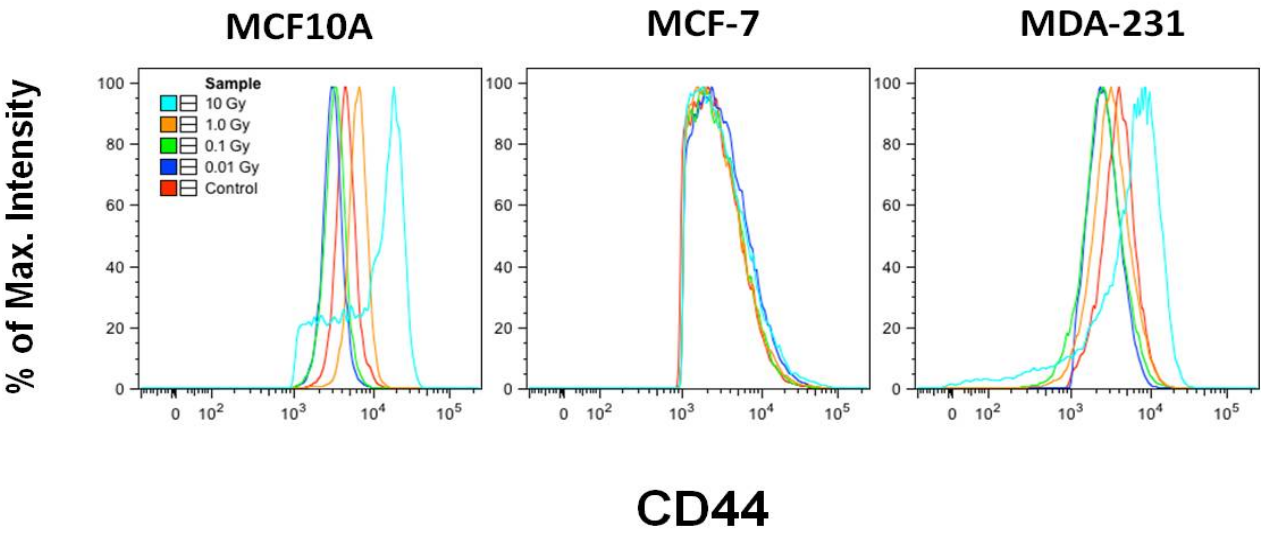

Figure 1. *CD44s Intensity measured in mammary cell lines.*

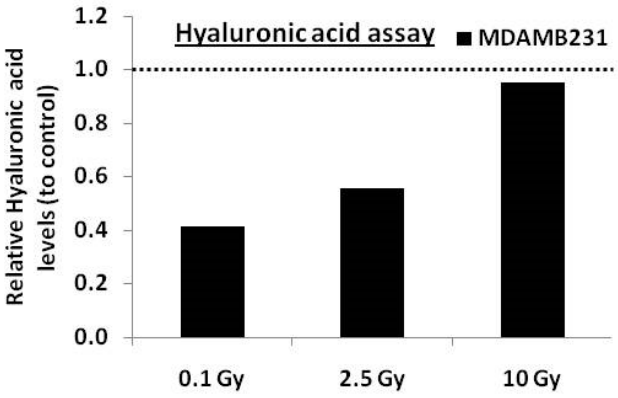

Figure 2*. HA measured following radiation exposure using the HA assay. Levels normalized to sham-irradiated controls shown as the dotted line.*

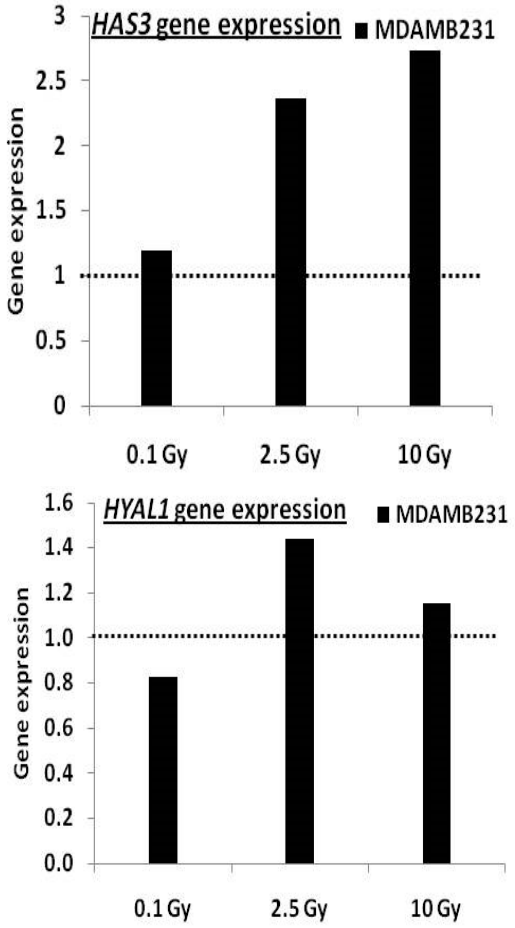

Figure 3*. Expression of HAS3 and HYAL1 genes at different doses of radiation. mRNA were measured by qRT-PCR and normalized to sham-irradiated controls.*

Taken together these experiments have shown that radiation influences the stem cell population in a dose dependent manner and that this may impact cellular invasion/metastasis through alterations in extracellular matrix signaling. *In vivo* experiments have been initiated to explore radiation effects on stem cells. Mice were exposed to either 1 Gy protons or 1 Gy gamma radiation and mammary epithelial tissue was harvested 24 hours later. Cells from the tissue were dissociated and grown in attachment-free conditions to allow mammosphere formation. Dontu et al. [*8*] developed a culture system for enriching $CD44^{+}/CD24^{low}$ breast cancer stem cells by culturing cells isolated from breast tissue in non-adherent and non-differentiating conditions to form mammospheres. Mammospheres are enriched in progenitor cells capable of differentiating along luminal, myoepithelial, and alveolar lineages. Ten days after culturing in these conditions the primary mammospheres were collected, dissociated into individual cells, and cultured as secondary mammospheres. After approximately 10 days these secondary mammospheres were collected and gene expression studies are currently being performed to determine radiation effects on stem cells.

References

1. M. Al-Hajj, M. S. Wicha, A. Benito-Hernandez, S. J. Morrison and M. F. Clarke, Prospective identification of tumorigenic breast cancer cells. *Proc Natl Acad Sci U S A* **100**, 3983-3988 (2003).
2. M. H. Barcellos-Hoff, C. Park and E. G. Wright, Radiation and the microenvironment - tumorigenesis and therapy. *Nat Rev Cancer* **5**, 867-875 (2005).
3. M. H. Barcellos-Hoff, Radiation-induced transforming growth factor beta and subsequent extracellular matrix reorganization in murine mammary gland. *Cancer Res* **53**, 3880-3886 (1993).
4. M. H. Barcellos-Hoff, The potential influence of radiation-induced microenvironments in neoplastic progression. *J Mammary Gland Biol Neoplasia* **3**, 165-175 (1998).
5. R. Setlow and B. Doyle, The direct action of fast charged particles on hyaluronic acid, hyaluronidase, and a combination of the enzyme and substrate. *Radiat Res* **2**, 15-25 (1955).
6. H. Kim, H. C. Cho, Y. C. Bae, H. W. Park and K. S. Chung, Heat and radiation effect on the degradation behaviors of polymeric liquids. *European Polymer Journal* **39**, 1431-1435 (2003).
7. K. K. Tsai, E. Y. Chuang, J. B. Little and Z. M. Yuan, Cellular mechanisms for low-dose ionizing radiation-induced perturbation of the breast tissue microenvironment. *Cancer Res* **65**, 6734-6744 (2005).
8. G. Dontu, M. Al-Hajj, W. M. Abdallah, M. F. Clarke and M. S. Wicha, Stem cells in normal breast development and breast cancer. *Cell Prolif* **36 Suppl 1**, 59-72 (2003). ■

Regulation and Mechanism of Arsenic-induced Apoptosis in Mouse Stem Cells

Vladimir N. Ivanov and Tom K. Hei

Arsenic is a well-characterized teratogen in animal models inducing general embryotoxicity and causing a substantial disturbance in embryonic neurogenesis [1, 2]. However, molecular mechanisms of these effects are still uncertain. Our main hypothesis is that arsenic (as sodium arsenite) may directly target embryonic stem cells (ESC) of the inner mass of the blastocyst by induction of apoptosis. Furthermore, at the subsequent stages of embryogenesis, arsenic might negatively affect self-renewal and differentiation of neural stem cells (NSC), which generate all the cells in the nervous system. NSC still persist in two specialized niches in the adult brain, initiating neurogenesis that is critically important for the functional recovery in the brain after injury or disease [3, 4]. Arsenic exposure induces a broad range of biochemical and pathological conditions, including mitochondrial damage and high levels of reactive oxygen species (ROS) production that might result in up-regulation of cell death levels in the nervous system [5, 6]. We further hypothesize that both embryonic and adult NSC might be the primary target of arsenic-induced death pathways. There are numerous scientific observations that indirectly support this hypothesis. Animal experiments demonstrated sensorimotor and cognitive behavioral deficits in mice and rats after prolonged arsenic treatment [7]. Epidemiological studies of human populations in Bangladesh exposed to higher sodium arsenite concentrations in drinking water demonstrated an inverse association between arsenic dose and IQ [8], suggesting an involvement of neurotoxic effects. Potentially immortal ESC in culture have long held promise as the next critical step of regenerative medicine. The self-renewal of mESC and the maintenance of their pluripotency are dependent on multifactorial stimulation of specific signaling pathways by the cytokine leukemia inhibitory factor (LIF) [9] and various growth factors from fetal bovine serum, such as IGF, BMP4 and WNT. Numerous investigations revealed a "minimal" combination of LIF-dependent [9, 10] and BMP-dependent signals [11] for the maintenance of mESC self-renewal and pluripotency together with a dynamic inhibition of differentiation pathways [12]. Alternatively, a combination of the small molecular inhibitors of the specific signaling pathways (FGFR, MEK-ERK and GSK3) could also be very efficient for the maintenance of mESC self-renewal via a suppression of differentiation [13]. In the present study, we investigated the effects of sodium arsenite on modulation of the major signaling pathways and their linkage to self-renewal, survival and induction of cell death in mouse ESC and NSC. We also elucidated the mechanism of the apoptotic death induced by sodium arsenite in stem cells with special attention to the mitochondrial death pathway, which is induced by arsenite exposure. Connection between stem cell biology and environmental health studies will allow us to better understand mechanisms of neurodegenerative diseases. It may result in better prevention and treatment of these diseases. In the current study we used ESC line W4 from 129/SvEvTac mice, and the surrogate mouse NSC clone C17.2, which was isolated initially from neonatal mouse cerebellum, and kindly provided by Dr. E.Y. Snyder. Propagation and stem-like behavior of the C17.2 cell line was augmented via vmyc transduced by MMLV retrovirus vector [14].

There is a substantial similarity in the downstream regulation of gene expression by "core" transcription factors Oct4, Sox2 and Nanog in mouse and human ESC. However, there is a significant difference in the upstream initiation of cytokine/growth factor-dependent signaling pathways in mouse ESC compared to human ESC [12]. The critical pathways, which are responsible for the self-renewal of mESC, are mediated by LIF/(LIFR,gp130)-JAK1/2 and LIF/(LIFR,gp130)-PI3K-AKT, while LIF-MAPK, as well as FGF2/FGFR-MAPK signaling pathways, which activate a differentiation program, should be partially suppressed in these conditions.

Our recent experimental data demonstrated a dramatic, dose-dependent effect of sodium arsenite (1-4 μM) exposure on proliferation and regulation of the cell cycle in mESC resulting in G2/M arrest 24 h after treatment and pronounced apoptosis 48 h after treatment (Figure 1). For cell cycle-apoptosis analysis, we have used propidium iodide staining of DNA and FACS analysis. Total death levels were determined using trypan blue staining and microscopic analysis. As expected, total levels of cell death were higher than apoptotic levels. However, relatively modest changes in cell cycle distribution and apoptosis levels were detected after sodium arsenite treatment of mouse embryonic fibroblasts (Figure 1), highlighting a strong sensitivity of mESC to cytotoxic effects of arsenic exposure. We further used the universal caspase inhibitor Z-VAD-FMK (50 μM) and specific caspase inhibitors, Ac-IETD-CHO (an inhibitor of caspase-8; 50 μM) and Ac-LEHD-CHO (an inhibitor of caspase-9; 50 μM), and obtained evidence of activation of the mitochondrial apoptotic pathway (caspase-9-dependent) in mESC after arsenite treatment. We also revealed a dramatic upregulation in levels of heme oxygenase-1 (HO-1) after sodium arsenite exposure that

correlated with internal protection against the mitochondrial apoptotic pathway [15]. Interestingly, specific inhibition of HO-1 enzymatic activity substantially accelerated arsenic-induced apoptosis in ESC (data not shown).

Furthermore, Western blot analysis of signaling proteins demonstrated strong negative effects of sodium arsenite on AKT activation via inhibition of its Ser473 phosphorylation and the subsequent inhibition of mTOR activation in mESC (data not shown). The PI3K-AKT connection, a cross-road of signaling pathways induced by growth factor receptor protein kinases, plays a central role for a general cell survival and anti-apoptotic response, while mTOR activation is well known as a critical target of PI3K-AKT. We and others have previously observed a negative regulation of JAK2/STAT3 and of IKK-NF-kappaB pathways in cancer cells following sodium arsenite treatment [16]. We have further demonstrated a negative regulation of these pathways and their downstream targets upon sodium arsenite treatment of mESC (data not shown). To evaluate the effect of sodium arsenite on regulation of the cell cycle and apoptosis in mESC, we compared the effects of the specific small molecular inhibitors of the cell signaling pathways, which were added to the culture media. The quickest response with pronounced induction of apoptosis in mESC was observed for BMS345541, an IKK-NF-kappaB inhibitor and LY294002, a PI3K-AKT inhibitor. Furthermore, PPP and PD153035, inhibitors of IGF-1R and EGFR, respectively, induced strong changes in the cell cycle distribution and increased apoptotic levels. On the other hand, a pronounced effect of STAT3 suppression (by STAT3 inhibitor-6) was observed only 48 h after treatment. These results indicated that suppression of PI3K-AKT, IKK-NF-kappaB and JAK2-STAT3 activities by sodium arsenite treatment of ESC could be critical for G2/M arrest and apoptosis induction.

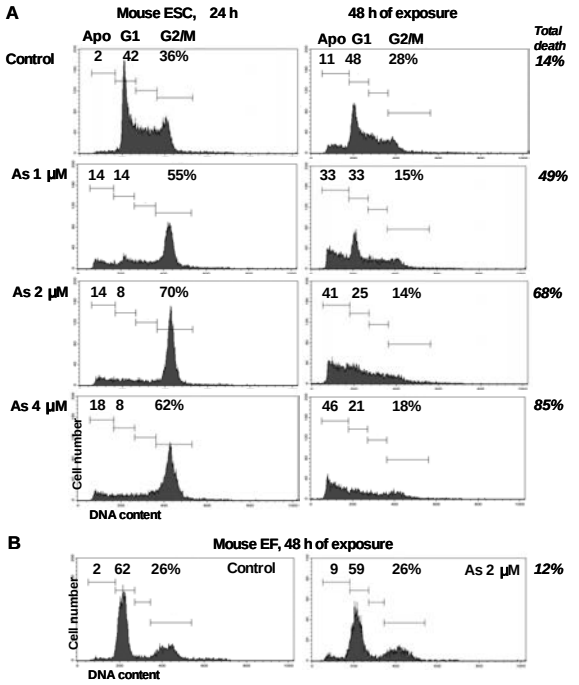

Figure 1. *Dose-dependent effects of sodium arsenite treatment on cell cycle and apoptosis of mouse ESC. Sodium arsenite induced G2/M arrest of ESC 24 h after exposure in a dose-dependent manner that was accompanied by increased levels of apoptosis 48 h after exposure. In contrast, MEF did not display a pronounced response to arsenite treatment.*

The effects of these same inhibitors, as well as effects of sodium arsenite, on downregulation of NF-kB/STAT3-dependent expression of cyclin D1 and B transcripts in mESC was investigated in the context of regulation of the cell cycle. Interestingly, the summary effects of sodium arsenite treatment were similar to total upstream inhibition of IGF1/IGF1R-mediated signaling by PPP. Quite similar results were also obtained after EGF/EGFR inhibition. In contrast, inhibitors of MAPKs (MEK-ERK, JNK and p38) did not demonstrate significant effects on upregulation of apoptosis (data not shown).

As expected, transferring mESC into minimal medium with 1.5% FBS without LIF was accompanied by induction of high apoptotic levels within 24 h (data not shown), highlighting a general significance of cytokine/growth factor signaling LIF/IGF-PI3K-AKT in anti-apoptotic protection. The presence of sodium arsenite in the minimal medium demonstrated only small additive effects, suggesting that growth factor withdrawal or arsenite treatment could affect a similar set of the downstream signaling modules (data not shown).

Negative regulation of PI3K-AKT, IKK-NF-kappaB and JAK2-STAT3 activities by sodium arsenite is a well-established phenomenon for many normal and cancer cell lines. However, mECS demonstrated especially high sensitivity to arsenite treatment that will be investigated further. In this respect, the IKK-NF-kappaB pathway represents a special interest. This pathway could be induced or upregulated in mESC via numerous upstream modules, including PI3K-AKT-IKK, JAK2-IKK and ATM-IKK. There are additional secondary mechanisms of negative regulation of PI3K-AKT and IKK-NF-kappaB by sodium arsenite: i) NF-kappaB-mediated transcriptional control of IGF1R expression that could be suppressed by sodium arsenite resulting in a massive blockage of IGFR1-mediated signals, including PI3K-AKT and IKK-NF-kappaB; and ii) NF-kappaB-regulated gp130 gene expression that after suppression by sodium arsenite may negatively affect LIF-gp130 signaling pathways.

In our current experiments, we use ectopic expression of constitutively active IKK-beta S178E/S181E [17] to upregulate activation of NF-kappaB, even after sodium arsenite exposure. Since NF-kappaB-dependent Bcl-xL overexpression suppresses the mitochondrial apoptotic pathway [18], we anticipate that activation of the NF-kappaB pathway will block (at least, partially) arsenite-induce apoptosis in mESC. Recently we found a negative

regulation of Oct4, Sox2 and Nanog by sodium arsenite in ESC (data not shown). Our next aim is to investigate the negative effects of sodium arsenite on STAT3/NF-kappaB-dependent gene expression of Oct4, Sox2 and Nanog, a common set of "core" transcription factors that are involved in the maintenance of pluripotency in mESC [19]. We anticipate that investigation of signal-dependent regulation of gene expression driven by "core" transcription factors and the modulating effects of sodium arsenite as a transcriptional regulator in ESC may open up new opportunities for understanding mechanisms of arsenic-mediated embryotoxicity.

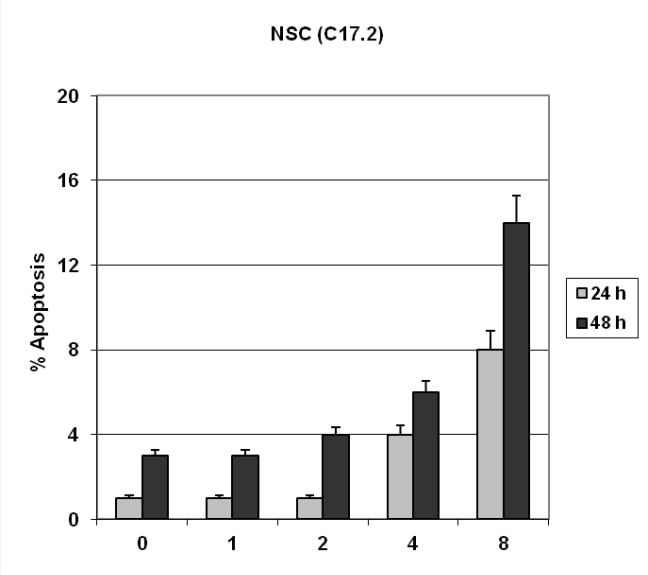

Figure 2. *Dose-dependent effects of sodium arsenite on apoptosis levels of mNSC cells 24 h and 48 h after treatment.*

Our preliminary data surprisingly demonstrated a high anti-apoptotic resistance of mNSC (clone C17.2) to sodium arsenite in culture conditions: modest apoptosis levels were detected only 24 h after arsenite treatment at 4-8 μM (Figure 2). However, prolonged (72 h) incubation of mNSC in the presence of 2 μM sodium arsenite caused a massive non-apoptotic cell death. Simultaneously, only LU294002, a PI3K-AKT inhibitor, was able to induce pronounced apoptosis in mNSC 24-48 h after treatment; the presence of 2 μM arsenite additionally increased apoptotic levels. In addition, arsenite further increases apoptosis induced by inhibition of the STAT3 or ATM pathways (by KU55933). The growth factor inhibitors PPP and PD153035 induced low levels of apoptosis alone, but demonstrated additive effects in combination with arsenite.

Taken together, these preliminary data indicate an efficient protection against sodium arsenite action in mNSC that is probably dependent on the PI3K-AKT pathway. This pathway could be permanently induced by FGF2 or FGF4 in complete medium. Indeed, PD173074 (1 μM), a FGFR inhibitor, was able to initiate apoptotic cell death in mNSC alone or, especially, in combination with PD153035 (an EGFR inhibitor).

Effects of sodium arsenite on downstream targets of PI3K-AKT in mNSC will be further investigated. We anticipate that suppression of mTOR and reactivation of GSK3beta following sodium arsenite exposure could dramatically change mNSC survival and induce both massive cell death and differentiation for a small number of surviving cells. Determination of mitochondrial damage (decrease of the mitochondrial membrane potential), ROS production, and ROS-dependent signaling pathways induced by sodium arsenite treatment of mNSC will provide additional information regarding metabolic homeostasis and protection against oxidative stress in these cells. This is especially relevant as NSC are progenitors of neurons, which exhibit high levels of oxidative metabolism.

A better understanding of the mechanisms of arsenic-induced embryotoxicity and neurotoxicity may result in better prevention and treatment of neurodegenerative diseases. Another important aspect of this problem is arsenic-mediated transformation of embryonic stem cells into cancer stem cells. This concern is based on the well-established mutagenic effects of arsenic and its role in regulation of gene expression, which is the main object of the present study. Paradoxically, we and other investigators observed higher sensitivity to arsenite in neuroblastoma cells, compared to NSC, especially in combination with STAT3-inhibitors [20, 21]. This might provide a new highly relevant approach for treatment of this type of cancer.

References

1. Robinson, J. F., Yu, X., Moreira, E. G., Hong, S., and Faustman, E. M. (2011) Toxicol Appl Pharmacol 250, 117-129
2. Lindgren, A., Danielsson, B. R., Dencker, L., and Vahter, M. (1984) Acta Pharmacol Toxicol (Copenh) 54, 311-320
3. Reynolds, B. A., Tetzlaff, W., and Weiss, S. (1992) J Neurosci 12, 4565-4574
4. Reynolds, B. A., and Weiss, S. (1992) Science 255, 1707-1710
5. Pulido, M. D., and Parrish, A. R. (2003) Mutat Res 533, 227-241
6. Partridge, M. A., Huang, S. X., Hernandez-Rosa, E., Davidson, M. M., and Hei, T. K. (2007) Cancer Res 67, 5239-5247
7. Rodriguez, V. M., Jimenez-Capdeville, M. E., and Giordano, M. (2003) Toxicol Lett 145, 1-18
8. Wasserman, G. A., Liu, X., Parvez, F., Ahsan, H., Factor-Litvak, P., Kline, J., van Geen, A., Slavkovich, V., Loiacono, N. J., Levy, D., Cheng, Z., and Graziano, J. H. (2007) Environ Health Perspect 115, 285-289
9. Niwa, H., Ogawa, K., Shimosato, D., and Adachi, K. (2009) Nature 460, 118-122
10. Hirai, H., Karian, P., and Kikyo, N. The Biochemical Journal (2011) 438, 11-23

11. Ying, Q. L., Nichols, J., Chambers, I., and Smith, A. (2003) Cell 115, 281-292
12. Hanna, J., Cheng, A. W., Saha, K., Kim, J., Lengner, C. J., Soldner, F., Cassady, J. P., Muffat, J., Carey, B. W., and Jaenisch, R. (2010) Proc Natl Acad Sci U S A 107, 9222-9227
13. Pera, M. F., and Tam, P. P. (2010) Nature 465, 713-720
14. Snyder, E. Y., Deitcher, D. L., Walsh, C., Arnold-Aldea, S., Hartwieg, E. A., and Cepko, C. L. (1992) Cell 68, 33-51
15. Fulda, S., and Debatin, K. M. (2006) Oncogene 25, 4798-4811
16. Ivanov, V. N., and Hei, T. K. (2004) J Biol Chem 279, 22747-22758
17. Zandi, E., Rothwarf, D. M., Delhase, M., Hayakawa, M., and Karin, M. (1997) Cell 91, 243-252
18. Khoshnan, A., Tindell, C., Laux, I., Bae, D., Bennett, B., and Nel, A. E. (2000) J Immunol 165, 1743-1754
19. Hanna, J. H., Saha, K., and Jaenisch, R. (2010) Cell 143, 508-525
20. Ivanov, V. N., and Hei, T. K. (2011) Apoptosis 16, 1268-1284
21. Pettersson, H., Karlsson, J., Pietras, A., Øra, I., and Påhlman, S. (2007) Journal of Bioenergetics and Biomembranes 39, 35-41

■

siRNA-Mediated Decrease in RAD9 Expression Alters Expression of Downstream Genes

Qingping Cui, Aiping Zhu, Howard B. Lieberman

Introduction

RAD9 is an evolutionarily conserved gene that has many functions, including a role in DNA repair, cell cycle checkpoint control and apoptosis [1]. An siRNA-mediated decrease in RAD9 protein levels reduces the tumorigenic potential of human prostate cancer cells, suggesting that RAD9 also has a functional role in human prostate carcinogenesis [2]. Recent research has provided evidence that human RAD9 can, like p53, act as a sequence specific transcription factor [3]. To fully understand this, using siRNA-mediated RAD9 knock down in human prostate cancer cells as previously reported [2], we have explored how RAD9 might regulate the cellular response to DNA damage by binding to and transactivating a network of relevant downstream target genes.

Materials and Methods

RAD9 has been knocked down by siRNA according to Zhu et al., 2008 [2]. Reduction in the level of RAD9 protein was confirmed by Western blot analysis (Figure 1A), before total RNA was extracted using the EXIQON RNA Isolation kit for subsequent microarray gene expression studies. Two independent microarray analyses were performed according to the Affymetrix protocol for labeling, hybridization, washes and chip reading. dChip (www.dchip.org) was used for hierarchical cluster analyses. Further analysis was performed using Ingenuity Pathway Analysis (IPA). Two independent ChIP assays were also performed using NimbleGen Human ChIP-chip 2.1 M Deluxe Promoter Arrays to identify the gene promoters bound by RAD9. According to the manufacturer's protocol, DU145 cells were fixed and DNA/protein cross-linked, then sonicated. DNA was then immuoprecipitated by RAD9 antibody, amplified by ligation-mediated PCR, fragmented, end-labeled and hybridized to NimbleGen chips. SignalMap was used for viewing ChIP-chip peaks. SYBR green real-time PCRs were performed on selected genes to confirm microarray data, for genes positive in both the microarray and ChIP-chip assays.

ChIP-chip using anti-RAD9 antibody (Abcam ab70810) and anti-mouse IgG antibody as negative control was performed in two independent DU145 cell cultures. Chromatin enrichment was confirmed by ChIP-PCR assays with positive primers located in the promoter of a known RAD9 target, p21 [3]. Primers located around the 3' region of p21 were used as a negative control for RAD9 binding.

Results

In the microarray expression study, 453 genes were identified after excluding background signals with average intensity lower than 100, and a fold change larger than 1.5 in DU145 RAD9 knocked down cells compared to either DU145 parental cells or DU145 cells transfected with an insertless vector.

Centroid-linkage hierarchical clustering using 1-correlation as the distance metric was applied to the normalized expression values to visualize the gene expression pattern among DU145 cells with different status. The blue color in Figure 1 indicates genes that have relative low expression while red indicates high

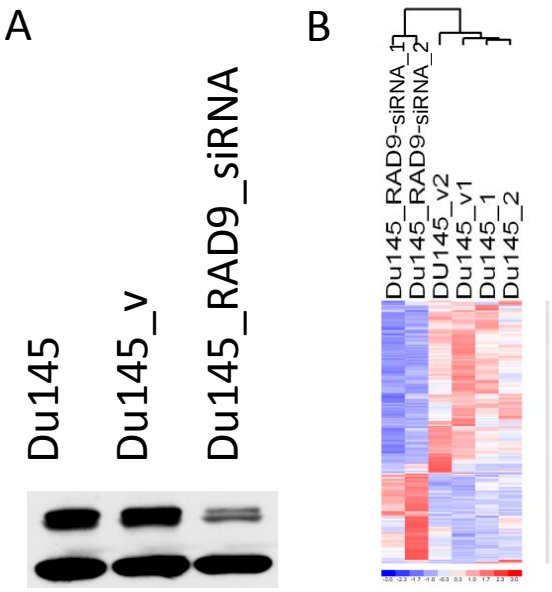

***Figure 1**. A) RAD9 protein reduced after being knocked down by siRNA in DU145 cells. DU145_v: DU145 with insertless vector. B) Heatmap of expression of 453 selected genes in DU145, DU145_v (transfected with an insertless vector), DU145_RAD9_siRNA.*

expression. The dendrogram divided the samples into two groups, siRNA-mediated RAD9 knock down in DU145 cells, and DU145 cells with or without vector.

Using IPA pathway analysis, we found that a significant number of genes in specific functional categories were enriched in this set of 453 genes (Table 1). There are 21 genes with cell cycle function, 26 involved in cellular development, 16 impacting on cell morphology, 20 with cellular function and maintenance activities, and 26 that contribute to cellular growth and proliferation.

Analysis of ChIP-chip experiments with SignalMap identified 3165 genes encoding proteins that bind RAD9 and met a Peak score > 1.5 in both independently conducted sets of experiments. Subsequent analysis revealed 48 genes also in the 453 positive microarray gene set. Among these 48 genes, ASF1B, CCL5, FOXP1, IGFBPs, JAK1 and NDRG1 were down regulated, and EPHA2 as well as PLK3 were up regulated, when RAD9 was knocked down in DU145 cells. qPCR was performed to confirm these gene expression results.

Table 1. IPA analysis of molecular and cellular functions.

Name	p-value	No. of Genes
Cell Cycle	1.78E-04 - 4.81E-02	21
Cellular Development	8.87E-04 - 4.78E-02	26
Cell Morphology	1.68E-03 - 3.38E-02	16
Cellular Function and Maintenance	2.07E-03 - 2.87E-02	20
Cellular Growth and Proliferation	2.07E-03 - 4.43E-02	26

Discussion

RAD9 can regulate expression of a number of genes, including p21, when overexpressed [3]. Our study has shown that the down regulation of RAD9 in prostate cancer cells, which reduces tumorigenic potential, alters the expression of a set of downstream target genes, consistent with its known transactivation function. 48 of these genes were also bound by RAD9 within their promoter region, as determined by ChIP-chip assays. The down-regulated genes participate in a variety of functions. For instance, depletion of Asf1b has been shown to severely compromise proliferation of breast cancer cells [4]. Interestingly, TLK1B, a gene involved in the regulation of chromatin assembly, repairs DSBs via its interaction with Asf1 and Rad9 [5]. Down regulation of CCL5 causes loss of the inflammatory immune response. Just like RAD9, FOXP1 is an androgen receptor (AR) transcription factor that negatively regulates AR signaling in prostate cancer cells [6]. IGFBP3 and NDRG1, both considered tumor suppressor genes, are also down regulated by RAD9 siRNA. The biological significance of these downstream genes is being pursued.

Up regulated genes include DCLK1 and PLK3. DCLK1 functions in maintaining the proliferation of cells. PLK3 can regulate mitosis, and might be up regulated by activator E2F [7].

In summary, our preliminary work has identified a set of differentially expressed genes as potential RAD9 downstream target genes. These genes function in DNA repair, cell division and tumor suppression. Changes in their expression suggest that RAD9 is an important sequence specific transcription factor that controls cell growth and stability of genetic material. Further experiments to define the biological significance of the genes identified as regulated by RAD9 will contribute to better understanding how RAD9 mediates the cellular response to DNA damage and acts as an oncogene with respect to prostate cancer.

References

1. H. B. Lieberman. Rad9, an evolutionarily conserved gene with multiple functions for preserving genomic integrity. Journal of cellular biochemistry. 97, 690-697 (2006).
2. A. Zhu, C. X. Zhang, and H. B. Lieberman. Rad9 has a functional role in human prostate carcinogenesis. Cancer Research 68, 1267-1274 (2008).
3. Y. Yin, A. Zhu, Y. Jin, Y.X. Liu, X. Zhang, K.M. Hopkins, H.B. Lieberman, Human RAD9 checkpoint control/proapoptotic protein can activate transcription of p21. Proceedings of the national Academy of

Sciences of the United States of America 101, 8864-8869 (2004).
4. A.Corpet, Koning De, J. Toedling, A. Savignoni, F. Berger, C. Lemaitre, R. J. O'Sullivan, J. Karlseder, E. Barillot, B. Asselain, X. Sastre-Garau, and G. Almouzni. Asf1b, the necessary Asf1 isoform for proliferation, is predictive of outcome in breast cancer. The EMBO journal 30, 480-493 (2011).
5. S. P. Sen, and A. De Benedetti. TLK1B promotes repair of UV-damaged DNA through chromatin remodeling by Asf1. BMC molecular biology 7, 37 (2006)
6. K. Takayama, K. Horie-Inoue, K. Ikeda, T. Urano, K. Murakami, Y. Hayashizaki, Y. Ouchi, and S. Inoue. FOXP1 is an androgen-responsive transcription factor that negatively regulates androgen receptor signaling in prostate cancer cells. Biochemical and biophysical research communications. Biochemical and biophysical research communications 374, 388-393 (2008)
7. M. Tategu, H. Nakagawa, K. Sasaki, R. Yamauchi, S. Sekimachi, Y. Suita, N. Watanabe, and K. Yoshid. Transcriptional regulation of human polo-like kinases and early mitotic inhibitor. Journal of genetics and genomics. 35, 215-224 (2008). ■




Top (l to r): Dr. Lubomir Smilenov, Dr. David Brenner, Dr. Eric Hall, Dr. Charles Geard. Bottom (l to r): Meeting of the Bystander Effects Program Project Grant team, Dr. Erik Young.

Variability of the Ionizing Radiation-Induced Bystander Response

Kevin M. Hopkins, Shanaz Ghandhi, Qingping Cui, Sally A. Amundson, and Howard B. Lieberman

When cells are exposed to ionizing radiation they can demonstrate a variety of phenotypes, including cell cycle delay, micronuclei formation, induction of mutation, apoptosis, or other modes of death. Interestingly, it was found that many of these same phenotypes can also be exhibited by cells neighboring those directly "hit" by charged particles. These cells are called bystanders and the reaction is called the bystander response [1, 2].

Variability has been observed with respect to the degree of the bystander response, between cell lines and even from experiment to experiment using the same parental cell population. Thus, efforts were made to ensure that cells examined for defining the molecular mechanism underlying the bystander response, an important goal, in fact were demonstrating such a response. A double Mylar dish configuration [3], illustrated in Figure 1 upper left panel, was used for bystander studies whereby directly hit cells and the bystanders are in contact during irradiation but can be separated for independent analyses. Our strategy involved the monitoring of micronuclei formation in bystander versus directly irradiated cells on a plate-by-plate basis, as outlined in Figure 1.

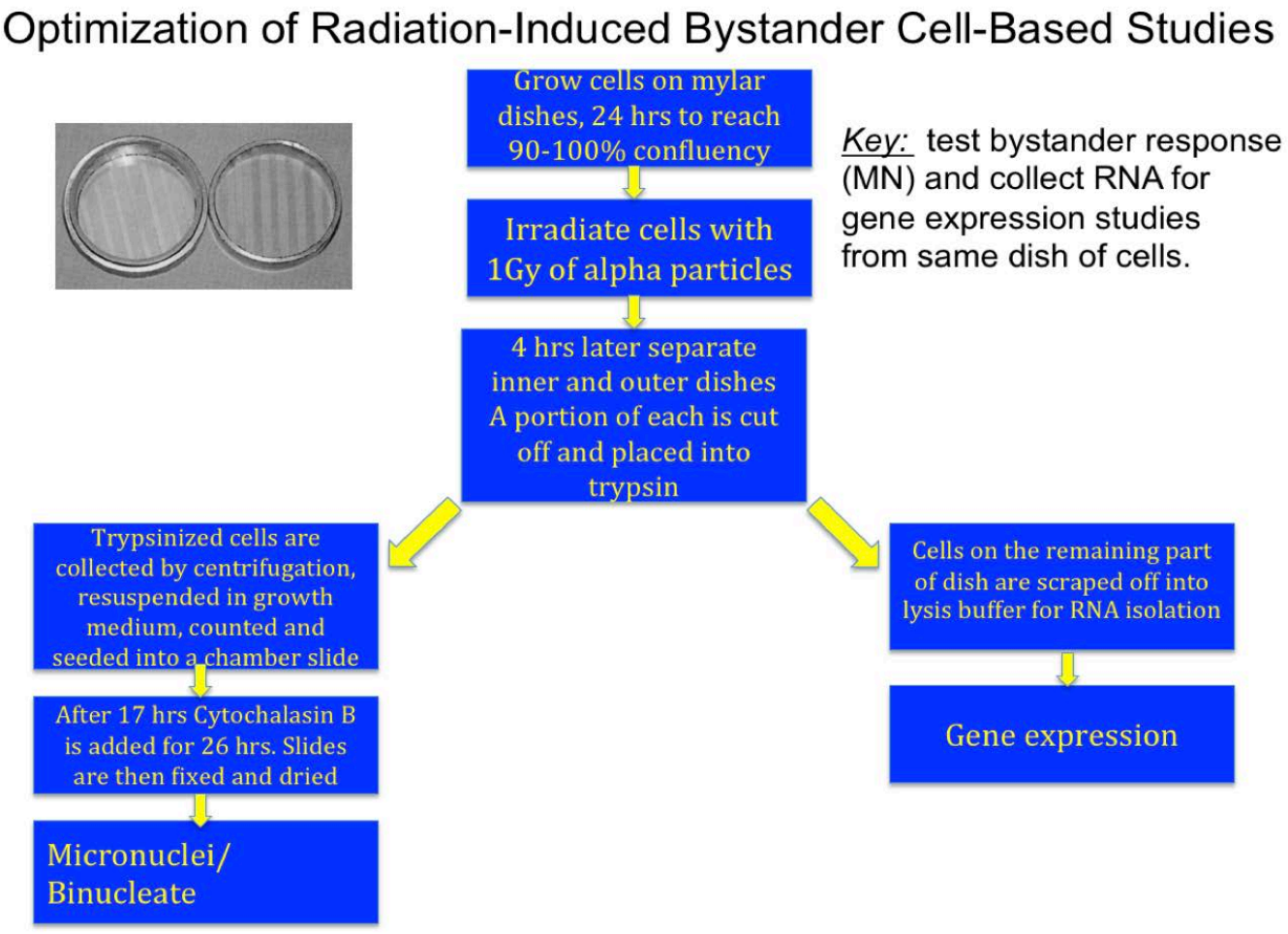

Figure 1. *Strategy used to test the bystander response in cells on a plate-by-plate basis. Micronuclei (MN) formation and the harvesting of RNA for subsequent gene expression analyses are illustrated and as noted both can be performed on samples from a single dish. As such, it is clear that RNA is taken from cells actually undergoing a bystander response. Cells are H1299, and alpha particles were used as the radiation of choice. The upper left panel depicts the double Mylar dishes used for the experiment.*

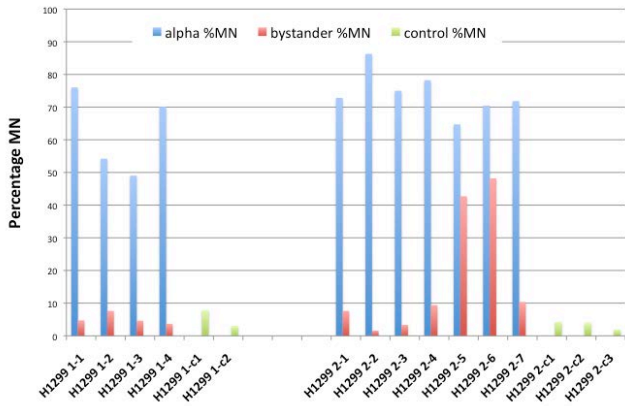

Figure 2. *Percentage of micronuclei (MN) formed in H1299 cells directly exposed to 1Gy of alpha particles (blue), as bystander cells (pink) or in unirradiated controls (green). Each bar represents an individual dish.*

The results for the micronuclei related experiments are illustrated in Figure 2. The number of micronuclei per binucleate cell in directly irradiated (1Gy alpha particles, blue), bystanders (red) and unirradiated cell controls (c, green) were scored. Fixed cells were stained with SYBR Green and subsequently counted by using a fluorescent microscope. Data are shown for individual dishes plated with one of two independent H1299 cell freezes (H12991-X; H12992-X). As illustrated, directly irradiated cells consistently demonstrated MN formation above unirradiated background levels. The frequency of MN formation in controls was low. However, only two dishes contained cells that demonstrated a dramatic bystander response, that is H1299 2-5 and H1299 2-6, even though to the best of the investigators knowledge all dishes were handled in essentially the same manner.

These results demonstrate the dramatic variation that can occur in experiments designed to address bystander responses. In conclusion, a system has been optimized such that the bystander response can be monitored and RNA can be isolated from cells that are known to have undergone a bystander response. Experiments are underway to determine the nature of the bystander signaling and reasons for the observed wide spread variability in that response to radiation exposure.

References

1. Hei TK, Zhou H, Ivanov VN, Hong M, Lieberman HB, Brenner DJ, Amundson SA, Geard CR. (2008) Mechanism of radiation-induced bystander effects: a unifying model. *J Pharm Pharmacol*. **60:**943-50.
2. Morgan WF, Sowa MB. (2007) Non-targeted bystander effects induced by ionizing radiation. *Mutat Res*. **616:**159-64
3. Zhu A, Zhou H, Leloup C, Marino SA, Geard CR, Hei TK, Lieberman HB. (2005) Differential impact of mouse Rad9 deletion on ionizing radiation-induced bystander effects. *Radiat Res*. **164:**655-61.■

Holiday prizes: Rob Morton, Antonella Bertucci, Margaret Zhu, David Brenner, Jarah Meador, Helen Turner, Adayabalam Balajee, Maria Taveras, Tom Hei.

Combined Haploinsufficiency and Genetic Control of the G2/M Checkpoint in Irradiated Cells

Erik F. Young , Lubomir B. Smilenov , Howard B. Lieberman, and Eric J. Hall

Radiation exposure culminating in chromosome aberrations causes cell cycle arrest at the G2/M checkpoint, facilitating DNA repair. Defects in checkpoint control genes can impart radiosensitivity. In a survey of radiation induced arrest kinetics, we monitored rapidly dividing mouse embryo fibroblasts (MEFs) at doses ranging from 10 mGy to 5.0 Gy of γ radiation over a time course of 0 to 12 h. We observed no significant checkpoint engagement at doses below 100 mGy. The checkpoint is only fully activated at doses where most of the cells are either bound for mitotic catastrophe or are reproductively dead. Atm null cells with ablated checkpoint function exhibited no robust arrest. Surprisingly, haploinsufficiency for ATM alone or in combination with other radioresistance genes did not alter checkpoint activation. Prior findings from this lab suggest that haploinsufficiency for several radioresistance genes imparts intermediate phenotypes for several end points including apoptosis, transformation and survival. The G2/M arrest findings suggest that checkpoint control does not contribute toward these intermediate phenotypes and that different biological processes can be activated at high doses compared to low doses.

Introduction

In establishing radiation protection standards, regulatory bodies make two assumptiuons. First, that the human population responds uniformly to radiation and second, that cancer risk is related to dose in a completely linear relationship. This may be untrue for lower doses, which may induce response programs that differ from programs engaged at higher doses [1-4]. At present, it is not clear whether such considerations will increase or decrease cancer risks at low doses compared with the linear, no-threshold convention.

This laboratory has previously demonstrated that haploinsufficiency for ATM, Mrad9 and BRCA1 can cause increased radiation sensitivity [5-9]. Are these otherwise silent haploinsufficiencies additive or cooperative in cumulative radiation sensitivity and checkpoint control? Such interplay would emerge in a survey of arrest kinetics of cells that are rapidly dividing and devoid of chemical manipulation of the cell cycle. Assessment of lower acute doses would also report differences in the response biology in higher versus lower doses and address concerns with the linear, no-threshold convention. To address this question, we chose to measure G2/M arrest kinetics in order to assess checkpoint function and accompanying radiation sensitivity in the context of combined haploinsufficiency.

The goals of this work were to assess rapidly dividing, minimally perturbed cell populations with combined haploinsufficiency for ATM, Mrad9 and PTEN, for their ability to halt at the G2/M checkpoint after irradiation with low and high doses. In so doing, we sought to test whether the radiosensitivity seen to accompany combined haploinsufficiency is coincident with the checkpoint control functions of these genes. In the context of partially ablated checkpoint components in various combinations, we also sought to gain more detailed mechanistic insight into checkpoint function – especially at low doses.

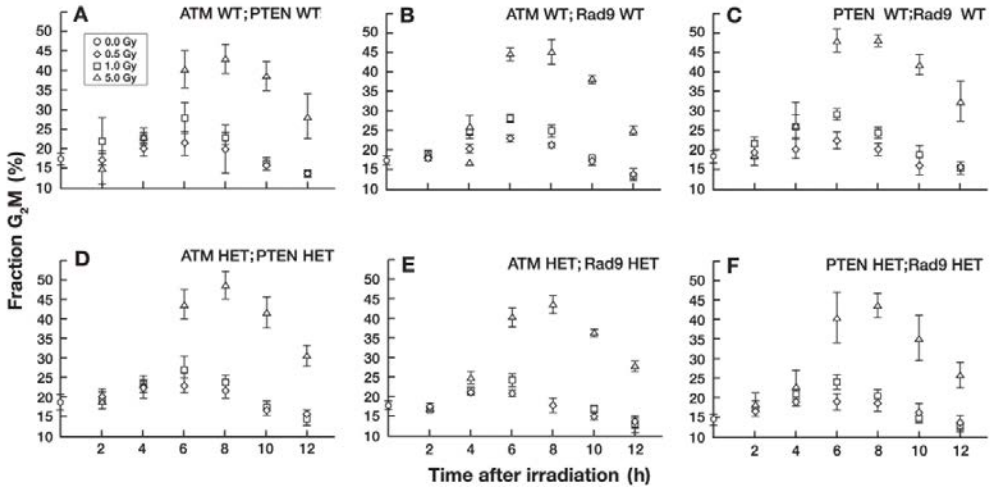

Figure 1. *Kinetics and magnitude of G2/M arrest in freshly isolated mouse embryo fibroblasts from wild type littermate control embryos (A-C) or those doubly haploinsufficient for PTEN and ATM (D), ATM and Mrad9 (E), and PTEN and Mrad9 (F). The fraction of G2/M is reported as the mean with standard deviation of three technical repeats of all available measurements from three different embryos.*

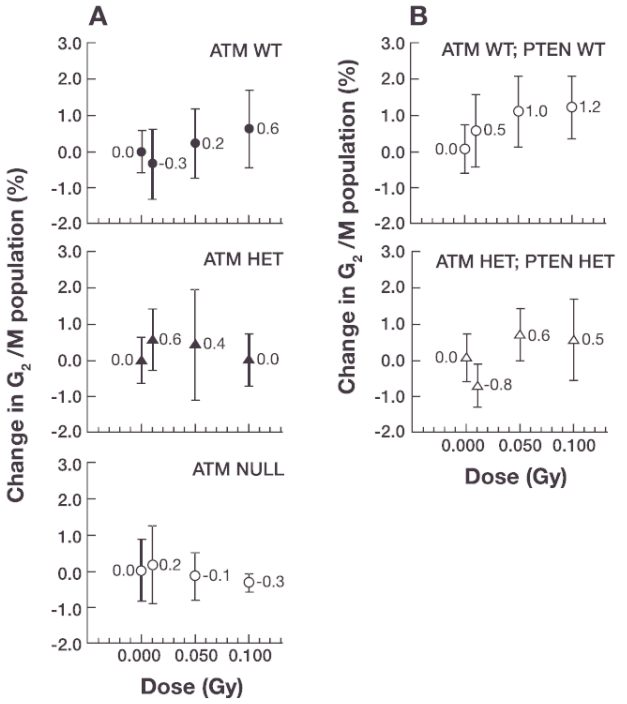

Figure 2. *Low dose survey of MEFs at 6 h after irradiation. Cells with various gene doses of ATM (A) and cells with combined haploinsufficiency for ATM and PTEN (B) were assessed for increases in G2/M population at 6 h after various acute low doses of γ radiation. Change is defined as the difference in acquired measurements relative to the mean of sham irradiated samples. Change in the fraction of G2/M is reported with the mean and standard deviation of six technical iterations shown for each dose.*

Results

MEFs were isolated from F1 pairings of mice heterozygous for a variety of radioresistance genes, split into dishes at early passage number and irradiated with doses from 0 to 5 Gy. Arrest kinetics were monitored over a subsequent 12 h timecourse by ethanol fixation, propidium iodide staining for ploidy and scoring by flow cytometry. Cells exhibited a prominent 6 h maximum in G2/M arrest after acute doses, and this shifted to around 8 h with the highest dose in the study, 5.0 Gy. This pattern was unchanged irrespective of combinatorial haploinsufficiency for a variety of radioresistance genes (Figure 1). Atm null cells failed to mount a robust arrest after irradiation [10].

Low dose comparisons over the range of 0-100 mGy were conducted 6 h after irradiation. Importantly, no significant increase in G2/M fraction was observed in wild type MEFs or those haploinsufficient for ATM (Figure 2A). Cells with combined haploinsufficiency for ATM and PTEN showed no significant induction in the G2/M population over the low dose range of interest (Figure 2B).

Conclusions

Previously, we demonstrated that MEFs haploinsufficient for both ATM and Mrad9 are more sensitive to transformation and DNA repair. Thymocytes haploinsufficient for both ATM and Mrad9 exhibit less apoptosis than wild type cells or those haploinsufficient for only one of the encoded proteins [6]. Radiation induced cataractogenesis in such haploinsufficient animals also exhibits an intermediate phenotype [5, 6]. G2/M arrest kinetics, a well characterized radiation induced process, should recapitulate these other findings, reporting intermediate phenotypes.

We observe statistically significant increases in the G2/M fraction of MEFs doubly haploinsufficient for ATM and PTEN at doses above 0.5 Gy. We do not see a statistically significant change in the G2/M fraction over the dose range of 0-100 mGy. The activation threshold for arrest appears to lie above 100 mGy and is in agreement with reports from other groups [11, 12]. Release from radiation induced arrest is also in this dose region [13, 14]. Activation of all cell cycle checkpoints occurs irrespective of haploinsufficiency contributed by various combinations of radioresistance genes when examined in freshly isolated MEFs after acute exposures to γ radiation. The G2/M checkpoint, irrespective of haploinsufficiency in MEFs, engages at a threshold greater than 0.1 Gy and less than 0.5 Gy.

Discussion

There is not a discernible connection between the radiosensitivity that arises from haploinsufficiency in our other systems of study and the control of the G2/M checkpoint. It is notable that a substantial dose must be applied for activation of the checkpoint, suggesting a paucity of checkpoint function at low doses. Activation of the checkpoint only occurs at doses where most of the cells are reproductively dead. Lastly, our findings confirm a threshold of activation for the G2/M checkpoint, hinting at two separate radiation response programs acting below and above this threshold.

References

1. Barcellos-Hoff MH, Brenner DJ, Brooks AL, Formenti S, Hlatky L, Locke PA, et al. Low-dose radiation knowledge worth the cost. Science 2011;332(6027):305-6.
2. Ding LH, Shingyoji M, Chen F, Hwang JJ, Burma S, Lee C, et al. Gene expression profiles of normal human fibroblasts after exposure to ionizing radiation: a comparative study of low and high doses. Radiat Res 2005;164(1):17-26.
3. Mezentsev A, Amundson SA. Global gene expression responses to low- or high-dose radiation in a human three-dimensional tissue model. Radiat Res 2010;175(6):677-88.

4. Yin E, Nelson DO, Coleman MA, Peterson LE, Wyrobek AJ. Gene expression changes in mouse brain after exposure to low-dose ionizing radiation. Int J Radiat Biol 2003;79(10):759-75.
5. Hall EJ, Worgul BV, Smilenov L, Elliston CD, Brenner DJ. The relative biological effectiveness of densely ionizing heavy-ion radiation for inducing ocular cataracts in wild type versus mice heterozygous for the ATM gene. Radiat Environ Biophys 2006;45(2):99-104.
6. Kleiman NJ, David J, Elliston CD, Hopkins KM, Smilenov LB, Brenner DJ, et al. Mrad9 and atm haploinsufficiency enhance spontaneous and X-ray-induced cataractogenesis in mice. Radiat Res 2007;168(5):567-73.
7. Smilenov LB, Lieberman HB, Mitchell SA, Baker RA, Hopkins KM, Hall EJ. Combined haploinsufficiency for ATM and RAD9 as a factor in cell transformation, apoptosis, and DNA lesion repair dynamics. Cancer Res 2005;65(3):933-8.
8. Worgul BV, Smilenov L, Brenner DJ, Junk A, Zhou W, Hall EJ. Atm heterozygous mice are more sensitive to radiation-induced cataracts than are their wild-type counterparts. Proc Natl Acad Sci U S A 2002;99(15):9836-9.
9. Worgul BV, Smilenov L, Brenner DJ, Vazquez M, Hall EJ. Mice heterozygous for the ATM gene are more sensitive to both X-ray and heavy ion exposure than are wildtypes. Adv Space Res 2005;35(2):254-9.
10. Young EF, Smilenov LB, Lieberman HB, Hall EJ. Combined Haploinsufficiency and Genetic Control of the G(2)/M Checkpoint in Irradiated Cells. Radiat Res 2012;177(6):743-50.
11. Jeggo P. The role of the DNA damage response mechanisms after low-dose radiation exposure and a consideration of potentially sensitive individuals. Radiat Res 2010;174(6):825-32.
12. Xu B, Kim ST, Lim DS, Kastan MB. Two molecularly distinct G(2)/M checkpoints are induced by ionizing irradiation. Mol Cell Biol 2002;22(4):1049-59.
13. Lobrich M, Jeggo PA. The impact of a negligent G2/M checkpoint on genomic instability and cancer induction. Nat Rev Cancer 2007;7(11):861-9.
14. Deckbar D, Birraux J, Krempler A, Tchouandong L, Beucher A, Walker S, et al. Chromosome breakage after G2 checkpoint release. J Cell Biol 2007;176(6):749-55. ■

Effect of Ionizing Radiation and Estrogen on Cell Adhesion Molecules in Breast Cancer Cells

Gloria M. Calaf[a], Adayabalam Balajee, Debasish Roy[b], and Tom K Hei

Introduction

Cell-cell adhesion is mediated by the cadherin-catenin system and within this system E-cadherin and β catenin are important epithelial adhesion molecules in epithelium as a prerequisite for normal cell function [1]. β catenin as a component of a complex signal transduction pathway may serve as a common switch in central processes that regulate cellular proliferation and differentiation [2]. It is associated with the cytoplasmic portion of E-cadherin necessary for the function of E-cadherin as an adhesion molecule. Loss of E-cadherin–β-catenin adhesion is an important step in the progression of many epithelial malignancies [1-7]. E-cadherin/alpha-catenin complex has a role in modulating cell-cell and cell-matrix adhesive properties of invasive colon carcinoma and there is an interaction of alpha-actinin with the cadherin/catenin cell-cell adhesion complex via alpha-catenin [5]. Frequent alterations have been found in E-cadherin, alpha and beta-catenin expression in human breast cancer cell lines [8].

Integrins are not considered to be bonafide oncogenes or tumor suppressors, but their expression levels are altered by transformation and breast cancer cells exhibit altered levels of integrin expression [3]. Integrin receptors are cell adhesion molecules that mediate primarily cell-matrix interactions, being localized to focal contacts, or in the case of the alpha6beta4 integrin heterodimer, to hemidesmosomes [5].

Cell-cell adhesion molecules include E-cadherin in adherens junctions and desmocollin (DSC) glycoproteins in desmosomes [6]. Desmosomes are sites of adhesion between adjacent cells in layers of epithelia, as well as in some non-epithelial tissues, and play an important role in the maintenance of tissue structure. Gap junction genes allow direct communication between cells. Loss of gap

[a]Instituto de Alta Investigación, Universidad de Tarapacá, Arica, Chile
[b]Department of Natural Sciences, Hostos College of the City University of New York

junction intercellular communication (GJIC) between cancer cells is a common characteristic of malignant transformation. Markers employed to differentiate between cell phenotypes are components of desmosomes such as Desmocollin 1-3 (DSC). These cell adhesion molecules are transmembrane proteins of the cadherin family that form the adhesive core of desmosomes. Desmosomal proteins such as DSC3 are integral to the maintenance of tissue architecture, and loss of these components leads to a lack of adhesion and a gain of cellular motility. DSC3 expression is down-regulated in breast cancer cell lines and primary breast tumors. Gamma-catenin is required for its high affinity binding to the cytoplasmic domains of E-cadherin and desmosomal cadherin, and the tumor suppressor APC protein [3].

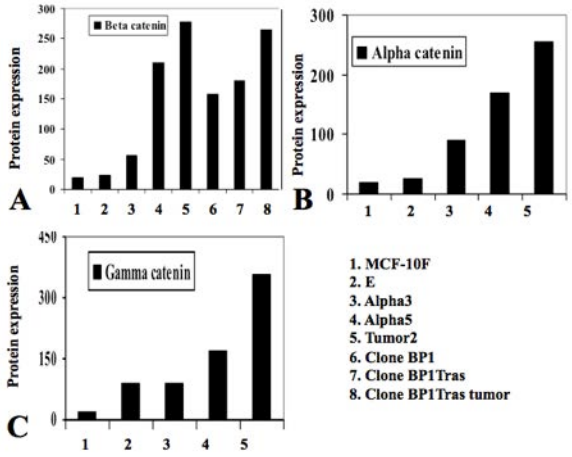

Figure 1. *Protein expression determined by immunofluorescent staining quantified by confocal microscopy after staining for A) Beta catenin, B) Alpha catenin and C) Gamma catenin in 1) MCF-10F, 2) Estrogen (E), 3) Alpha3, 4) Alpha5, 5) Tumor2, 6) Clone BP1, 7) BP1Tras and 8) BP1Tras Tumors.*

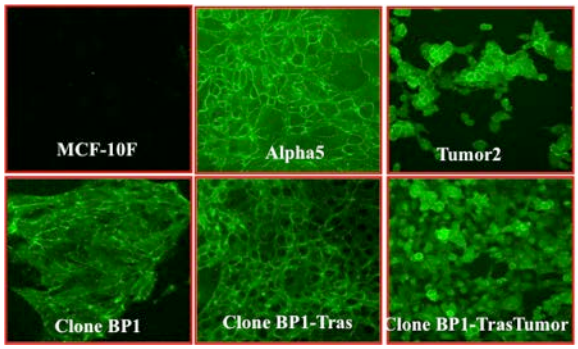

Figure 2. *Representative images of protein expression of Beta catenin in MCF-10F, Alpha5, Tumor2, Clone BP1, BP1Tras and Clone BP1Tras Tumor cell lines.*

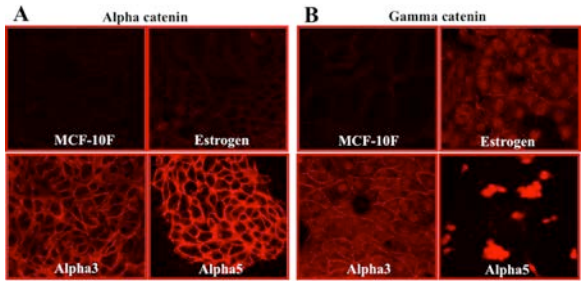

Figure 3*. Representative images of protein expression of A) Alpha catenin and B) Gamma catenin in MCF-10F, Estrogen, Alpha3 and Alpha5 cell lines.*

In vitro model systems have been used to study initiation and transformation in cancer, and they provide a unique opportunity for studying proteins involved in breast cancer [7]. The human breast epithelial cell line MCF-10F, spontaneously immortalized and derived from the breast tissue, has the morphological characteristics of a normal breast epithelial cell line [8]. The aim of this work was to study the effect of radiation and estrogen on cell adhesion molecules in a breast cancer cell model [9].

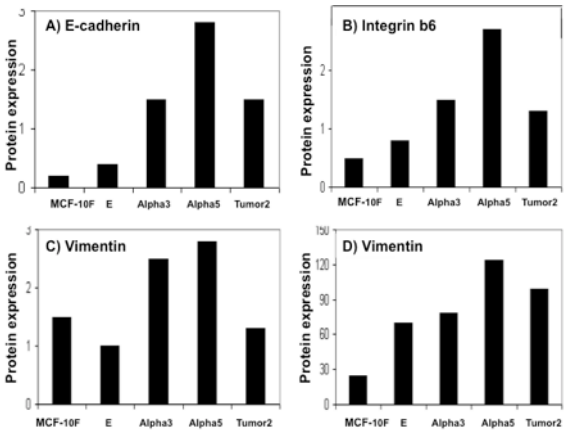

Figure 4. *Protein expression in MCF-10F, Estrogen (E), Alpha3, Alpha5 and Tumor2 cells determined by peroxidase staining of A) E-cadherin, B) Integrin b6 and C) Vimentin. D) immunofluorescent staining of Vimentin.*

Results and Conclusions

These studies analyzed several cell adhesion molecules altered by radiation and estrogen in a breast cancer progression model. We confirmed the reported significance of the E-cadherin/beta-catenin complex in breast cancer [1]. Beta catenin, alpha and gamma catenin expression were significantly ($P<0.05$) greater in Alpha5 and Tumor2 than MCF-10F, Estrogen and Alpha3 cell lines as seen by immunofluorescent studies (Figure 1). Representative images are seen in Figures 2 and 3. Nakopoulou *et al.* [2] reported that abnormal alpha-catenin expression in invasive breast cancer correlates with poor patient survival. E-Cadherin, Integrin b6 and Vimentin protein expression were significantly ($P<0.05$) greater in Alpha5 than MCF-10F, Estrogen and Alpha3 cell lines. However, Tumor2 showed decreased protein expression in comparison to Alpha5 (Figure 4). Representative images of E-Cadherin, Integrin b6 and Vimentin protein expression are seen in Figure 5.

Differential gene expression analyzed using Affymetrics microarrays (Figure 6) showed several genes involved in cellular adhesion functions (Figure 7). In pairwise comparisons, the MCF-10F cell line was not

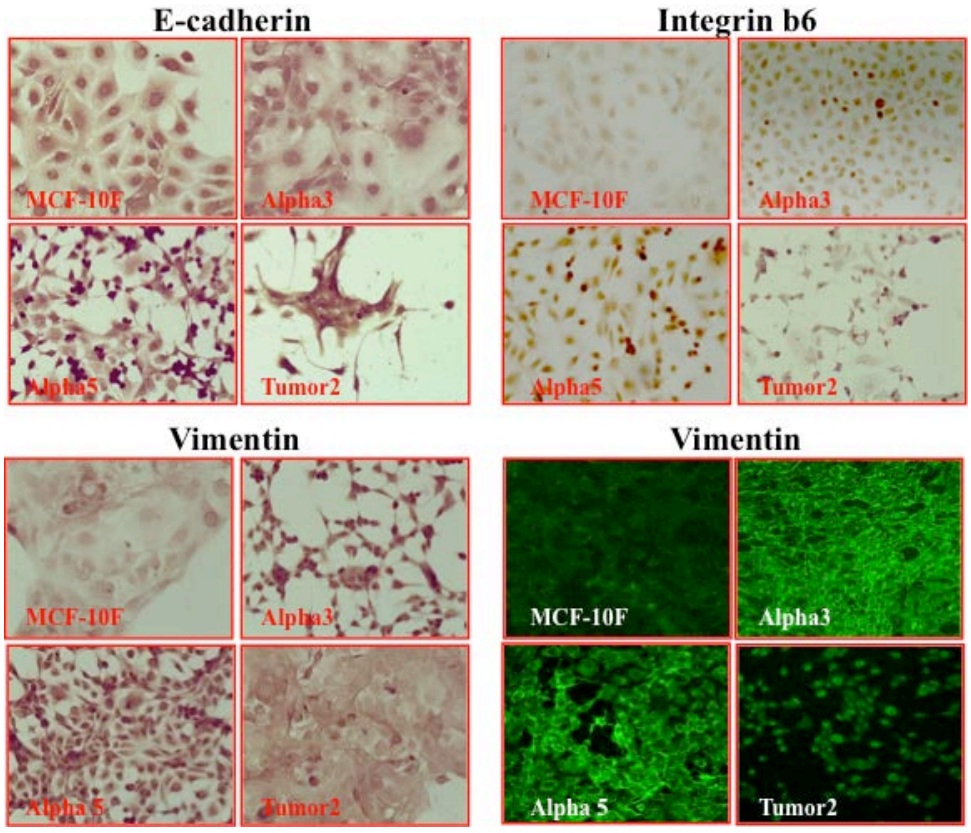

Figure 5. *Protein staining in MCF-10F, Alpha3, Alpha5 and Tumor2 cell lines using peroxidase detection A) E-cadherin, B) Integrin b6 and C) Vimentin. D) immunofluorescent staining of Vimentin protein in the same cell lines.*

significantly different from the Estrogen cell line in terms of E cadhein expression (Figure 7A). The Estrogen cell line was also not different from the Alpha5 cell line. There was a decrease in gene expression in MCF-10F/Alpha3, however. There was also an increase in gene expression in Alpha3/Alpha5, Alpha3/Tumor2 and Alpha5/Tumor2.

Integrin b6 gene expression (Figure 7B) showed no difference in MCF-10F/Estrogen, but decreased expression in MCF-10F/Alpha3, as well as in the Estrogen/Alpha5 cell line comparison. There was no difference between Alpha3/Alpha5, and an increase in Alpha5/Tumor2 as well as in Alpha3/Tumor2.

MCF-10F/Alpha3 and Estrogen/Alpha5 cell line comparisons were made. There was a decrease in Vimentin gene expression between Alpha3/Alpha5, Alpha5/Tumor2 and Alpha3/Tumor2.

Figure 7D shows differential expression of a gene for a Gap Junction protein. There was no difference between MCF-10F/Estrogen, an increase in MCF- 10F/Alpha3, Alpha3/Tumor2 and Alpha5/Tumor2.

Expression of DSC3 (Figure 7E) gene expression decreased in MCF-10F/Alpha3 and Estrogen/Alpha5 cell line comparisons. There was an increase in DSC3 gene expression in MCF-10F/Estrogen, Alpha3/Alpha5, Alpha5/Tumor2, and Alpha3/Tumor2. There was no

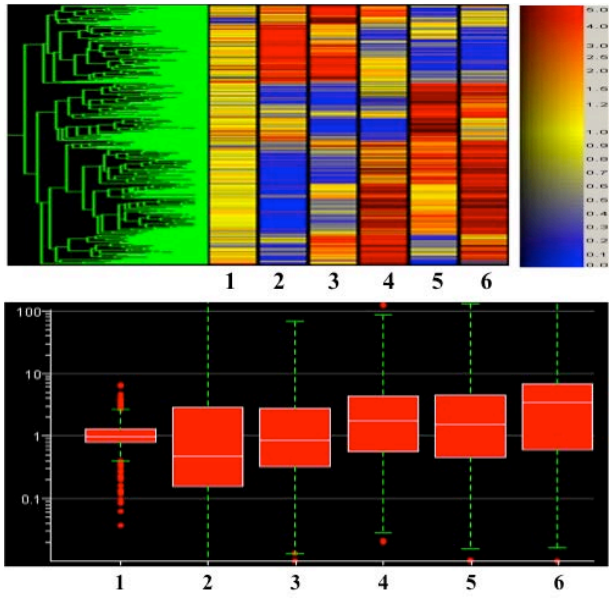

Figure 6. *Heatmap of Affymetrix array (U133A) data comparing the following cell lines: **1)** MCF-10F/Estrogen, **2)** MCF-10F/Alpha3, **3)** Estrogen/Alpha5, **4)** Alpha3/Alpha5, **5)** Alpha5/Tumor2 and **6)** Alpha 3/Tumor2. Red indicates higher expression in the first cell line, blue lower expression, and yellow indicates equal expression in both cell lines (top panel). The box plot summarizes the range of differential gene expression in the same pairwise cell line comparisons (lower panel).*

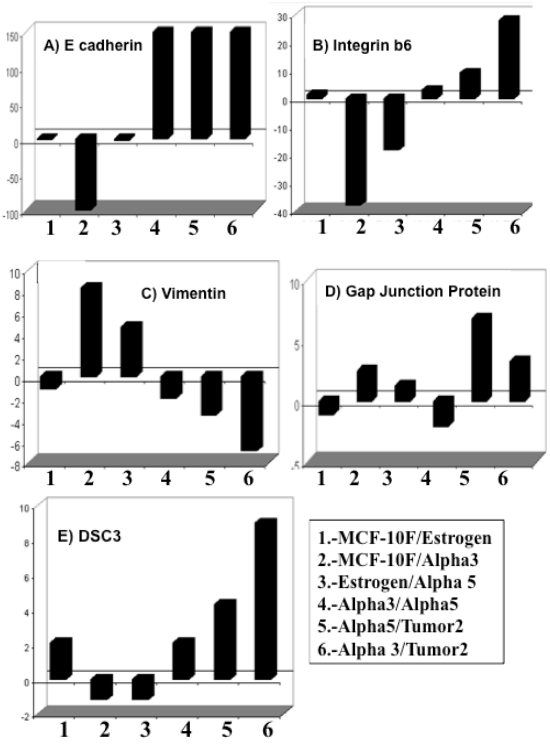

Figure 7. *Differential gene expression of A) E-cadherin, B) Integrin b6, C) Vimentin, D) Gap Junction protein and E) Desmocollin (DSC3) derived from Affymetrix array U133A data comparing the following cell lines: 1) MCF-10F/Estrogen, 2) MCF-10F/Alpha3, 3) Estrogen/Alpha5, 4) Alpha3/Alpha5, 5) Alpha5/Tumor2 and 6) Alpha3/Tumor2.*

significant difference between MCF-10F and E cell line; E/Alpha5 and Alpha3 /Alpha5 cell line, an increase in Alpha3 and Alpha5, Alpha5/Tumor2 and Alpha3/Tumor2. It can be concluded that cell-to-cell adhesion is mediated by the cadherin-catenin system and that adhesion molecules are important for malignant transformation.

References

1. Lim SC and Lee MS: Significance of E-cadherin/beta-catenin complex and cyclin D1 in breast cancer. *Oncol Rep* **9(5):** 915-928, 2002.
2. Nakopoulou L, Gakiopoulou-Givalou H, Karayiannakis AJ, Giannopoulou I, Keramopoulos A, Davaris P and Pignatelli M: Abnormal alpha-catenin expression in invasive breast cancer correlates with poor patient survival. *Histopathol* **40(6):** 536-546, 2002.
3. Ozawa M, Terada H and Pedraza: The fourth armadillo repeat of plakoglobin (gamma-catenin) is required for its high affinity binding to the cytoplasmic domains of E-cadherin and desmosomal cadherin Dsg2, and the tumor suppressor APC protein. *J Biochem* **118(5):** 1077-1082, 1995.
4. Breen E, Steele G Jr and Mercurio AM: Role of the E-cadherin/alpha-catenin complex in modulating cell-cell and cell-matrix adhesive properties of invasive colon carcinoma cells. *Ann Surg Oncol* **2(5):** 378-385, 1995.
5. Knudsen KA, Soler AP, Johnson KR and Wheelock MJ: Interaction of alpha-actinin with the cadherin/catenin cell-cell adhesion complex via alpha-catenin. *J Cell Biol* **130(1):** 67-77, 1995.
6. Takayama T, Shiozaki H, Shibamoto S, Oka H, Kimura Y, Tamura S, Inoue M, Monden T, Ito F and Monden M: Beta-catenin expression in human cancers. *Am J Pathol* **148(1):** 39-46, 1996.
7. Pierceall WE, Woodard AS, Morrow JS, Rimm D and Fearon ER: Frequent alterations in E-cadherin and alpha- and beta-catenin expression in human breast cancer cell lines. *Oncogene* **11(7):** 1319-1326, 1995.
8. Soule HD, Maloney TM, Wolman SR, Peterson WD Jr, Brenz R, Mc Grath CM, Russo J, Pauley RJ, Jones RF and Brooks SC: Isolation and characterization of a spontaneously immortalized human breast epithelial cell line. MCF-10. *Cancer Res* **50(18):** 6075-6086, 1990.
9. Calaf GM, Hei TK. Establishment of a radiation and estrogen-induced breast cancer model. *Carcinogenesis* **21 (4):** 769-776, 2000. ■

(l to r): Dr. Tom Hei, Mr. Carl Elliston, Dr. David Brenner, Dr. Debra Wolgemuth, Dr. Norman Kleiman, Dr. Charles Geard

Short and Longer-term Effects of Gamma Radiation on Endothelial Barrier Function: Uncoupling of PECAM

Preety Sharma, Thomas Templin, and Peter Grabham

An increase in vascular permeability is a common event that follows radiotherapy and is considered to be a critical element in the development of radiation-associated complications of edema and subsequent fibrosis. In the brain, radiotherapy patients may suffer long-term effects including vasculopathy, stroke, white matter damage, necrosis, and memory loss. These late effects are preceded by early changes in blood–brain barrier (BBB) permeability, increased leukocyte-endothelial interactions, and astrogliosis. The molecular mechanisms of radiation effects on the human endothelial barrier remain poorly understood.

We have previously investigated the effect of ionizing radiation on angiogenesis and DNA damage in human endothelial cultures [1, 2]. In the present study, we investigated the effects of radiation on human endothelial barriers using cultured human primary brain microvascular endothelial cells (HBMEC) and large vessel derived human endothelial cells (HUVEC). We assessed the permeability of these two types of endothelial barrier using 3 endpoints: 1) transendothelial electrical resistance (TEER), 2) the passage of tracer molecules through the barrier, and 3) localization of the actin cytoskeleton, adhesion proteins, adherens junction proteins and tight junction proteins.

Development of endothelial barriers

First we used these endpoints to find the best culture conditions for the development of impermeable endothelial barriers. For TEER, the cells were seeded on the substrate in electrode arrays and monitored by recording the TEER at a frequency of 4000 Hz. Confluency was observed when the resistance reached 1000-1200 Ωcm^2 at 15-20 hours. Continued culturing induced more differentiated monolayers. At over 60 hours post plating the properties of the monolayers were consistent with an impermeable endothelial barrier. TEER values peaked at 1850 - 2000 Ωcm^2 for HBMEC and ~ 1600-1750 Ωcm^2 for HUVEC. The cells had the typical 'cobblestone' morphology of less motile cells and there were no dividing cells. Adherens and tight junction proteins were present at the cell borders and permeability to tracer molecules (10 kDa dextran and 70 kDa ovalbumin) was very low.

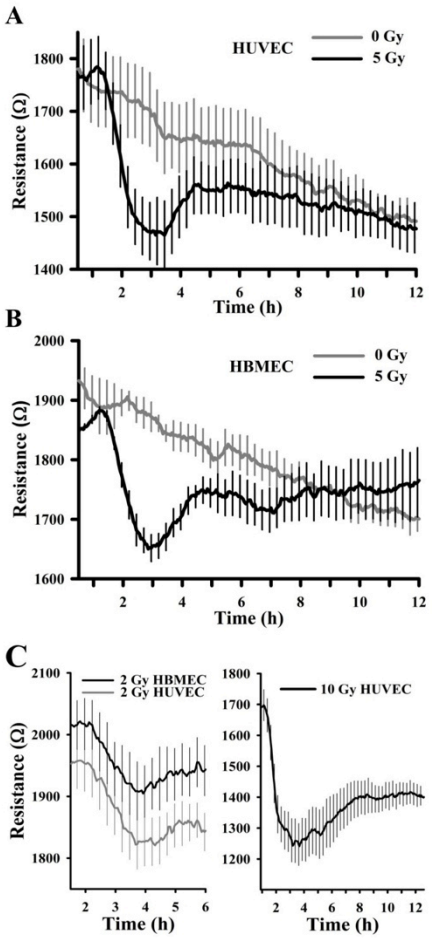

***Figure 1**. Effect of gamma radiation on transendothelial resistance. The electrical resistances across HUVEC (panels A, C) and HBMEC (panels B, C) monolayers after irradiation with 5 Gy γ-rays are shown. Curves show averages of 4 technical repeats, and error bars indicate SEMs of every 5th resistance measurement. γ-irradiation leads to a pronounced dip in electrical resistance at about 3 h after irradiation.*

Effects of gamma radiation on TEER

The effects of radiation on the permeability of HBMEC and HUVEC barriers was assessed by TEER measurements from 0 to 12 hours after irradiation with 0,

2, 5, or 10 Gy gamma rays. At all doses tested, a rapid and transient decrease in resistance was observed to peak at 3 hours post irradiation (Figure 1). The range of the resistance drop was dose dependent. At 2 Gy the drop in resistance was around 100 Ωcm^2 (5%) (Figure 1C). At 5 Gy the drop in resistance was around 200Ω cm^2 (Figure 1A and 1B) and at 10 Gy the drop in resistance was around 450 Ωcm^2 (Figure 1C). Both HUVEC and HBMEC responded to radiation dose with similar kinetics and magnitude.

Effects of gamma radiation on the morphology of endothelial barriers.

To determine what morphological changes in the endothelial barrier might be associated with a transient drop in TEER, we investigated phenotypic changes in the cells at the time of lowest electrical resistance. Parallel cultures were fixed at 3 hours after irradiation and stained with a whole cell stain (Figure 2). Control cultures showed a confluent monolayer of cells with almost complete substrate coverage. Treatment with 5 Gy gamma radiation resulted in no general cell shape change but gaps or holes appeared in the monolayer. A small proportion of cells had detached and floated into the media creating spaces in the monolayer (Figure 2 C-D). Both HUVEC and HBMEC cell types showed similar responses. At 6 hours post irradiation no empty cell spaces were visible for either cell type: presumably the remaining cells had migrated to fill in the spaces (Figure 2E - G). The number of cells per unit area had also reduced.

Effects of gamma radiation on junction proteins

To better understand the events following irradiation leading to cell detachment and the generation of spaces in the endothelial monolayers, we examined the localization of key proteins involved in maintaining the endothelial barrier. These include: the actin cytoskeleton, the adherens junction protein - VE Cadherin, the tight junction protein - ZO-1 and the cell adhesion molecule – Platelet endothelial cell adhesion molecule (PECAM). Each cell type was grown in parallel cultures and fixed 3 hr and 6 hr after either sham irradiation or a dose of 5 Gy gamma radiation. The actin cytoskeleton, VE Cadherin and ZO-1, showed no appreciable difference in localization at 3 hours after irradiation (not shown). PECAM localization however, appeared to have been disrupted for both cell types since the normal pattern of staining around and between the cell borders had become discontinuous in discrete areas (Figure 3). Observations indicated that complete absence of PECAM on an entire cell boundary of a cell correlated with cell detachment and a gap in the monolayer. A cell was often missing at the center of small areas where PECAM was missing. We examined the colocalization of ZO-1 and PECAM to determine the relationship between loss of tight junctions and the loss of PECAM. In the cells with partial loss of PECAM tight junctions often remained intact, as indicated by the presence of ZO-1(Figure 3 F). PECAM is lost more extensively and is thus likely to precede the loss of tight junctions

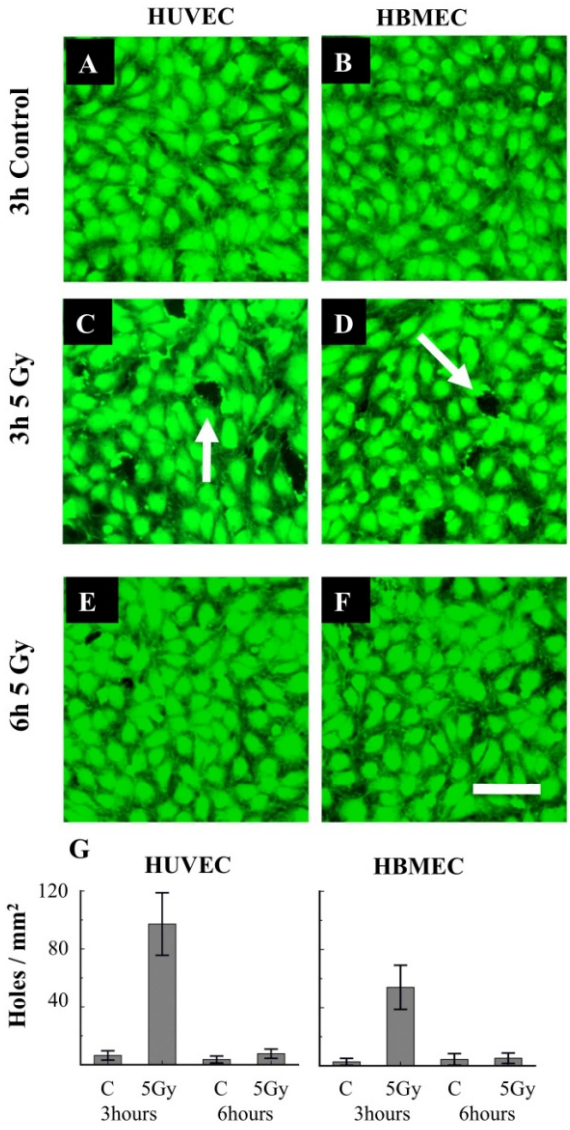

Figure 2. *Effects of gamma radiation on HUVEC and HBMEC monolayers at 3 hr and 6 hr post radiation. Control cultures exhibit intact monolayers (A and B). Irradiated cells exhibit gaps in the monolayer indicated by arrows (C and D). By 6 hr post irradiation gaps in the monolayer were no longer visible (E and F). Bar = 100 μm. (G) Quantitation of gaps. Error bars = SD.*

Uncoupling of PECAM

Low temperatures are well known to cause changes in the cytoskeleton and relax homophilic binding of cell adhesion molecules. We utilized this phenomenon to examine further the uncoupling of PECAM in response to gamma radiation. Relaxing these homophilic bonds with low temperatures changes the cell shape to a rounded

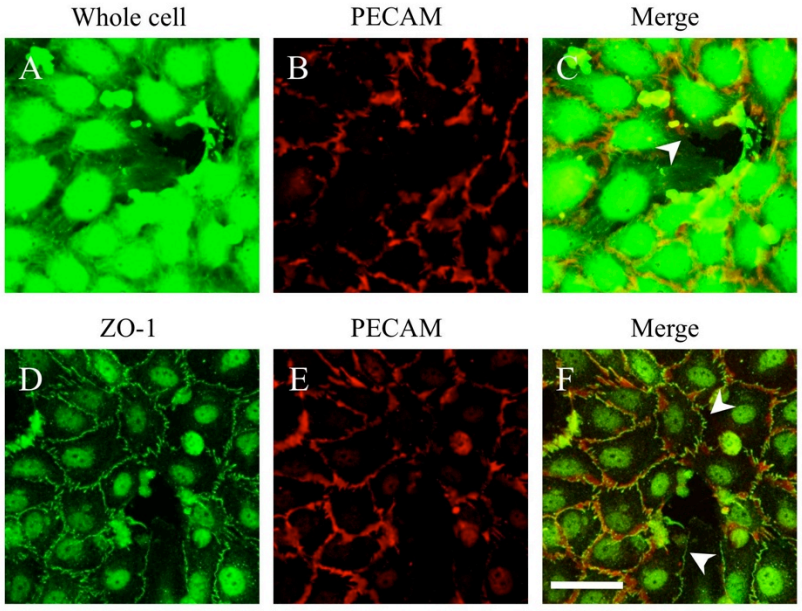

Figure 3. *Loss of PECAM is associated with gaps in monolayers, but not with loss of tight junctions. HBMEC barrier 3 hours after exposure to 5 Gy gamma radiation. A-C stained for the whole cell (DTAF – green) and PECAM (red). At the center of a region where PECAM is lost a cell has detached. Loss of PECAM is associated with the appearance of gaps between cells (arrowhead C). D-F stained for the tight junction protein – ZO-1 (green) and PECAM (red). ZO-1 without associated PECAM can be seen (arrowheads F). Bar = 50 μm.*

morphology and renders the binding of the adhesion molecule visible for the assessment of further uncoupling. fifteen minutes incubation at 15ºC before fixation was sufficient to cause cell rounding and the relaxation of homophilic PECAM bonds such that the adhesion molecule had become hyper-extended or stretched like gum between the cells (Figure 4A and B). When cells were irradiated with 5 Gy gamma rays followed by fifteen minutes incubation at 15ºC, an additional effect of the radiation on PECAM was observed. The cells rounded as in Figure 4B, but the adhesion protein was no longer stretched between cells, it was severed leaving PECAM localized to the edge of the cells and larger gaps between cells (Figure 4C). Thus, gamma radiation had an additive effect with low temperatures resulting in a more complete uncoupling of PECAM between cells.

Permeability changes

Permeability of the endothelial barrier to various molecules is the physiological endpoint and the most direct measurement of barrier function. We therefore determined the traversal of fluorescent tracers of two different sizes (10 kDa and 70 kDa) across the monolayer in transwell inserts.

Tracer molecules were added to the top wells and permeability determined by sampling and detection of tracer molecules in the bottom wells. Initially we monitored the traversal of tracer molecules over the first 6 hours, but found little difference in permeability

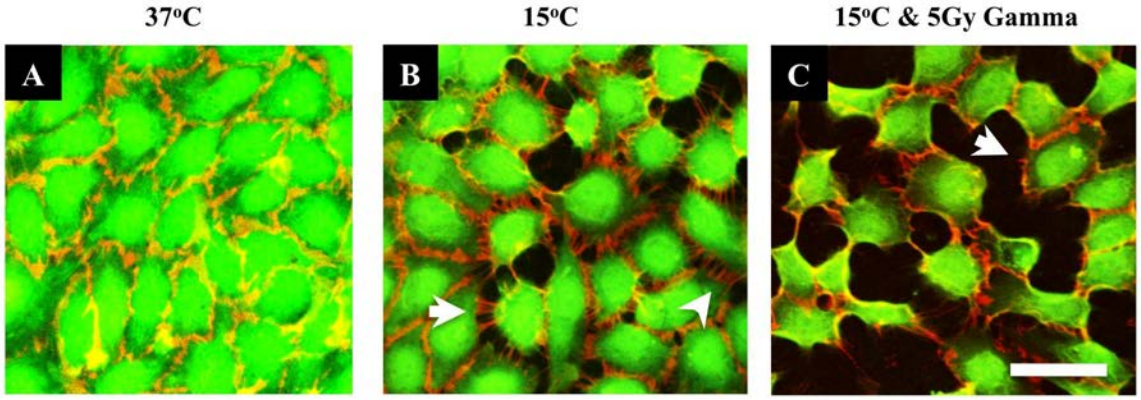

Figure 4. *Uncoupling of PECAM in response to low temperature and gamma rays. Control and 5 Gy irradiated cells were fixed 3 hours after irradiation and stained for the whole cell (green) and for PECAM (red). (A) When fixed at 37 °C the cells had an intact monolayer with PECAM bordering the cells. Incubation for 15 minutes at 15°C before fixation (B) resulted in cell contraction creating spaces with PECAM stretched or hyperextended between the cells (arrowheads). When irradiated cells were fixed at 15°C (C) the adhesion protein was no longer stretched between cells. It was severed leaving PECAM localized to the edge of the cells (arrowhead). Bar = 50 μm.*

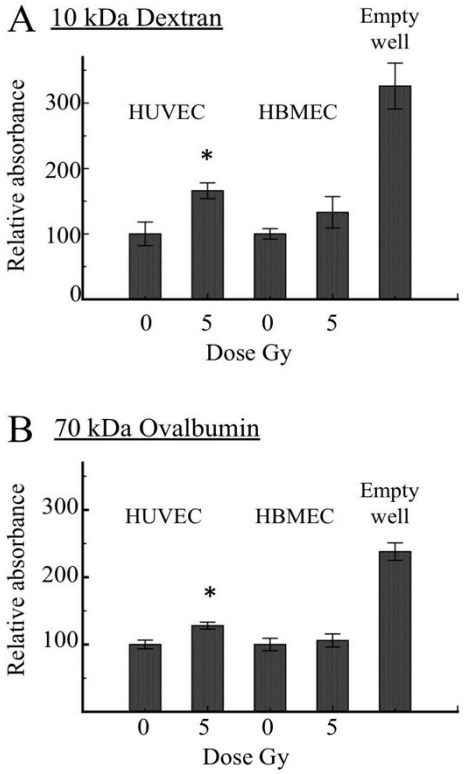

Figure 5. *Irradiation induced increase in permeability to fluorescently labeled 10 kDa dextran and 70 kDa ovalbumin tracers. Tracer molecules were added to the top well of transwell inserts one hour after irradiation with 5 Gy gamma rays and spectrofluorometer measurements made at 24 hr on both control and irradiated cultures. A significant increase in the traversal of 10 kDa dextran and 70 kDa ovalbumin was observed at 24 hr in irradiated HUVEC monolayers but not in HBMEC.*

compared to controls over this time period. The temporary effect of lowered resistance, gaps in the monolayer, and loss of PECAM did not translate to increased permeability in this assay, the sensitivity of which was not sufficient (not shown). The extremely tight barrier, however, allowed us to monitor permeability to these molecules over a period of 24 hours after irradiation and the addition of tracer molecules to the top well. Control samples showed only 30% (10 kDa dextran) or 40% (70 kDa ovalbumin) traversal compared to wells without cells (Figure 5). A significantly increased permeability to dextran (10 kDa) and at a lower level to 70 kDa ovalbumin was observed in HUVEC over 24 hrs post irradiation. HBMEC barriers, which have been consistently less compromised by gamma radiation, did not show any significant increase in permeability.

In conclusion, we have shown that doses of gamma rays as low as fractionated therapy doses (2 Gy) cause a reversible dip in TEER, which is coupled with the loss of cells from the endothelial barrier. This acute effect is associated with uncoupling of the cell adhesion molecule PECAM, but not tight junctions. Although TEER was not reduced 24 hours after irradiation compared to controls, permeability of dextran in HUVEC barriers was in fact reduced over this time. It is likely that the acute effects of gamma radiation cause a longer-term weakening of the endothelial barrier.

This work was supported by NASA grants NNJ09ZSA001N and NNJ11ZSA001N.

References

1. Grabham P.W, B. Hu, P. Sharma, and C. Geard. (2010) Effects of ionizing radiation on 3-dimensional human vessel models: Differential effects according to radiation quality and cellular development. *Radiation Research* **175**: 21-28.

2. Grabham P.W, Bigelow A and C. Geard (2012) DNA damage foci formation and decline in two-dimensional monolayers and in three-dimensional human vessel models: Differential effects according to radiation quality. *International Journal of Radiation Biology*. **88**: 493–500. ■

(l to r): Dr. Sunirmal Paul, Dr. Sally Amundson, Dr. Eric Hall, Ms. Catherine Geard, Dr. Charles Geard, Dr. Gerhard Randers-Pehrson.

Transient Radiation Induced Changes in Human Coronary Endothelium

Erik F. Young and Lubomir B. Smilenov

Introduction

Several different radiotherapy interventions in humans admit energy to the heart [1, 2]. More recently, interest in the effects of occupational, low dose irradiation on the heart has been piqued with particular attention drawn to the paucity of information available on the radiation sensitivities of the various subcompartments of the heart [3, 4]. At higher doses, overt damage to the relatively radioresistant myocardium is seen to occur [5, 6], but at doses that are closer to therapeutic values, radiation induced heart disease is believed to be a disorder of the endothelial cells in the heart.

Beyond effects on contractility and paracrine signaling, which are ablated in radiation response [7-11], radiation also causes overt changes in barrier function to the extent that dyes and tracers can flow out of permeabilized vasculature [12]. The ramifications of radiation induced barrier failure in smaller vessels have been studied and the result appears to be a modified immune response resulting in the deposition and remodeling of the extracellular matrix leading to fibrosis [13, 14]. In the heart, ectopic remodeling of the matrix will have deleterious effects on cardiac function [15, 16]. Failure of the endothelial barrier can inappropriately admit soluble factors from blood, which, once retained in the intimal space of great vessels, can serve as stimulants for leukocyte homing and smooth muscle cell proliferation, resulting in an atherosclerotic lesion [17-19]. Such lesions are also induced in young radiotherapy patients with no pre-existing atherosclerosis [20]. The mechanism underlying the genesis of radiation induced lesions and cardiac fibrosis is of great interest.

We adopted a highly sensitive bioelectric assay for assessment of radiation induced changes in endothelial monolayers. We seeded primary human coronary endothelial cells on planar gold arrays and employed alternating current of less than 45 μA at a range of frequencies from 62 to 60 x 10^3 Hz. This modality evolved from apparatus originally designed to prove the existence of superconducting electron tunneling in insulators by the Nobel Laureate Ivar Giaver. The resultant biologically oriented technology is known by the name Electric Cell Substrate Impedance Sensing (ECIS). The method is exquisitely sensitive, successfully reporting micromovement in confluent monolayers and cellular changes in response to fluctuations in ambient CO_2 of ± 0.5 % in tissue culture incubators [21, 22]. The transmonolayer impedance of endothelial cells, in particular, responds robustly when treated with compounds known to perturb endothelial barrier function, including thrombin, histamine and calcium chelating agents. A model has been tested allowing for electronic assessment of permeability changes in response to these stimuli [23-25]. Importantly this technology allows for continuous cell monitoring over a considerable timecourse. The goal of this work was to assess radiation induced barrier changes in human coronary endothelial monolayers using an impedance based micromorphometry technique. Particular attention was paid to rearrangements of the cytoskeleton, which could alter the barrier function of the tissue.

Impedance measurements

All measurements were performed using an Applied Biophysics ECIS Zθ instrument, which allows measurement of complex impedance of cell monolayers over a range of frequencies. For the impedance related experiments, "8W10E+" type ECIS arrays (Applied Biophysics, Troy, NY) were coated with extracellular matrix substrate by addition of 400 μL of a Rat Tail collagen 1 solution to each well. This array type (Figure 1A) allows for measurements at 40 regularly spaced working electrodes over the 0.8 cm^2 surface of the culture with an interdigitated array of counterelectrodes forming the other terminus of the circuit. Impedance

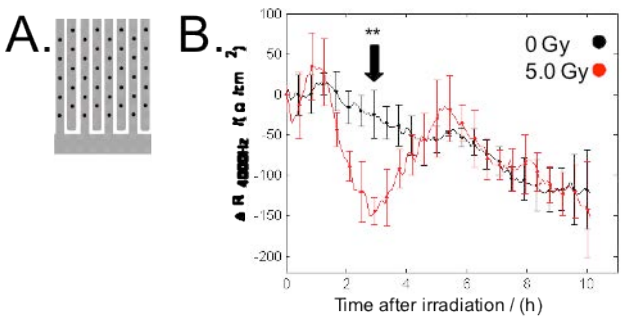

Figure 1. *Transmonolayer impedance measurement of irradiated HCAEC monolayers. Cells were seeded on collagen-coated, interdigitated 40-point gold planar electrode arrays (A). The change in the real ohmic component of impedance after irradiation is plotted (B) with the average and standard deviation of technical triplicates shown. HCAEC monolayers exhibit a transient and statistically significant decrease in resistance 3 hours after irradiation.*

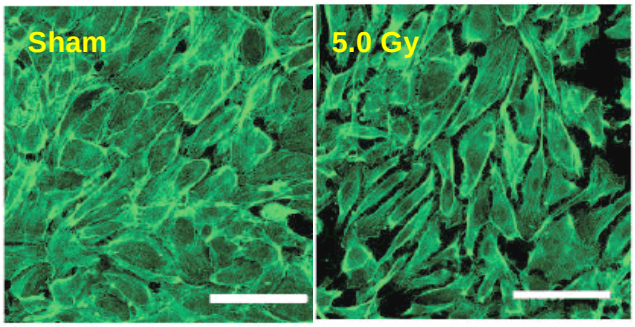

***Figure 2**. Cytoskeletal rearrangement in HCAEC monolayers after irradiation. Cells were seeded on collagen-coated glass coverslips and allowed to mature into monolayers for 18-20 h. Mature monolayers were irradiated with 5.0 Gy γ radiation and subsequently fixed and stained 3 h after irradiation with fluorescent phalloidin. HCAECs exhibit cytoskeletal rearrangement with some gaps between the cytoskeletons of neighboring cells as compared to sham irradiated controls. (Scale bars = 100 μm).*

measurements were made at 11 frequencies with an ECIS Zθ instrument at 5-minute intervals and logged on a command laptop computer running proprietary ECIS software.

Results

When competent human coronary arterial endothelial (HCAEC) monolayers are irradiated with 5.0 Gy, a small initial rise in the resistance values precedes a statistically significant (P = 0.001) drop, which appears at 3 hours post irradiation (Figure 1B).

Cytoskeletal rearrangement is known to occur in endothelial cells exposed to radiation of 15-20 Gy [26]. We conducted a survey of the cytoskeleton in HCAECs at various times after irradiation, including the 3 hour time point at which the impedance measurements suggested such a rearrangement might take place. In comparison with sham irradiated controls, phalloidin stained preparations of irradiated HCAECs showed cells with a slightly more polygonal shape with bundling of actin fibers at the periphery of the cells and a notable retraction from neighboring cells (Figure 2). Taken together, these findings reveal a transient rearrangement of the cytoskeleton in response to radiation, which coincides with a loss in barrier function as assessed by ECIS.

Discussion

Several studies have shown that endothelial function is compromised after high doses of radiation over 15 Gy [7-11, 17]. Since the relative sensitivities of cardiac substructures to radiation damage have not been assessed, we studied the coronary endothelium. It is also apparent that the details of endothelial dysfunction in radiation induced heart disease remain unclear. We chose to investigate the changes in coronary endothelial function using ECIS. This is a unique, highly sensitive technology, which allows us to monitor changes in live cell monolayers for days after irradiation.

We chose to irradiate HCAEC monolayers with a dose of 5.0 Gy, as this dose constituted the threshold of detection for cytoskeletal rearrangement in a survey of irradiated endothelia in the literature [26]. The transmonolayer resistance measurements in our studies are made at 4 kHz as this frequency exhibits the greatest response seen in a multifrequency spectrum for our monolayers in comparisons of early and mature time points.

The coronary endothelium is a component of a complete cardiopulmonary system. The ultimately detrimental effect of radiation induced heart disease is reduction of cardiac function. Irradiation of the thorax for diagnostic or therapeutic reasons includes exposure of the lungs, myocardium, pericardium, great vessels and coronary circulation. Radiation induced effects on any of these components can cause feedback into others in a decompensating feedback loop resulting in failure [27]. We anticipate that future studies will further detail the role of endothelial dysfunction in radiation induced heart disease and that additional sub-compartments of the heart will be assessed for their respective radiation sensitivities.

References

1. Basavaraju SR, Easterly CE. Pathophysiological effects of radiation on atherosclerosis development and progression, and the incidence of cardiovascular complications. Med Phys 2002;29(10):2391-403.
2. Nieder C, Pawinski A, Andratschke NH, Molls M. Does prophylactic breast irradiation in patients with prostate cancer influence cardiac toxicity? J Natl Cancer Inst 2007;99(21):1646-7.
3. Darby SC, Cutter DJ, Boerma M, Constine LS, Fajardo LF, Kodama K, et al. Radiation-related heart disease: current knowledge and future prospects. Int J Radiat Oncol Biol Phys 2010;76(3):656-65.
4. Little MP, Gola A, Tzoulaki I. A model of cardiovascular disease giving a plausible mechanism for the effect of fractionated low-dose ionizing radiation exposure. PLoS Comput Biol 2009;5(10):e1000539.
5. McChesney SL, Gillette EL, Powers BE. Radiation-induced cardiomyopathy in the dog. Radiat Res 1988;113(1):120-32.
6. Powers BE, Thames HD, Gillette EL. Long-term adverse effects of radiation inhibition of restenosis: radiation injury to the aorta and branch arteries in a canine model. Int J Radiat Oncol Biol Phys 1999;45(3):753-9.
7. Allen JB, Sagerman RH, Stuart MJ. Irradiation decreases vascular prostacyclin formation with no concomitant effect on platelet thromboxane production. Lancet 1981;2(8257):1193-6.
8. Furchgott RF, Vanhoutte PM. Endothelium-derived relaxing and contracting factors. Faseb J 1989;3(9):2007-18.

9. Menendez JC, Casanova D, Amado JA, Salas E, Garcia-Unzueta MT, Fernandez F, et al. Effects of radiation on endothelial function. Int J Radiat Oncol Biol Phys 1998;41(4):905-13.
10. Qi F, Sugihara T, Hattori Y, Yamamoto Y, Kanno M, Abe K. Functional and morphological damage of endothelium in rabbit ear artery following irradiation with cobalt60. Br J Pharmacol 1998;123(4):653-60.
11. Soloviev A, Prudnikov I, Tsyvkin V, Tishkin S, Kyrychenko S, Zelensky S, et al. Electrophysiological and contractile evidence of the ability of human mesenchymal stromal cells to correct vascular malfunction in rats after ionizing irradiation. J Physiol Sci 2010;60(2):161-72.
12. Jolles B, Harrison RG. Radiation skin reaction and depletion and restoration of body immune response. Nature 1963;198:1216-7.
13. Baker DG, Krochak RJ. The response of the microvascular system to radiation: a review. Cancer Invest 1989;7(3):287-94.
14. Griem ML, Robotewskyj A, Nagel RH. Potential vascular damage from radiation in the space environment. Adv Space Res 1994;14(10):555-63.
15. Caulfield JB, Norton P, Weaver RD. Cardiac dilatation associated with collagen alterations. Mol Cell Biochem 1992;118(2):171-9.
16. Kim HE, Dalal SS, Young E, Legato MJ, Weisfeldt ML, D'Armiento J. Disruption of the myocardial extracellular matrix leads to cardiac dysfunction. J Clin Invest 2000;106(7):857-66.
17. Aarnoudse MW, Lamberts HB, Dijk F, Vos J, de Vries AJ. Monocytes and radiation-induced atheromatosis in rabbits. Virchows Arch B Cell Pathol Incl Mol Pathol 1984;47(3):211-6.
18. Hoving S, Heeneman S, Gijbels MJ, te Poele JA, Bolla M, Pol JF, et al. NO-donating aspirin and aspirin partially inhibit age-related atherosclerosis but not radiation-induced atherosclerosis in ApoE null mice. PLoS One 2010;5(9):e12874.
19. Hoving S, Heeneman S, Gijbels MJ, te Poele JA, Russell NS, Daemen MJ, et al. Single-dose and fractionated irradiation promote initiation and progression of atherosclerosis and induce an inflammatory plaque phenotype in ApoE(-/-) mice. Int J Radiat Oncol Biol Phys 2008;71(3):848-57.
20. Huff H, Sanders EM. Coronary-artery occlusion after radiation. N Engl J Med 1972;286(14):780.
21. Giaever I, Keese CR. Micromotion of mammalian cells measured electrically. Proc Natl Acad Sci U S A 1991;88(17):7896-900.
22. Lo CM, Keese CR, Giaever I. pH changes in pulsed CO2 incubators cause periodic changes in cell morphology. Exp Cell Res 1994;213(2):391-7.
23. Moy AB, Van Engelenhoven J, Bodmer J, Kamath J, Keese C, Giaever I, et al. Histamine and thrombin modulate endothelial focal adhesion through centripetal and centrifugal forces. J Clin Invest 1996;97(4):1020-7.
24. Moy AB, Winter M, Kamath A, Blackwell K, Reyes G, Giaever I, et al. Histamine alters endothelial barrier function at cell-cell and cell-matrix sites. Am J Physiol Lung Cell Mol Physiol 2000;278(5):L888-98.
25. Tiruppathi C, Malik AB, Del Vecchio PJ, Keese CR, Giaever I. Electrical method for detection of endothelial cell shape change in real time: assessment of endothelial barrier function. Proc Natl Acad Sci U S A 1992;89(17):7919-23.
26. Gabrys D, Greco O, Patel G, Prise KM, Tozer GM, Kanthou C. Radiation effects on the cytoskeleton of endothelial cells and endothelial monolayer permeability. Int J Radiat Oncol Biol Phys 2007;69(5):1553-62.
27. Schultz-Hector S. Radiation-induced heart disease: review of experimental data on dose response and pathogenesis. Int J Radiat Biol 1992;61(2):149-60. ■

(l to r): Ms. Monique Rey, Ms. Mary Coady, Dr. Sally Amundson, Dr. John Ng, Dr. Eric Hall, Dr. Tony Wang, Mr. David Cuniberti, Mr. Robert Morton.

Distinct Mechanisms of the Inhibition of Vasculogenesis by Different Species of Ionizing Particles

Peter Grabham, Preety Sharma and Charles Geard

Travel into space will result in exposure to both low LET (proton) ionizing radiation and high LET (eg. iron ion [Fe]) ionizing radiation. Very little is known about the effects of these types of radiation on the human body. The present study is aimed at understanding the non-cancer effects of space ionizing radiation on the formation and maintenance of blood vessels with particular relevance to neurodegenerative diseases.

We have previously shown that ionizing radiation has damaging effects on the development of vessels and on the structure of mature vessels in 3-D tissue culture models using human umbilical vein (HUVECs) [1] (Figure 1) and that these damaging effects include DNA damage and repair [2].

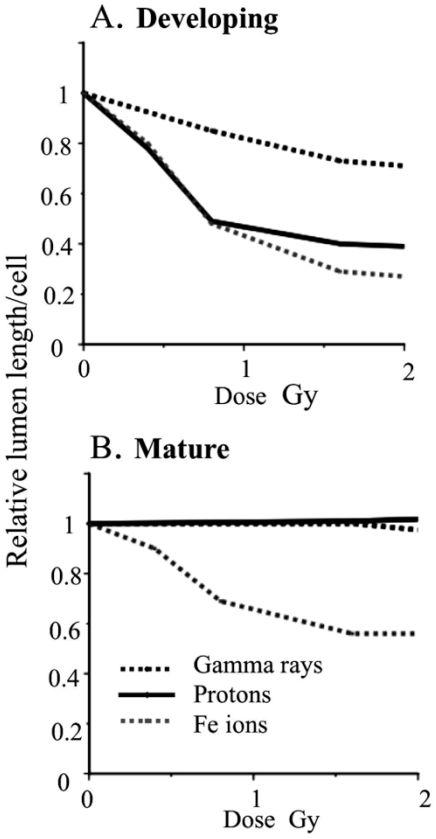

Figure 1. *Combined data for effects of high-energy protons and Fe ions on the mature structure and the development of human vessel tissue models. A. Developing vessels are more sensitive to protons than mature vessels. B. Mature vessels are resistant to low LET protons and gamma rays but not Fe ions.*

For space radiation, high-energy (1 GeV/n) Fe ions were most damaging and caused significant structural loss in both developing and mature vessels at a dose of 0.8 Gy. High-energy (1GeV) protons had no effect on mature vessels up to a dose of 3.2 Gy but did inhibit vessel formation at 0.8 Gy. The relative biological effect (RBE) of Fe ions compared to protons is greater than 4 for mature vessels but only 1 for developing vessels (Figure 1).

The action of low LET protons on developing vessels was surprisingly effective, and this effect on the developing tissue suggests that radiosensitivity might depend on the context of the cell behavior and signal activation. Vessel formation or angiogenesis requires coordinated regulation by multiple signaling pathways. Binding of the cell surface receptors collagen, hFGF-B and hVEGF activates several signaling pathways that regulate the steps required for angiogenesis. Pathways involving the extracellular signaling kinases (ERKs) and Rho GTPases are activated. Differential gene expression occurs and the cytoskeleton is highly dynamic as endothelial cells migrate and form tubes. Under these conditions, low LET protons and photons are able to influence development perhaps by influencing signaling pathways in a distinct way from the effects of heavy ions. Support for this is found in the difference in the morphology of vessels inhibited by each particle (Figure 2). Irradiation is carried out on day 2 of culture and vessels are assayed on day 6. Cells exposed to protons failed to make connections with other cells, cellular processes extended short distances into the gel matrix and terminated in a dead end. Conversely, cells exposed to Fe ions extended cellular processes and made connections to other cells but did not develop a central lumen. This result suggests that protons inhibit motile tip extension whereas Fe ions inhibit a later stage of vasculogenesis when endothelial cells migrate to form a tube. We investigated this hypothesis by looking at the specialized motile tip of the extending cell up to 24 hours after irradiation by each particle (Figure 3). As early as 1.5 hours after exposure we found differences in the actin and microtubule cytoskeletons. At this time the endothelial cells in the matrix are extending cellular processes that

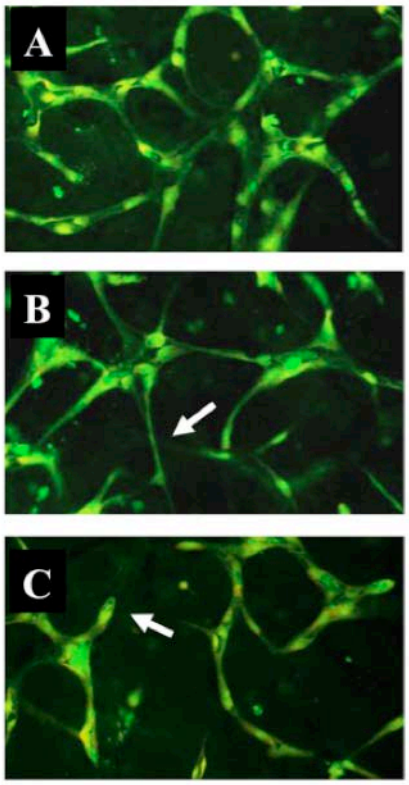

Figure 2. *Morphological differences between vessel development inhibited by Fe ions and protons. A. Control. B. Cells exposed to 1Gy Fe ions make connections but fail to form tubes. C. Cells exposed to 1Gy protons fail to connect but make short tubes with rounded ends.*

are tipped by motile structures penetrating the matrix. Low power images do not show large differences between controls and cultures irradiated with 1 Gy high-energy protons (Figure 3 A and B) although the microtubule staining in the shaft of extending processes appeared to be more concentrated in the control cultures. High power microscopy however, revealed significant differences (Figures 3 C-F). The processes of the control cultures contain tightly bundled microtubules that are associated with motile actin structures. Exposure to 1 Gy of high-energy protons resulted in a significant decrease in the number of these motile tips per cell. Conversely exposure to high-energy Fe ions did not significantly reduce the frequency of motile tips (Figure 3 G). Thus these ionizing radiations induce different responses in the formation of motile structures. Protons inhibit motile structures while Fe ions do not.

Protein kinase C (PKC) has long been known to stimulate angiogenesis and studies have implicated PKC in vessel formation and the effects of radiation. There is evidence that PKC inhibition sensitizes vessel development to gamma irradiation, supporting the notion that radiosensitivity might depend on the context of the cell behavior and signal activation. Also, in support of the involvement of PKC, a dose of 3 Gy gamma radiation can inhibit vessel development in a 2 –dimensional model and

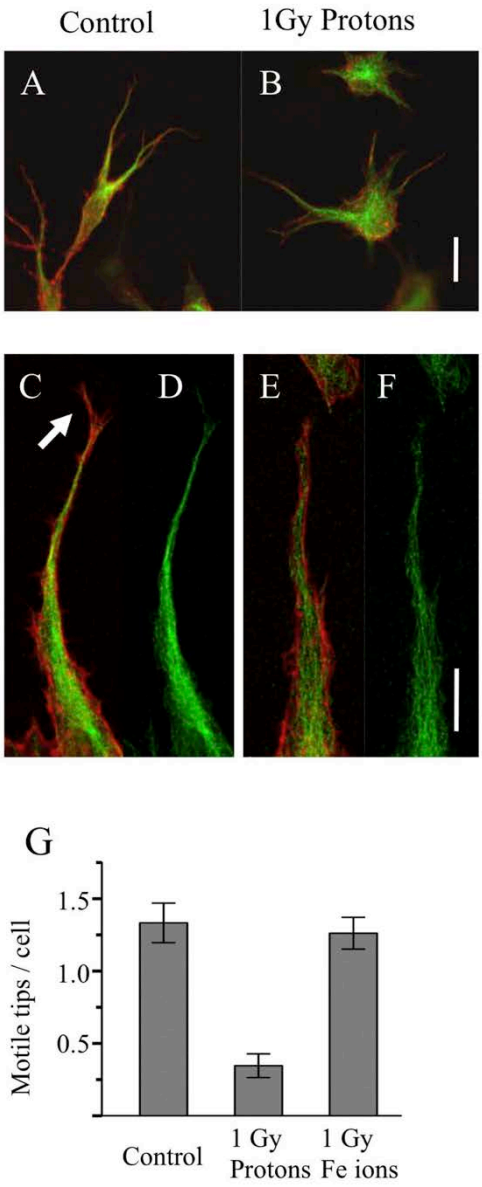

Figure 3. *High-energy protons but not high-energy Fe ions reduce the frequency of specialized motile tips of endothelial cells extending into the matrix. A) and B) low magnification 3-D images (projected onto a single plane) of endothelial cells 1 day after plating and 1.5 hours after sham exposure (A) or exposure to 1Gy 1GeV protons (B). Cultures are stained for microtubules (green) and actin (red). Cells appear similar although microtubules are more concentrated in un-irradiated cultures. Bar=20 μm. C-F) High magnification reveals bundled microtubules and motile actin structures such as filopodia (arrow in C) in controls but not in cells exposed to protons. Bar = 5μm. G) Quantitation reveals that motile tips are inhibited 4-fold by protons but not by 1Gy of 1GeV/n Fe ions.*

PKC inhibition sensitizes vessels to radiation, suggesting that vessel formation is mediated by PKC. We hypothesized that either protons or Fe ions or both might be inhibiting vasculogenesis in our model by inhibiting PKC. Rescue of the capillary phenotype would then be possible by stimulating PKC before irradiation. One day-

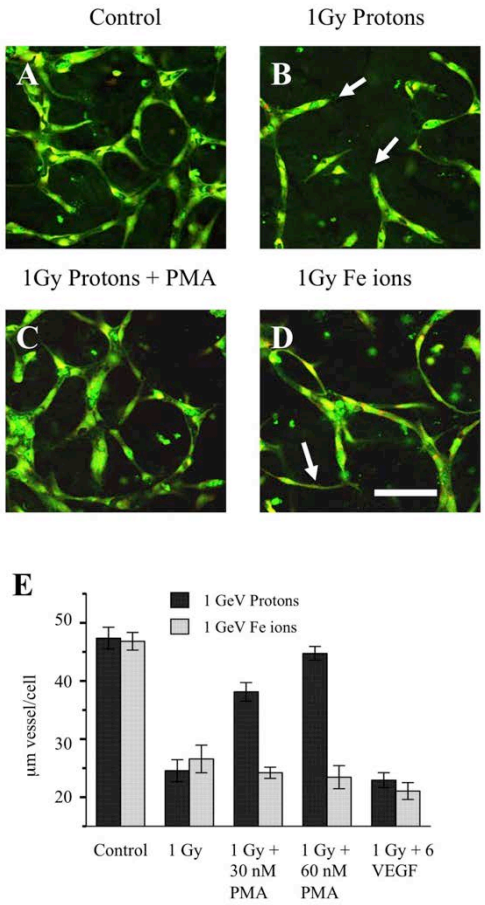

Figure 4. *Rescue of vessel formation in endothelial cultures treated with high-energy protons and Fe ions. Human brain microvascular cells were allowed to begin vessel development for 24 hours. Cultures were then treated with PMA or VEGF 20 minutes before irradiation. 5 days later cultures were fixed and stained for all proteins (green) and for nuclei (red). A. Unirradiated controls show robust vessel formation. B. 1GeV Protons reduce vessel formation. Cellular processes extended short distances into the gel matrix and terminated in a dead end (arrows). C. 30nM PMA restores vessel growth. D. Fe ions inhibit vessel formation but cells still make connections. E. Quantitation of vessels under all conditions. PMA rescues vessel formation inhibited by protons but not Fe ions. VEGF does not rescue vessel formation inhibited by either particle.*

old vessel cultures were treated with 30 nM and 60 nM phorbol ester (PMA) 15 minutes before irradiation with both ions. VEGF was also tested since it is a critical angiogenic factor. After irradiation, the developing vessels were cultured for a further 5 days before fixation and then assayed for capillary formation. Figure 4 shows that stimulation of PKC restored capillary formation in proton treated cultures but not in Fe ion treated cultures. VEGF did not restore capillary formation in cultures irradiated with either protons or Fe ions. Thus, the mechanisms for inhibition of vessel formation by protons and Fe ions must be distinct.

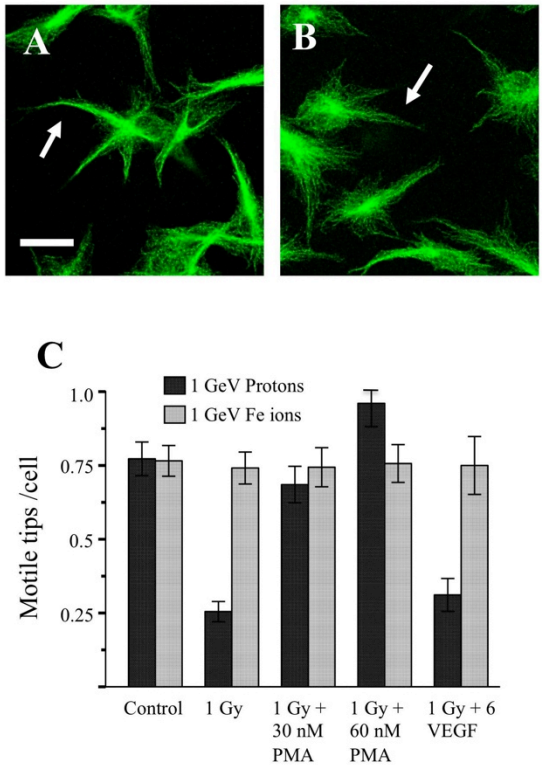

Figure *5 Rescue of motile tips in endothelial cultures treated with high-energy protons and Fe ions. Human brain microvascular cells were allowed to begin vessel development for 24 hours. Cultures were then treated with PMA or VEGF for 20 minutes, irradiated and then fixed after 2 hours. In control cultures (A) tubulin staining shows bundling at motile tips (arrow). In cultures irradiated with 1 Gy protons (B), microtubules in cell projections were not bundled (arrow). C. Quantitation of motile tips under all conditions. PMA rescues motile tip formation inhibited by protons. Motile tips are not inhibited by Fe ions.*

These results indicate that inhibition of vessel formation by protons but not Fe ions involves the inhibition of PKC. Since inhibition by protons but not Fe ions also shows a phenotype at the motile tip that suggests that the initial extension of endothelial cells into the matrix is obstructed, we tested whether stimulation of PMA could also restore tip motility. Endothelial cells were cultured for 24 hours and treated with PMA and VEGF 20 minutes before irradiation as above. Two hours after irradiation the cultures were fixed and stained for microtubules. In this case we assayed for motile tips by imaging those cells that were in the gel but also resting on the substrate. This allowed us to analyze motile tips more readily and quickly since non-motile tips spread out more when in contact with substrate but motile tips remain spear-shaped with tightly bundled microtubules (Figure 5). This analysis gave the same difference between un-irradiated and proton irradiated seen in the matrix except that the absolute values were lower. It is likely that the

increased spreading on the substrate eliminates some false positives. We found that, as for vessel development, stimulation of PKC by PMA but not VEGF was able to restore the motile tips inhibited by protons (Figure 5 E). As seen in Figure 5, Fe ions did not inhibit motile tips and PMA and VEGF had no additional effect. Thus the phenotype of motile tips correlates with vessel formation and inhibition of this phenotype by protons leads to inhibition of vessel formation.

In conclusion, we have shown that low LET protons and high LET Fe ions inhibit the formation of brain capillaries by different mechanisms. In the case of protons, inhibition involves regulation of PKC-dependent motile tips leading to a failure of cellular processes to migrate through the matrix and meet up with other processes. In the case of Fe ions, inhibition does not involve PKC-dependent motile tips since these structures are not affected and cellular processes succeed in making connections. Rather, the cells fail to form tubular structures.

The effect of protons on vessel development is of interest here for two reasons. First, the dose required for 50% inhibition is only 40 cGy, which is within the range of the doses encountered in space, especially during solar particle events (SPEs). Secondly, the difference in RBE between mature vessels and developing vessels suggests that developing cells are hypersensitive to low LET protons and that PKC, a common second messenger signal, is involved. This raises the possibility that signaling activity in the cell can change its sensitivity to low LET radiation.

This work was supported by NASA grants NNJ09ZSA001N and NNJ11ZSA001N.

References

1. Grabham P.W, B. Hu, P. Sharma, and C. Geard. (2010) Effects of ionizing radiation on 3-dimensional human vessel models: Differential effects according to radiation quality and cellular development. Radiation Research 175: 21-28.
2. Grabham P.W, Bigelow A and C. Geard. (2012) DNA damage foci formation and decline in two-dimensional monolayers and in three-dimensional human vessel models: Differential effects according to radiation quality. International Journal of Radiation Biology. 88, 493–500. ■

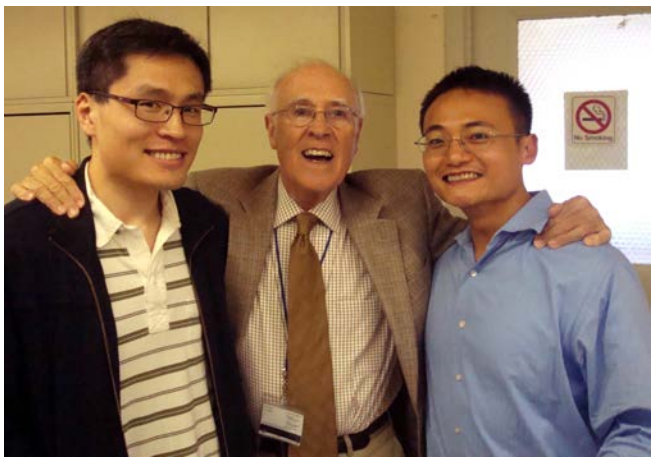

Above: Dr. Charles Geard explains chromosome aberration formation.

Top left (l to r): Dr. Tony Wang, Dr. Eric Hall, Dr. John Ng.

Lower left (l to r): Dr. Richard Miller, Dr. David Brenner, Dr. Tom Hei.

Faculty and students of the first microbeam training course. Standing (l-r): Mr. Stephen Marino, Dr. Ying Nie, Dr. Mykola Onyshchenko, Ms. Stefanie Girst, Dr. Andrew Harken, Ms. Manuela Buonanno, Dr. Anne Marie Adamczyk, Dr. Gerhard Randers-Pehrson, Dr. Diana Pignalosa, Dr. Charles Geard, Dr. Marcelo Vazquez. Kneeling (l to r): Dr. Alan Bigelow, Dr. Guy Garty.

Standing (l to r): Dr. Manuella Buonanno, Dr. Helen Turner, Dr. David Brenner, Dr. Igor Shuryak, Dr. Sally Amundson, Dr. Tom Hei, Dr. Antonella Bertucci. Seated: Dr. Marcelo Vazquez, Teresa Vazquez.

What Do We Mean by "Safe"? The Example of Airport X-Ray Backscatter Scanners

David J. Brenner

What do we mean by safe? The most direct interpretation of "safe" refers to an exposed individual. One may ask what is the best estimate of the lifetime cancer risk to an individual receiving one or more x-ray backscatter scans. Using the standard "5%/Sv" cancer mortality risk formula, this would result in an estimated lifetime cancer mortality risk estimate of about 10^{-7} for two 1-mSv screening scans. "Safe" by almost any standard!

Of course this individual risk estimate is exceedingly uncertain. Some have argued that the risk at very low doses is zero; others have argued that phenomena such as tissue/organ microenvironment effects, bystander effects, and "sneaking-through" immune surveillance, imply that low-dose radiation risks could be higher than anticipated. The bottom line is that individual risk estimates at very low doses are extremely uncertain.

But when extremely large populations are involved, with up to 10^9 scans per year in this case, risk should also be viewed from the perspective of the entire exposed population. Population risk quantifies the number of adverse events expected in the exposed population as a result of a proposed practice, and so depends on both the individual risk and on the number of people exposed. Population risk is described by ICRP as "one input to ... a broad judgment of what is reasonable", and by NCRP as "one of the means for assessing the acceptability of a facility or practice". Population risk is considered in many other policy areas where large populations are exposed to very small risks, such as nuclear waste disposal or vaccination.

It has sometimes been suggested that moving from individual risk to population risk is "bad science". In fact there's *no* science at all here. An individual cancer risk of 1 in X is just another way of saying that if X people are exposed to that risk, the expected number of induced cancers is 1; and if (say) X times 100 people are exposed to that risk, it's essentially certain that there will be some induced cancers. One can argue what the individual risk actually is, but one can't argue about the average population consequences of a given individual risk – it's simply what we mean when we talk of individual risk.

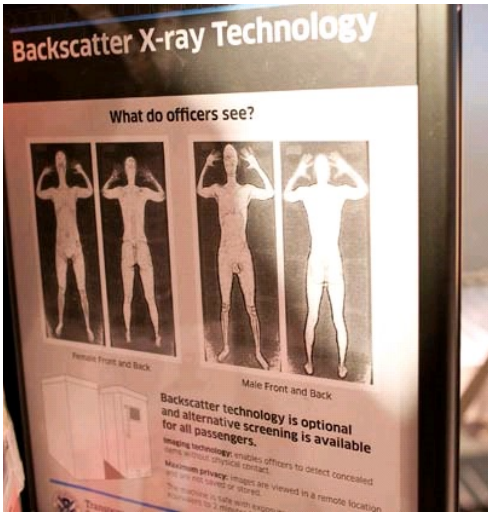

Public concerns about airport scanners have focused more on privacy issues than on health risks.

So x-ray backscatter scanners are associated with very small but very uncertain individual risks. This uncertainty is irrelevant for an individual – whether the individual risk is zero, or 10^{-8} or 10^{-6}, these are all small enough risks for any individual not to be concerned. But if 10^9 scans per year are performed, the uncertainties in individual risk mean that we have little idea whether the population consequences of this activity will be zero or 10 or 1,000 cancers per year.

Of course it could well be argued that any such population risks would be more than balanced by the benefits of reducing the risk of a terrorist event. This may be true, but it's a tough argument to make, quantitatively. X-ray backscatter scanners are probably "safe" from an individual perspective, but their population safety, if they are to be used up to a billion times annually, is unknown.

Reference

Brenner DJ. Are x-ray backscatter scanners safe for airport passenger screening? For most individuals, probably yes, but a billion scans per year raises long-term public health concerns. Radiology 2011 Apr; 259:6-10. ■

Cancer Risks from CT Scans: Now We Have the Data, What Next?

David J. Brenner and Eric J. Hall

It is more than a decade since a paper was published from the CRR that drew the attention of the wider community to the radiation exposures associated with pediatric CT [1]. The paper provided the first quantitative risk estimates of radiation risks associated with pediatric CT. The following day the story hit the front page of USA Today, and the world of CT scans was changed forever.

There was never a question that CT is a remarkably effective modality. It provides for better surgery, better diagnosis and treatment of cancer, better treatment after injury, better treatment of stroke, and better treatment of cardiac conditions. Nonetheless, the suggestion that there might be some potential downside in terms of cancer risks has been vigorously challenged by many in the field.

The original risk estimates for pediatric CT [1] were derived from organ doses and risk data from Japanese atomic bomb survivors. Clearly there are many differences between a CT scan and an atomic bomb exposure - though about 30,000 atomic bomb survivors, located a couple of miles from the epicenter, did indeed receive radiation exposures comparable to those from a few CT scans, and did show a significant increase in cancer risk. Of course, CT scans are typically focused on a particular part of the body, whereas the atomic-bomb exposures were to the whole body. As far as possible these differences were taken into account in estimating CT scan risks, but the prediction that there is a small but real cancer risk associated with the radiation exposure from CT did not convince everyone. Many in the field suggested that the evidence for a small cancer risk associated with CT scanning was simply speculation.

Now the first results of the first of several ongoing epidemiological studies of pediatric CT have been published, by Pearce et al. [2]. The authors identified 180,000 patients who had about 280,000 CT scans in the UK between 1985 and 2002, when they were younger than age 22. They first estimated individual brain and bone marrow doses for every patient. They next ascertained the subsequent cancer history of these 180,000 patients up to 2008, using the UK National Health Service Registry - a study that can be done in the UK and in various other countries, but would be extraordinarily difficult to do in the US! Because they are the cancers that might be expected to appear first in irradiated children, the authors restricted their initial study to leukemia and brain tumors – and as best as they could they eliminated patients who had cancer at the time of their CT scans.

The bottom line [2] is that there were statistically significant linear associations between the radiation dose to the brain and the brain tumor risk ($p<0.0001$), and between the bone-marrow dose and leukemia risk ($p=0.01$). The risks were small but they are undoubtedly real. How small is small? Pearce *et al.* estimated that a single head CT scan given in the first decade of life would

www.usatoday.com THE NATION'S NEWSPAPER 50 CENTS

FINAL SPORTS

Super Bowl

Let the hype begin

Clock is ticking toward Sunday. Full report, 1-4C
▸ 10 years ago, war was on our minds, 1C
▸ Coming Friday: Bonus Section

USA TODAY

NO. 1 IN THE USA

The Golden Globes

'Gladiator' wins best drama film

Julia Roberts, Tom Hanks honored for drama roles; *Almost Famous* named best comedy film ■ 1-2D
▸ The red carpet, 5D

By Robert Hanashiro, USA TODAY

Roberts: Smiles for *Erin Brockovich*.

Monday, January 22, 2001

Newsline

■ News ■ Money ■ Sports ■ Life

usatoday.com's new look

USA TODAY .com

Get the latest news, stocks, scores and more right now at USA TODAY's 24-hour online news site, all with a clean new interface. Plus, a stand-alone Tech section.

■ Asia stocks mixed overnight

Japan's Nikkei average is down 137 points, 1.0%, to 13,852 early today. Hong Kong's Hang Seng index is up 136 points, 0.9%, to 16,069.

CT scans in children linked to cancer later

By Steve Sternberg
USA TODAY

Each year, about 1.6 million children in the USA get CT scans to the head and abdomen — and about 1,500 of those will die later in life of radiation-induced cancer, according to research out today.

What's more, CT or computed tomography scans given to kids are typically calibrated for adults, so children absorb two to six times the radiation needed to produce clear images, a second study shows. These doses are "way bigger than the sorts of doses that people at Three Mile Island were getting," David Brenner of Columbia University says. "Most people got a tenth or a hundredth of the dose of a CT."

Both studies appear in February's *American Journal of Roentgenology*, the nation's leading radiology journal. The first, by Brenner and colleagues, is the first to estimate the risks of "radiation-induced fatal cancer" from pediatric CT scans. Until a decade ago, CT scans took too long to perform on children without giving them anesthesia to keep them still. Today's scanners spiral around the patient in seconds, providing cross sections, or "slices," of anatomy.

Doctors use CT scans on children to search for cancers and ailments such as appendicitis and kidney stones.

"There's a huge number of people who don't just receive one scan," says Fred Mettler of the University of New Mexico, noting that CT scans are used for diagnosis and to plan and evaluate treatment. "The breast dose from a CT scan of the chest is somewhere between 10 and 20 mammograms. You'd want to think long and hard about giving your young daughter 10 to 20 mammograms unless she really needs it."

Mettler recently published a study showing that 11% of the CT scans at his center are done on children younger than 15, and they get 70% of the total radiation dose given to patients. Children have more rapidly dividing cells than adults, which are more susceptible to radiation damage. Children also will live long enough for cancers to develop.

Researchers led by Lane Donnelly at Cincinnati's Children's Hospital found that children often get radiation doses six times higher than necessary. Cutting the adult dose in half would yield a clear image and cut the risk a like amount, Brenner says. "Radiologists genuinely believe the risks are small," he says. "I suspect they've never been confronted with numbers like this."

produce approximately 1 excess case of leukemia and 1 excess brain tumor per 10,000 scanned patients, in the decade after exposure.

So now we have the data, what next?

First, it is clear that we have now passed a watershed in our field, where it is no longer tenable to claim that CT risks are "too low to be detectable and may be non-existent". A large well-designed epidemiological study has clearly shown that the individual risks are small, but real.

The second conclusion follows from the fact that estimated individual CT-related cancer risks are very small. It follows that if a CT exam is clinically justified, there is no doubt that its benefits will by far exceed its risks – no need for any complicated benefit-risk calculations: Reassurance for the patient and, of course, for the physician.

A third conclusion is a caveat: The follow-up times in the Pearce et al. study [2] were, on average, less than 10 years. From long-term studies of other irradiated populations, we expect that not all the radiation-induced cancers that are going to appear have actually yet appeared. Based on the time-post-exposure patterns in these other long-term studies, we can extrapolate the risk estimates with ten-year follow-up that Pearce et al. published, to produce lifetime risk estimates:

A. Leukemia: From A-bomb data [3], about 70% of all radiation-associated leukemias that were ultimately detected after childhood exposure, were actually detected within ten years of exposure. Thus we might extrapolate the estimated [2] 1 in 10,000 leukemia risk from a single head CT scan after 10 years follow-up, to a lifetime 1.3 in 10,000 lifetime leukemia risk.

B. Brain tumors: Based on the long-term study of brain tumors after pediatric scalp irradiation for tinea capitis [4], about 8% of all radiation-associated brain tumors that were ultimately detected, were detected within ten years of exposure. Thus we might extrapolate the estimated [2] 1 in 10,000 brain-tumor risk from a single head CT scan after 10 years follow-up, to a lifetime 12 in 10,000 lifetime brain-tumor risk.

A fourth conclusion that follows from these new risk estimates is that the various risk estimates from CT that have appeared in the past decade were pretty near the mark: For a pediatric head CT scan, our 2001 paper [1] estimated a lifetime leukemia risk of about 1 in 10,000 (cf. the 1.3 in 10,000 lifetime estimate based on Pearce et al.), and it estimated a lifetime brain tumor risk of about 5 in 10,000 (cf. the 12 in 10,000 lifetime estimate based on Pearce et al). It follows that the standard methodology [1] of estimating radiological risks - estimating organ doses and applying A-bomb survivor data – is not unreasonable. Fortunately so: given that we will need to wait many more decades for epidemiologically-based lifetime risk estimates, we will remain reliant on this standard risk-estimation methodology for many years to come.

In summary, ten years after our suggestion [1] that CT scans might produce a small cancer risk, Pearce et al. [2] have shown that this is almost certainly the case, and confirmed the numerical magnitude of the risks. The new risk estimates clearly confirm that, for every clinically justified CT scan, the benefit by far outweighs the risk. That being said, there are still far too many clinically unnecessary CT scans being performed – in the tens of millions per year in the US. It is to be hoped that the publication of this historic paper [2] will provide an added stimulus towards justifying and optimizing every CT scan – both for children and also for adults.

References

1. Brenner DJ, Elliston CD, Hall EJ, Berdon WE. Estimated risks of radiation-induced fatal cancer from pediatric CT. *AJR Am J Roentgenol.* 2001;**176:**289-96.
2. Pearce MS, Salotti JA, Little MP, *et al*. Radiation exposure from CT scans in childhood and subsequent risk of leukaemia and brain tumors: A retrospective cohort study. *Lancet*. 2012; **380**:499-505.
3. Preston DL, Kusumi S, Tomonaga M, *et al*. Cancer incidence in atomic bomb survivors. Part III. Leukemia, lymphoma and multiple myeloma, 1950-1987. *Radiat Res.* 1994;**137**(2 Suppl):S68-97.
4. Ron E, Modan B, Boice JD, Jr., *et al*. Tumors of the brain and nervous system after radiotherapy in childhood. *N Engl J Med.* 1988;**319**:1033-9. ■

Impact of Reduced Patient Life Expectancy on Potential Cancer Risks from Radiologic Imaging

David J. Brenner, Igor Shuryak, and Andrew J. Einstein[a]

The purpose of this study was to quantify the effect of reduced life expectancy on cancer risk by comparing estimated lifetime risks of lung cancer attributable to radiation from commonly used computed tomographic (CT) examinations in patients with and those without cancer or cardiac disease.

With the use of clinically determined life tables, reductions in radiation-attributable lung cancer risks were estimated for coronary CT angiographic examinations in patients with multi-vessel coronary artery disease who underwent coronary artery bypass graft (CABG) surgery and for surveillance CT examinations in patients treated for colon cancer. Statistical uncertainties were estimated for the risk ratios in patients who underwent CABG surgery and patients with colon cancer versus the general population.

Patients with decreased life expectancy had decreased radiation-associated cancer risks. For example, for a 70-year old patient with colon cancer, the estimated reduction in lifetime radiation-associated lung cancer risk was approximately 92% for stage IV disease, versus 8% for stage 0 or I disease. For a patient who had been treated with CABG surgery, the estimated reduction in lifetime radiogenic lung cancer risk was approximately 57% for a 55-year-old patient, versus 12% for a 75-year-old patient.

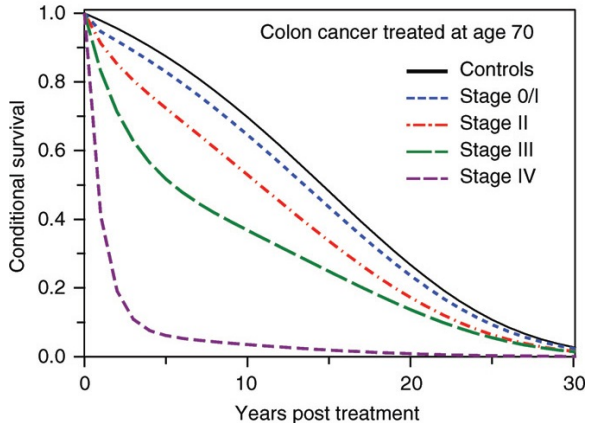

***Figure 1**. Comparison of long-term conditional survival functions for patients diagnosed with different stages of colon cancer at age 70 years (the median age for colon cancer diagnosis) and for healthy control subjects. Derived from SEER results reported by Ward et al. [1].*

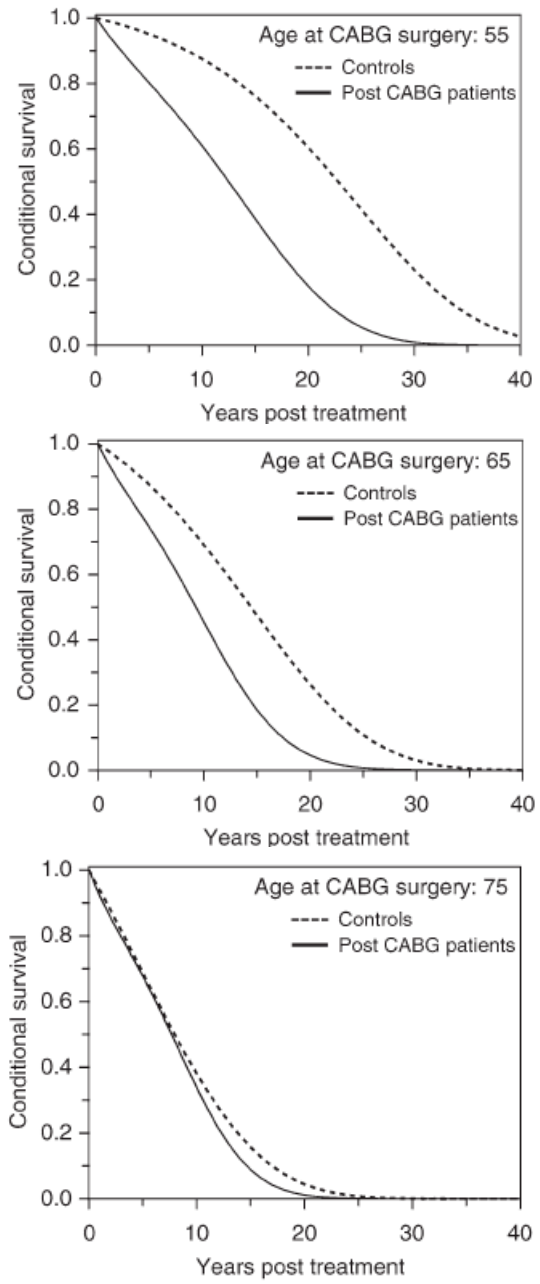

***Figure 2**. Comparison of long-term conditional survival functions for patients who had undergone CABG surgery (solid line) and an age-, sex-, and location-matched control population (dashed line). Derived from results reported by Gao et al. [2].*

[a]Department of Medicine, Division of Cardiology, Columbia University Medical Center, New York

The information needed for comparison of the estimated lifetime radiation risks for CT examinations for these patients, relative to the risks for the same CT examinations in individuals with normal life spans, is as follows: (a) life tables (age specific mortality data) for the two scenarios being considered (after treatment for colon cancer or after CABG surgery) and for the corresponding healthy population, (b) the excess relative risk (ERR) per unit dose for radiation-induced lung cancer, and (c) the background lung cancer rate for the population.

For patients with colon cancer undergoing surveillance after treatment, we used relative survival data in a population of 129,000 patients with colon cancer in the 1998–2001 Surveillance, Epidemiology, and End Results (SEER) database [1], stratified by time since diagnosis, cancer stage, and sex, together with sex-specific U.S. life tables for the year 2000.

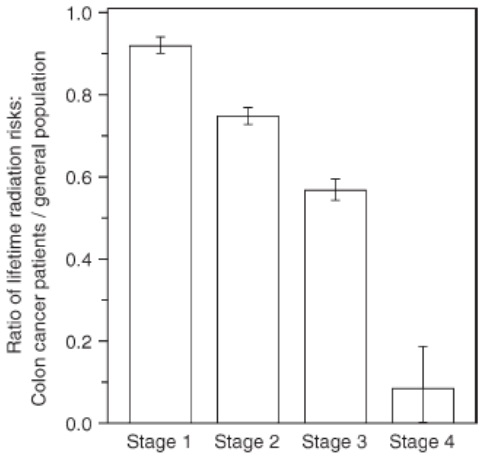

Figure 3*. The ratio of predicted lifetime risk for radiation-induced lung cancer due to post-treatment surveillance CT examinations in patients with various stages of colon cancer (mean age at exposure, 70 years) relative to the corresponding lifetime risk of radiation-induced lung cancer in individuals with a normal life span who undergo the same CT examinations. Error bars show 95% confidence intervals for the estimated ratios.*

For patients who had undergone CABG surgery, we used long-term survival data after CABG surgery, stratified by age at surgery and time after surgery, in more than 20,000 patients who underwent CABG surgery from 1968 through 2003 in Portland, Oregon [2]. Corresponding calendar year–specific life tables for the general population in Oregon were obtained from state-specific U.S. life tables.

The mathematical techniques used to estimate radiation-induced excess cancer risks are based on the recent Biological Effects of Ionizing Radiation (BEIR) VII National Academies report [3]. The details are discussed in reference [4].

Our results suggest that the importance of radiation exposure in determining optimal imaging usage is much

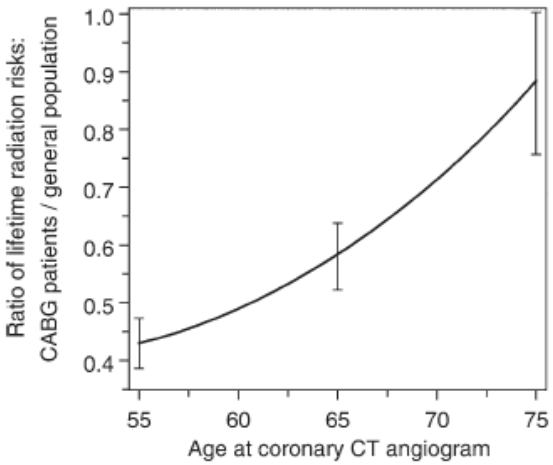

Figure 4*. The ratio of predicted lifetime radiation-induced lung cancer risks for a coronary CT angiographic examination in patients who had undergone CABG surgery relative to the lifetime risks for the same CT examination in an age-, sex-, and location-matched normal–life span population. Error bars show 95% confidence intervals for the estimated ratios.*

reduced for patients with markedly reduced life expectancies. Reduced life expectancy is an important factor in determining the potential radiation-associated lifetime risk associated with radiologic examinations and thus should play a substantial role in assessing the justification and optimization of these examinations. Estimates of radiation risks in reduced life-expectancy scenarios that do not take this into account may well result in unrealistically large risk estimates. It follows that imaging justification and optimization criteria for patients with substantially reduced life expectancies should not necessarily be the same as for those with normal life expectancies.

References

1. Ward KC, Young JL, Ries LAG. Cancers of the colon and rectum. In: Ries LAG, Young JL, Keel GE, Eisner MP, Lin YD, Horner MJ, eds. SEER survival monograph: cancer survival amongst adults: U.S. SEER Program, 1998-2001, patient and tumor characteristics. NIH Pub. No. 07-6215. Bethesda, Md: National Institutes of Health, 2007.
2. Gao G, Wu Y, Grunkemeier GL, Furnary AP, Starr A. Long-term survival of patients after coronary artery bypass graft surgery: comparison of the pre-stent and post-stent eras. Ann Thorac Surg 2006; 82 (3): 806 – 810.
3. National Research Council. Health risks from exposure to low levels of ionizing radiation. BEIR VII. Washington, DC: The National Academies Press, 2006.
4. Brenner DJ, Shuryak I, Einstein AJ. Impact of reduced patient life expectancy on potential cancer risks from radiologic imaging. Radiology. 2011; 261 (1):193-8. ■

Radiation-Induced Carcinogenesis: Mechanistically Based Differences between Gamma-Rays and Neutrons, and Interactions with DMBA

Igor Shuryak, David J. Brenner, and Robert L. Ullrich[a]

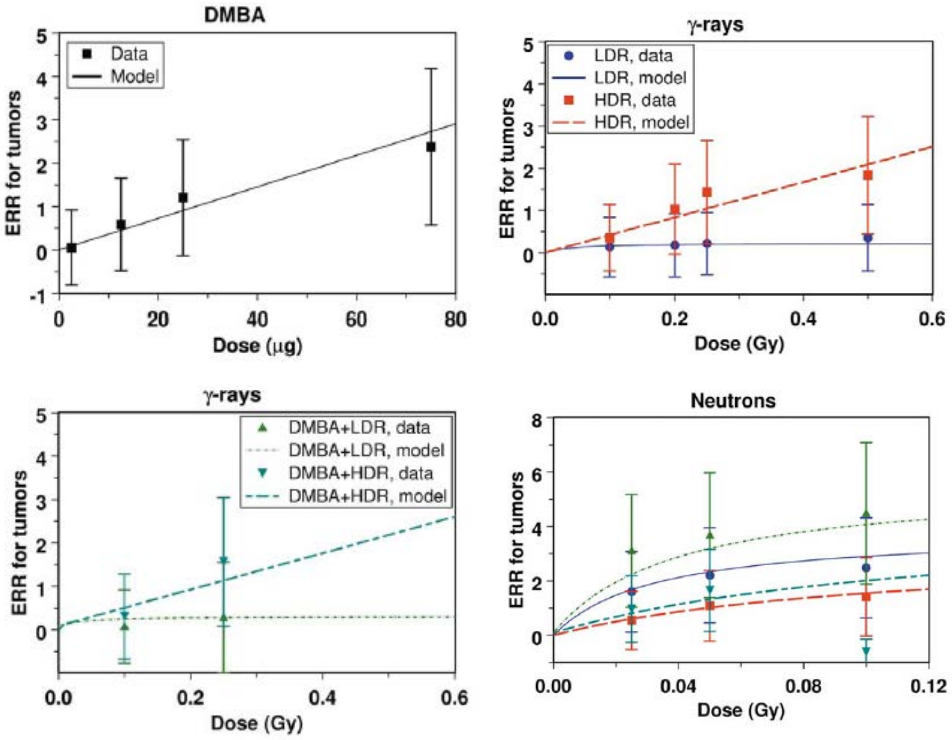

Figure 1. *The data and model predictions for mammary tumor excess relative risk (ERR) after gamma-ray, neutron and/or DMBA exposure. In the panels showing effects of gamma-rays and neutrons, the legend is the same: HDR = high dose rate; LDR = low dose rate; DMBA= 2.5 mg of DMBA. Error bars represent 95% confidence intervals.*

Different types of ionizing radiation produce different dependences of cancer risk on radiation dose/dose rate. Sparsely ionizing radiation (e.g. gamma-rays) generally produces linear or upwardly curving dose responses at low doses, and the risk decreases when the dose rate is reduced (direct dose rate effect). Densely ionizing radiation (e.g. neutrons) often produces downwardly curving dose responses, where the risk initially grows with dose, but eventually stabilizes or decreases. When the dose rate is reduced, the risk increases (inverse dose rate effect). These qualitative differences suggest qualitative differences in carcinogenesis mechanisms.

We hypothesize that the dominant mechanism for induction of many solid cancers by sparsely ionizing radiation is initiation of stem cells to a pre-malignant state, but for densely ionizing radiation the dominant mechanism is radiation bystander-effect mediated promotion of already pre-malignant cell clone growth.

We generated a mathematical model based on these assumptions and tested it using data on the incidence of dysplastic growths and tumors in the mammary glands of mice exposed to high or low dose rates of gamma-rays and neutrons, either with or without pre-treatment with the chemical carcinogen 7,12-dimethylbenz-alpha anthracene (DMBA).

Details of the model formalism are provided in reference [1]. Results of model fitting to the data for gamma-rays and neutrons are shown in Figures 1-3.

Our analysis provided a mechanistic quantitative model based on the hypothesis that carcinogens such as DMBA and gamma-rays act mainly as initiators of pre-malignant cells, whereas neutrons act mainly to promote the growth of already existing pre-malignant cell clones.

[a]Department of Radiation Oncology, The University of Texas Medical Branch, Galveston, TX.

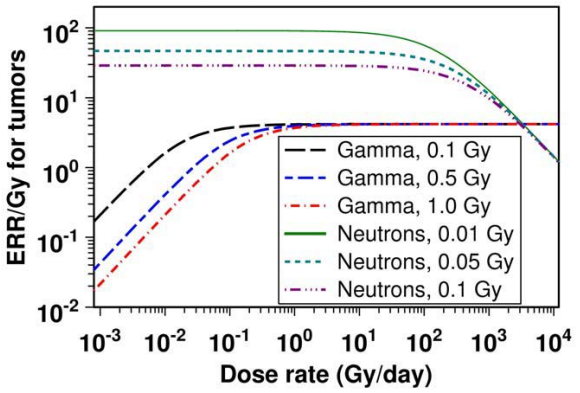

***Figure 2**. Model predictions for tumor ERR/Gy as a function of dose/dose rate for gamma-rays and neutrons.*

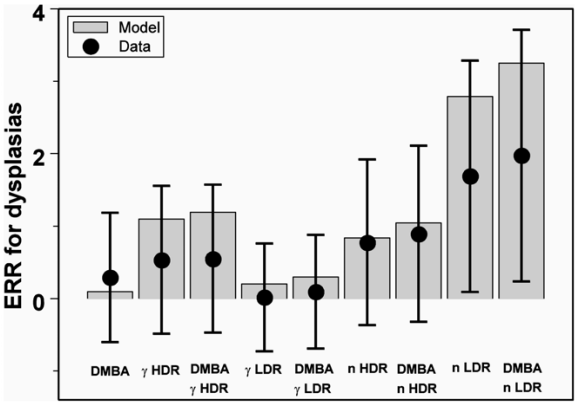

***Figure 3**. The data and model predictions for the ERR for ductal mammary dysplasias observed in the fat pads of untreated mice after transplant of mammary epithelial cells from carcinogen-treated mice. Legend: DMBA= 2.5 mg of DMBA; gamma = 0.25 Gy of gamma-rays; n = 0.025 Gy of neutrons; HDR = high dose rate; LDR = low dose rate.*

The model was then directly tested using data for mammary carcinogenesis as well as early events in the carcinogenic process induced by DMBA, gamma-rays and neutrons in a well-established mouse mammary cancer animal model. Importantly, the results support the animal cancer model. The results also support other evidence [2-4] suggesting that densely ionizing radiation, such as neutrons and alpha particles, induces cancer mainly through promoting effects on premalignant cell clones. Such promoting effects may occur due to disruption of intercellular signaling by radiation, which can happen even if only a small fraction of the cells are actually traversed by ionizing tracks. This analysis may provide useful insight into human carcinogenesis.

References

1. Shuryak I, Brenner DJ, Ullrich RL. Radiation-induced carcinogenesis: mechanistically based differences between gamma-rays and neutrons, and interactions with DMBA. PLoS One. 2011; 6(12):e28559.
2. Curtis SB, Hazelton WD, Luebeck EG, Moolgavkar SH. From mechanisms to risk estimation–bridging the chasm. Adv Space Res. 2004; 34:1404–1409.
3. Hazelton WD, Moolgavkar SH, Curtis SB, Zielinski JM, Ashmore JP, et al. Biologically based analysis of lung cancer incidence in a large Canadian occupational cohort with low-dose ionizing radiation exposure, and comparison with Japanese atomic bomb survivors. J Toxicol Environ Health A. 2006; 69:1013–1038.
4. Heidenreich WF, Paretzke HG. Interpretation by modeling of observations in radon radiation carcinogenesis. Radiat Prot Dosimetry. 2004; 112:501–507. ■

(l to r): Dr. Eric Hall, Dr. Chang W. Song, Professor and Director of Radiation Biology and Molecular Cancer Therapeutics at the University of Minnesota, and Dr. Tom Hei.

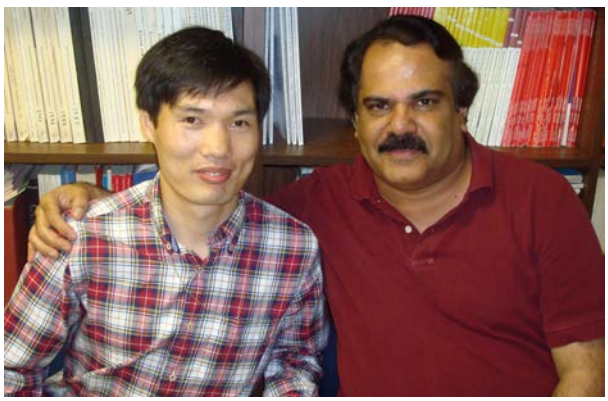

(l to r): Dr. Hongbo Fang, and Dr. Adayabalam Balajee

Effective Dose in Cardiac CT Scans Study

Andrew Einstein[a], Radoslaw Pieniazek, and Sigal Trattner[a]

Current methods to estimate effective dose in cardiac CT are based on single-slice scanners, which technologically are markedly different from the CT scanners currently in use for cardiac computed tomography angiography (CCTA). Several studies show that these methods underestimate the true dose by at least 50%, for a wide range of current scanners [1].

The overall goal of the project is to develop an improved methodology to estimate radiation doses from cardiac CT using solid-state physics experiments with metal-oxide-semiconductor field-effect transistors (MOSFETs) and anthropomorphic radiologic phantoms. These experiments will be performed using a variety of cardiac CT scanners and different scan protocols.

MOSFET

The dosimeters used for this study were the TN: 1002RD-H high sensitivity MOSFET dosimeters manufactured by Best Medical Canada (Figure 1). It is

***Figure 1**. Reader with five attached MOSFETS.*

necessary to use high sensitivity MOSFETs for diagnostic studies due to the low radiation exposures that must be measured. In preparation for these studies a full day was spent ensuring transfer of knowledge from Carl Elliston, who had previously worked on similar experiments with these MOSFETs [2, 3]. The training covered topics like mobileMOSFET software, device preparation, maintenance, and proper dosimeter placement inside a modified anthropomorphic phantom (Figure 2). This

***Figure 2**. Modified anthropomorphic phantom.*

phantom was modified from a commercially available anthropomorphic phantom (ATOM 701; CIRS, Norfolk, Va). Additional holes were drilled so that absorbed dose could be determined for each organ with a significant tissue- weighting factor from the ICRP 2007 guidelines. Discussions were also held with Abdelbasset Hallil, the Director of Research & Development at Best Medical Canada, to broaden knowledge of MOSFET calibration.

Calibration

In order to use the MOSFET dosimeters for our study calibration is required. Calibration is commonly performed by using an ion chamber that is placed inside a nested acrylic head/body phantom before the actual scan. We compared several ion chambers (and one solid state detector) for stability, repeatability and accuracy. The comparison was done by testing the different devices on the Philips 16-slice CT scanner with a variety of pre-programmed protocols in different radiation ranges. Once an ion chamber was selected we were able to proceed to the calibration process. Without new MOSFETs this was a practice run using ones that already had a significant dose accumulated from pervious experiments. We noticed non-zero readouts without any source of radiation, which made the calibration troublesome. After consulting the Best Medical Canada support team we found out we can only use fresh MOSFETs for our study, because with accumulated dose, the fading effect increases adding

[a]Department of Medicine, Division of Cardiology, Columbia University Medical Center, New York

noise to the readings. One restrictive factor of MOSFET dosimetry is the limited life span of the detectors. After a large accumulated dose, the linearity of the detector decreases and larger doses are required to produce the same differential potential change. As such we have investigated a relatively new MOSFET dosimetry system for accuracy at low applied doses (less than 10 mGy) using high-energy X-rays produced by a pulsed radiation linear accelerator. This approach could prolong the life of the MOSFET detectors without severely compromising accuracy of results. Once a MOSFET dosimeter surpasses a certain threshold of accumulated dose it will be relocated to an area in the phantom that receives larger amounts of radiation (more than 10 mGy) making the fading effect negligible.

Conclusion

Once the calibration is concluded we plan to take measurements on as many CT scanners as available. This methodology will in turn be used for the comparison of cumulative and procedural radiation effective doses to symptomatic patients in a real-world U.S. population.

References

1. Einstein AJ, Henzlova MJ, Rajagopalan S. Estimating risk of cancer associated with radiation exposure from 64-slice computed tomography coronary angiography. *JAMA.* (2007) **298(3):**317-23.
2. Einstein AJ, Elliston CD, Arai AE, Chen MY, Mather R, Pearson GD, Delapaz RL, Nickoloff E, Dutta A, Brenner DJ. Radiation dose from single-heartbeat coronary CT angiography performed with a 320-detector row volume scanner. *Radiology*. (2010) **254(3):**698-706.
3. Einstein AJ, Elliston CD, Groves DW, Cheng B, Wolff SD, Pearson GD, Robert Peters M, Johnson LL, Bokhari S, Johnson GW, Bhatia K, Pozniakoff T, Brenner DJ. Effect of bismuth breast shielding on radiation dose and image quality in coronary CT angiography. *J Nucl Cardiol. (*2012) **19(1):**100-8. Epub 2011 Nov. ■

Holiday lunch party with Dr. Lieberman's and Dr. Hei's laboratories.

Divergent Gene Expression Responses to Radiation in Human and Murine Exposure Models

Sally A. Amundson, Lihua Ming, and Sunirmal Paul

In our ongoing development of gene expression as a potential tool for radiation biodosimetry, we have amassed a large amount of microarray data from an *ex vivo* irradiation model using human peripheral blood lymphocytes (PBL) drawn from healthy volunteers [1]. These data have been further supplemented by data from cancer patients undergoing total body irradiation (TBI) prior to bone marrow transplant [2], and more recently, by data from mice irradiated *in vivo*. Our original comparisons between human blood irradiated *ex vivo* and *in vivo* suggested that the responses seen in the *ex vivo* model were generally conserved *in vivo*, but that many additional genes responded *in vivo*. This finding made the exploration of an animal model of *in vivo* irradiation, where dose and time after exposure could be controlled without the many constraints of patient treatment, of high importance. We have exposed cohorts of mice to between 1 and 6 Gy gamma rays and sacrificed them after 24 hours. One of the most immediately striking features of the gene expression data was the significant response of a number of the genes previously identified as potential biodosimetry genes in humans, but with a dose response trend moving in the opposite direction to that seen previously in the human studies.

At least eight male C57/Bl6 mice (Charles River Laboratories) per point were exposed to radiation doses from 0 to 6 Gy using a Gammacell-40 ^{137}Cs irradiator (AECL, Ontario, Canada). After irradiation, mice were returned to their home cages until the time of sacrifice, when blood was collected via cardiac puncture. RNA was prepared from the blood using the PAXGene protocol. All experiments involving mice were approved by the Columbia University Medical Center Institutional Animal Care and Use Committee (IACUC).

Agilent Whole Mouse Genome Microarrays were hybridized to Cyanine-3 (Cy3) labeled cRNA prepared from RNA, then washed and scanned as recommended by the manufacturer. Image extraction, data import and filtering in BRB-ArrayTools [3] were conducted as previously described [1]. Class comparisons were conducted using BRB-ArrayTools and a random-variance t-test to identify genes that were differentially expressed in the blood of irradiated mice.

Class comparison identified 3417 genes with significantly different expression ($p<0.001$, False Discovery Rate (FDR)<0.7%) across the doses used. This is compared with 130 genes significantly differentially expressed ($p<0.001$, FDR<10%) at 24 hours in the human *ex vivo* model [1] and 1588 differentially expressed genes

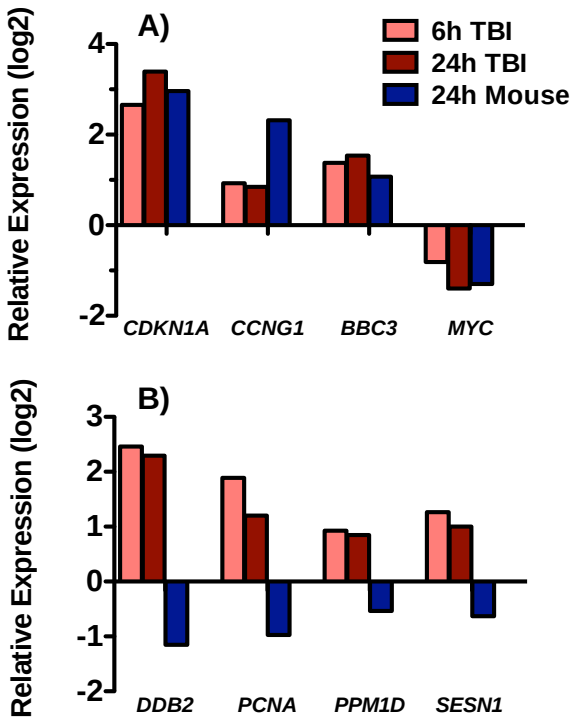

Figure 1. *Examples of genes with similar (A) or opposite (B) patterns of response to in vivo radiation exposure in mice and humans. 6h TBI represents patients after the first 1.25 Gy fraction of total body irradiation, 24h TBI is after accumulation of 3 fractions (3.75 Gy), and the mouse samples represent the response at 24 hours after a single 4 Gy dose.*

($p<0.001$, FDR<1.3%) at 24 hours after the first fraction of TBI [2]. Although the mouse study found about twice the number of responding genes seen in the human *in vivo* study, this may be due at least in part to the fact that the TBI patients had only accumulated 3.75 Gy, distributed across 3 fractions, while the mouse study included both higher doses, and the additional power of multiple doses in the analysis.

We then looked for genes significantly altered by radiation exposure in both the mouse whole body and human TBI *in vivo* exposures and found 238 genes with matching gene names in both gene sets. Of these genes, only 76% showed the same direction of expression change in response to radiation (Figure 1A), while 24% unexpectedly responded in the opposite direction in mice and humans (Figure 1B). Of the genes showing opposite directions of response, 44 (77%) were over-expressed in humans and under-expressed in mice following

irradiation, and the remaining 13 were under-expressed in humans and over-expressed in mice.

When the selected genes were examined in more detail, we found the pattern of expression response was maintained across the range of doses used. Although the limitations on measurements of *in vivo* responses in humans prevented us from comparing *in vivo* dose-responses directly between the two species, the mouse dose responses were compared to *ex vivo* dose responses of the same genes in human peripheral blood (Figure 2).

An examination of the Gene Ontology (GO) functions of the sets of genes showing the same or opposite response in mice and humans revealed many of the functions commonly seen in radiation experiments among the similarly expressed genes (Table 1). Among the small set of genes showing opposite responses in the two species, only the p53 pathway was significantly over-represented (Benjamini corrected p=0.015). The genes regulated by and/or regulating TP53 were examined in Ingenuity Systems Pathway Analysis (IPA), which identified 43 genes associated with TP53 among the set of 238 genes. One third of these (14 genes) showed opposite regulation in mouse and human TBI (Figure 3).

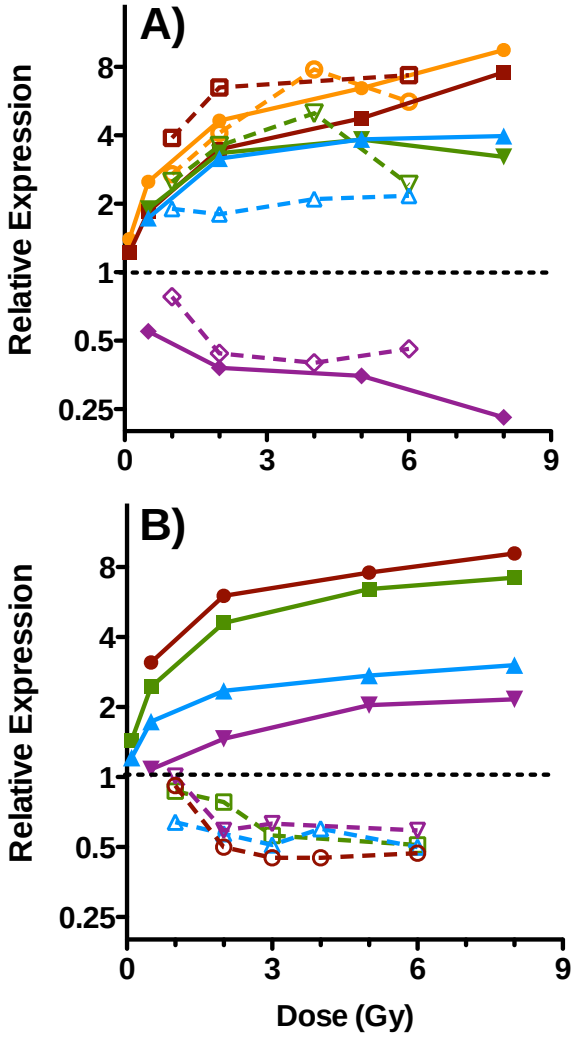

Figure 2. *Radiation dose response of genes with similar (A) or opposite (B) responses in human (solid lines and symbols) and mouse (dashed lines and open symbols) peripheral blood measured at 24 hours after exposure. Panel A: GDF15 (red), CDKN1A (gold), CCNG1 (green), BBC3 (blue), MYC (purple). Panel B: DDB2 (red), PCNA (green), SESN1 (blue), PPM1D (purple).*

Table 1. *GO analysis of genes with similar response in humans and mice*

Term	p-value	Benjamini p-value
Phosphoprotein	2.9×10^{-7}	6.38×10^{-5}
SH2 domain	1.43×10^{-6}	1.58×10^{-4}
T-cell receptor complex	1.87×10^{-6}	3.56×10^{-4}
Acetylation	9.21×10^{-5}	6.73×10^{-3}
Transmembrane protein	2.33×10^{-4}	0.0127
Regulation of T-cell activation	8.03×10^{-5}	0.0208
DNA-dependent DNA replication	1.59×10^{-4}	0.0235
Regulation of apoptosis	2.49×10^{-4}	0.0285

The over-representation of genes associated with TP53 among genes showing this reverse response to radiation in human and mouse is especially interesting, as there are known differences in p53 between the two species that could contribute to the observed effects. For instance, several non-conserved phosphorylation sites have been documented in p53. The mouse Ser34 and Thr76/86 sites have no apparent human homologs, and the human Ser33, Ser46 and Thr81 sites have no apparent mouse homologs [4]. All three of the human sites are known to be involved in p53 stabilization and activation after exposure to UV radiation [5, 6], although less is known about their roles in the ionizing radiation response. Ser46, however, is known to play a role in regulating apoptosis in response to ionizing radiation exposure [7].

The regulation of p53 also differs between mouse and human. For instance, in human cells the p14ARF protein localizes to the nucleus and activates p53. The larger p19ARF mouse ortholog interacts with Pex19p, which prevents its entry into the nucleus, thus modifying its effect on p53 function [8]. Such differences in interactions with additional proteins may help to shape the specificity of gene regulation by p53 and other transcription factors following irradiation in different species.

Binding sites for p53 in the genome show considerable heterogeneity in the sequence of the response elements of different genes. In light of our current findings it is also of note that the conservation of the sequences of these response elements can vary greatly from gene to gene, with some being almost identical in mouse and human, and some having little similarity.

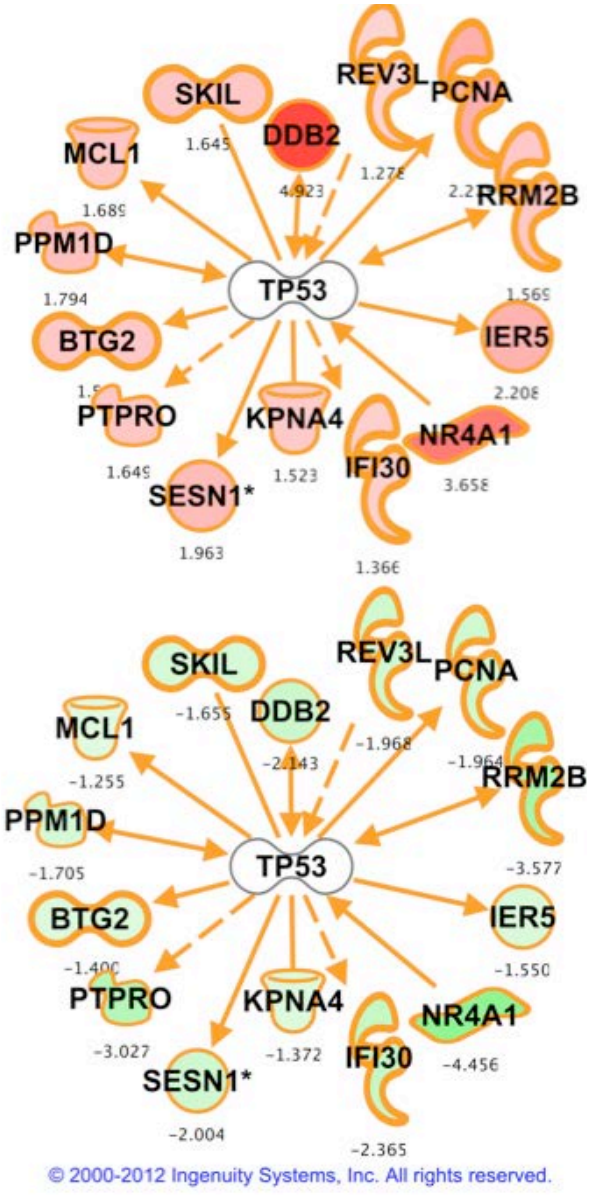

Figure 3. *IPA network of p53 interacting genes. Red nodes indicate genes over-expressed 24 hours after irradiation, green indicates under-expression. The top figure is the response in human peripheral blood, the bottom figure is the same network overlaid with the response in mouse peripheral blood.*

Genes involved in apoptosis generally showed poor conservation of p53 response elements [9]. Interestingly, *PCNA*, one of the genes we identified as responding differently in mice and humans, was one of the genes found by the same study to have little if any homology between rodent and human p53 response elements.

These findings underline the importance of including human models, despite their limitations, in the development of potential gene expression signatures for radiation biodosimetry. They also point to differences between species in coordinate gene expression responses that may have broad implications for many other mechanistic based studies.

References

1. Paul, S, and Amundson, S A (2008) Development of gene expression signatures for practical radiation biodosimetry. *Int J Radiat Oncol Biol Phys* **71:** 1236-1244.
2. Paul, S, Barker, C A, Turner, H C, McLane, A, Wolden, S L, and Amundson, S A (2011) Prediction of In Vivo Radiation Dose Status in Radiotherapy Patients using Ex Vivo and In Vivo Gene Expression Signatures. *Radiat Res* **175:** 257-265.
3. Simon, R, Lam, A, Li, M-C, Ngan, M, Menenzes, S, and Zhao, Y (2007) Analysis of gene expression data using BRB-Array Tools. *Cancer Informatics* **2:** 11-17.
4. Xu, Y (2003) Regulation of p53 responses by post-translational modifications. *Cell Death Differ* **10:** 400-403.
5. Bulavin, D, Saito, S I, Hollander, M C, Sakaguchi, K, Anderson, C W, Appella, E, and Fornace, Jr, A J (1999) Phosphorylation of human p53 by p38 kinase coordinates N-terminal phosphorylation and apoptosis in response to UV radiation. *EMBO J.* **18:** 6845-6854.
6. Buschmann, T, Potapova, O, Bar-Shira, A, Ivanov, V N, Fuchs, S Y, Henderson, S, Fried, V A, Minamoto, T, Alarcon-Vargas, D, Pincus, M R, Gaarde, W A, Holbrook, N J, Shiloh, Y, and Ronai, Z (2001) Jun NH2-terminal kinase phosphorylation of p53 on Thr-81 is important for p53 stabilization and transcriptional activities in response to stress. *Mol Cell Biol* **21:** 2743-2754.
7. Mi, J, Bolesta, E, Brautigan, D L, and Larner, J M (2009) PP2A regulates ionizing radiation-induced apoptosis through Ser46 phosphorylation of p53. *Mol Cancer Ther* **8:** 135-140.
8. Wadhwa, R, Sugihara, T, Hasan, M K, Taira, K, Reddel, R R, and Kaul, S C (2002) A major functional difference between the mouse and human ARF tumor suppressor proteins. *J Biol Chem* **277:** 36665-36670.
9. Horvath, M M, Wang, X, Resnick, M A, and Bell, D A (2007) Divergent evolution of human p53 binding sites: cell cycle vs apoptosis. *PLoS Genet* **3:**e127. ■

In Vivo Micronuclei Formation in Radiotherapy Patients Undergoing Partial Body Irradiation

Antonella Bertucci, Israel Deutsch[a], Maria Taveras, Helen Turner, and David J. Brenner

Introduction

Analysis of mature biomarkers of radiation exposure could potentially be used for triage and treatment decisions for acute radiation exposure such as after a radiological accident as well as for long term assessment of late effects such as cancer and cardiac disease. Partial body biodosimetry is also likely to be required after a radiological exposure to determine the fraction of the body irradiated and the relevant absorbed dose.

The *in vitro* cytokinesis-block micronucleus assay (CBMN) is one of the most reliable and widely used methods to assess cytogenetic damage resulting from radiation exposure. In this system, chromosome fragments or whole chromosomes become detectable as micronuclei (MN) in the cytoplasm of cells that have undergone mitotic division (Figure 1). Moreover the incidence of micronuclei in peripheral blood lymphocytes (PBLs) is a well-known bio-indicator of radiation damage. Studies have shown that the damage to a cell's chromosomes can give us a good idea of how much radiation a person has been exposed to. However, direct data on the persistence of radiation-induced MN in human PBLs *in vivo* is limited.

In the present study we analyze MN frequencies in lymphocytes of radiotherapy (RT) patients undergoing partial body irradiation of the pelvic region. Blood samples were acquired from RT volunteers treated for prostate or cervical cancer at the Radiation Oncology Department of the Columbia University Medical Center.

Methods

Sample Preparation and Cell Harvesting: fresh peripheral blood samples were acquired into heparinized vacutainers at six time points:

- before RT
- immediately after the first fraction (POST 1)
- immediately before the second fraction (POST 2)
- immediately after the final fraction (LAST)
- 2 days after the final fraction and
- 7 days after the final fraction.

Blood was cultured in RPMI 1640 medium supplemented with 10% fetal calf serum, penicillin, streptomycin and phytohemagglutinin (PHA) to stimulate mitosis. Whole blood cultures for the MN assay were processed in duplicate for all samples.

Cytochalasin-B was added 44 h after stimulation in order to inhibit cytokinesis in cells undergoing their first mitotic division.

Lymphocytes were then harvested by centrifugation at 72 h after PHA addition, and cells were treated with 0.075M KCl. The cells were fixed with a cold solution of methanol and acetic acid (3:1 v/v) and dropped onto slides. Air-dried slides were then stained with DAPI.

Radiotherapy treatment: For this study we have recruited eight cancer patients who received a targeted radiotherapy regimen of 1.8-2 Gy per fraction to the pelvic region. The calculated mean total blood dose for

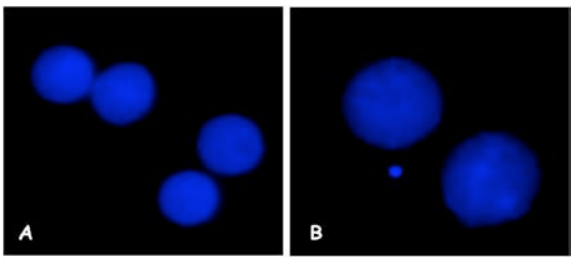

Figure 1. *DAPI stained normal binucleate cells (A) and a cell with damaged DNA showing a micronucleus (B).*

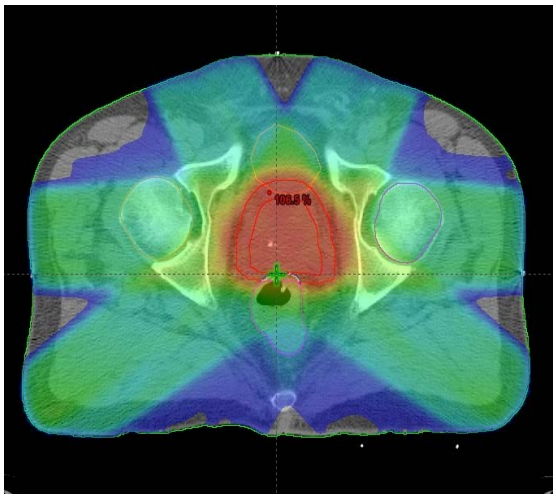

Figure 2. *3D images of a pelvic treatment plan used in our study. The area of high dose (red) corresponds precisely to the area being treated, which corresponds to the entire prostate.*

[a]Department of Radiation Oncology, Columbia University Medical Center.

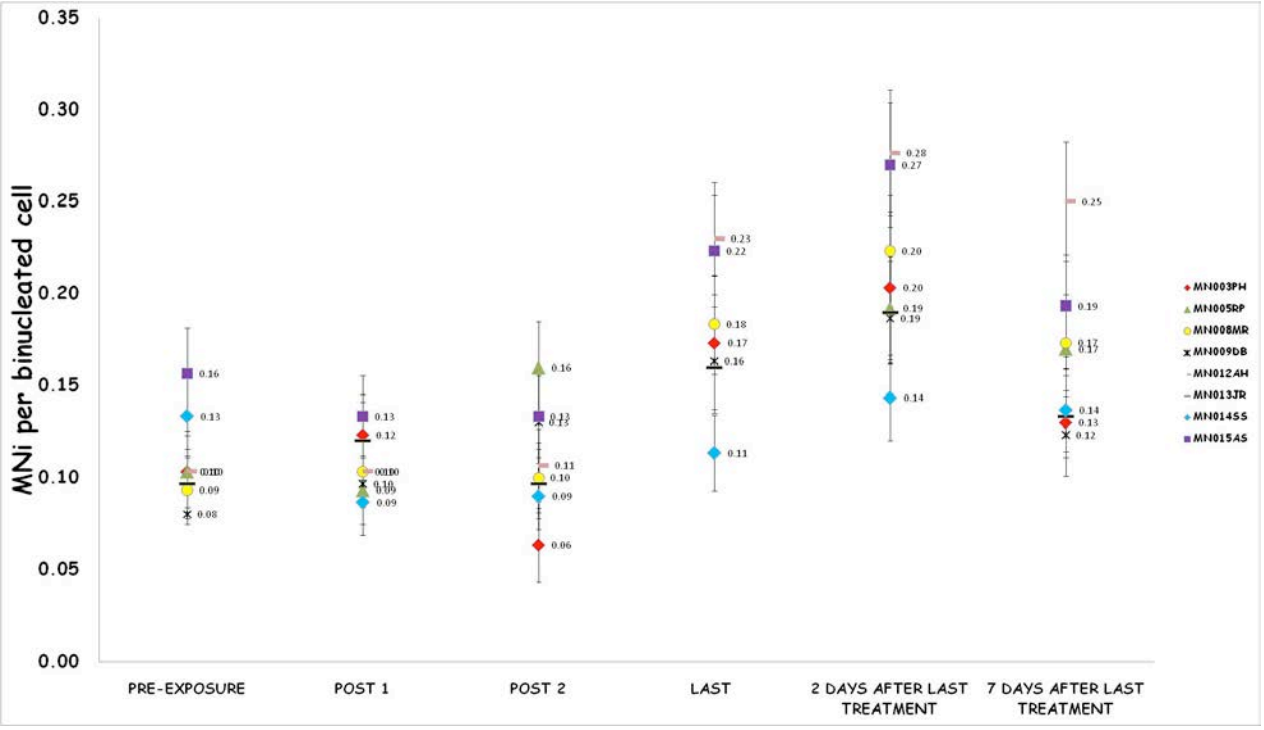

Figure 3. *Frequency of micronuclei in binucleated peripheral blood lymphocytes from radiotherapy patients. The different symbols represent individual patients. The error bars are standard deviation of duplicate measurements.*

these patients was in the range of 2 to 4 Gy.

The patients were treated using Intensity Modulated Radiation Therapy (IMRT), which more precisely shapes radiation beams to the size and contour of a tumor (Figure 2). This helps avoid healthy tissue and enables treatment of difficult-to-reach tumors.

Results

The measured micronuclei frequencies are shown in Figure 3. The pre-treatment baseline micronuclei frequencies, as well as the frequencies in the samples immediately after the first fraction and immediately before the second fraction, fall within the normal range. In principle, the extent of micronuclei induction should be similar in patients irradiated at the same site with similar integral doses. In fact in each case a dose-related increase in MN frequency was observed. The results also showed a persistence of an elevated MN yield 7 days after the completion of the radiotherapy, which is indicative of radiation-induced residual damage. ■

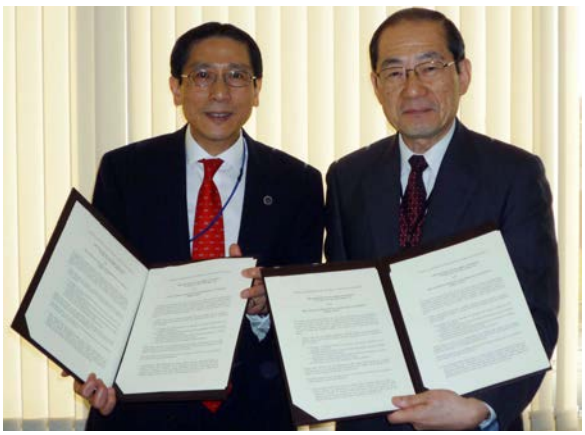

(l to r): Dr. David Brenner, Dr. Charles Geard, Dr. Peter Grabham. Dr. Tom Hei and Dr. Yoshiharu Yonekura, President of NIRS.

Implementing Quality-control at the Center for High Throughput Minimally Invasive Biodosimetry

Guy Garty, Jay R. Perrier, Helen C. Turner, Sally Quataert[a], and David J. Brenner

According to the code of federal regulations [1][b] studies that support or are intended to support applications for research or marketing permits for products regulated by the Food and Drug Administration must be conducted under a quality control system. This is intended to assure the quality and integrity of the data filed to the FDA. As opposed to basic scientific research, where the integrity of the researcher is assumed, in quality controlled (QC) studies the burden is on the investigator to prove that all studies were performed according to predetermined criteria.

Establishing a quality control system typically incorporates documentation and control of four general fields: Controlled Documents, Personnel, Equipment, and Experimental Assays.

Document control

One of the most important things in performing a quality controlled study is documentation. Everything needs to be documented and in many cases signed by a member of the management team. When a new document (such as a Standard Operating Procedure; SOP) is written, it is given a document number and version number or date. The document must be reviewed by a member of the management team (other than the author) and signed by the study director. If it is determined that a change needs to be made, the revision must also be reviewed by the management team and study director and a new version number assigned. A system needs to be put in place so that only the latest version of each document is available to all laboratory personnel and that prior versions are archived. This allows, in case of an audit, to reconstruct the protocols and procedures in effect in the lab when a specific experiment was conducted. In implementing a document control system we have initially drafted a document management SOP and SOP template and then used that for creating all subsequent documents. In total, over 40 SOPs and 27 forms and templates were written as described in the table below.

***Figure 1**. QC Documentation shelf in our laboratory, including protocols, personnel records and data collection forms, sorted by category.*

Table I: Classification of documents generated

Description	Number of documents
Forms	6
Maintenance log sheets	18
Templates	3
Administrative protocols	14
Equipment operation protocols	18
Regent preparation protocols	10
Assay protocols	3

Assay control

The FDA requires the lab to have "*standard operating procedures [SOPs] in writing setting forth […] methods that management is satisfied are adequate to insure the quality and integrity of the data generated in the course of a study.*" (§58.81(a)). At the minimum SOPs must be written for (where applicable):

(1) Animal room preparation.
(2) Animal care.
(3) Receipt, identification, storage, handling, mixing, and method of sampling of the test and control articles.
(4) Test system observations.
(5) Laboratory tests.
(6) Handling of animals found moribund or dead during study.
(7) Necropsy of animals or postmortem examination of animals.
(8) Collection and identification of specimens.
(9) Histopathology.
(10) Data handling, storage, and retrieval.
(11) Maintenance and calibration of equipment.

[a] Compliant Systems Integration, Inc., Rochester, NH
[b] All italicized text is quoted directly from this document.

(12) Transfer, proper placement, and identification of animals.

(§58.81(b)) These SOPs are controlled documents and need to be periodically reviewed by the management. In case of deviation from the SOP, the management team must be notified and the study director must approve the deviation or reject the experiment. If a protocol is changed, the change must also be approved by management following a study of its consequences. A current copy of all SOPs must be kept in the lab, where they can be accessed by all personnel performing the experiments.

Additionally, *"all reagents and solutions in the laboratory areas shall be labeled to indicate identity, titer or concentration, storage requirements, and expiration date."*(§58.83)

This pertains both to stock solutions, where appropriate labeling is typically provided by the vendor as well as for prepared solutions, where the lab personnel must affix an appropriate label that also indicates who made the solution. In this case the guidelines for determining the expiration date are to be determined by management and specified in the SOP for preparing that reagent. Care must be taken that expired reagents are NOT used in the study.

In order to facilitate reagent control we have designed labels containing all pertinent information as well as a machine readable barcode which is unique to each type of reagent. This allows the Laboratory Information Management System to recognize the different reagents and ensure that the proper reagent is used at each step of the assay.

We have also written both a master reagent preparation and labeling SOP and individualized SOPs for each specific reagent used in our laboratory. These specific SOPs specify how the reagent is made and how it's expiration date is determined.

***Figure 2**. Sample reagent label used in our laboratory.*

Personnel control

At the core of personnel control is the requirement that *"Each individual engaged in the conduct of or responsible for the supervision of a nonclinical laboratory study shall have education, training, and experience, or combination thereof, to enable that individual to perform the assigned functions."* (§58.29(a))

In order to ensure this requirement, the facility needs to define the following:

- **Organizational chart**: The organizational chart should define the title and hierarchy of all people involved in the study (Figure 1 shows as an example a CRR organizational chart from 2010).

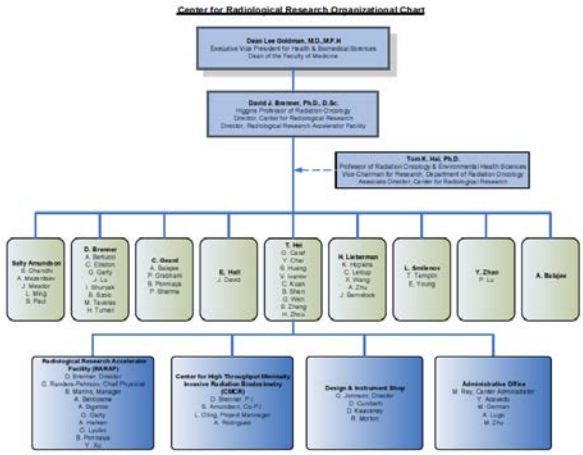

***Figure 3**. CRR organizational chart (January 2010).*

- **Job descriptions**: For each job description, a comprehensive list of responsibilities is defined. The responsibilities associated with each job title allow the definition of **training requirements** for that job description
- **Training Records**: For each individual working on the study an up to date record of all training must be maintained. This ensures that the individual is indeed able to perform their function, as specified in the Job description. Training should include safety courses and any other general courses mandated by the University (for Example HIPPA) as well as internal lab training on operation of equipment and assays used in the lab. All training must be documented and reviewed periodically to ensure that it is up to date.

In general, the job titles and descriptions defined for the facility are flexible and may be set to reflect the existing hierarchy and responsibilities in the lab, with one exception:

The **study director** whose roles and responsibilities are defined in §58.33 is the ultimate authority. He has *"overall responsibility for the technical conduct of the study, as well as for the interpretation, analysis, documentation and reporting of results, and represents the single point of study control."* Specifically he is responsible for approving all study protocols as well as all deviations from them. The study director is appointed by the "**management team**" who has subordinate responsibility for ensuring that the studies are performed according to the protocols approved by the study director.

The **Quality Assurance Unit** (§58.35) who is *"entirely separate from and independent of the personnel engaged in the direction and conduct of that study"* has the responsibility to maintain copies of all protocols and periodically check that they are indeed being followed. The QA unit reports to the management and study director.

In our laboratory, we defined job descriptions for a Study Director, a Project Manager, a Project Science Manager, a Documentation Manager, a Laboratory Manager, a Lead Scientist and multiple Laboratory Assistants. Furthermore, we developed both the training requirements for each one and forms for keeping track of training and qualifications.

Equipment control

Equipment control is required to assure that "Equipment used in the generation, measurement, or assessment of data and equipment used for facility environmental control shall be of appropriate design and adequate capacity to function according to the protocol and shall be suitably located for operation, inspection, cleaning, and maintenance." (§58.61). In order to assure this, every piece of equipment used in the study must be "*adequately inspected, cleaned, and maintained*" and, when relevant, "*tested, calibrated and/or standardized.*"

In order to do this each piece of equipment must have an SOP for its operation (in addition to the manufacturer supplied manual). The SOP should specify how to use the equipment in as much detail as possible.

Additionally, records must be kept of scheduled maintenance/service and calibration as well as of any malfunctions and repairs. When available, the maintenance/calibration schedule recommended by the manufacturer is to be adhered to, but if such a schedule is not available, the management team must establish a reasonable schedule independently.

The above is all that is needed for simple off-the-shelf pieces of equipment where there is only one way to use the equipment. For more elaborate pieces of equipment, which can be reconfigured for different experiments, or for home-built equipment, a longer SOP is generally required. Additionally, in such a case the appropriateness of the equipment for its intended use must be demonstrated. This is done via a set of "qualification documents":

- The **Design Qualification** documents list the requirements from the equipment for performing the study and are usually written prior to purchase or installation.
- The **Installation Qualification** documents record that the equipment was properly installed and has appropriate power, cooling and any other prerequisite specified by the manufacturer. This ensures that the instrument will work in a safe manner.
- The **Operation Qualification** documents record the results of a series of tests specified by the manufacturer or the management team and which demonstrate that the equipment works according to the manufacturer's specifications. This does not ensure, however, that the equipment is appropriate for use in the specific study performed.
- The **Performance Qualification** documents record the results of a series of tests designed to show that the equipment operates properly in the context of the study to be performed. This typically entails performing the actual assay on a set of samples for which the result is known and verifying that the assay works as expected. When relevant, it requires performing the assay with common "errors" and demonstrating that the equipment is able to trap these errors and report them appropriately. The performance qualification needs to be repeated following any software upgrade or modification to the equipment.

Table II: *list of "simple" and "elaborate" equipment for which SOPs were written.*

Simple Equipment	Elaborate Equipment
Fyrite CO_2 gas analyzer	epMotion 5070 liquid handling system
Manual Micropipettes	LIMS system
Fridge/Freezer	96-well filtration system
CO_2 Incubator	Fluorescent microscope
Refrigerated Centrifuge	Underdrain removal tool
Thermometer	Image acquisition software
Biosafety hood	Image analysis software
Water bath	
Barcode readers	
Label printer	
Manual pipette	
Temperature logger	
Plate shaker	
Light meter	

LIMS system

While a computerized Laboratory Information Management System (LIMS) is not mandated by 21CFR58, implementation of one greatly facilitates the requirement for storage and retrieval of records and data: "*All raw data, documentation, protocols, final reports, and [non-perishable] specimens […] shall be retained.*" (§58.190(a)). Furthermore: "*All data entries shall be dated on the date of entry and signed or initialed by the person entering the data*." (§58.130(e)).

A major part of our work revolved around the configuration of the LIMS system. We have implemented a LIMS based on the Progeny software package (Progeny Software LLC, Delray Beach, FL). Progeny LIMS is a complete sample inventory system with an intuitive, flexible database that can be configured by the user.

Within the framework provided by the vendor, we configured the LIMS system database to contain all data relevant to our studies. We programmed the workflows defined by our SOPs into Progeny LIMS allowing a simple interface where each sample can be scanned, using

a barcode reader, and the next step to be performed on it is displayed. This allows the LIMS system to cross check that the assay is indeed performed as specified in the SOP. Furthermore we have implemented checks for reagent identity so that it is impossible to accidentally use a reagent other than the one appropriate for that step.

In addition, as Progeny LIMS requires the user to log in, an audit trail is maintained as to who entered which piece of data and when.

Implementation of a Quality Control System

In conclusion, implementation of a quality Control system is neither rapid nor easy. If it is to be done properly, resources on the order of 2-3 FTE (Full Time Equivalent) need to be allocated. While it is beneficial to have an outside consultant familiar with the FDA requirements, there is no replacement for having most of the work done by people who actually "live" in the lab and are intimately familiar with the assays to be controlled. During our work we relied heavily on training, advice and templates (sample SOPs) from SQ but the bulk of the writing was done by HCT and JRP (The latter working full time on QC implementation) on the science SOPs and GG and JRP on the administrative ones. In addition to writing and reviewing protocols, a lot of effort was placed into re-organizing the lab such that the experiments can be performed in an efficient manner and that all reagents and consumables are properly labeled and stored. Two shelves were designated locations for Good Laboratory Practice (GLP) documents and equipment manuals.

However, as we have seen, a big advantage of implementing QC is that the act of writing things down in a clear yet detailed manner requires one to consider carefully the critical parts of an experiment, locate the common pitfalls, and devise ways to overcome them. This results in improved experimental control and repeatability.

Reference

1. Good Laboratory Practice Regulations, (2009) Code of Federal Regulations, Title 21, Part 58 (21 CFR 58). ■

A Pilot Trial to Correlate Radiotherapy-Induced Skin Reactions with Markers of Radiosensitivity

Brian Ponnaiya, Preety Sharma, Helen Turner, Silvia C Formenti[a], and David J. Brenner

In an attempt to develop predictors of individual sensitivity to acute radiation response, a study was initiated to examine the correlation between acute (early onset) erythema in breast-cancer patients and previously established biomarkers of radiation exposure, i.e. micronuclei formation and induction of γH2AX.

Erythema is an acute radiation effect in humans, typical peaking at the end of the radiotherapy (RT) course [1] and the inter-patient variation in the severity has been seen to differ greatly [2]. In addition, acute radiation-induced skin response and radiation-induced LD50 values have been seen to correlate in mice [3-5]. Eligibility for the pilot study was limited to women who were about to undergo breast radiotherapy in the Radiation Oncology Department at the NYU School of Medicine. Before and at the end of the radiotherapy, the degree of redness of the skin was measured at fixed points on the skin of the patient; two points within the irradiated field (avoiding areas of pigmentation or scarring) and a contralateral control point. Measurements of skin color were performed using a sensitive computer-controlled reflectance spectrometer color analyzer, the Chroma Meter CR-400 (Konica Minolta). These measurements were conducted at NYU and as per the study design, the results will not be shared until the end of the study.

Before the first RT treatment, a blood sample was acquired by conventional venipuncture and shipped to the CRR within 24 hours. A portion of each blood sample was irradiated to 4 Gy and processed for γH2AX foci formation or micronuclei induction as described previously [6].

[a]Department of Radiation Oncology, NYU Langone Medical Center.

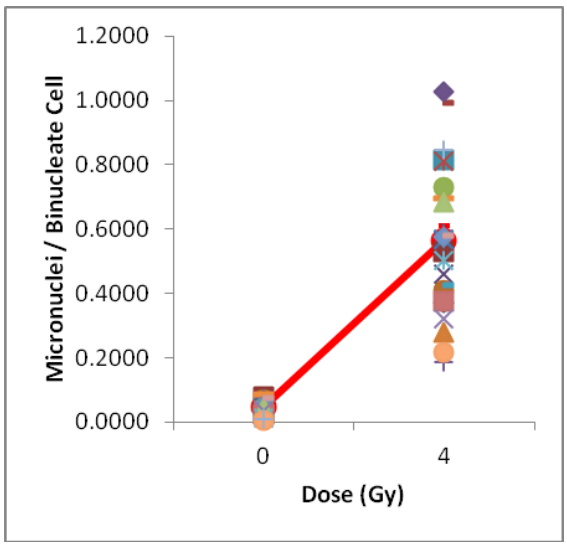

***Figure 1**. Yields of micronuclei in binucleate cells in individuals following ex-vivo irradiation with 4 Gy. Red line represents mean ±SEM of 24 patients.*

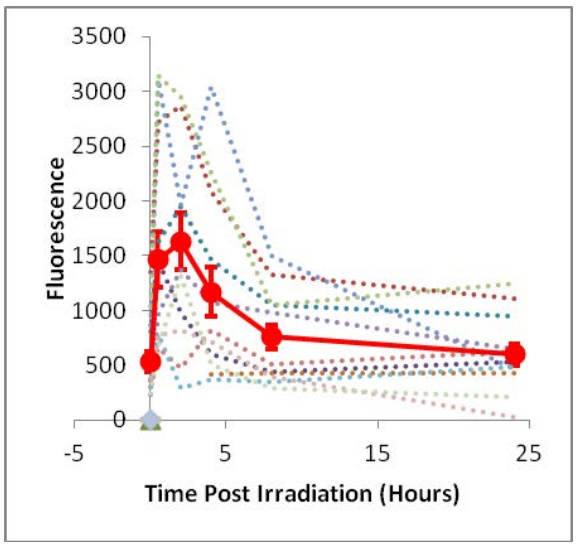

***Figure** 2. Induction of γH2AX in individual samples following 4 Gy exposure. The red line represents mean ±SEM (n=15).*

As can be seen in Figure 1, background yields of micronuclei (0 Gy) were relatively similar among all patients (with an average yield of 0.046 ± 0.005). While there were statistically significant differences in micronuclei yields between 0 and 4 Gy for every individual, there appeared to be a fair degree of variability among individuals following ex-vivo exposure to 4 Gy. The frequencies ranged from a mean of 1 micronucleus in every binucleate to a mean of only 1 in 5 binucleate cells containing a micronucleus.

γH2AX fluorescence in individual samples following ex-vivo irradiation is presented in Figure 2. Taken as a mean of 15 patient samples, staining intensities increased significantly within 0.5 hours of irradiation and remained significantly elevated up to 8 hours post irradiation before returning to control levels at 24 hours. However, similar to the trends observed for micronuclei induction, there appear to be some inter-patient variations in both the maximum intensities and kinetics of foci formation. While the peaks of fluorescence intensities were seen at 0.5 hours for some patients, this peak was extended to 2 and even 4 hours post irradiation for others. By 24 hours γH2AX staining intensities were back to near control levels for most (but not all) patient samples.

In conclusion, there appears to be a good deal of inter-patient variation in both the yields of micronuclei and γH2AX induction following ex-vivo irradiation. It remains to be determined whether these variations correlate with variations in acute erythema in these patients.

References

1. Russell, N.S., et al., Quantification of patient to patient variation of skin erythema developing as a response to radiotherapy. Radiother Oncol, 1994. 30(3): 213-21.
2. Tucker, S.L., I. Turesson, and H.D. Thames, Evidence for individual differences in the radiosensitivity of human skin. Eur J Cancer, 1992. 28A(11): 1783-91.
3. Rojas, A., F.A. Stewart, and J. Denekamp, Interaction of radiosensitizers and WR-2721. I. Modification of skin radioprotection. Br J Cancer, 1982. 45(5): 684-93.
4. Rasey, J.S., et al., Radioprotection of normal tissues against gamma rays and cyclotron neutrons with WR-2721: LD50 studies and 35S-WR-2721 biodistribution. Radiat Res, 1984. 97(3): 598-607.
5. Biedermann, K.A., et al., scid mutation in mice confers hypersensitivity to ionizing radiation and a deficiency in DNA double-strand break repair. Proc Natl Acad Sci U S A, 1991. 88(4): 1394-7.
6. Turner HC, Brenner DJ, Chen Y, Bertucci A, Zhang J, Wang H, Lyulko OV, Xu Y, Shuryak I, Schaefer J, Simaan N, Randers-Pehrson G, Yao YL, Amundson SA, Garty G. Adapting the γ-h2ax assay for automated processing in human lymphocytes. 1. Technological aspects. Radiat Res, 2011. 175: 282–290. ■

High-Throughput Immunofluorescence Assay of γ-H2AX Decay Kinetics in Multiple Individuals

Preety Sharma, Brian Ponnaiya, Guy Garty, Helen Turner, Antonella Bertucci, and David Brenner

The Columbia University RABiT (Rapid Automated Biodosimetry Tool) quantifies DNA damage and estimates past radiation exposure levels, based on fingerstick volumes of blood. This robotically based system is fully automated, and its high throughput is based on robotically based handling, a multiwell plate platform, and rapid image analysis. One RABiT protocol quantifies the γ-H2AX assay, a measure of DNA double strand breaks (DSB). The RABiT γ-H2AX assay was initially optimized for a single time point. The practicality and scalability of the system is demonstrated by quantifying γ-H2AX foci at multiple time points after irradiation. Fingerstick blood samples were collected in heparin-coated capillaries from multiple healthy individuals with no prior radiation exposure. The samples were irradiated *ex vivo* with 4 Gy of gamma radiation. After irradiation, the lymphocytes were fractionated using separation medium and released into multiwell filter bottom plates at 0.5 hr, 2 hr, 4 hr, 7 hr and 24 hr post irradiation. The γ-H2AX foci were detected using anti-human γ-H2AX monoclonal antibody, visualized using an Alexa Fluor 555 secondary antibody, and the nuclei were counterstained with DAPI. Functional validation of the system is presented by the global DSB repair kinetics of total γ-H2AX fluorescence at different time points post-irradiation.

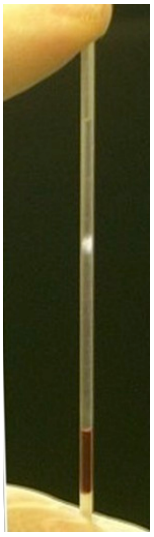

Figure 1.

The RABiT is designed to process blood samples collected, using a standard finger stick lancet, into bar-coded heparin-coated plastic capillary tubes. In the RABiT the capillary is spun to separate lymphocytes from red blood cells (Figure 1). The red blood cells are discarded while the isolated lymphocytes are transferred to filter bottom multiwell plates, immunostained and later imaged [1].

Results and Discussion

The primary goal here is to validate the extended system for high throughput measurements of DSB repair in a population of healthy adults. Finger stick samples were collected from 65 healthy individuals with demographic information recorded for gender, age, ethnicity, smoking and alcohol consumption status.

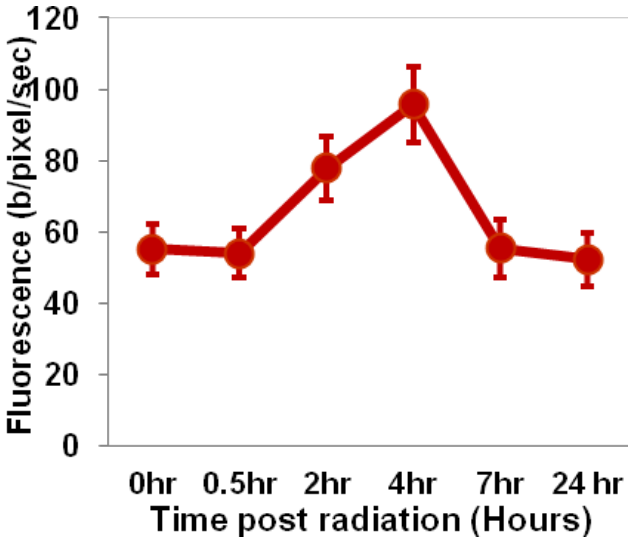

Figure 2. *Mean of gamma-H2AX DNA repair kinetics obtained from 42 donors.*

These samples were irradiated to a dose of 4 Gy of gamma-rays and the RABiT assay was used to establish the DNA repair capabilities using the γ-H2AX endpoint measured up to 24 hr post irradiation. Samples were processed for immunofluorescence measurements of γ-H2AX repair kinetics. The imaging and analyses of DNA repair kinetics on the processed samples are currently in progress. Shown here is the mean of total fluorescence yields for γ-H2AX at different time points obtained from 42 donors. Data are plotted as total fluorescent yield normalized to nuclear area and to image exposure time (Figure 2). The large inter-individual variability is evident.

To determine if there were any differences in the DNA repair kinetics between males and females, the data from these 42 donors was sorted based on gender (Figure 3). These results, obtained using a well-calibrated, conventional gamma-ray source (Atomic Energy of Canada, Gammacell 40 Cesium Unit) will serve as the basis of comparison for the initial biological testing of the compact irradiator being built in house.

DNA double-strand breaks are critical DNA lesions that can promote genomic instability. Organisms have evolved complex repair pathways, often with multiple redundancies, to respond to and repair DSB. Not surprisingly, there is much evidence that links global DSB repair capacity with cancer risks [2], with radiation sensitivity [3], and with response to cancer therapy [4, 5].

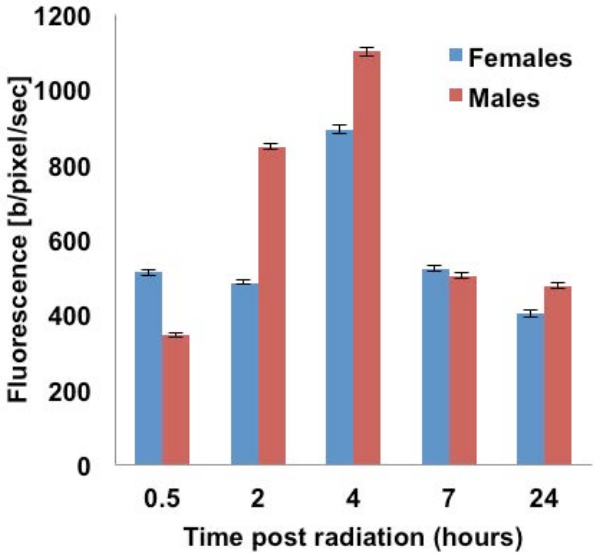

Figure 3. *Gamma H2AX DNA repair kinetics characterized for gender.*

There is now a great deal of interest in mechanistic biomarkers that could ultimately lead to predictive or preventive strategies [6-11], and also in potential individualized biomarkers for cancer therapy. Until now, there has been no corresponding high-throughput technology for assaying global DSB repair – as we are developing here. Having the technology for a high throughput, inexpensive assay for global DSB repair would allow a new approach - DSB-repair association studies.

Thus our goal is to be able to characterize, with very high throughput, DNA repair protein kinetics in fingerstick samples of human lymphocytes. Assessing the kinetics of these repair protein foci will provide a practical, rapid, high-throughput, and inexpensive tool for assessing global DSB repair capacity on an individual-by-individual basis.

Potential applications are for epidemiological studies relating to cancer therapy strategies, and also to facilitate development of preventive strategies for a variety of diseases – either in standalone epidemiological studies, or to complement molecularly-based association studies.

Future goals include analyzing DNA repair kinetics in 85 additional healthy individuals. In parallel with this we will work on developing a quantitative approach for comparing the measured DNA repair kinetics of different endpoints and different samples, and to be able to identify outliers.

References

1. Turner, H.C., et al., Adapting the γ-H2AX assay for Automated Processing in Human Lymphocytes. 1. Technological Aspects. Radiation Research, 2011. **175**(3): p. 282-290.
2. Bau, D.T., et al., DNA double-strand break repair capacity and risk of breast cancer. Carcinogenesis, 2007. **28**(8): p. 1726-30.
3. Rube, C.E., et al., DNA double-strand break repair of blood lymphocytes and normal tissues analysed in a preclinical mouse model: implications for radiosensitivity testing. Clin Cancer Res, 2008. **14**(20): p. 6546-55.
4. Chistiakov, D.A., N.V. Voronova, and P.A. Chistiakov, Genetic variations in DNA repair genes, radiosensitivity to cancer and susceptibility to acute tissue reactions in radiotherapy-treated cancer patients. Acta Oncol, 2008. **47**(5): p. 809-24.
5. Fernet, M. and J. Hall, Genetic biomarkers of therapeutic radiation sensitivity. DNA Repair (Amst), 2004. **3**(8-9): p. 1237-43.
6. Perera, F., et al., Biologic markers in risk assessment for environmental carcinogens. Environ Health Perspect, 1991. **90**: p. 247-54.
7. Berwick, M. and P. Vineis, Markers of DNA repair and susceptibility to cancer in humans: an epidemiologic review. J Natl Cancer Inst, 2000. **92**(11): p. 874-97.
8. Kyrtopoulos, S.A., Biomarkers in environmental carcinogenesis research: striving for a new momentum. Toxicol Lett, 2006. **162**(1): p. 3-15.
9. Au, W.W., Usefulness of biomarkers in population studies: from exposure to susceptibility and to prediction of cancer. Int J Hyg Environ Health, 2007. **210**(3-4): p. 239-46.
10. Kennedy, D.O., et al., DNA repair capacity of lymphoblastoid cell lines from sisters discordant for breast cancer. J Natl Cancer Inst, 2005. **97**(2): p. 127-32.
11. Reinlib, L. and E.C. Friedberg, Report of the Working Group on Integrated Translational Research in DNA Repair. DNA Repair (Amst) 2007 **6**(1):145-7. ■

Radiation Biodosimetry in Patients Treated with Radiation to Prevent Heterotopic Ossification

Jay R. Perrier, Helen C. Turner, David J. Brenner, and Sally A. Amundson

One of the major problems that the Columbia CMCR program has faced in our biodosimetry studies is that our study blood samples are either taken from unirradiated healthy humans with the blood irradiated *ex vivo*, or are from *in-vivo* irradiated cancer patients. One constraint on studies using cancer patients is the fractionated nature of their therapy, which makes it impossible to monitor changes that occur over time since a single initial exposure. Also, this model raises some questions as to the relative effects of radiation exposure on healthy individuals. Recently, we have set up a collaboration with a team at the University of Maryland Medical Center (UMMC) to collect blood samples from patients receiving a localized radiotherapy fraction to prevent heterotopic ossification after hip or elbow surgery. In each case, a single high-dose fraction of 7 to 8 Gy is typically given, which results in an average dose to the blood of 15 to 55 cGy. For the patients recruited in this study, information about the details of their radiotherapy treatment plan will allow us to use standard analytic modeling techniques to estimate the distribution of dose to the blood. Blood samples will be collected before, and at defined times up to seven days after the radiation treatment and analyzed for cytogenetic biomarkers and transcription across the whole genome. Our aim for this study is to accrue 20 patients, who will each provide a pre-irradiation blood sample and two post-irradiation samples, the timing of which will be agreed upon at the time of recruitment. In this report, we present our preliminary data using the micronucleus assay, to examine the *in vivo* effect of single-fraction radiation exposure on micronucleus frequency in peripheral lymphocytes from healthy human donors.

Blood collection and shipping requirements

One aspect of this collaboration with the Maryland team was to develop a standard operating procedure (SOP), for the collection and shipment of blood samples from UMMC to Columbia University Medical Center in New York while ensuring the integrity of these valuable samples. The cytogenetics assays require 5-6 ml of blood be collected into a BD Lithium Heparin Vacutainer Tube (Becton Dickinson) and kept at room temperature prior to shipping, whereas the gene expression assays require 2.5 ml of blood be collected into a PAXgene RNA tube (PreAnalytiX) and kept at 4˚C until shipping. The shipping requirements specify that the collected samples must be shipped the day of collection, overnight, at ambient temperature to assure arrival at Columbia the next morning. Samples were kept at ambient temperatures using a preconditioned Credo 22-248 (Minnesota Thermal Science Inc.) certified shipping box with the internal temperature of the box monitored by the inclusion of an EL-USB1 Temperature Data Logger. Samples that have been exposed to temperatures outside the range from 18 to 37 degrees Celsius will be rejected and not used. Prior to the start of the study the shipping boxes, packaging materials and temperature loggers, together with detailed instructions of use, were provided to UMMC.

Micronucleus Assay Analysis

To date we have received blood samples from three patients. For the first two individuals, we received blood samples from two time points, the pre-irradiation and 4 hours post-irradiation. For the third patient, we received blood samples from three time points, the pre-irradiation and 4 and 24 hours after radiation. Upon receiving samples they were processed for the micronucleus assay [1]. Briefly, whole blood samples (1ml) were cultured in complete RPMI 1640 medium containing phytohemagglutinin (PHA), to stimulate mitosis, followed by the addition of cytochalasin B, to block cytokinesis and obtain binucleate cells. For analysis, the cells were fixed with Carnoy's solution and spread onto a Fisherbrand Superfrost Plus slide. The cells were stained with the nuclear stain DAPI and scored manually using an Olympus BX43 fluorescent microscope with a 40x air objective. Scoring was based on the Fenech micronuclei scoring criteria [1]. At least 1000 binucleates were scored per time point.

Figure 1 shows the micronuclei frequency in the blood samples shipped from Patient 3. The results show a significant increase (>1.5%; P<0.05) in micronuclei per

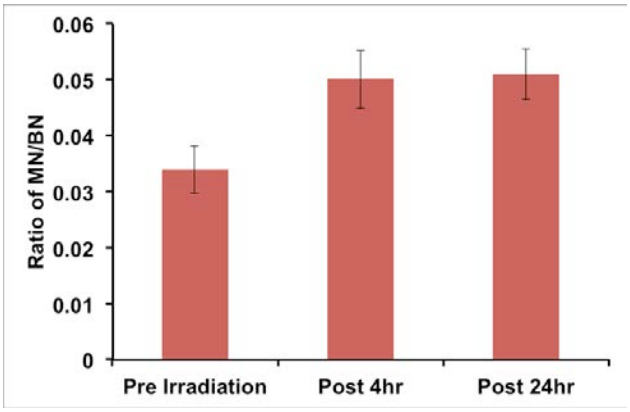

Figure 1. *Micronucleus frequency, scored as micronuclei per binucleate for Patient 3. Error bars show ± SEM.*

binucleate in both the 4 hr (1.6%) and 24 hr (1.61%) post-irradiation time points compared to the pre-irradiation control sample. There is no apparent increase or decrease in micronuclei formation between the 4 hr and 24 hr time points. Analysis of blood samples collected from Patients 1 and 2 exhibited a similar increase in micronuclei induction 4 hours post-irradiation, 1.3% with $P<0.001$ and 1.3% with $P< 0.05$, respectively (data not shown).

In summary, we provide preliminary data for the induction of micronuclei in cultured peripheral blood lymphocytes after single-fraction partial body irradiation in individuals with no history of cancer or previous radiation therapy. The results show that we have been able to detect a small but significant increase in the induction of micronuclei formation 4 hours post-irradiation that persists 24 hours later. This study is ongoing as we expect to recruit more patients and expand these preliminary data.

Reference

1. Michael Fenech (2000) The in vitro micronucleus technique. *Mutation Research*. **455:** 81-95. ■

Proton Radiation-Induced miRNA Signatures in Mouse Blood: Characterization and Comparison with ^{56}Fe-Ion and Gamma Radiation

Thomas Templin, Erik F. Young, and Lubomir B. Smilenov

Background

MicroRNA (miRNA) are a class of small non-coding RNA that are important regulators of gene expression [1]. *In vivo* and *in vitro* studies have found that miRNA control is essential for the proper execution of many processes in normal cells, including cell metabolism, cell differentiation, and cell signaling [2, 3]. A host of recent findings demonstrate that radiation has a significant impact on miRNA expression (reviewed in [4]). Among these studies are several examples of low linear energy transfer (LET) effects on normal human fibroblasts and various immortalized cell lines [3, 5-10, 11].

We have reported a strong effect of radiation on miRNA expression profiles derived from the circulating blood of radiotherapy patients [12]. We also showed that blood miRNA expression signatures of mice exposed to low- or high-LET radiation (γ-rays or ^{56}Fe ions) are highly dependent on radiation energy and dose [13]. Classifiers based on these signatures reliably predicted the irradiation type and dose of mice with unknown irradiation status. Together, these results demonstrate that miRNA signatures may be used as both radiation biodosimeters and indicators of radiation-induced functional changes in cells and tissues.

In this study, we investigate the potential of miRNA signatures to be used as biomarkers for exposure to 600 MeV protons. Protons are the main type of high-LET radiation encountered by astronauts in low earth orbit. They are components of the solar wind, the Van Allen radiation belts, and galactic cosmic rays and cumulatively pose a health threat to astronauts, particularly during heightened solar activity. In this *in vivo* proof-of-principle study, we exposed C57BL/6 mice to 600 MeV proton total body irradiation and measured miRNA expression levels in the blood of the irradiated and control animals. Using these results and the results that we obtained from prior work [13], we developed statistical classifiers that can be used in the estimation of exposure parameters. Finally, we analyzed the involvement of the differentially expressed miRNA in cellular processes.

miRNA expression signatures induced by irradiation

A total of 119 mouse miRNA (out of an average 188 per sample that were amplified above background level) were differentially expressed with *p*-values of less than 0.05. The differentially expressed miRNA were subjected to an FDR analysis, which controls for the expected proportion of false positives [14]. The FDR was set to 0.07 which means that only 7% of the miRNA declared as differentially expressed are expected to be false positives. After applying this restrictive adjustment, we determined that 26 miRNA were differentially expressed (FDR < 0.07, average *p*-value of 0.0002; Table 1). The differentially expressed miRNA were expressed in either one condition (77%) or multiple conditions (23%). Notably, the majority of differentially expressed miRNA (79%) were downregulated after proton irradiation.

Table 1. *MicroRNA differentially expressed in whole mouse blood after exposure to 600 MeV protons in vivo. Mice were irradiated with doses of 0.5 or 1.0 Gy, 250 μl blood were collected directly in lysis solution, and total RNA was purified at 6 and 24 h after irradiation. miRNA expression levels were determined by 384-well low-density TaqMan® real-time PCR miRNA expression assays. The expression data was preprocessed and normalized. Fold changes in expression level, relative to non-irradiated control samples, with a false discovery rate of < 0.07 were considered to be statistically significant.*

Irradiation condition	miRNA ID	Fold change[a] ± SEM	*p*-value	FDR	Avg. C_T controls[b]	Avg. C_T irradiated[b]
p 6 h 0.5 Gy	miR-10b	-5,000.0 ± 1.67	2.9E-04	0.0135	27.7	40.0
	miR-292-3p	-90.9 ± 1.54	0.0011	0.0426	33.5	40.0
	miR-495	-120.5 ± 1.20	8.8-05	0.0056	33.1	40.0
	miR-501-3p	5,970.0 ± 1.23	4.2E-05	0.0040	40.0	27.5
	miR-667	-384.0 ± 1.08	7.4E-06	0.0014	31.4	40.0
p 6 h 1.0 Gy	miR-1	-4.4 ± 1.29	0.0041	0.0482	24.5	26.7
	miR-10b	-4,760.0 ± 1.67	1.3E-05	6.1E-04	27.7	40.0
	miR-34c	-16.1 ± 1.65	0.0012	0.0325	35.9	40.0
	miR-99a	-2.4 ± 1.19	0.0074	0.0615	24.1	25.4
	miR-100	-2.4 ± 1.29	0.0098	0.0633	24.2	25.6
	miR-125b-5p	-3.3 ± 1.26	0.0019	0.0415	23.2	25.1
	miR-127	-4.8 ± 1.32	0.0035	0.0482	25.9	28.2
	miR-143	-13,000.0 ± 1.39	1.4E-06	1.4E-04	26.2	40.0
	miR-200a	-16,400.9 ± 1.18	1.0E-07	1.9E-05	25.9	40.0
	miR-203	-5.6 ± 1.53	0.0118	0.0633	21.0	23.6
	miR-204	-4.8 ± 1.47	0.0130	0.0646	26.7	29.0
	miR-218	-4.8 ± 1.29	0.0025	0.0427	25.3	27.7
	miR-224	-3.3 ± 1.40	0.0082	0.0615	28.7	30.6
	miR-294	34.0 ± 1.32	1.6E-04	0.0050	40.0	35.0
	miR-379	-6.7 ± 1.39	0.0029	0.0427	28.5	31.4
	miR-380-5p	-52.6 ± 2.79	0.0046	0.0495	34.2	40.0
	miR-411	-7.1 ± 1.68	0.0147	0.0697	27.2	30.1
	miR-511	361.1 ± 1.35	2.6E-05	9.9E-04	40.0	31.6
	miR-598	-62.50 ± 1.22	8.0E-06	5.2E-04	33.9	40.0
p 24 h 0.5 Gy	miR-200a	-6,250.0 ± 1.38	1.1E-05	0.0020	27.4	40.0
	miR-292-3p	-137.0 ± 1.37	9.9E-05	0.0091	32.9	40.0
	miR-379	-123.5 ± 1.62	5.6E-04	0.0341	33.1	40.0
p 24 h 1.0 Gy	miR-342-5p	-1,790.0 ± 1.41	2.7E-05	0.0012	29.2	40.0
	miR-379	-122.0 ± 1.63	6.1E-04	0.0226	33.1	40.0
	miR-598	107.1 ± 1.19	1.1E-05	7.1E-04	40.0	33.2
	miR-667	302.4 ± 1.06	1.0E-07	9.3E-06	40.0	31.7
	miR-685	1,830.0 ± 1. 09	1.0E-07	9.3E-06	40.0	29.1
	miR-741	33.6 ± 1.63	0.0020	0.0617	40.0	34.9

Abbreviations: ID = identification; SEM = standard error of the mean; FDR = false discovery rate.
[a] Compared to the non-irradiated control sample.
[b] Average C_T values of non-irradiated control and irradiated samples, respectively.

Comparison of miRNA signatures for different types and energies of radiation

In a previous study using the same mouse strain (from the same vendor) and experimental conditions, we assessed the miRNA response to γ-rays and 1 GeV/n ^{56}Fe ions. As compared to the 600 MeV proton irradiations, the prior ^{56}Fe-ion particle exposures had comparable relative biological effectiveness (RBE) magnitudes. Data in the previous study was processed with the same criteria for statistical significance [13]. Based on these factors, we believe that a reliable comparison between the two studies is possible. A comparison of the differentially expressed miRNA shows that a total of 39 miRNA are differentially expressed 6 h after irradiation with γ-rays, protons, or ^{56}Fe ions and that 22 miRNA are differentially expressed 24 h after exposure to any of these 3 radiation types. For each time point, 5 miRNA are differentially expressed upon exposure to either of two different types of radiation, amounting to, respectively, 12.8% and 22.7% of all differentially expressed miRNA at the 6 h and 24 h time point, but no miRNA are differentially expressed in response to all 3 radiation types (Figure 1).

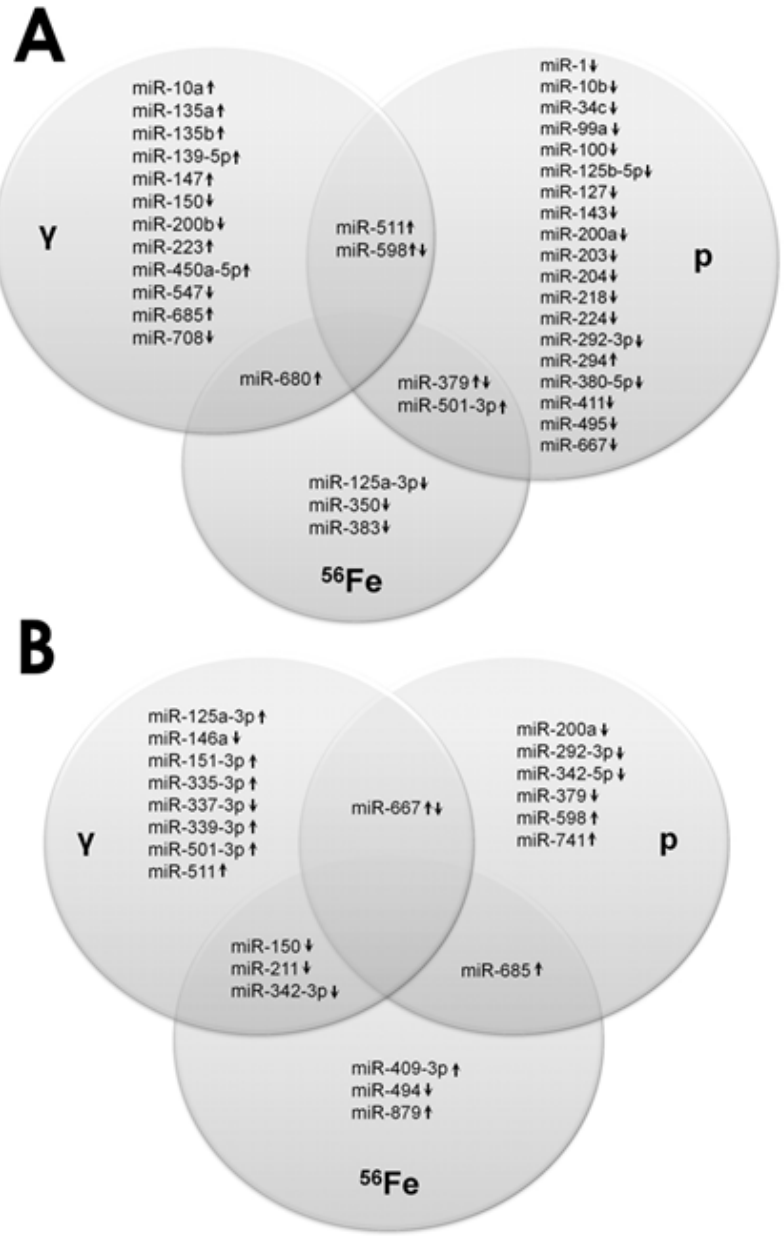

Figure 1. *Venn diagrams showing miRNA differentially expressed upon irradiation with γ-rays, 600 MeV protons, or 1 GeV/n ^{56}Fe ions, regardless of radiation dose, at 6 h (**A**) or 24 h (**B**) after radiation exposure. Areas of overlap among different circles depict miRNA differentially expressed after exposure to either of two different types of radiation. Arrows indicate up or down regulation of the specific miRNA after irradiation.*

miRNA signature-based class prediction

The differentially expressed miRNA obtained in this study together with the miRNA expression results obtained in our previous study were used to build classifiers in order to test to what degree blood miRNA signature-based class prediction is able to indicate the irradiation status of mice. The leave-one-out cross validation method was used to test the robustness of the classifiers. In this method, all samples—except one—are used to build the classifier, and the ability of the classifier to correctly predict the class membership of the left-out sample is computed. This process is continued until each sample has been left out once, and the parameters that characterize the performance of the classifier are based on the overall ability of the classifier to correctly assign the samples to their respective classes.

Three parameters were calculated to gauge classifier performance: accuracy, sensitivity, and specificity. Accuracy is the percentage of samples correctly assigned to the class they belong to. Sensitivity is the probability for a sample belonging to a class to be correctly predicted as belonging to that class. Specificity is the probability for

a sample not belonging to a class to be correctly predicted as not belonging to that class.

Three different types of classifiers were created. The performance of these classifiers is illustrated in Table 2. The first classifier was designed to classify samples according to radiation type (γ, proton, ^{56}Fe, or control), irrespective of time point after irradiation and radiation dose. Thirty-two miRNA were included in this predictor. This predictor correctly classified 81% of the unknown samples, with specificities and sensitivities ranging from 0.583 to 1.00.

Table 2. *Performance of class-prediction classifiers. Accuracy, sensitivity, and specificity of the class-prediction classifiers designed to predict the irradiation type, proton-irradiation dose or time after proton irradiation based on miRNA expression signatures.*

Irradiation condition	Accuracy	Sensitivity	Specificity
γ	81%	0.583	0.902
p		1	1
^{56}Fe		0.75	0.902
Control		0.882	0.944
p 0.0 Gy	88%	1	0.833
0.5 Gy		1	1
1.0 Gy		0.667	1
p 6 h	83%	0.778	0.889
24 h		0.889	0.778

Abbreviation: p = protons.

The second classifier was designed to classify samples according to proton radiation doses irrespective of the time point after radiation exposure. This type of predictor may be used for a sample known to be exposed to proton radiation. This predictor contained 3 miRNA (miR-292-3p, miR-379, and miR-667) and correctly classified 88% of the unknown samples, with specificities and sensitivities ranging from 0.667 to 1.00. The third classifier was designed to classify samples according to the time after receiving proton irradiation. It can be used for a sample known to be exposed to proton radiation and contained the same miRNA used in the dose prediction classifier. This predictor correctly classified 83% of the unknown samples with specificities and sensitivities ranging from 0.778 to 0.889.

It is important to consider that class predictors can be employed in combinations. For example, once the radiation type has been determined using this classifier, the miRNA expression data obtained from blood samples can be further classified using separate radiation type-specific predictors, such as the one for protons shown above or the γ ray- or ^{56}Fe ion-specific predictors we developed previously [13]. We conclude that, in principle, blood miRNA expression profiles derived from C57BL/6 mice can be used to correctly predict the type and dose of radiation received by the animal.

Acknowledgements: This study was supported in part by NASA, grant number NNX07AT41G, and by the Center for High-Throughput Minimally-Invasive Radiation Biodosimetry, National Institute of Allergy and Infectious Diseases, grant number U19 AI067773.

References

1. Bartel DP. MicroRNAs: target recognition and regulatory functions. Cell 2009;136:215-33.
2. Shkumatava A, Stark A, Sive H, Bartel DP. Coherent but overlapping expression of microRNAs and their targets during vertebrate development. Genes Dev 2009;23:466-81.
3. Maes OC, An J, Sarojini H, Wu H, Wang E. Changes in MicroRNA expression patterns in human fibroblasts after low-LET radiation. J Cell Biochem 2008;105:824-34.
4. Dickey JS, Zemp FJ, Martin OA, Kovalchuk O. The role of miRNA in the direct and indirect effects of ionizing radiation. Radiat Environ Biophys 2011;50:491-9.
5. Simone NL, Soule BP, Ly D, et al. Ionizing radiation-induced oxidative stress alters miRNA expression. PLoS One 2009;4:e6377.
6. Shin S, Cha HJ, et al. Alteration of miRNA profiles by ionizing radiation in A549 human non-small cell lung cancer cells. Int J Oncol 2009;35:81-6.
7. Chaudhry MA. Real-time PCR analysis of micro-RNA expression in ionizing radiation-treated cells. Cancer Biother Radiopharm 2009;24:49-56.
8. Josson S, Sung SY, Lao K, Chung LW, Johnstone PA. Radiation modulation of microRNA in prostate cancer cell lines. Prostate 2008;68:1599-606.
9. Marsit CJ, Eddy K, Kelsey KT. MicroRNA responses to cellular stress. Cancer Res 2006;66:10843-8.
10. Ishii H, Saito T. Radiation-induced response of micro RNA expression in murine embryonic stem cells. Med Chem 2006;2:555-63.
11. Nikiforova MN, Gandi M, Kelly L, Nikiforov YE. MicroRNA dysregulation in human thyroid cells following exposure to ionizing radiation. Thyroid 2011;21:261-6.
12. Templin T, Paul S, Amundson SA, et al. Radiation-induced micro-RNA expression changes in peripheral blood cells of radiotherapy patients. International journal of radiation oncology, biology, physics 2011;80:549-57.
13. Templin T, Amundson SA, Brenner DJ, Smilenov LB. Whole mouse blood microRNA as biomarkers for exposure to -rays and (56)Fe ion. Int J Radiat Biol 2011;87:653-62.
14. Benjamini Y, Hochberg Y. Controlling the false discovery rate: A practical and powerful approach to multiple testing. Journal of the Royal Statistical Society B 1995;57:289-300. ■

In vivo Effect of Dose Rate on Residual γ-H2AX Levels and Apoptosis Frequency in Peripheral Mouse Lymphocytes Exposed to X-rays

Helen C. Turner, Maria Taveras, Antonella Bertucci, Jay R. Perrier, Congju Chen, Lubomir B Smilenov, Guy Garty, Sally A. Amundson, and David J. Brenner

Many IND (Improvised Nuclear Device) and RDD (Radioactive Dispersal Device) scenarios involve significant components of the dose being delivered over many hours. The duration of radiation exposure will vary in different situations, from fractions of a second to hours or days. A given dose is generally less effective if it is spread over a period of hours, days or weeks as opposed to being administered acutely within a few minutes [1]. The dose-rate effect is due in large part to the capacity of cells to repair important molecular lesions, such as DNA double strand breaks (DSBs) [1].

The immunofluorescence-based detection of γ-H2AX is a reliable and sensitive method for quantitatively measuring DSBs in irradiated samples. The phosphorylation of histone H2AX at serine 139 is one of the earliest responses of mammalian cells to ionizing radiation-induced DNA breaks [2]. Apoptosis is a physiological mode of cell death under genetic control that may result from hormonal or growth factor manipulations, aberrant gene expression and DNA damage [3]. It is characterized morphologically by increased cytoplasmic granularity, cell shrinkage, chromatin condensation, membrane blebbing and the formation of nuclear bodies [4]. In the present study, we used the γ-H2AX assay to examine the *in vivo* formation of γ-H2AX in mouse peripheral lymphocytes following exposure to acute and low dose rate (LDR) doses of X-rays over a period of 24 hours. Apoptosis frequency was quantified by terminal deoxynucleotidyl transferase d-UTP Nick End Labeling (TUNEL) [5,6].

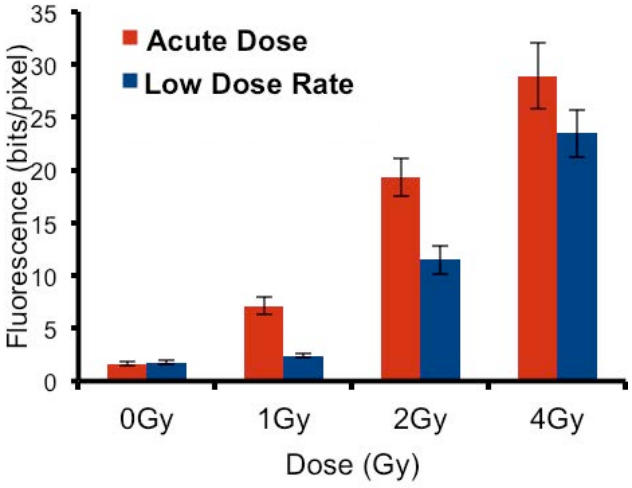

Figure 1. *In vivo dose-rate response of residual γ-H2AX protein levels, 24 hours after the start of irradiation. The data is pooled from 8 mice and the errors bars show ± SEM.*

The Center for Radiological Research has recently acquired a Precision X-Rad 320 biological X-Ray rradiator (Precision X-Ray Inc.), which is a self-shielded self-contained system that allows a range of dose rates from 1 Gy/day up to > 10 Gy/minute, with programmable irradiation times from 1 sec to > 24 h. Importantly, 1) the environment in the irradiation chamber can be controlled in terms of both temperature and humidity/CO_2 levels, and 2) the irradiation chamber and the irradiation field are both large enough for protracted, uniform simultaneous irradiation of up to 12 mice [7]. Our study was performed in 10-week old C57BL/6 male mice. The experiments included 7 doses in total: controls, acute (1, 2 and 4 Gy) and LDR (1, 2 and 4 Gy) with eight mice for each dose point. The dose rate for the acute, high dose rate exposure was ~1.03 Gy/min whereas the low dose rate was ~0.31 cGy/min. (or about 4 Gy per day). All mice were euthanized by CO_2 asphyxiation at 24 hours after the start of irradiation. Blood was collected by cardiac puncture. Lymphocytes were isolated using lymphocyte separation media (Histopaque 1083) and fixed with ice-cold methanol. For the immunocytochemical detection of γ-H2AX, the cells were incubated with a primary rabbit polyclonal antibody, visualized using Alexa Fluor 488 (AF488), and counterstained with the nuclear stain DAPI. Images of cells were obtained using an Olympus epifluorescence microscope (Olympus BH2-RFCA). Fluorescent images of DAPI-labeled nuclei and AF488-labeled γ-H2AX were captured separately for each dose using a 60x oil immersion objective. Quantification of γ-H2AX yields was determined by measuring the total γ-H2AX nuclear fluorescence per lymphocyte at a fixed exposure time of 2 seconds and analyzed using image analysis software [8].

The *in vivo* dose-rate response of residual γ-H2AX expression levels is presented in Figure 1. The results show that at the higher dose rate, there is a dose-response in residual γ-H2AX levels. Overall, the residual levels of γ-H2AX are higher in mice exposed to acute doses versus low dose rate irradiation. For the 1 Gy LDR samples, the results show that the total γ-H2AX fluorescence level appears to be close to background levels of γ-H2AX. At

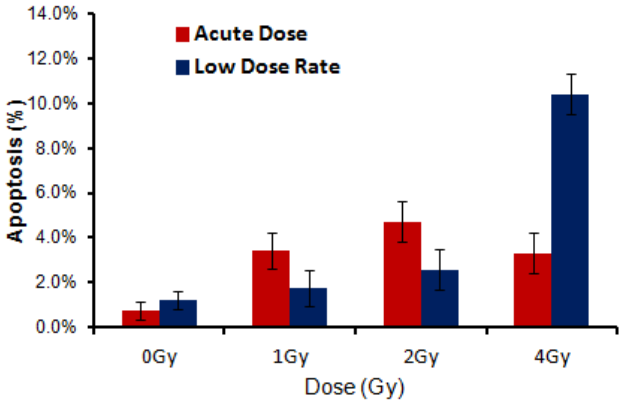

Figure 2. *Radiation-induced apoptosis frequency 24 hours after the start of radiation. The errors bars show ± SE.*

the highest dose, 4 Gy, the *in vivo* dose rate effect appears smaller due to increased residual γ-H2AX levels measured in lymphocytes isolated from the 4 Gy LDR mice.

Apoptosis was detected using a commercially available APO-BrdU TUNEL Assay Kit (Invitrogen). DNA fragments were labeled with a DNA labeling mixture containing terminal deoxynucleotidyl transferase (TdT) and the deoxythymidine analog 5-bromo-2'-deoxyuridine 5'-triphosphate (BrdUTP). Then, the breaks were labeled with Alexa Fluor 488 dye-labeled anti-BrdU antibody and the nuclei were counterstained with propidium iodide (PI). For this study, only nuclei fully labeled with Alexa 488 were considered TUNEL positive within the total PI stained population. At least 600 cells per dose were counted under a fluorescent microscope using a 20x air objective. Percentages of apoptotic cells were calculated for every dose (Figure 2). The results show that radiation-induced apoptosis was higher in the mice exposed to acute doses of 1 Gy and 2 Gy x-rays compared to the equivalent low dose rate exposure, whereas, the reverse was seen at 4 Gy; the induction of apoptosis was significantly ($P < 0.05$) larger in the 4 Gy LDR samples compared to 4 Gy acute dose samples.

In summary, residual DNA damage was measured 24 hours after radiation exposure with the γ-H2AX biomarker. The results show that the residual levels of γ-H2AX are higher in mice exposed to an acute dose rate as opposed to low dose rate, 24 hours after the start of irradiation. These data highlight differences in the effect of dose rate on the *in vivo* repair of DSBs. Radiation-induced apoptosis frequency after 1 Gy and 2 Gy X-ray exposures showed a higher percentage of apoptotic cells in the high dose rate samples compared to the low dose rate samples. Interestingly, a reverse response was seen at 4 Gy, where the lymphocytes isolated from the 4 Gy LDR mice showed a much larger apoptosis frequency compared to the mice exposed to 4 Gy at a high dose rate. These analyses are ongoing and future studies will look to quantify other biodosimetric markers and examine the dose rate effect 7 days post irradiation.

References

1. T.A. Kato, H. Nagasawa, W.M. Weil, P.C. Genik, J.B. Little, J. S. Bedford. γ-H2AX foci after low-dose-rate irradiation reveal atm haploinsufficiency in mice. Radiat Res. 166: 47-54 (2006).
2. E. P. Rogakou, D. R. Pilch, A. H. Orr, V. S. Ivanova and W. M. Bonner. DNA double-stranded breaks induce histone H2AX phosphorylation on serine 139. J. Biol. Chem. 273: 5858–5868 (1998).
3. S. Czene, E. Testa, J. Nygren, I. Belyaev, M. Harms-Ringdahl. DNA fragmentation and morphological changes in apoptotic human lymphocytes. Biochem Biophys Res Commun. 294(4): 872-878 (2002).
4. R.C. Wilkins, B. C. Kutzner, M. Truong, J. Sanchez-Dardon, J. R. N. McLean. Analysis of radiation-induced apoptosis in human lymphocytes: flow cytometry using Annexin V and propidium iodide versus the neutral comet assay. Cytometry, 48 (1): 14-19 (2002).
5. Douglas RS, Tarshis AD, Pletcher Jr, Nowell PC and Moore JS. A simplified method for the coordinate examination of apoptosis and surface phenotype of murine lymphocytes. Journal of Immunological Methods 188: 219-228 (1995).
6. Darzynkiewicz Z, Galkowski D and Zhao H. Analysis of apoptosis by cytometry using TUNEL assay. Methods 44(3): 250-254 (2008).
7. Elliston CD, Amundson SA, Paul S, Johnson GW, Smilenov LB and Brenner DJ (2011) Progress in adapting the x-ray machine to low dose rate studies. Center for Radiological Research, Annual Report 2010, pp.87-89.
8. H.C. Turner, D.J. Brenner, Y. Chen, A. Bertucci, J. Zhang, W. Wang, O.V. Lyulko, Y. Xu, I. Shuryak, J. Schaefer, N. Simaan, G. Randers-Pehrson, Y.L. Yao, S.A. Amundson, G. Garty. Adapting the γ-H2AX Assay for Automated Processing in Human Lymphocytes. 1. Technological Aspects. Radiat Res. 175(3): 282-90 (2011). ■

THE RADIOLOGICAL RESEARCH ACCELERATOR FACILITY

An NIH-Supported Resource Center

WWW.RARAF.ORG

Director: David J. Brenner, Ph.D., D.Sc.
Associate Director: Gerhard Randers-Pehrson, Ph.D.
Manager: Stephen A. Marino, M.S.

Research Using RARAF

For over a decade, many of the biology studies at RARAF, including those involving animals, have examined the "bystander" effect - the response of cells that are not directly irradiated when in close contact with, or are even only in the presence of, irradiated cells. The emphasis of most of the present biological experiments is to determine the mechanism(s) by which the effect is transmitted, primarily via direct gap junction communication through cell membrane contact. Both the Microbeam and the Track Segment Facilities continue to be utilized in various investigations of this phenomenon. Research into bystander effects in 3-D systems continued this past year with the irradiations of *C. elegans* nematodes using a "worm clamp" system adapted for use on the microbeam system.

The experiments performed using the RARAF Singletron between January 1 and December 31, 2011 and the number of shifts each was run in this period are listed in Table I. Fractional shifts are assigned when experimental time is shared among several users (*e.g.*, track segment experiments) or when experiments run for more or less than an 8-hour shift. Use of the accelerator for experiments was 26% of the regularly scheduled time (40 hours per week), about 1/4 higher than last year. Five different experiments were run during this period. Two experiments were undertaken by members of the CRR, supported by grants from the National Institutes of Health (NIH). Three experiments were performed by external users, supported by grants and awards from the Department of Defense (DoD), the National Air and Space Administration (NASA), and The Israel Science Foundation. Brief descriptions of these experiments follow.

Hongning Zhou and Tom Hei of the CRR continued experiments to identify the signaling transduction pathways involved in radiation-induced bystander responses (Exp. 110). Using the Microbeam Facility, they observed that cytoplasmic irradiation with ^{4}He ions could induce mutagenesis in mitochondrial functional human skin fibroblasts, although the mutation induction rate is relatively low compared with nuclear-irradiated cells. However, cytoplasmic irradiation could induce very little, if any, mutagenesis in directly irradiated cells without mitochondrial DNA. Furthermore, using real time quantitative PCR, they found that targeted cytoplasmic irradiation induced a transient increase in mitochondrial DNA contents as a function of time post-irradiation. To detect mitochondrial alteration after cytoplasmic irradiation, small airway epithelia cells labeled with GFP glycoprotein linked to their mitochondrial membranes were irradiated through their

Table I. *Experiments Run at RARAF January 1 - December 31, 2011*

Exp No.	Experimenter	Institution	Exp. Type	Title of Experiment	Shifts Run
110	H. Zhou, B. Zhang, K. K. Lam, T. K. Hei	CRR	Biol.	Identification of molecular signals of alpha particle-induced bystander mutagenesis	47.8
112	Y. Horowitz	Ben Gurion Univ., Israel	Phys.	HCP and neutron irradiation of LiF:Mg, TI TLD chips	6.5
113	A. Miller	AFRRI	Biol.	Role of alpha particle radiation in depleted uranium-induced cellular effects	1.0
152	B. Ponnaiya, H. Lieberman	CRR	Biol.	The role of Rad9 in mediating global gene expression in directly irradiated and bystander cells and chromosome abnormalities.	5.2
153	C. Zeitlin	Southwest Research Institute	Phys.	Fast neutron detection efficiency of boron-loaded plastic scintillators.	3.5

cytoplasm with ^{4}He ions. After irradiation, mitochondrial fusion was observed using the RARAF multiphoton imaging system that is available on the microbeam end station. One day post-irradiation, cells were stained with a cell-permeant green-fluorescent dye that is selective for the mitochondria of live cells. When compared to similarly-treated controls, irradiated cells showed a significant reduction in mitochondrial membrane potential, indicating a loss of function. These results indicate that mitochondria play a critical role in cytoplasmic irradiation-induced genotoxicity and impact on our understanding of the cellular response to DNA damage and low dose radiation risk assessment.

Yigal Horowitz of Ben Gurion University, Israel resumed studies of the responses of different types of thermoluminescent devices (TLDs) to high-LET charged particles and monoenergetic neutron irradiation (Exp. 112). TLDs were irradiated with doses of 1 and 100 Gy of 6 MeV neutrons produced using the D(d,n)^{3}He reaction. Both TLD-600 (^{6}LiF:Mg,Ti) chips, which are sensitive to neutrons and γ rays, and TLD-700 (^{7}LiF:Mg,Ti) chips, which are only sensitive to γ rays were irradiated. The lower dose was to determine the sensitivities of the TLDs and the larger dose was to obtain good measurable optically stimulated luminescence (OSL).

The exposure of military personnel and civilians to the alpha emitter and heavy metal depleted uranium (DU) is of concern to the Department of Defense. Alexandra Miller of the Armed Forces Radiobiological Research Institute (AFRRI) continued studies using the Track Segment Facility to evaluate DU radiation-induced carcinogenesis and other late effects using *in vitro* models and to test safe and efficacious medical countermeasures (Exp. 113). Human osteoblast cells (HOS) were irradiated with ^{4}He ions to evaluate the effect of the biological countermeasure phenylbutyrate (PB) on cell survival, neoplastic transformation, chromosomal aberrations, and global DNA methylation status.

Rad9 has been implicated in a wide range of cellular processes (including the regulation of cell cycle checkpoints and DNA damage repair) that are thought to play roles in the development of tumors. Brian Ponnaiya and Howard Lieberman continued investigations of the effects of Rad9 on radiation-induced changes in chromosome status and gene expression in human and mouse cells directly irradiated or as bystanders (Exp. 152). The three genotypes used in this study were wild-type mouse ES cells, Rad9-/- cells and Rad9-/- cells ectopically expressing the mouse Rad9 gene. Cells were seeded onto double-ring mylar dishes and irradiated with 1 Gy of ^{4}He ions using the Track Segment Facility. Irradiated and bystander populations were separated 24 hours after irradiation and reseeded into T25 flasks. Chromosome preparations were made at 7 day intervals and metaphases were analyzed for gross chromatid- and chromosome-type aberrations. The data supports previous findings of a role for Rad9 in both genomic instability and bystander responses. In addition, differential expression of chromatid- and chromosome-type aberrations as a function of Rad9 status suggests that Rad9 might play different roles in the appearance of delayed chromosomal aberrations in directly irradiated and bystander cells.

Cary Zeitlin of the Southwest Research Institute, along with several colleagues, began to characterize the efficiency of a neutron spectrometer based on a boron-loaded plastic scintillator (Exp. 153) for use in space. Neutrons are thermalized in the large detector as they lose energy in elastic collisions, primarily with the hydrogen nuclei in the scintillator material. Since these collisions occur extremely rapidly, the energy of the neutron is observed as a single pulse. The low-energy neutrons are often captured by the boron, which has a very large thermal neutron cross section and releases a 1.5 MeV alpha particle a very short time after the pulse from the neutron collisions. The pulse from this alpha particle is of constant amplitude and indicates that the first pulse was caused by a neutron that has given up all its energy. An advantage of this design is the direct measurement of the neutron spectrum. Most other spectroscopy systems require complicated deconvolution programs to determine the neutron spectrum. The detector was irradiated with essentially monoenergetic neutrons with energies from 0.5 to 3.0 MeV and 6 MeV to obtain initial neutron spectra.

Development of Facilities

Development continued on a number of extensions of our irradiation facilities and capabilities for imaging and irradiating biological specimens:

- Focused particle microbeams
- Focused x-ray microbeam
- Neutron microbeam
- Non-scattering particle detector
- Advanced imaging systems
- Targeting and manipulation of cells
- Small animal systems
- New neutron source

Focused particle microbeams

The electrostatically focused microbeam has continued operating very reliably this past year, consistently producing a beam spot 1-2 μm in diameter using a 500 nm thick silicon nitride exit window. A window only 100 nm thick is used when a sub-micron beam spot is desired.

Emphasis on quality control was maintained. We perform a microbeam test run the evening before an irradiation so that the next morning, after the accelerator has warmed up, the charged particle beam is found immediately and has a minimal beam spot diameter. This provides an earlier and trouble-free start for irradiations and consequently a greater throughput.

Twelve new ceramic quadrupole triplet rods were machined in our shop. The rods were then sent to the Institute of High Current Electronics in Russia for implantation of platinum ions to increase the surface resistivity, which reduces ion charge build-up on the insulating sections between the electrodes, and were returned in early 2011. The conductivities of the insulating sections will be measured, the sections carefully masked and the rods sent out to have a gold layer 1 μm thick plated on the electrode sections to make them conducting. The rods then will be tested in vacuum with high voltage using the test fixture described in last year's report. After testing, eight of the rods will be assembled into two quadrupole triplet lenses and the lenses mounted in an alignment tube for insertion into the microbeam beam line, where the voltages on the lens elements will be adjusted to produce a beam spot with a sub-micron diameter.

The permanent magnet microbeam (PMM) uses a compound quadrupole triplet lens system made from commercially available precision permanent magnets. Its design is similar to that of the electrostatic lens system for the sub-micron microbeam, the major difference being that it uses magnetic rather than electrostatic lenses. After tuning, it consistently produced a ^{4}He beam spot 5 μm in diameter. The quadrupole magnet strengths used to focus the beam were adjusted to produce a focused 4.4 MeV proton beam for development of the Flow And ShooT (FAST) microfluidics system, described below, and for irradiation of *C. elegans* nematodes.

Focused x-ray microbeam

We have developed a microbeam to provide characteristic K_{α} x rays generated by proton-induced x-ray emission (PIXE) from Ti (4.5 keV). Charged particle beams can generate nearly monochromatic x rays because, unlike electrons, they have a very low bremsstrahlung yield.

A small x-ray source is produced by bombarding a Ti target with 1.8 MeV protons using an electrostatic quadrupole quadruplet lens to focus the beam to ~50 x 120 μm on the target. The x rays used are emitted at 90° to the proton beam direction. A zone plate is used to focus the x-ray source to a beam spot 5 μm in diameter. The system is mounted on its own horizontal beam line on the 1st floor of RARAF and the x-ray beam is oriented vertically, so that the geometry of the microscope and stage is the same as for our charged particle microbeam systems.

A new quadrupole quadruplet lens with an 8mm bore, significantly larger than the 2 mm bore on the previous quadruplet, has been constructed and installed. The new lens has five ground planes, one between each set of electrodes (five), providing better definition of the electric field than the previous lens, which only had ground planes

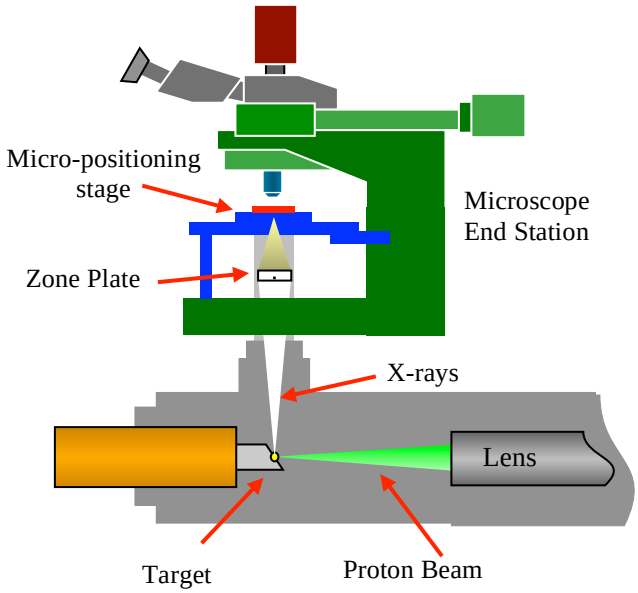

***Figure 1**: Schematic layout diagram of the x-ray microbeam endstation.*

at the ends and between the 2nd and 3rd elements. The increased bore allows much higher proton beam currents to be obtained (>2 μA), greatly increasing the dose rate. We have begun irradiations of cell nuclei with the focused x-ray beam to observe foci formed by single-strand repair proteins tagged with GFP in XRCC1 cells, from our collaborator David Chen at the University of Texas Medical Branch, and γH2AX foci in normal human fibroblasts.

Neutron microbeam

Neutrons produced by the ^{7}Li(p,n)^{7}Be reaction are emitted only in a forward conical volume when the proton energy is just above the reaction threshold (1.881 MeV). The half-angle of this cone is dependent on the proton energy and increases with increasing energy. A focused proton microbeam 5 μm in diameter will be incident on a 1 μm thick lithium fluoride target. The backing material will be 20-μm thick Au, selected for its high density and thermal conductivity, which will stop the incident proton beam. Using a 1.886 MeV proton beam, thin samples in contact with the target backing will be exposed to a beam of neutrons 20 μm in diameter having energies from 10-50 keV. This will be the first neutron microbeam in the world.

The facility is being constructed on a dedicated horizontal beamline using a quadrupole quadruplet to focus the proton beam. The microscope, stage, video camera and computer systems already have been assembled and tested. Construction of the support and alignment system for the quadruplet lens and the LiF target has been completed and installation of the beam line is about to proceed.

As soon as the beamline is completed, the voltages on the quadruplet lens will be adjusted to produce a small focused proton beam. In order to measure the beam spot size, a thin Havar metal window will be used in place of the gold target. The protons will pass through this window and the beam spot size will be determined in the same manner as for the particle microbeams: a knife-edge scan using thin Havar strips. Unlike the other microbeams in which the charged particle or x-ray fluence is low, the proton beam current for the neutron microbeam will be at least 1 nA ($6x10^9$ protons/s – too high to count) so an ionization chamber, instead of a solid state detector, will be used to observe the change in the proton beam as it is scanned.

Non-scattering particle detector

The RARAF microbeam endstation presently delivers a precise number of particles to thin samples by counting the particles traversing them using a gas proportional counter placed immediately above the sample. Because ^{4}He ions have a very short range (≤50 μm), the medium over cells must be removed to count the ions. To allow cell medium to remain in place during cell irradiations or to irradiate samples thicker than the range of the incident ions, a very thin particle detector is necessary between the beam exit window and the samples.

An under-dish detector design was investigated several years ago in which an aluminum electrode was evaporated on one side of a thin silicon wafer and three parallel gold electrodes were evaporated on the opposite side, with only a small horizontal gap between the ends of the electrodes. The prototype detector produced a usable signal but was fragile, even with a 10 μm thickness, and was broken in use. We have been unable to obtain wafers thinner than 10 μm and efforts to thin down these wafers to ~2 μm have been unsuccessful.

Other thin detector designs are being investigated in collaboration with the Mechanical Engineering Department of Columbia University. In one design, an amorphous silicon layer ~1 μm thick, was deposited on the surface of a silicon nitride microbeam vacuum window. The detector behaved as a diode, as expected, however no pulses were observed when the detector was traversed by ^{4}He ions. This design may be investigated further since such a thin silicon layer might not absorb enough energy to produce a usable signal; a thicker silicon layer and reduced electronic noise might make this design useful.

Advanced imaging systems

We continue to develop new imaging techniques to obtain two- and three-dimensional images of cells without using stain. This is of great importance for the microbeam irradiation facilities in order to avoid damage to the cells, to maintain physiological conditions, and to image thick samples, especially small animals, for targeting and observation.

SIMI

Immersion-based Mirau interferometry (IMI) was developed at RARAF by constructing an objective to function as an immersion lens using standard interferometric techniques; however interferometry is very sensitive to vibrations, even as small as a fraction of a wavelength. Although this system provides usable images in a vibration-free environment; on the electrostatic microbeam endstation small vertical motions due to vibrations in the building greatly reduce the image quality, and passive and active systems to reduce these vibrations were unsuccessful.

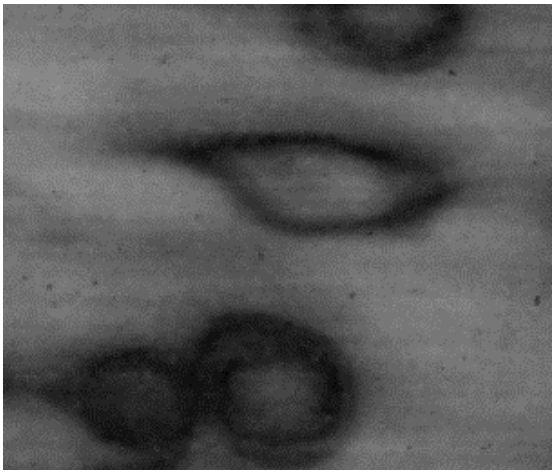

Figure 2*. Simultaneous Immersion Mirau image of HT 1080 fibrosarcoma cells expressing the XRCC1 gene. The cells were plated on glass slides and imaged in phosphate-buffered saline.*

Recently, a new approach to overcome the vibration problem using Simultaneous Immersion Mirau Interferometry (SIMI) was demonstrated. Polarized light is split into equal components in the x and y planes, one of which undergoes a phase shift of 90º by use of 1/8 wavelength (λ/8) waveplates. A polarization beam splitter is used to send the x and y components to form interferograms on a single camera. Since the images are taken simultaneously, there is no effect from vibration. This system is also much faster than Immersion Mirau because only one image is necessary instead of four images at different distances, requiring 3 vertical movements of the stage.

New optical elements were fabricated to adapt the Immersion Mirau objective for Simultaneous Immersion Mirau Interferometry. The small, thin glass discs required (8 mm D, 0.2-0.3 mm thick) were coated, either as spot mirrors or partially reflective (10-85%) beam splitters. This year the discs have been assembled into 2- or 4-piece elements with 1/8λ polycarbonate film waveplates sandwiched between the glass discs. These elements have been installed in the SIMI objective housing, designed and constructed in our machine shop, and the value of the partially reflective beam splitter that produces the best image has been determined. SIMI will be incorporated

into the sub-micron microbeam endstation as an imaging option.

UV microspot

A multi-photon microscope was developed and integrated into the microscope of the Microbeam Facility several years ago to detect and observe the short-term molecular kinetics of radiation response in living cells and to permit imaging in thick targets, such as tissue samples and *C. elegans*. Two photons delivered very closely together in space and time can act as a single photon with half the wavelength (twice the energy). The longer wavelength of the light beam allows better penetration into the sample while still being able to excite fluorophors at the focal volume and less damage is produced in the portion of the sample not in the focal volume. This system also can be used as a laser "microspot" to induce UV damage in the focal volume of the laser. Several users, both internal and external, have made use of this facility this year, particularly for 3-D imaging.

Targeting and manipulation of cells

We have purchased a micro-milling machine and a variety of small mill and drill bits. This system was used to manufacture the single cell dispenser and microfluidics chips for the FAST. It eliminates the need to use Mechanical Engineering Department facilities at the Morningside campus of Columbia.

FAST

A Flow And ShooT (FAST) targeting system based on microfluidics is being developed to increase the throughput of the microbeam and to provide irradiation of non-adherent cells, such as lymphocytes, that do not plate on surfaces and therefore do not have stable positions.

Cells moving through a narrow capillary are imaged by a high-speed camera to track their trajectory. The point-and-shoot system is used to aim the particle beam to the projected position of the cell on the trajectory and the particle beam is enabled. The deflection coil currents are changed continuously to follow the path of the cell until the required number of particles is delivered. The final system will be capable of tracking several cells at a time.

We have manufactured polydimethylsiloxane (PDMS) microfluidic chips using soft lithography. The channel has a width of 200 µm and height of 20 µm, so that the cells, when targeted by the microbeam, flow in the immediate vicinity of the exit window. The bottom of the irradiation section of the microfluidic channel is 10 µm thick and the top is 20 µm thick, so particles can reach the cells and the detector above the channel. The flow rate is controlled by a syringe pump.

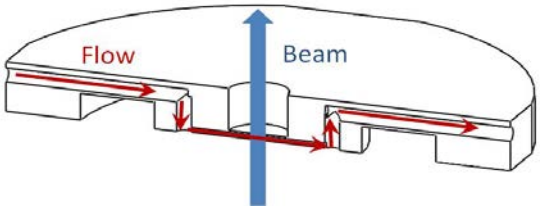

Figure 3*. FAST microfluidics chip cross section.*

Initial tests with fluorescent beads flowing through the channel and imaging at 25 frames/s resulted in the predicted bead position being within 1 µm of the actual position 90% of the time and within 2.5 µm 98% of the time. A new fast camera has been installed that allows imaging of the irradiation area at up to 1,000 frames/s. The increased imaging speed will make possible more accurate cell targeting and permit a higher flow rate, increasing throughput to as high as 100,000 cells/hr.

During the past year the permanent magnet lens system was tuned to reduce the diameter of the 4.5 MeV proton beam spot and the beam alignment was adjusted to minimize changes in the beam spot size with position when the beam is deflected.

OET

A novel cellular manipulation technique is being adapted to irradiate non-adherent cells on the sub-micron microbeam endstation. We are developing an OptoElectronic Tweezer (OET) system, initially developed by our collaborators, the Ming Wu group at Berkeley National Laboratory.

The OET consists of two parallel-plate electrodes. The top electrode is Indium Tin Oxide (ITO), which is transparent and is covered with a 1 µm thick layer of hydrogenated amorphous silicon (a-Si:H) that acts as a photoconductive layer. When light is focused on the surface of the a-Si:H, the conductivity of the layer increases by several orders of magnitude. By patterning a dynamic light image on the electrode, a reconfigurable virtual electrode is created. When the virtual electrode and its opposing plate electrode are biased with an AC voltage, a non-uniform AC field is created.

In the presence of a non-uniform electric field, a dielectric particle (*e.g.*, a cell) will feel a force caused by dielectric polarization (dielectrophoresis, DEP). The conductivity of the fluid in the chamber must be carefully controlled as it will strongly affect the electric field in the fluid layer of the OET device. If the resistance of the fluid layer is less than that of the a-Si:H, then the voltage drop will occur in the a-Si:H layer, and the DEP effect will be reduced in the liquid. The direction of the force is a function of the AC voltage frequency and the fluid conductivity. Below a certain frequency the cells are attracted by the force; at higher frequencies they are repelled.

Initial tests demonstrated the ability to manipulate fluorescent beads, moving them around with an image projected by a laser; tests this year have been performed using computer-generated images projected into the microscope using a standard LCD projector. To better understand the system, the finite element software COMSOL Multiphysics Simulation was used this year to simulate the electric field in the ET device.

Cell dispenser

Another cell manipulation device that is under development is a single cell dispenser. The dispenser consists of a microfluidic channel in which selected cells can be dispensed into a multi-well plate. In a system where cells normally travel across a T-intersection, a pressure pulse can eject a droplet containing a single cell as it passes the nozzle. The pressure pulse is generated by applying a pneumatic backpressure and quickly opening and closing a solenoid valve. The size of the droplet is determined by the precise control of the timing of the opening and closing of the valve and the applied liquid backpressure. The valve requires a 12 V 'peak' voltage pulse 150 μs long to open the nozzle, and a hold voltage to keep it open for the specified amount of time. A function generator specifies the length of the pulse and a microprocessor applies the 'peak' and 'hold' voltages to the solenoid. The device is made from a polymethyl methacrylate (PMMA) slab with 100 μm x 50 μm channels directly milled using a micromilling machine.

Presently this system is manual and very laborious. An automated system is being developed to control the dispenser based on the fluorescence of the cells or other selected criteria.

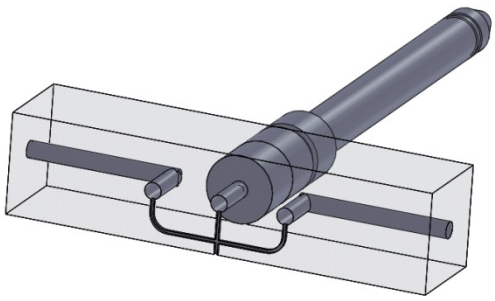

Figure 4*. CAD model of the dispenser.*

Small animal systems

C. elegans is a multi-cellular eukaryotic organism that is simple enough to be studied in great detail and is well-established as a research tool. From a practical perspective, it is small enough (~100 μm diameter, ~1 mm long) to be compatible with microbeam irradiation and a wide variety of mutants and transgenics are readily available, as is a large community of *C. elegans* researchers.

Initial irradiations required worms to be anesthetized and manually handled individually, a slow and laborious process. In order to provide high-throughput irradiations, we have developed, in collaboration with the Whitesides group at Harvard University, a microfluidic worm clamp for rapid immobilization of large numbers of live worms for morphological analysis and fluorescence imaging. We have manufactured worm clamps with four channels and a 10 μm thick PDMS bottom to allow charged particle penetration. We have begun using these chips for anesthetic-free irradiation of *C. elegans* worms and have seen that the worms indeed remain immobilized. The clamp design is being expanded to accommodate 16 worms with a possible further expansion to 64 worms

New neutron source

Development has begun on a fast neutron source with a broad spectrum that will emulate that of the "Little Boy" atomic bomb at Hiroshima. The neutron spectrum will extend to 10 MeV. A mixed beam of 5 MeV monatomic, diatomic and triatomic protons and deuterons will be incident on a thick beryllium target, producing neutrons from the $^{9}Be(d,n)^{10}B$ and $^{9}Be(p,n)^{9}B$ reactions. The diatomic and triatomic particles break up on contact with the target into individual ions with 2.5 MeV and 1.67 MeV energies, respectively, enhancing the lower-energy portion of the spectrum. In order to produce this mixed ion beam, a gas source with a specific ratio of hydrogen to deuterium will be placed in the terminal of our Singletron accelerator and a new, 0º beam line has been installed. Since this beamline does not involve deflecting the particle beam from the accelerator, there will be no separation of different ions and the full beam from the accelerator will be utilized.

The beryllium targets have been purchased and a high-capacity water-cooling system has been designed and constructed. Studies of the focusing of the ion beam have begun.

Because the area in which this source will be located was not originally intended for such a strong source of neutrons, additional shielding will have to be installed and a radiation survey performed.

Singletron Utilization and Operation

Table II summarizes accelerator usage for the past year. The Singletron normally is started between 8 and 9 am and the nominal accelerator availability is one 8-hour shift per weekday (~250 shifts per year); however the

Table II. *Accelerator Use, January - December 2011.*
Usage of Normally Scheduled Shifts

Radiobiology and associated dosimetry	**22%**
Radiological physics and chemistry	**4%**
On-line facility development and testing	**14%**
Microbeam Training Course	**4.5%**
Safety system	**2%**
Accelerator-related repairs/maintenance	**0.1%**
Other repairs and maintenance	**2%**
Off-line facility development	**40%**

***Table III**. Students for the first RARAF Microbeam Training Course.*

Name	Position	Affiliation
Anne Marie Adamczyk	Postdoctoral Associate	University of Tennessee, Knoxville, TN
Manuela Buonanno	Ph.D. student	New Jersey Medical School (UMDNJ), NJ
Stefanie Girst	Undergraduate	University of the Armed Forces, Munich, Germany
Ying Nie	Asst. Professor	Loma Linda University, CA
Mykola Onyshchenko	Postdoctoral Associate	NIH, MD
Diana Pignalosa	Scientist	GSI, Darmstadt, Germany

accelerator is frequently run well into the evening, often on weekends, and occasionally 24 hours a day for experiments or development.

Accelerator use for radiobiology and associated dosimetry was about 25% more than for last year. About 72% of the use for all experiments was for microbeam irradiations, about 12% for track segment irradiations and 16% for neutron irradiations. Approximately 1/3 of the experiment time was for experiments proposed by external users, and 2/3 was for internal users.

On-line facility development and testing was about 14% of the available time, primarily for development and testing of the electrostatically focused microbeam, the x-ray microbeam and the Flow And Shoot (FAST) system. This was significantly less use than for the last number of years because many of our current projects deal with imaging and cell manipulation and therefore do not require the use of the accelerator for much or all of their development.

There was only a fraction of a shift of Singletron maintenance to investigate a small leak in the insulating tank gas. The accelerator was not opened for maintenance or repair this year. This is the lowest amount of time spent on accelerator repair since RARAF was moved to Nevis Laboratories in 1982. The Singletron charging system continues to be very stable and reliable.

Training

We continue to participate in the Research Experiences for Undergraduates (REU) project in collaboration with the Columbia University Physics Department. For 10 weeks during the summer students attend lectures by members of different research groups at Nevis Laboratories, work on research projects, and present oral reports on their progress at the end of the program. Among other activities, the students receive a seminar about RARAF and take a tour.

This year Hamin Jeon from Emory University in Atlanta, Georgia participated in the program and worked with Alan Bigelow on UV sterilization of human wounds.

Microbeam Training Course

The first RARAF microbeam training course "Single-Cell Microbeams: Theory and Practice" (http://raraf.org/microbeamtraining.htm) was given from

***Figure 5**. The students for the first RARAF Microbeam Training Course at the Singletron accelerator console.*

May 3-5 this year. This three-day course consisted of lectures, demonstrations, and hands-on experience. The course was designed for specific needs (*e.g.*, imaging, designing a microbeam facility). Because of the intimate nature of the course, it was limited to 6 participants.

To assist in the design and operation of the course, we recruited Dr. Marcelo Vazquez of Loma Linda University Medical Center as the Director. Dr. Vazquez has had significant experience from his prior employment by NASA at the NASA Space Radiation Laboratory (NSRL) at Brookhaven National Laboratory (BNL). He helped establish the first NASA Space Radiation Summer School and assisted in running the course for three years. He is familiar with the requirements of educating students on the utilization of specialized irradiation facilities.

Notification of the course was made by e-mail using the contact lists for the 2008 and 2010 Microbeam Workshops. Flyers announcing the course were handed out at the 9th International Microbeam Workshop, July, 2010 in Darmstadt, Germany and at the 56th Annual Meeting of the Radiation Research Society, September 2010 in Hawaii and verbal announcements were made in sessions at these meetings.

Students

In response to our notifications, we received 17 applications with CVs. The prospective students covered a wide range of educational levels – from undergraduate to postdoc to scientist - and were from the U.S., Europe, the Middle East, and South America. Candidates were about evenly split in gender and field (physics or radiobiology). The six applicants selected for the course

Figure 6*. From left to right: Steffi and Ying plating cells on Day 1; Anne Marie optically locating the microbeam beam spot on Day 2; Mykola making a slide for the γH2AX assay on Day 2; Anne Marie, Mykola, Manuela and Diana discussing results with Brian Ponnaiya on Day 3.*

are given in Table III and shown in Figure 5. No fee was charged for the course and some assistance was provided for travel, housing and food.

Course

Most of Day 1 involved lectures on the physics and biology of microbeams. The students received a tour of the various RARAF microbeam facilities. There was a demonstration of the procedure for plating cells on the special microbeam dishes, after which the students were divided into pairs with each person plating 3 dishes for irradiation on Day 2. Another demonstration showed the formation of foci in cells with a repair protein tagged with a fluorescent protein. After irradiation, fluorescent spots could be seen forming in seconds directly under the cross-hairs indicating the position of the irradiation. This very visual demonstration was so impressive it actually evoked gasps from the students.

Day 2 consisted mostly of demonstrations and hands-on work by the students. After observing the accelerator start-up and the characterization of the ^{4}He beam, the students performed a γH2AX assay on cells that had been irradiated previously by Brian Ponnaiya. Between the steps in the assay, one pair of students alternately prepared their cells for irradiation or actually irradiated cells with the microbeam for micronucleus assay. They each also performed the procedure to optically locate the beam spot. The other pairs either had lunch or observed a demonstration of microbeam irradiation protocols and had a tour of the neutron and broad beam facilities at RARAF.

On Day 3, the students processed their cells for the micronucleus assay and then heard lectures on microbeam developments occurring at RARAF and on biological results obtained by RARAF users. That evening there was a group dinner at which the students received certificates of completion. Each student took home a notebook containing copies of all the slides from the lectures as well as the instructions on all the physics and biology procedures that were demonstrated and that they had performed.

At the end of the course, the students were given a questionnaire on which they rated various aspects of the course and gave comments. Students thought the course was interesting and informative. They gave high ratings to the content, program structure, hands-on activities and demos, relevance, the materials provided, actual irradiation of samples and sample preparation, and interaction with faculty.

A virtual course created from this training course is described in the Dissemination section below. A second course will be given next year in conjunction with the 10th Microbeam Workshop, to be held at Columbia University.

Dissemination

The content of our website is updated continually to reflect the current state of research at RARAF. For present users, the current month's accelerator schedule is posted and the Experiment Scheduling Request form can be filled out and printed for submission to request beam time. For prospective new users, there is information about the irradiation facilities at RARAF as well as forms and instructions for proposing new service or collaboration experiments. In the Dissemination section, we offer a list of papers detailing research performed at RARAF and published in peer-reviewed journals. Many of these papers, and almost all recent papers, are available in PDF format free from our web site.

To further disseminate general information about microbeam technology, we are active participants in Wikipedia. We have created or significantly expanded encyclopedic entries for a number of topics, such as microbeam, RARAF, and Mirau interferometry, and have encouraged others in the microbeam community to participate in these efforts as well.

We are developing a virtual microbeam training course, based on the three-day microbeam training course "Single-Cell Microbeams: Theory and Practice" held at RARAF in May of this year. For interested scientists unable to attend the course, our virtual microbeam training course allow users to tailor the curriculum to best meet their needs ─ providing concise summary information for an overview and more detailed knowledge in specific topics of interest. Eleven Powerpoint-based lectures from our three-day training course were recorded and converted into enhanced podcasts. Each podcast consists of audio, synched with the accompanying PowerPoint slides (viewable on a video iPod or a PC), as well as a PDF handout of the PowerPoint slides (http://raraf.org/educationalmaterials.htm).

We plan to augment these podcast lectures with video demonstrations and a virtual tour. High-resolution video (640x480 or higher, with audio) will be used to document

demonstrations of all aspects of a microbeam experiment from making microbeam dishes to irradiating cells and online analysis. The full microbeam training course is scheduled to be completed in time for the International Conference on Radiation Research.

The 10th International Workshop: Microbeam Probes of Cellular Radiation Response will be hosted at Columbia University March 15-17, 2012 by RARAF personnel with Alan Bigelow as the organizer. Over 80 participants from around the world have registered for the three-day Workshop. This workshop provides a forum for the microbeam community to come together and discuss the present and future of microbeam research. The third day of the Workshop will be a tour of the RARAF microbeam facilities. The RARAF web site will be the central repository for information on this meeting (http://raraf.org/meeting/index.html).

Personnel

The Director of RARAF is Dr. David Brenner, the Director of the Center for Radiological Research (CRR). The accelerator facility is operated by Mr. Stephen Marino, the manager, and Dr. Gerhard Randers-Pehrson, the Associate Director of RARAF.

Dr. Charles Geard, the former Associate Director of the CRR, retired this year and is now Professor Emeritus. He continues to spend most of the work-week at RARAF.

Dr. Brian Ponnaiya, an Associate Research Scientist, is the biology advisor for RARAF. He presently spends about half his time at the CRR.

Dr. Alan Bigelow, an Associate Research Scientist, is continuing the development of the multiphoton microscopy system, which includes the UV "microspot" irradiation facility, as well as Optical Electronic Tweezers for manipulating cells.

Dr. Guy Garty, a Research Scientist, is developing the Flow And Shoot (FAST) system. He spends about half his time working on the National Institute of Allergy and Infectious Diseases (NIAID) project, for which he is the project manager.

Dr. Andrew Harken, a Postdoctoral Fellow, is responsible for the x-ray microbeam. He is also working on the imaging of cells without stain using a highly sensitive EMCCD camera.

Dr. Yanping Xu, a Postdoctoral Fellow, has been working on the development of a neutron microbeam. He is also working on the NIAID project, developing an accelerator-generated neutron source with a spectrum similar to that of the Hiroshima atomic bomb.

Sasha Lyulko, a graduate student in the Physics Department at Columbia University, is involved in developing the Simultaneous Immersion Mirau Interferometry (SIMI) system and also worked on imaging for the NIAID project.

Manuela Buonanno, a Postdoctoral Fellow, began working at RARAF in August.

Michael Grad, a graduate student in the Mechanical Engineering Department, has spent most of his time since September working at RARAF, making microfluidics chips for FAST, developing a single cell dispenser and working on the Optoelectronic Tweezers with Alan Bigelow.

Recent Publication of Work Performed at RARAF

1. Bigelow, A.W., Randers-Pehrson, G., Garty, G.,. Geard, C. R, Xu Y., Harken, A.D., Johnson, G.W. and Brenner, D.J. Ion, X-ray, UV and neutron microbeam systems for cell irradiation. AIP Conf. Proc. **1336**, pp. 351-355.
2. Fuks, E., Horowitz, Y.S., Horowitz, A., Oster, L., Marino, S., Rainer, M., Rosenfeld, A. and Datz, H. Thermoluminescence solid state nanodosimetry – the peak 5a/5 dosimeter. Radiat. Prot. Dosim. **143**: 416-426 (2011) PMCID: PMC310827.
3. Garty, G., Grad, M., Jones, B.K., Xu, Y., Randers-Pehrson, G., Attinger, D. and Brenner, D.J. Design of a novel flow-and shoot (FAST) microbeam, Radiat. Prot. Dosimetry **143**: 344-348 (2011) PMCID: PMC3108275.
4. Harken, A.D., Randers-Pehrson, G., Johnson, G.W. and Brenner, D.J. The Columbia University proton-induced soft x-ray microbeam. Nucl. Inst. Meth. B **269**(18): 1992-1996 (2011) PMCID: PMC3146766.
5. Hu, B., Grabham, P., Nie, J., Balajee, A.S., Zhou, H., Hei, T.K. and Geard, C.R. Intrachromosomal changes and genomic instability in site-specific microbeam-irradiated and bystander human-hamster hybrid cell. Radiat. Res. 2011 Nov 11. [Epub ahead of print].
6. Ivanov, V.N., Ghandhi, S.A., Zhou, H., Huang, S.X., Chai, Y., Amundson, S.A. and Hei, T.K. Radiation response and regulation of apoptosis induced by a combination of TRAIL and CHX in cells lacking mitochondrial DNA: a role for NFκB- and STAT3-directed gene expression. Exp. Cell Res. **317**: 1548-1566 (2011) PMCID: PMC2860693.
7. Marino, S.A., Johnson, G.W., Schiff, P.B. and Brenner, D.J. Modification of shirt buttons for retrospective radiation dosimetry after a radiological event. Health Phys. **100**: 542-547 (2011) PMCID: PMC3079536.
8. Mezentsev, A., Ming, L. and Amundson, S.A. Involvement of HNF4A in the low-dose radiation response of a human 3-dimensional tissue model. Radiat. Res. **175**: 677-688 (2011) PMCID: PMC3148653.
9. Miller, A.C. Development of models to study radiation-induced late effects. In "HFM Panel-099 RTG-033 Activity: Radiation Bioeffects and Countermeasures -The Radiation Bioeffects and Countermeasures RTG-033 Final Report", NATO, 2011. ■

Publications

1. **Amundson SA,** and **Smilenov LB** (2011) Integration of biological knowledge and gene expression data for biomarker selection: FN1 as a potential predictor of radiation resistance in head and neck cancer. *Cancer Biol Ther* **10:** 1252-1255.
2. Autsavapromporn N, De Toledo SM, **Buonanno M**, Jay-Gerin JP, Harris AL, Azzam EI (2011) Intercellular communication amplifies stressful effects in high-charge, high-energy (HZE) particle-irradiated human cells. *J Radiat Res.* **52(4):** 408-14.
3. Barcellos-Hoff MH, **Brenner DJ**, Brooks AL, Formenti S, Hlatky L, Locke PA, Shore R, Tenforde T, Travis EL, Williams J. (2011) Low-dose radiation knowledge worth the cost. *Science* **332(6027):** 305-6.
4. **Bigelow AW, Randers-Pehrson G, Garty G, Geard CR, Xu Y, Harken AD, Johnson GW**, and **Brenner DJ** (2011) Ion, X-ray, UV and Neutron Microbeam Systems for Cell Irradiation. *AIP Conference Proceedings* **1336:** 349-353.
5. **Brenner DJ**. (2011) Are x-ray backscatter scanners safe for airport passenger screening? For most individuals, probably yes, but a billion scans per year raises long-term public health concerns. *Radiology* **259(1):** 6-10.
6. **Brenner DJ, Shuryak I.** (2011) Ten years of follow-up is not long enough to assess lifetime cancer risks caused by computed tomography scans in a young population. *J Clin Oncol*. **29(30):**4062; author reply 4062.
7. **Brenner DJ, Shuryak I**, Einstein AJ. (2011) Impact of reduced patient life expectancy on potential cancer risks from radiologic imaging. *Radiology*. **261(1)**: 193-8.
8. **Buonanno M**, de Toledo SM, Azzam EI (2011) Increased frequency of spontaneous neoplastic transformation in progeny of bystander cells from cultures exposed to densely ionizing radiation. *PLoS One* **6(6):** e21540.
9. **Buonanno M**, de Toledo SM, Pain D, Azzam EI (2011) Long-term consequences of radiation-induced bystander effects depend on radiation quality and dose and correlate with oxidative stress. *Radiat Res.* **175(4):** 405-15.
10. **Calaf GM**, Echiburú-Chau C, Roy D, **Chai Y, Wen G, Balajee AS**. (2011) Protective role of curcumin in oxidative stress of breast cells. *Oncol Rep.* **26(4):** 1029-35.
11. **Calaf GM**, Garrido F. (2011) Catechol estrogens as biomarkers for mammary gland cancer. *Int J Oncol.* **39(1):** 177-83.
12. **Chen C, Brenner DJ**, Brown TR. (2011) Identification of urinary biomarkers from X-irradiated mice using NMR spectroscopy. *Radiat Res.* **175(5):** 622-30.
13. de Toledo SM, **Buonanno M**, Li M, Asaad N, Qin Y, Gonon G, Shim G, Galdass M, Boateng Y, Zhang J, Azzam EI (2011) The impact of adaptive and non-targeted effects in the biological responses to low dose/low fluence ionizing radiation: the modulating effect of linear energy transfer. *Health Phys.* **100(3):** 290-2.
14. Echiburú-Chau C, Roy D, **Calaf GM**. (2011) Deleterious MnSOD signals lead to abnormal breast cell proliferation by radiation and estrogen exposure. *Int J Oncol.* **38(6):** 1703-11
15. Echiburú-Chau C, Roy D, **Calaf GM**. (2011) Metastatic suppressor CD44 is related with oxidative stress in breast cancer cell lines. *Int J Oncol.* **39(6):** 1481-9.
16. Einstein AJ, **Elliston CD**, Groves DW, Cheng B, Wolff SD, Pearson GD, Robert Peters M, Johnson LL, Bokhari S, Johnson GW, Bhatia K, Pozniakoff T, **Brenner DJ**. (2011) Effect of bismuth breast shielding on radiation dose and image quality in coronary CT angiography. *J Nucl Cardiol.* **19(1):** 100-8.
17. Fuks E, Horowitz YS, Horowitz A, Oster L, **Marino S**, Rainer M, Rosenfeld A, and Datz H (2011) Thermoluminescence solid state nanodosimetry – the peak 5a/5 dosimeter. *Radiat. Prot. Dosim*. **143**: 416-426.
18. **Garty G**, Chen Y, **Turner HC**, Zhang J, **Lyulko OV, Bertucci A, Xu Y**, Wang H, Simaan N, **Randers-Pehrson G**, Lawrence Yao Y, **Brenner DJ** (2011) The RABiT: a rapid automated biodosimetry tool for radiological triage. II. Technological developments. *Int J Radiat Biol*. **87(8):** 776-90.
19. **Garty G**, **Grad M,** Jones BK, **Xu Y**, Xu J, **Randers-Pehrson G**, Attinger D, **Brenner DJ**. (2011) Design of a novel flow-and-shoot microbeam. *Radiat Prot Dosimetry*. **143(2-4):** 344-8.
20. **Garty G**, Karam A, **Brenner DJ** (2011) Infrastructure to support ultra high throughput biodosimetry screening after a radiological event. *Int J Radiat Biol*. **87(8):** 754-65.

21. **Ghandhi SA**, Sinha A, Markatou M, and **Amundson SA** (2011) Time-series clustering of gene expression in irradiated and bystander fibroblasts: an application of FBPA clustering. *BMC Genomics* **12:** 2.

22. **Grabham P**, Hu B, Sharma P, Geard C (2011) Effects of ionizing radiation on three-dimensional human vessel models: differential effects according to radiation quality and cellular development. *Radiat. Res.* **175(1):** 21-28.

23. **Harken AD, Randers-Pehrson G, Johnson GW, Brenner DJ** (2011) The Columbia University proton-induced soft x-ray microbeam. *Nucl Instrum Methods Phys Res B.* **269(18):** 1992-1996.

24. **Hei TK, Zhao Y, Zhou HN**, and **Ivanov VN** (2011) Mechanism of radiation carcinogenesis: Role of the TGFBI gene and the inflammatory response. *Adv. Exp. Med. Biol.* **720:**163-170.

25. **Hei TK, Zhou H, Chai Y, Ponnaiya B** and **Ivanov VN**. (2011) Radiation Induced Non-targeted Response: Mechanism and Potential Clinical Implications. *Curr Mol Pharmacol.* **4**:96-105.

26. Hricak H, **Brenner DJ**, Adelstein SJ, Frush DP, **Hall EJ,** Howell RW, McCollough CH, Mettler FA, Pearce MS, Suleiman OH, Thrall JH, Wagner LK. (2011) Managing radiation use in medical imaging: a multifaceted challenge. *Radiology* **258(3):** 889-905.

27. **Huang SX**, Jaurand MC, Kamp DW, Whysner J, and **Hei TK** (2011) Role of mutagenicity in asbestos fiber induced carcinogenicity and other diseases. *J. Toxicol. Environ. Hlth*. **14**:1-67.

28. Huang TC, **Paul S**, Gong P, Levicky R, Kymissis J, **Amundson SA**, and Shepard KL (2011) Gene expression analysis with an integrated CMOS microarray by time-resolved fluorescence detection. *Biosens Bioelectron* **26:** 2660-2665.

29. Hyduke DR, **Amundson SA**, and Fornace, AJ, Jr. (2011) Complexity of Stress Signaling. *Regulation of Organelle and Cell Compartment Signaling: Cell Signaling Collection.* (Bradshaw, R A, and Dennis, E A, eds) pp. in press, Academic Press,

30. **Ivanov VN, Ghandhi SA, Zhou H, Huang SX, Chai Y**, **Amundson SA**, and **Hei TK** (2011) Radiation response and regulation of apoptosis induced by a combination of TRAIL and CHX in cells lacking mitochondrial DNA: a role for NF-kappaB-STAT3-directed gene expression. *Exp Cell Res* **317:** 1548-1566.

31. **Ivanov V** and **Hei TK**. (2011) Regulation of apoptosis in human melanoma and neuroblastoma cells by statins, sodium arsenite and TRAIL. *Apoptosis* **16**:1268-1284.

32. **Ivanov V., Partridge MA, Huang SX**, and **Hei TK**. (2011) Suppression of the proinflammatory response of metastatic melanoma cells increases TRAIL induced apoptosis. *J. Cell Biochem*. **112(2):**463-75.

33. **Lieberman HB**, **Bernstock JD, Broustas CG, Hopkins KM, Leloup C, Zhu A.** (2011) The role of RAD9 in tumorigenesis. *J Mol Cell Biol* **3**:39-43.

34. **Marino SA, Johnson GW,** Schiff PB, **Brenner DJ** (2011) Modification of shirt buttons for retrospective radiation dosimetry after a radiological event. *Health Phys.* **100(5):** 542-7.

35. **Meador JA, Ghandhi SA**, and **Amundson SA** (2011) p53-Independent Downregulation of Histone Gene Expression in Human Cell Lines by High- and Low-LET Radiation. *Radiat Res* **175:** 689-699.

36. **Mezentsev A**, and **Amundson SA** (2011) Global Gene Expression Responses to Low- or High-Dose Radiation in a Human Three-Dimensional Tissue Model. *Radiat Res* **175:** 677-688.

37. Montalvo MT, Lobato I, Villanueva H, Bórquez C, Navarrete D, Abarca J, and **Calaf GM**. (2011) Prevalence of human papillomavirus in young university women. *Oncology Letters* **2***:* 701-706.

38. **Paul S,** and **Amundson SA** (2011) Gene expression signatures of radiation exposure in peripheral white blood cells of smokers and non-smokers. *Int J Radiat Biol* **87:** 791-801.

39. **Paul S**, Barker CA, **Turner HC**, McLane A, Wolden SL, and **Amundson SA** (2011) Prediction of in vivo radiation dose status in radiotherapy patients using ex vivo and in vivo gene expression signatures. *Radiat Res* **175:** 257-265.

40. **Ponnaiya B**, Suzuki M, Tsuruoka C, Uchihori Y, **Wei Y** and **Hei TK**. (2011) Detection of chromosomal instability in bystander cells after Si490 ion irradiation. *Radiat. Res*. **176**:280-290.

41. **Repin MV,** Repina LA. (2011) Rapid dicentric assay of human blood lymphocytes after exposure to low doses of ionizing radiation. *Radiats Biol Radioecol*. **51(4):** 411-8.

42. Rivas M, Araya MC, Caba F, Rojas E, **Calaf GM**. (2011) Ultraviolet light exposure influences skin cancer in association with latitude. *Oncol Rep.* **25(4):** 1153-9.

43. **Shuryak I, Brenner DJ,** Ullrich RL (2011) Radiation-induced carcinogenesis: mechanistically based differences between gamma-rays and neutrons, and interactions with DMBA. *PLoS One*. **6(12):**e28559.

44. **Shuryak I**, Sachs RK, **Brenner DJ** (2011) A new view of radiation-induced cancer. *Radiat Prot Dosimetry*. **143(2-4):**358-64.

45. **Templin T, Amundson SA, Brenner DJ**, and **Smilenov LB** (2011) Whole mouse blood microRNA as biomarkers for exposure to γ-rays and (56)Fe ion. *Int J Radiat Biol* **87:** 653-662.

46. **Templin T, Paul S, Amundson SA, Young EF**, Barker CA, Wolden SL, and **Smilenov LB** (2011) Radiation-Induced Micro-RNA Expression Changes in Peripheral Blood Cells of Radiotherapy Patients. *Int J Radiat Oncol Biol Phys* **80:** 549-557.

47. **Turner HC, Brenner DJ,** Chen Y, **Bertucci A**, Zhang J, Wang H, **Lyulko OV, Xu Y, Shuryak I,** Schaefer J, Simaan N, **Randers-Pehrson G**, Yao YL, **Amundson SA**, and **Garty G** (2011) Adapting the gamma-H2AX assay for automated processing in human lymphocytes. 1. Technological aspects. *Radiat Res* **175(3):** 282-290.

48. Wang J, Su F, **Smilenov LB**, Zhou L, Hu W, Ding N, Zhou G. (2011) Mechanisms of increased risk of tumorigenesis in Atm and Brca1 double heterozygosity. *Radiat Oncol.* **6**: 96.

49. **Wen G**, Hong M, Li B, Liao W, Cheng SK, **Hu B, Calaf G**, **Partridge MA,** Tong J, and **Hei TK**. (2011) Transforming growth factor-B induced protein (TGFBI) suppresses mesothelioma progression through the AKT/mTOR pathway. *Int. J. Oncology* **39**: 1001-1009.

50. **Wen G, Partridge MA**, Li B, Hong M, Liao W, Cheng SK, **Zhao Y, Calaf GM**, Liu T, Zhou J, Zhang Z, **Hei TK**. (2011) TGFB1 expression reduces in vitro and in vivo metastatic potential of lung and breast tumor cells. *Cancer Letter* **308**: 23-32, 2011.

51. Williams JP, Huser AK, **Brenner DJ**. (2011) Introduction. *Int J Radiat Biol*. **87(8):** 747.

52. Williams PD, Owens CR, Dziegielewski J, Moskaluk CA, Read PW, Larner JM, Story MD, Brock WA, **Amundson SA**, Lee JK, and Theodorescu D (2011) Cyclophilin B expression is associated with in vitro radioresistance and clinical outcome after radiotherapy. *Neoplasia* **13:** 1122-1131.

53. **Xu Y, Randers-Pehrson G, Marino SA, Bigelow AW**, Akselrod MS, Sykora JG, **Brenner DJ** (2011) An accelerator-based neutron microbeam system for studies of radiation effects. *Radiat Prot Dosimetry* **145(4)**: 373-376.

54. **Young EF, Smilenov LB**. (2011) Impedance-based surveillance of transient permeability changes in coronary endothelial monolayers after exposure to ionizing radiation. *Radiat Res*. **176(4)**: 415-24.

55. Zhang S, **Wen G, Huang SX**, Wang J, Tong J and **Hei TK. (2012)** Mitochondrial alterations in malignantly transformed human small airway epithelial cells induced by alpha particles. *Int. J. Cancer*, in press. ■

Margaret German with the completed 2010 Annual Report